Characterisation of Protein-Protein Interactions Involved in Type 2 Diabetes

Chloé Grace Myers

Submitted in accordance with the requirements for the degree of

Doctor of Philosophy

The University of Leeds

Leeds Institute of Cardiovascular and Metabolic Medicine

Faculty of Medicine and Health

June 2022

The candidate confirms that the work submitted is her own and that appropriate credit has been given where reference has been made to the work of others.

Acknowledgments

First of all, I would like to thank the most wonderful group of supervisors: Dr. Katie Simmons, Dr. Paul Meakin and Prof. Mark Kearney for their guidance and continued support throughout all my years at Leeds – I certainly could not envision better mentors to have on this journey with me. In particular, Katie, thank you for giving me the chance to work with you on these projects and ultimately for being an amazing boss and friend.

To all of the Kearney group, past and present. Thank you so much for taking me in as one of your own, from day one. Your endless support, tutelage and daily lab banter have taught me *so* much and have kept me wanting to come back day after day for more! I will miss you all dearly and I wish each of you every success. Special thanks to Alex Bruns, Hema Viswambharan, Jane Brown, Lia De Faveri, Katie Simmons, Katherine Paradine and Samuel Turvey for training and help managing cell work – particularly through the re-opening of LICAMM after the first lockdown! A huge thank you to Alex and Hema again for imparting your expert knowledge of western blotting onto me, I hope to keep building onto it throughout the years to come – I think I'd miss it if I didn't! Thank you to Natalie North for PCR training and, to Tom Slater for scratch wound healing and bead sprouting assay training. A massive thank you to Eva Clavane for her time in preparing bead sprouts and, Katie Simmons and Ric Cubbon for the proximity ligation work for my thesis. It has been such a help, especially towards the end – I'm so grateful to you all!

For their extensive expertise and answering of my many questions, I would like to thank Dr. Brian Jackson and Dr. Fatima Nadat from the Protein Production Facility for their help in producing the eNOS reductase domain and PYK2 kinase domain proteins and, to Dr. Iain Manfield from the Centre for Biomolecular Interactions facility with SPR training and experiments.

My project has been funded by the British Heart Foundation – being able to perform research in field is something I've wanted to do for the longest time, and I am eternally grateful to have been given the opportunity to work in this facility.

To my family and friends. Thank you for all the love and support throughout these studies… and the twenty years before that! Nothing has ever felt out of reach, and I wouldn't be where I am today if you didn't have complete faith in me and my abilities.

And lastly, to my husband and life partner, Conal. Thank you so much for everything. You have always been my biggest supporter in encouraging me to follow my dreams and for that, I couldn't be more grateful. I genuinely couldn't have this without you.

Abstract

The study of protein-protein interactions (PPIs), notably those involved in mechanisms of disease can be exploited in design of effective therapeutics. Type-2 diabetes can induce a dysfunctional endothelial cell phenotype which is also intrinsically linked to the progression of atherosclerosis and further cardiovascular disease, observing increased expression of transmembrane insulin receptor/insulin-like growth factor 1 receptor (IR/IGF1R) hybrid receptors and intracellular protein tyrosine kinase 2β (PYK2) proteins.

IR/IGF1R hybrids are composed of one IR and IGF1R α- and β-subunit. Unlike their homodimeric counterparts, the physiological function of hybrids is yet unknown however, their ability to activate insulin signalling pathways is markedly reduced. Small molecule inhibitors have been identified and validated through rounds of iterative screening. Compound HI-2 has been shown to selectively inhibit the formation of hybrid receptors in human umbilical vein (HUVEC) and saphenous vein endothelial cells (SVEC). The effect of reducing hybrids using HI-2 has resulted in altered insulin signalling and wound healing.

Autophosphorylation of PYK2 Y402 can inhibit endothelial nitric oxide synthase (eNOS) enzymatic activity by phosphorylation of its Y657 site and, subsequently reduces production of NO. Characterisation of the eNOS-PYK2 interaction has been demonstrated in HUVEC, SVEC and ATEC using co-immunoprecipitation and proximity ligation assays. Biophysical techniques such as surface plasmon resonance have been employed, however further method development is required. Inhibition of PYK2 using siRNA knockdown

in HUVEC has shown a 45% reduction in expression; inhibition using pharmacological inhibitor, PF-10e in vitro and in vivo has not been effective.

Molecular dynamics simulations have been employed in modelling protein-protein interactions utilizing a coarse-grained/atomistic (CGAT) hybrid simulation method. A series of apo-IR, IGF1R and IR/IGF1R hybrid receptor models have been produced and simulations of each have been performed on the ARC3 high-performance computer server, at the University of Leeds.

Characterisation of these interactions through biochemical, biophysical and computational techniques have contributed to a larger understanding of their mode of action, and subsequently highlighted their potential for modulation for therapeutic benefit. Further investigation is required to elucidate these interactions and design novel small molecule inhibitors for in vivo use.

Table Of Contents

List of Figures

List of Tables

Abbreviations

a.a.	Amino acids
Ach	Acetylcholine
α-CT	α-Charge Transfer
Akt	Ak Strain Transforming
AMPK	5’ Adenosine Monophosphate-activated Protein Kinase
AS160	Akt Substrate 160 kDa
AT	Adipose Tissue
ATEC	Adipose Tissue Endothelial Cells
ATF6	Activating Transcription Factor 6
BH_4	Tetrahydrobiopterin
BRET	Bioluminescence Resonance Energy Transfer
CAD	Coronary Artery Disease
CaM	Calmodulin
CaMKII	Calmodulin-dependent protein kinase II
Cav-1	Caveolin-1
CEB	Cell Extraction Buffer
CG	Coarse-Grained
CGAT	Coarse Grained-Atomistic
cGMP	Cyclic Guanosine Monophosphate
CHOP	C/EBP-Homologous Protein
CR	Cysteine-rich Region
DFG	Asp-Phe-Gly motif
DM	Diabetes Mellitus
DMEM	Dulbecco’s Modified Eagle Medium

DMSO	Dimethyl Sulfoxide
DPBS	Dulbecco Phosphate Buffered Saline
E. coli	*Escherichia coli*
EC	Endothelial Cell
EC_{50}	50% Concentration Required for Maximal Receptor Activation
ECD	Ectodomain
ECGM	Endothelial Cell Growth Medium
ED	Endothelial Dysfunction
EDRF	Endothelium-derived Relaxant Factor
EdU	5-ethylnyl-2'-deoxyuridine
EGF	Epidermal Growth Factor
EGFR	Epidermal Growth Factor Receptor
ELISA	Enzyme-Linked Immunosorbent assay
EM	Electron Microscopy
eNOS	Endothelial Nitric Oxide Synthase
EPC	Endothelial Progenitor Cell
ER	Endoplasmic Reticulum
Erk	Extracellular Signal-Related Kinase
ESMIRO	Endothelial-Specific Overexpression of Dominant-Negative Human Mutant Insulin Receptor
ET-1	Endothelin-1
FAD	Flavin Adenine Dinucleotide
FAK	Focal Adhesion Kinase
FAT	Focal Adhesion Targeting

FCS	Foetal Calf Serum
FERM	4.1 Ezrin Radixin Moesin
FGF	Fibroblast Growth Factor
FLIM	Fluorescence Lifetime Imaging
FMN	Flavin Mononucleotide
FnI-III	Fibronectin I-III
FOXO1	Forkhead Box O 1
FRET	Fluorescence Resonance Energy Transfer
GH	Growth Hormone
GHBP	Growth Hormone Binding Protein
GHRH	Growth Hormone-Releasing Hormone
GLUT	Glucose Transporter
GM	Growth Medium
GCPR	G Protein Coupled Receptor
GRP78	Glucose-Regulated Protein 78kDa
GSK3	Glycogen Synthase Kinase 3
GST	Glutathione-*S*-Transferase
GTPCH	Guanosine Triphosphate Cyclohydrolase
HBSS	Hank's Balanced Salt Solution
HI	Hybrid Inhibitor
HIF-1α	Hypoxia-Inducible Factor-1α
hIRECO	Endothelial Cell-Specific Overexpression of Human Insulin Receptor
HOMO	Highest Occupied Molecular Orbital
HPC	High-Performance Computer

HR	Hybrid Receptor
HSP	Heat Shock Protein
HUVEC	Human umbilical vein endothelial cells
i-EC-FAK-KO	Inducible Endothelial Cell-Specific Focal Adhesion Kinase Knockout
IGF	Insulin-like Growth Factor
IGF1R	Insulin-like Growth Factor 1 Receptor
IGF2R/M6PR	Insulin-like Growth Factor 2 Receptor/Mannose-6-Phosphate Receptor
IGFBP	Insulin-like Growth Factor Binding Protein
IL-1/8	Interleukin-1/8
iNOS	Inducible Nitric Oxide Synthase
IR	Insulin Receptor
IR/IGF1R	Insulin Receptor/Insulin-like Growth Factor 1 Receptor
IRE1α	Inositol Requiring Enzyme 1α
IRR	Insulin-Related Receptor
IRS	Insulin Receptor Substrate
JM	Juxtamembrane
L1/L2	Leucine-rich 1/2
LC-MS	Liquid Chromatography in tandem with Mass Spectrometry
LDL	Low-Density Lipoprotein
LGI	Leeds General Infirmary
LICAMM	Leeds Institute of Cardiovascular & Metabolic Medicine
L-NAME	N^G-nitro *L*-arginine methyl ester

L-NIO	N^5-(1-iminoethyl)-*L*-ornithine
L-NMMA	N^G-monomethyl *L*-arginine
LUMO	Lowest Unoccupied Molecular Orbital
mAb	Monoclonal Antibody
MALDI-TOF	Matrix-Assisted Laser Desorption/Ionization-Time Of Flight
MAPK	Mitogen-Activated Protein Kinase
MBP	Maltose Binding Protein
MCP-1	Monocyte Attractant Protein 1
MD	Molecular Dynamics
MS	Mass Spectrometry
MST	Microscale Thermophoresis
mTORC	Mammalian Target of Rapamycin Complex
NADPH	Nicotinamide Adenine Dinucleotide Phosphate
ND	Non-Diabetic
NMR	Nuclear Magnetic Resonance
nNOS	Neuronal Nitric Oxide Synthase
NO	Nitric Oxide
NOS	Nitric Oxide Synthase
OEC	Outgrowth Endothelial Cell
PACA	Plate Antibody Capture Assay
PCR	Polymerase Chain Reaction
PDGF	Platelet-Derived Growth Factor
PDK-1	Phosphoinositide-Dependent Kinase 1
PEC	Pulmonary Endothelial Cell

PEG	Polyethylene Glycol Precipitation Binding Assay
PERK	Protein Kinase RNA-activated-like ER Kinase
PF	Pfizer Inhibitor
PH	Plekstrin Homology
PI3K	Phosphoinositide 3-Kinase
PIP_2	Phosphatidylinositol 4,5-biphosphate
PIP_3	Phosphatidylinositol 3,4,5-triphosphate
PKA	Protein Kinase A
PKC	Protein Kinase C
PLA	Proximity Ligation Assay
PPF	Protein Production Facility
PYK2	Protein Tyrosine Kinase 2β
RLF	Relaxin-like Factor
Rluc	*Renilla luciferase*
RMSD	Root mean-squared deviation
RMSF	Root mean-squared fluctuation
ROS	Reactive Oxygen Species
RTK	Receptor Tyrosine Kinase
SFM	Serum-Free Media
sGC	Soluble Guanylate-Cyclase
siRNA	Short Interfering RNA
SPA	Scintillation Proximity Binding Assay
SPR	Surface Plasmon Resonance
SSM	Serum-Starved Media
SV	Saphenous Vein

SVEC	Saphenous Vein Endothelial Cell
T1DM	Type-1 Diabetes Mellitus
T2DM	Type-2 Diabetes Mellitus
TIM	mTOR Interaction Motif
TK	Tyrosine Kinase
TM	Transmembrane
TNF-α	Tumour Necrosis Factor α
UPR	Unfolded Protein Response
VCAM-1	Vascular Adhesion Molecule 1
VEGF	Vascular Endothelial Growth Factor
VEGFR	Vascular Endothelial Growth Factor Receptor
VSMC	Vascular Smooth Muscle Cell
XBP-1	Xbox-Binding Protein 1
YFP	Yellow Fluorescent Protein

An Introduction to Insulin Signalling

1. Introduction

1.1. Type-2 Diabetes Mellitus

Type-2 diabetes mellitus (T2DM) is a highly degenerative and increasingly prevalent disease, affecting approximately 3.5 million people in the UK alone as of 2019 (UK, 2020), with a further 13.6 million at risk of developing the condition (UK, 2021). T2DM assumes one of two phenotypes: where an individual's metabolism is incapable of producing sufficient levels of insulin in response to elevation of serum glucose or, where insulin signalling is impaired within cells which function by stimulus of insulin (Balakumar et al., 2016). By definition, T2DM can be simply characterized by an elevation of serum glucose levels, insulin resistance and a lack of available insulin. The Emerging Risk Factors Collaboration reported that DM can apply a two-fold risk of acquiring severe co-morbidities such as coronary artery disease (CAD), stroke and other vascular causes (Collaboration, 2010) such as myocardial infarction, retinopathy, renal disease and neuropathy (Balakumar et al., 2016; Leon and Maddox, 2015). As a result of a multitude of complications arising from the disease and its co-morbidities, diabetes treatment costs the NHS over £9.8 billion annually, equating to 10% of the total budget (Hex et al., 2012). Nearly 80% of this expenditure is used in treatment of complications associated with T2DM and the primary causes relate to cardiovascular diseases.

T2DM is also becoming increasingly common in young children and adolescents, responsible for close to 50% of all childhood diabetes (Mozaffarian, 2016) in the US. This increase results from higher rates of obesity in developed countries but other factors such as hypertension,

smoking and poor diet can contribute to an increased risk of diabetes. An epidemic is looming; a disease which previously was considered to affect the aging population will have a substantial knock-on effect in the years to come in terms of population health and management of condition, and the subsequent cost associated with ensuring quality of life.

However, markers of premature diabetes can be identified prior to development of the condition and one such marker is endothelial insulin resistance, which is also an independent risk factor in the progression of cardiovascular atherosclerosis.

1.2. The Endothelium

The endothelium lines all blood vessel lumens, forming a semipermeable barrier between the blood and vascular smooth muscle cells (Figure 1-1). Endothelial cells (EC) are mediators between the adjacent parties, moderating blood flow and fulfilling metabolic demands by supplying the local tissues with oxygen and other nutrients. By design, these cells are therefore exposed to changes in shear and frictional forces as blood flows through the vascular network and in response, may stimulate a shift in production of various molecular messengers, such as nitric oxide (NO). In addition, the endothelium also reacts to changes in chemical stimuli; vascular endothelial growth factor (VEGF) is crucial in modulation of endothelial cell specification and activity (Ferrara et al., 1992).

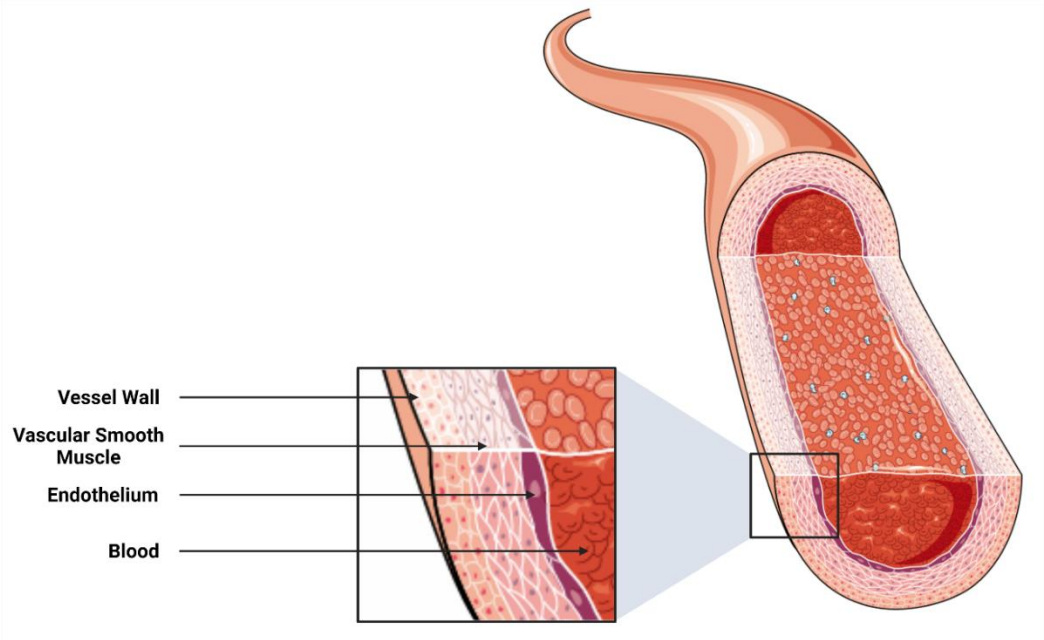

Figure 1-1: Schematic of an artery

Endothelial cells line the lumen of all vasculature. It separates vascular smooth muscle cells and flowing blood and mediates signals between the two. Image modified from smart.servier.com and created with BioRender.com.

1.2.1. Angiogenesis

Angiogenesis is the process of forming new blood vessels. Sprouting morphogenesis, intussusceptive growth, splitting, remodelling, stabilisation and differentiation of new and pre-existing vessels into arterioles, venules and capillaries are all enabled by mechanisms of angiogenesis. Angiogenesis requires a combination of proliferation, migration, cell survival, differentiation and specialisation mechanisms to carry out the aforementioned actions (Gerhardt, 2000-2013).

Development of the human vascular system begins early within embryogenesis, occurring concomitantly with the formation of the heart; vasculogenesis may be detected from as early as day 18 and in addition, fully-formed endothelial cells may also be observed in both the yolk sac and embryo from 23 days post-gestation (Larsen, 1998; Tavian et al., 1996). Formation of this network is intrinsically linked to the success of survival of

any mammalian species, providing transport of essential nutrients and oxygen to maturing cells and organs. The development of new vessels is termed neovascularization, which may be broken down into distinct signalling behaviours, comprising of angiogenesis, arteriogenesis and vasculogenesis (Simons, 2005). Vasculogenesis describes *de novo* formation of blood vessels from progenitor cells, namely angioblasts and haemangioblasts (Carmeliet, 2000). The angioblast cells aggregate and differentiate into endothelial and haematopoietic precursors, which form the basis for nascent blood vessels of each type (Carmeliet, 2005; Risau and Flamme, 1995). The newly forming vessels develop into small vesicular structures which fuse and form networks which further combine, extend and invade embryonic tissues to form the arterial, venous and lymphatic systems (Larsen, 1998; Rossant and Howard, 2002). Sprouting of new vessels in this manner is one mechanism of angiogenesis. The channels of endothelial cells are subsequently coated with pericytes, and vascular smooth muscle cells (VSMC) otherwise collectively known as mural cells, providing structural integrity and enabling regulation of haemostasis (Carmeliet, 2000; Carmeliet, 2005). The mural cells may be recruited by platelet-derived growth factor (PDGF)-BB and angiopoietin-1 (Carmeliet, 2005). Arteriogenesis encompasses the recruitment of mural cells and further remodelling of pre-existing vasculature to form larger conductance vessels (Carmeliet, 2000).

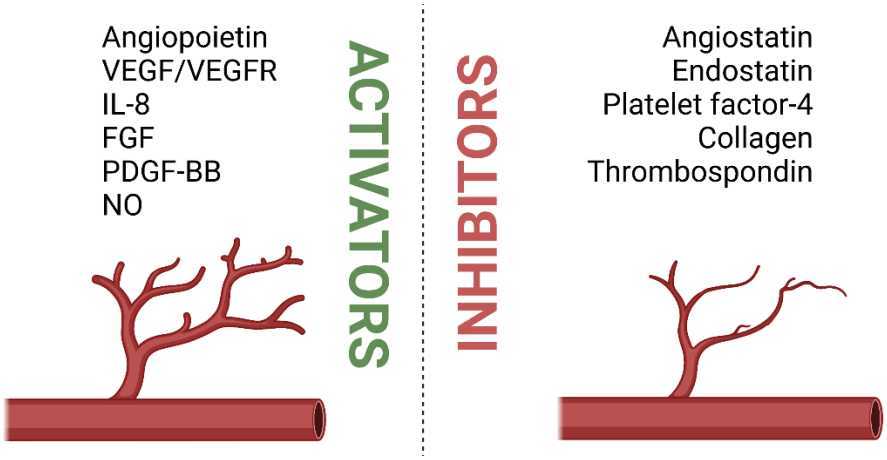

Figure 1-2: Regulators of Angiogenesis

Angiogenesis is regulated by many different activators and inhibitors. Angiopoietin, vascular endothelial growth factor (VEGF) and its receptor (VEGFR), interleukin-8 (IL-8), fibroblast growth factor (FGF), platelet-derived growth factor-BB (PDGF-BB) and nitric oxide (NO) are examples of activators of angiogenesis of endothelial cells. Angiostatin, endostatin, platelet factor-4, collagen and thrombospondin are all types of inhibitors of endothelial cells angiogenesis. Image of own design and created with BioRender.com.

In adulthood, most vessels remain quiescent, until re-activated as required for wound repair or neointima formation; continued angiogenesis typically occurs only in cycling ovaries and the placenta during pregnancy, as described above (Carmeliet, 2005). Yet mature endothelial cells retain their ability to divide rapidly in response to stimuli (Carmeliet, 2003). This process is activated and inhibited by many stimulatory and inhibitory signals from integrins, angiopoietins, chemokines, junctional molecules, oxygen sensors and endogenous inhibitors (Figure 1-2). Hypoxia and ischaemia are two principal activators of angiogenesis in endothelial cells. Hypoxia-induced angiogenesis is stimulated by upregulation of hypoxia-inducible factor (HIF)-1α in response to a lack of oxygen in surrounding tissues which results in increased expression of VEGF. VEGF, predominantly VEGF-A, and its homologue VEGF-C are key regulators of vascular and lymphatic endothelial cell sprouting, respectively; VEGF may stimulate enhanced proliferation, migration and survival, in addition to increased invasion and permeability of

pre-existing vessels (Gerhardt, 2000-2013; Carmeliet, 2005; Niu and Chen, 2010). NO production originating from endothelial cells is similarly important in angiogenesis: increasing NO bioavailability by oral administration of *L*-arginine substrate, required in the production of NO by endothelial nitric oxide synthase (eNOS) (section 1.6.2.2) saw improved revascularization, limb perfusion, capillary density and vasomotor function in rabbit hindlimb ischaemia models (Murohara et al., 1998).

When poorly regulated, mechanisms of angiogenesis may become contributing factors in development of malignancies, ischaemia, inflammatory, infectious and immune disorders. As an example, in ischaemic heart disease, angiogenesis may not be activated by normal means which may result in endothelial dysfunction, vessel malformation and prevention of revascularization, healing and regeneration (Carmeliet, 2005). Pro- and anti-angiogenic agents have become a focus of therapeutic design to promote revascularization in ischaemia and prevent vascular perfusion in cancers. Two anti-VEGF antibody therapies, Avastin (Genentech) in conjunction with conventional chemotherapy and monotherapeutic Sorafenib/Sutent (Bayer and Onyx/Pfizer) have demonstrated clinical benefit in cancer patients, targeting endothelial cells – in addition to oncogenic, stromal and haematopoietic cells (Carmeliet, 2005). The success of the monotherapy treatment suggests that a multi-targeting approach may be of benefit when designing anti-angiogenic therapies, including endothelial cells, mural and stromal cells, haematopoietic and neoplastic cells. The Endothelial Modulation in Angiogenic Therapy trial suggested a combination of intramyocardial VEGF and oral *L*-arginine may promote angiogenesis in patients with severe diffuse coronary artery disease, noting improved anterior

wall contractility and fewer perfusion defects post-coronary artery bypass graft (Ruel et al., 2008). Use of *L*-arginine as therapy for reperfusion of hypoxic lung has noted similar success, observing increased proliferation of endothelial cells of extra- and intra-acinar vessels leading to significant increases in vascular length accompanied by a reduction in resistance (Howell et al., 2009). These data suggest *L*-arginine might also serve as a treatment for pulmonary hypertension – and these are a few such examples where *L*-arginine therapy may prove efficacious in tandem with current treatments and surgeries.

1.2.2. Endothelial Dysfunction

Endothelial dysfunction (ED) describes endothelial cell function when impaired, typically characterised by reduced NO bioavailability (Dhananjayan et al., 2016; Carmeliet, 2005). ED can be caused by injury or intracellular damage which triggers compensatory mechanisms to regain a state of homeostasis. In endothelial dysfunction, the balance between release of NO and production of reactive oxygen species (ROS) in response to chemical or mechanical triggers is lost. Endothelial dysfunction is often observed in people at risk of developing T2DM and, can lead to insulin resistance which further aggravates their condition (Dhananjayan et al., 2016). The compensatory responses, such as exaggerated production of ROS, causing a reduction in NO bioavailability and the formation of peroxynitrate species, can lead to development and progression of cardiovascular co-morbidities, including accelerated atherosclerosis, coronary artery disease and hypertension (Cooke and Losordo, 2002).

1.2.3. Atherosclerosis

Atherosclerosis describes the process of plaque formation in arteries, which may result in further cardiovascular complications. The pathology of atherosclerosis is attributed as the main cause of death in the Western world (Mc Namara et al., 2019; Libby et al., 2019). Hypertension, hyperlipidaemia, obesity and diabetes are independent risk factors which contribute to the development of endothelial dysfunction, and subsequently for atherogenesis (Libby et al., 2019).

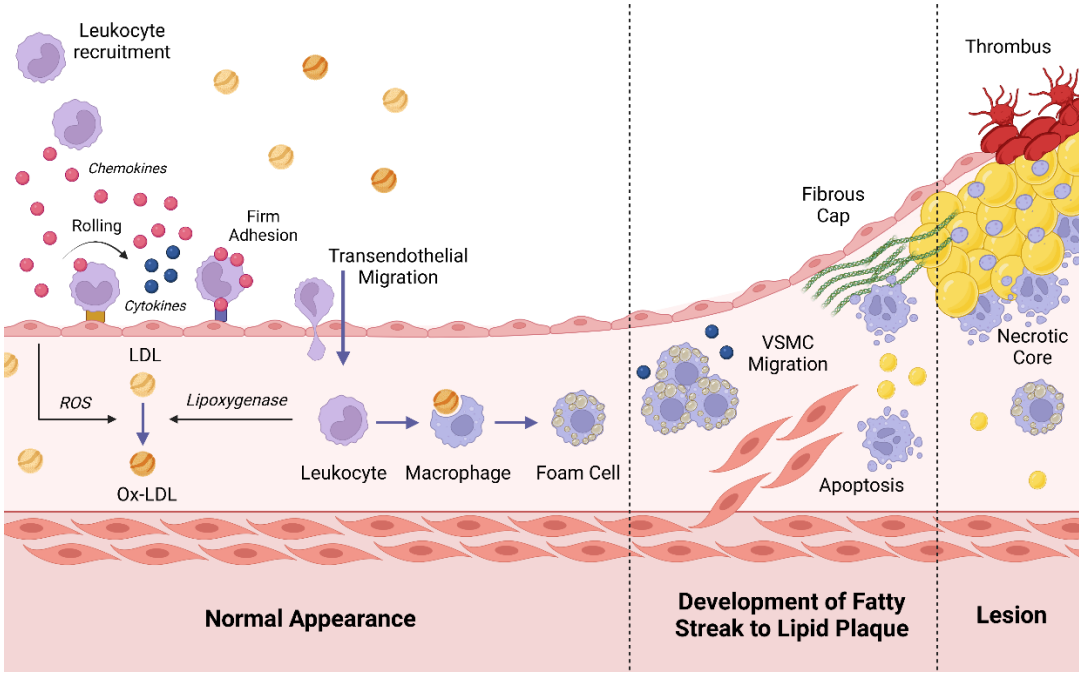

Figure 1-3: Development of Atherosclerotic Plaque

An overview of key mechanisms involved in the development and progression of atherosclerosis. Endothelial dysfunction can lead to lipid (LDL) infiltration in the intima, upregulation of expression of adhesion molecules and recruitment of leukocytes which adhere and transmigrate into the vessel wall. Oxidized-lipids (ox-LDL) are consumed by macrophages, resulting in formation of foam cells. Migration of vascular smooth muscle cells (VSMC), apoptosis of lipid-rich foam cells and accumulation of collagen-rich matrix proteins contribute to development of a necrotic core. The plaque can become destabilized and rupture, initiating platelet activation, resulting in thrombus formation. Image adapted from (Thayse et al., 2020) and created with BioRender.com.

Atherosclerosis frequently occurs at branch points in arteries; branching arteries are notably at risk as they are exposed to variable rates of blood flow.

The initial lesions in the intimal lining are caused by infiltration of cholesterol rich, low-density lipoproteins (LDL), accompanied by leukocytes and T-lymphocytes (Tavafi, 2013; Kume et al., 1992). Under normal conditions, the endothelium does not allow the adhesion of circulating leukocytes, prevented by endogenous NO (Kubes et al., 1991) however, dysfunctional endothelial cells become damaged by oxidative stress arising from an imbalance between NO and ROS, which further exaggerates ROS production through eNOS uncoupling and activation of nicotinamide adenine dinucleotide phosphate (NADPH) oxidases (Avogaro et al., 2006). ROS is involved in coordination of systemic oxidative stress and inflammation at these sites, enabling activation and recruitment of leukocyte adhesion molecules, including vascular cell adhesion molecule-1 (VCAM-1), to the plasma membrane which promotes endothelial cell permeability and leukocyte adhesion, respectively (Libby, 2002). The LDLs become oxidized by ROS originating from endothelial cells, to produce ox-LDL (Burke-Gaffney et al., 2002). Macrophages express cell-surface scavenger receptors, enabling absorption of available ox-LDL which transform into foam cells (Steinbrecher et al., 1984). LDLs and leukocytes accumulate in the vessel wall, due to an increase in vascular permeability – associated with endothelial dysfunction. Endothelial and vascular smooth muscle cells secrete cytokines and growth factors, such as interleukin-1 (IL-1) and tumour necrosis factor-α (TNFα), triggering the migration of VSMC into the luminal wall. Migration of VSMC, together with synthesis of extracellular matrix forms a fibrous cap, protecting the lesion from the lumen. The atherosclerotic lesions grow larger, until the accumulated macrophages and VSMC begin to necrose, releasing their high-lipid contents at the center of the plaque (Steinbrecher et al., 1984). The

development of atherosclerotic plaques causes a narrowing of the artery lumen which causes more regions of disturbed blood flow and subsequent endothelial cell damage in a vicious cycle of events. Unstable plaques can rupture and trigger luminal thrombosis *via* exposure of blood platelets and pro-coagulant factors, causing obstruction of vessels downstream (Tabas, 2017). Blockages of this kind prevent supply of oxygen to the heart and brain and may lead to myocardial infarction or ischaemic stroke (Ross, 1999; Fisher, 2016; Tabas, 2017).

1.3. An Introduction to Class II Receptor Tyrosine Kinases

Receptor Tyrosine Kinases (RTK) are a superfamily of proteins, existing in all multi-cellular organisms and involved in regulation of key cellular processes such as migration, metabolism, survival, proliferation and differentiation (Figure 1-4). RTKs are functionally distinct from other receptors by their activation of kinase subdomains, induced by binding of the cognate ligand to the ligand-binding region. Each RTK receptor is composed of an extracellular domain containing ligand-binding sites, a hydrophobic transmembrane domain and an intracellular domain containing the kinase sub-domain.

Class II RTKs specifically concerns the insulin receptor family: the insulin receptor (IR), insulin-like growth factor 1 receptor (IGF1R) and insulin receptor-related receptor (IRR). Agonists of both IR and IGF1R are naturally-occurring insulin and insulin-like growth factors 1 and 2 (IGF-1, IGF-2) – IRR however does not appear to be activated by either of these ligands (Zhang, B. and Roth, 1992; Jui et al., 1994). Activation of the insulin receptor by its cognate ligand triggers signalling cascades involving insulin receptor substrates (IRS), Cbl, Shc and STAT proteins (Hanke and Mann, 2009; De

Meyts, 2016). This thesis focusses upon IR and IGF1R, and a hybridized receptor species: the insulin receptor/insulin-like growth factor 1 receptor (IR/IGF1R) – and their effect on homeostasis in disease (Figure 1-4).

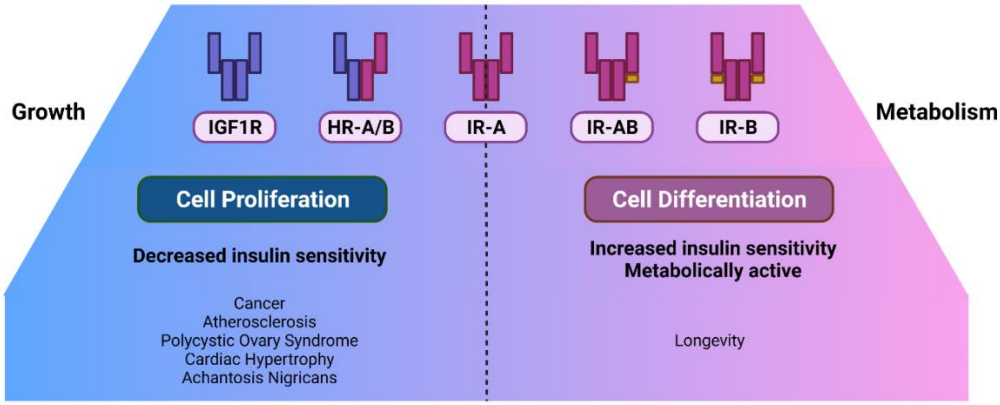

Figure 1-4: Diversification in signalling of Insulin Receptors, IGF1Rs and IR/IGF1R Hybrids

Metabolic and mitogenic signalling diversification of all isoforms of insulin receptor, IGF1R and their hybrid receptor species, including examples where overactivation of species to the left side, increasing IGF-signalling may result in development of disease, whereas restrained IGF-signalling and increased metabolic effect is observed in healthy patients. Image adapted from (Belfiore et al., 2009) and created with BioRender.com.

1.3.1. Insulin Receptor

The insulin receptor, the cognate receptor for the ligand insulin is a transmembrane tyrosine kinase where upon binding of insulin to its extracellular domain induces a conformational change in structure, stimulating tyrosine kinase phosphorylation in response, within the cell (Petruzzelli et al., 1982; Kasuga et al., 1982). Insulin-dependent activation may trigger the phosphorylation cascades of the phosphoinositide 3-kinase/Ak strain transforming protein (PI3K/Akt), mitogen-activated protein kinase/extracellular signal-related kinase (MAPK/Erk) and 5’ adenosine monophosphate-activated protein kinase (AMPK) pathways. More recently, it has also been discovered that IR may directly regulate gene transcription by

association with RNA polymerase II and Host Cell Factor 1 (Hancock et al., 2019).

These receptors functionally form a dimerized structure, composed of two identical monomer units – each containing an α- and β-subunit – linked by disulphide bonds (Schaffer and Ljungqvist, 1992; Sparrow et al., 1997). The subunits may be further characterized by their binding regions or protein domains. Each α-subunit is comprised of two leucine-rich regions (L1 and L2), a cysteine-rich (CR) region and two of the three fibronectin domains (FnI/II); the β subunit contains an extension of the fibronectin domain (FnII/III), a transmembrane (TM) domain, a juxtamembrane (JM) domain, the intracellular tyrosine kinase (TK) domain and the C-terminus (Figure 1-5) (Ullrich et al., 1985; De Meyts and Whittaker, 2002). Tyrosine kinase activity was assumed by Petruzzelli prior to confirmation by Kasuga and in fact, that the β subunit, containing the kinase domain was capable of autophosphorylation and able to interact with intracellular proteins as a consequence of its activation (Petruzzelli et al., 1982; Kasuga et al., 1982). Autophosphorylation sites were happened upon by chance when Ullrich and Ebina were cloning constructs of human IR; this gene was eventually isolated in 1989 and found to contain 22 exons (Ullrich et al., 1985; Ebina et al., 1985; Seino et al., 1989). An interesting aspect to elucidation of the IR gene sequence presented possibility for two alternately-spliced isoforms at exon 11, namely IR-A (Ex11-) and IR-B (Ex11+), where the latter contains an additional twelve amino acid-long sequence tagged onto the C-terminus (Ebina et al., 1985; Ullrich et al., 1985; Seino and Bell, 1989; Seino et al., 1989). Despite a seemingly inconsequential difference between isoforms, each possesses distinct binding affinities for ligands, kinase activity and intracellular transduction capability (Mosthaf et al.,

1990; McClain, 1991; Vogt et al., 1991; Kellerer et al., 1992; Yamaguchi, Y. et al., 1991). The most distinct functional difference between the insulin receptor isoforms relates to the high affinity of IR-A for IGF-2. As IR-A is predominantly expressed prenatally, signalling of IGF-2 is enhanced by this increase in cell sensitivity, encouraging embryogenesis and foetal development. It is also significantly expressed in adult tissues, notably in the brain. By contrast, IR-B is predominantly expressed in well-differentiated tissues, such as the liver, enhancing metabolic signalling *via* insulin (Belfiore et al., 2009).

Our understanding of the human insulin receptor IR structure is derived primarily from x-ray crystallographic and nuclear magnetic resonance (NMR) research of protein fragments (Hubbard et al., 1994; Hubbard, 1997; McKern et al., 2006; Menting et al., 2009; Cabail et al., 2015; Croll et al., 2016). The IR extracellular region or ‘ectodomain’ (ECD) garners most attention as it contains the binding sites for a variety of ligand species. This specific region of the protein was initially described by McKern and Lou, with an improved resolved crystal structure, in combination with molecular dynamics mapping, later provided by Croll in 2016 to 3.3 Å, demonstrating improved modelling *N*-linked glycans, fibronectin domains and the insert domain (Figure 1-5) (McKern et al., 2006; Lou et al., 2006; Croll et al., 2016). In the inactive state, the ECD forms an inverted ‘V’ shape, where the two leucine-rich and single cysteine-rich domains are folded over, maintained by the association of reciprocal L1 and FnII domains of the opposing subunits (One monomer shown in Figure 1-5) (McKern et al., 2006). This discovery contradicts the previous models showing the conformation of the receptor in a ‘T’ shape allowing binding of insulin the middle of the two ectodomain arms (De Meyts,

2004). However, there is good reason to suggest that the aforementioned conformation of McKern's x-ray crystal structure where the L1 domains are far apart would comply with evidence that the structural separation of these domains maintains the receptor in the inactive state; data from binding interactions also supports this model and are discussed in section 1.5.1 (Kavran et al., 2014).

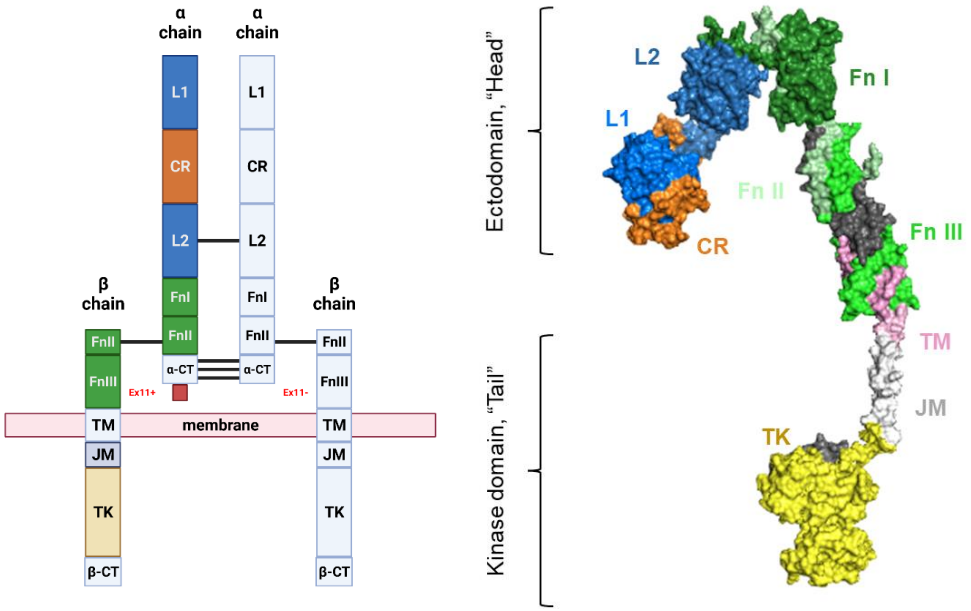

Figure 1-5: Structure of the Insulin Receptor

Left: Schematic of insulin receptor dimer modular structure of both α- and β-chains, comprised of leucine-rich (L1, L2, blue), cysteine-rich (CR, orange), fibronectin (FnI-III, green), transmembrane (TM), juxtamembrane (JM), tyrosine kinase (TK, yellow) domains and the inclusion of the additional 11-amino acid N-terminus tail for IR-A isoforms. Image adapted from (Scapin et al., 2018), created with BioRender.com. **Right:** Model of insulin receptor monomer combining x-ray diffraction and NMR solution PDB structures 4ZXB (Croll et al., 2016), 2MFR (Li, Q. et al., 2014)) and 1IRK (Hubbard et al., 1994) to produce a 'whole' receptor monomer structure, domains are colour-coded as shown in adjacent image. Model adapted from (Ye et al., 2017), created using PyMOL Molecular Graphics System, version 2.0 Schrödinger, LLC.

1.3.2. Insulin-like Growth Factor 1 Receptor

The IGF1R is the cognate ligand for both IGF-1 and IGF-2. Similarly to the insulin receptor, the IGF1R is also a dimerized, transmembrane tyrosine kinase however activation of this particular receptor transduces insulin-

receptor substrate-1 to activate cell growth and proliferation signalling pathways (Adams et al., 2000; Chitnis et al., 2008). As a consequence, IGF1R are expressed by most organs and tissues – notably abundant in embryo and the brain, and in minute levels in the liver due to downregulation of hepatic IGF-1. IGF1R research predominantly centres around their involvement, or lack thereof, in many human cancers and growth disorders, such as microcephaly or Beckwith-Wiedemann syndrome (BWS) (Chen and Sharon, 2013; Juanes et al., 2015; Gkourogianni et al., 2020; Giabicani et al., 2019).

IGF1R and IR have high structural similarities, possessing the same domain-centric formation and sharing 57% sequence identity (Section 1.3.1, Figure 1-5) (Kasuga et al., 1981; Chernausek et al., 1981; Massagué and Czech, 1982; Bhaumick et al., 1981; Kull et al., 1983). The majority of structural differences lie within the ectodomain region, governing ligand specificity of each receptor (Lou et al., 2006). The genes of the insulin receptor and IGF1R also share similar genomic organisation. While the *Ir* gene is composed of 22 exons, including the possibility for alternative splicing upon exon-11, IGF1R is composed of 21 exons but does not possess this same splicing ability which results in a single isoform of the receptor (Rosenfeld and Roberts, 1999). The apo structure of the IGF1R ectodomain was also deduced to form an inverted ‘V’-shaped dimer (Garrett et al., 1998; Xu et al., 2018).

1.3.3. Insulin Receptor/Insulin-like Growth Factor 1 Receptor Hybrids

The existence of hybrid receptors was first proposed by Kasuga in 1983 and confirmed before the turn of the new decade by Soos and Siddle, a highly homologous species of receptor which demonstrated high affinity for IGF-1 and showing immunoreactivity with insulin receptor-specific antibodies

(Kasuga et al., 1983; Soos and Siddle, 1989). Since their discovery, evidence has suggested IR/IGF1R hybrid receptors may be distributed across most cells and tissues, though notably present in EC and VSMC (Nitert et al., 2005; Chisalita and Arnqvist, 2005; Gomez-Hernandez et al., 2013). As referenced in section 1.3.2, the insulin receptor and IGF1R share a high degree of structural similarity and as a consequence, may form these functional heterodimers in place of their homodimer counterpart (Belfiore et al., 2009). More precisely, two types of hybrid receptors may form. Due to the inherent splicing ability of insulin receptors, hybrid receptor isoforms A (IR-A/IGF1R or HR-A) and B (IR-B/IGF1R or HR-B) may be produced – each possessing distinct properties as observed for the insulin homoreceptor isoforms. Heterodimerization is believed to occur by comparable efficiency to homodimerization; the proportion of hybrid receptors is believed to be dependent on the relative abundance of ‘free’ receptor monomers (Bailyes et al., 1997; Pandini et al., 1999) however modulation by proportion in availability of ligands or other biological factors may also be contributing factors. Several sources have reported a reduction in IR expression in human patients and animal models with diabetes, though not shown in endothelial cells, it is assumed the same behaviour would occur (Tiwari et al., 2007; Ojamaa et al., 1988; Chiefari et al., 2011).

The structural composition of hybrid receptors allows for interaction with all three cognate ligands: insulin, IGF-1 and IGF-2. It may be viewed that only ‘half’ of the available binding sites are now present in these species. It is no surprise therefore, that one might expect a high abundance of hybrid receptors populating cell membranes would result in a loss of signalling *via* either insulin or IGF cascades. From numerous observations, affinities for IGFs have been

demonstrated as considerably higher than those for insulin, described by Benyouncef as comparable to their interactions with the IGF1R (Slaaby et al., 2006; Benyoucef et al., 2007; Pandini et al., 2002). Furthermore, their differing affinities appear to have functional consequences; IGF-1 has been shown to functionally activate IR/IGF1R hybrids at low concentrations, whereas insulin did not (Nitert et al., 2005; Li, G. et al., 2005). This invokes some interesting considerations regarding interactions with these ligands: would harmonic oscillation theory still be regarded as an appropriate mechanism to describe ligand binding to this species – or open the door to new theoretical models for both homo- and heterodimer receptors – and, how correlation between loss of affinity for insulin, but not insulin-like growth factors, could be attributed to this new structural arrangement.

A higher abundance of hybrid receptors has been observed in many cancers and T2DM. In over 75% of human breast cancer specimens, hybrid receptors exceeded native IGF1R levels (Pandini et al., 1999). It was further observed that these receptors were readily activated by IGF-1, but not insulin – and in fact, most of the IGF-1-mediated effect was due to hybrid receptor activation. This was similarly noted in human thyroid cancer tissue and cell line samples, where higher levels of IR, IGF1R and hybrids were present and overstimulation of the IGF-1 system resulted from high affinity interactions of IGF1R and hybrids with this ligand (Belfiore et al., 1999). In prostate cancer cells, IGF1R was selectively upregulated by androgen and oestrogen receptors, favouring the formation of hybrid receptors (Pandini et al., 2007a; Pandini et al., 2005). All studies highlight the importance of the hybrid receptor’s role in mitogenic signalling. Therapies targeting the IGF1R have been shown to have a simultaneous effect on hybrid receptor population.

Pandini *et al.* evaluated the h7C10 human monoclonal antibody (mAb), an anti-tumoural growth inhibitor of the IGF1R (Pandini et al., 2007b). They noted that both IGF1R and hybrid receptors were downregulated with long-term use of h7C10, independent of ligand concentration. The anti-tumoural effect of h7C10 was distinctly more potent than mAbs targeting specifically IGF1R or hybrids alone, leading to consideration of dual-action antibody therapeutics in clinical settings. However, studies by Zhang and Fulzele in human breast cancer, MDA-435 and osteoblast cells demonstrated some adverse side effects of targeting IGF1R expression (Zhang, H. et al., 2007; Fulzele et al., 2007). Reduction of available IGF1R monomers, by an siRNA knockdown, resulted in fewer hybrid species being formed and so less IR were sequestered in formation of these receptors. They reported an increase in IRS-1, Erk/Akt activation, proliferation and glucose uptake in response to insulin – suggesting insulin sensitivity was increased. In addition, upregulation of genes downstream of the Erk pathway, including *Glut-1* and genes involved in angiogenesis, such as *Vegf* and *iNos*, were observed. Insulin signalling must be carefully balanced; enhanced IR signalling may contribute to IGF1R therapy resistance and result in selection of cancer cell clones with activated IR-A. In the case of diabetes, due to the hybrid receptor's intrinsic preference for binding IGFs over insulin, insulin sensitivity is lost across the plasma membrane, which is particularly devastating in cells of insulin-action (Federici et al., 1996). Development of insulin resistance may occur prior to onset diabetes and obesity; it is characteristically associated with further progression of the disease. Fernandez *et al.* noted the development of insulin resistance when overexpressing the IGF1R, as the available IR became sequestered into newly forming hybrid receptors (Fernandez et al., 2001) –

and has been observed in many diabetic tissues including pre-adipocytes, adipose tissue and skeletal muscle (Back and Arnqvist, 2009; Federici et al., 1996; Federici et al., 1997a; Federici et al., 1997b; Federici et al., 1998). The most interesting aspect to this phenomenon is that the stimulus driving formation of hybrids over their homodimeric counterparts is still unknown, as is the physiological role of these. Spampinato *et al.* contemplated the enigma of how hybrid receptor-related insulin resistance might occur: as a result of pre-existing high levels of hybrid receptors or, that the overexpression of hybrid receptors may result from pre-existing insulin resistant states (Spampinato et al., 2000). Obtaining reliable data through many traditional assays proves difficult; studies are complicated by the variable expression of IR and IGF1R moieties and differences in regulation of receptors through degradation and recycling in different cells and tissues, and further by a lack of specific antibodies recognizing hybrid receptors (Yamaguchi, Y et al., 1993; Soos et al., 1993; Soos et al., 1990). Elucidation of this information and development of high specificity assays will prove most valuable in hybrid receptor research.

Research by the Kearney group has focused on the effects of obesity on hybrid formation. Most recently, Mughal *et al.* determined levels of hybrid expression in a murine obesity-induced model of diabetes, distinguishing groups by high- or low-fat feeding regimens (Mughal et al., 2019). They observed a sustained increase in hybrid formation in the high-fat feeding group from short-term (5-weeks) to longer-term (16-weeks) from 30% to 60%, compared with the low-fat feeding group. An opportunity to design and evaluate a novel therapy targeting reduction of hybrid formation, with the

purpose of restoring native IR:IGF1R balance as a side effect of this modulatory action, became apparent.

1.4. The Cognate Ligands to Class II Receptor Tyrosine Kinases

The human insulin superfamily is comprised of ten members: insulin, IGF-1 and IGF-2, and seven peptides related to relaxin (RLF) (Chan, S.J. and Steiner, 2000; Conlon, 2001; Steiner et al., 1985; Hsu, 2003; Hsu et al., 2003). Insulin and the IGFs bind RTKs; relaxin-like peptides appear to bind leucine-rich repeat-containing G protein coupled receptors (GPCRs), and as such RLFs will not be further discussed in this thesis hereafter (Hsu, 2003).

Proteins of this family share a high degree of structural similarities. They are synthesized as prepro-proteins, consisting of four domains: pre, B, C and A. Proteolytical cleavage of the pre-domain, and in some circumstances the C-domain, and subsequent folding of the remaining components produces the mature form of the protein. IGF precursors also possess additional C-terminus D and E peptides, where the latter is also proteolytically removed post translation (De Meyts et al., 2013). This structural relationship enables interesting cross-interaction between receptors and ligands (Table 1-1).

Receptor	**Homodimers**			**Heterodimers**		
	IR-B	IR-A	IGF1R	IR-AB	HR-B	HR-A
	IR-B/IR-B	*IR-A/IR-A*	*IGF1R/IGF1R*	*IR-B/IR-A*	*IR-B/IGF1R*	*IR-A/IGF1R*
Ligand	Insulin	Insulin	IGF-1	Insulin	IGF-1	IGF-1
		IGF-2	IGF-2	IGF-2	IGF-2	IGF-2
						Insulin

Table 1-1: Receptors and Their Interacting Ligands

Binding preference of insulin receptors (IR-A/IR-B), insulin-like growth factor 1 receptors (IGF1R) and hybrid receptors (HR-A/HR-B) for insulin and insulin-like growth factors 1 and 2, in descending order. Adapted from (Belfiore et al., 2009).

1.4.1. Insulin

The hormone, insulin is secreted by β-cells within the islets of Langerhans. The role of insulin provides regulation of metabolism, by promotion of cellular uptake of glucose and amino acids, particularly in locations requiring either rapid energy release (muscle cells) or for storage (adipose cells). Glucose homeostasis regulated by insulin promotes glucose transport into these cells by translocation of glucose transporter 4 (GLUT-4), *via* the PI3K/Akt pathway. Downstream of the insulin receptor, phosphorylation of phosphatidylinositol 4,5-biphosphate (PIP_2) by PI3K, activates Akt and generates increased levels of intracellular phosphatidylinositol 3,4,5-triphosphate (PIP_3) at the plasma membrane. Akt stimulates this migration through phosphorylation of Akt substrate 160 kDa (AS160) (Alessi et al., 1996). In addition to this mechanism of activation, insulin provides an anabolic role in stimulation of glycogenesis, fatty acid and protein syntheses, and inhibition of gluconeogenesis in liver cells.

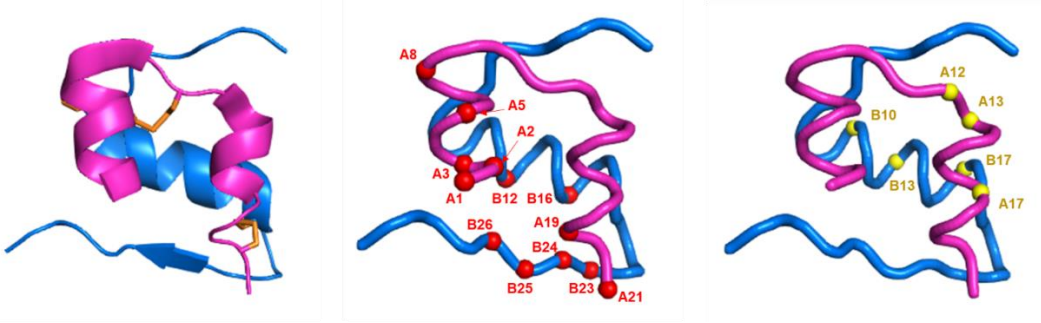

Figure 1-6: Classical and Hexamer Binding Sites of Insulin

Left: Insulin A- and B-chains (pink and blue, respectively) showing disulphide linkages between cysteine residues (orange). **Center:** Classical (dimerization) site of insulin, involved residues are shown in red. **Right:** Hexamerisation site of insulin, involved residues are shown in yellow. Model produced using x-ray diffraction PDB structure 4INS (Baker et al., 1988). Image adapted from (Ward et al., 2013), created using PyMOL Molecular Graphics System, version 2.0 Schrödinger, LLC.

Insulin is composed of two polypeptide chains (A and B) containing 21 and 30 amino acid residues respectively joined by two inter-chain disulphide bonds (Figure 1-6.A), and is produced by cleavage of single-chain proinsulin (Steiner et al., 1967; Steiner and Oyer, 1967). Numerous studies have investigated the structure and flexibility to gain insight into the structural basis for its function and aggregation properties (Blundell, T. et al., 1972; Chothia et al., 1983; Baker et al., 1988; Hua et al., 1991; Jorgensen et al., 1992; Jorgensen et al., 1996). Insulin may form a dimer with a second insulin protein and in the presence of Zn^{2+} and at neutral pH, may also form a hexamer (Scott and Fisher, 1938). The hexameric insulin complex may transition between three different conformations, designated T_6, T_3R_3 and R_6, relating to their symmetry groups (Kaarsholm et al., 1990). Each state is composed of a trimer of dimers, arranged with point group 32 symmetry (Figure 1-7.B). The structure was initially thought to possess a single binding site, it's "classical" binding site, however a secondary site was located opposite this site, enabling hexamerisation (Figure 1-6.B/C) (Blundell, T. et al., 1972; Baker et al., 1988).

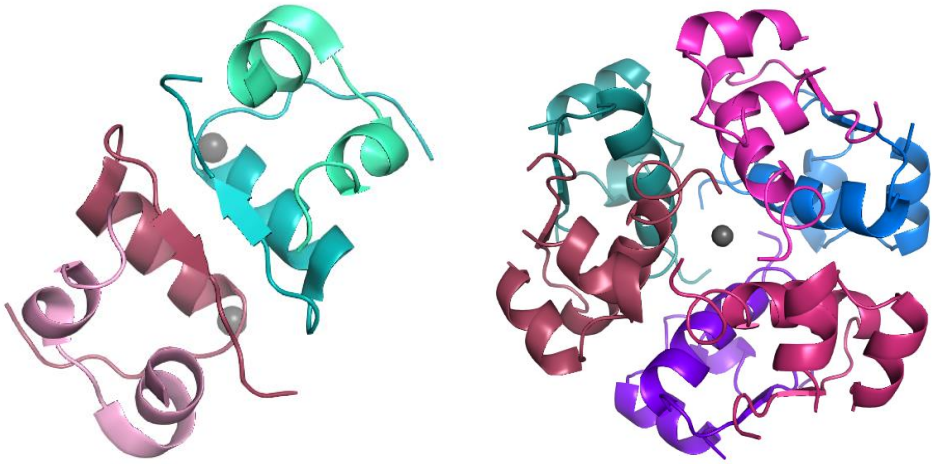

Figure 1-7: Insulin in Dimer and Hexamer Conformations

Left: Insulin dimer, formed by hydrogen bonding between residues at the junction between anti-parallel β-sheets of each distinct protein (1-turquoise, 1-mauve). Model produced using x-ray diffraction PDB structure 4INS (Baker et al., 1988). **Right:** Insulin hexamer, formed by histidine co-ordination to two zinc ions (center, grey) to three insulin dimers (pink and blue colour variations for each pair). Model produced using NMR solution PDB structure 3AIY (O'Donoghue et al., 2000) and manual insertion of zinc ions. Both models created using PyMOL Molecular Graphics System, version 2.0 Schrödinger, LLC.

Schaffer discovered the hexamer-forming site by use of insulin analogues containing two mutations at A13L and B17L – located opposite the dimerization site (Schaffer, 1994). While only the monomer form of insulin is biologically active, dimerization and hexamerisation of insulin provides greater stability. Dimeric association is driven by the formation of four hydrogen bonds of residues Tyr24-Phe25-Phe26 at the junction between the anti-parallel β-sheets of each insulin monomer. Zoete *et al.* determined the free energy of dimerized insulin to be -11.9 kcal mol^{-1} (Zoete et al., 2005). Insulin dimers may be further stabilized as a hexamerized conformer, where BHis10 of each monomer may become coordinated to two Zn^{2+} ions (Hill et al., 1990). Carpenter and Wilcox demonstrated that hexamer formation further improves the total free energy change to -26 kcal mol^{-1} (Carpenter and Wilcox, 2014). Hexamerisation of insulin allows for better storage in the β-cells of the pancreas, but has also been shown to prevent aggregation which is a major

contributor in other diseases such as Alzheimer's and Parkinson's disease (Lisi et al., 2014; Chiti and Dobson, 2006; Thirumalai et al., 2012).

1.4.1.1. Insulin Analogues

Insulin analogues are orthosteric variants of the native insulin protein, mimicking physiological insulin action as a clinical therapy for diabetic patients (Vajo et al., 2001; Hirsch and Vega, 2005). The use of insulin analogues has far surpassed synthetic human insulins, notably in the US, where the use of improved glycaemic controls agents have completely swapped: in 2000, 96% of insulin users were prescribed human insulins *vs*. 19% analogues; by 2010, 15% were still using human insulin, while 92% were using analogue products (Lipska et al., 2014). The reason for this progression is tied to the potential for modulation of pharmacokinetic and/or pharmacodynamic properties of these analogue structures and therefore, demonstrate more efficacious results in patients. In the 1990's, long-acting and rapid-acting analogues were introduced. The beauty of these time-sensitive release products allows for improved personalized care regimes for the level of treatment required. Of the rapid-acting analogues products, the three most popular products are Aspart (Novolog, Novo Nordisk), Glulisine (Apidra, Sanofi-Aventis) and Lispro (Humalog, Eli Lilly). Each possesses one or multiple residue substitutions of the native human insulin amino acid sequence: Aspart, Pro at B28 is changed for Asp; Glulisine, Asn at B3 to Lys and Lys at B29 to Glu and; Lispro, inversion of Pro B28 and Lys B29 residues (Figure 1-8) (PubChem, 2021d; PubChem, 2021b; PubChem, 2021a). All are provided in the form of subcutaneous injection and continuous subcutaneous insulin infusion (CSII) devices, allowing for quick absorption into the bloodstream – showing activity within

5-to-15 minutes, peaking at 60-120 minutes and completely diminished after 4 hours. These properties are aligned for use as basal insulin replacement, in addition to prandial insulin replacement and high glucose correction. In comparison with human insulin, which is typically administered 30 minutes prior to eating, the analogues are more quickly absorbed resulting in higher peaks and shorter durations of action which reduces the risk of late postprandial hypoglycaemia and early postprandial hyperglycaemia (Sperling et al., 2014). Long-acting products, such as insulin detemir (Levemir®, Novo Nordisk) and insulin glargine (Lantus®, Sanofi-Aventis) are similarly structured as the rapid-acting analogues: detemir, myristic acid is bound to Lys at B29 and B30 Thr is deleted from sequence; glargine, Asn at A21 substituted for Gly and two Arg residues are added to the C-terminus of B-chain (B31, B32) (Figure 1-8) (PubChem, 2021c; PubChem, 2021e). These insulins provide relatively constant levels of insulin over a 12-to-24-hour period, reaching an active level after 60-90 minutes. The mode of action of these is particularly interesting. Insulin detemir possesses a fatty acid side chain as part of its structure, promoting the formation of hexamers and reversible binding with albumin – producing the ‘free’ and active detemir protein slowly over a 24-hour period (Waller and Sampson, 2018; Phillips and Scheen, 2006; Havelund et al., 2004). Insulin glargine is far less soluble at physiological pH than human insulin – addition of Arg and substitution of Gly increases the isoelectric point from pH 5.4 to neutral. Therefore, upon subcutaneous injection of an acidic solution, insulin glargine becomes crystalline – forming microprecipitates where individual units are slowly released into blood circulation over a 24-hour period (Furman, 2017; Atkinson, 2016). As such, these analogues are highly suitable as basal insulin

replacement therapies. Pre-mixed insulin, combining both fast- and long-acting or short- and intermediate-acting products are also available, improving ease of use and reducing frequency of administration for the user.

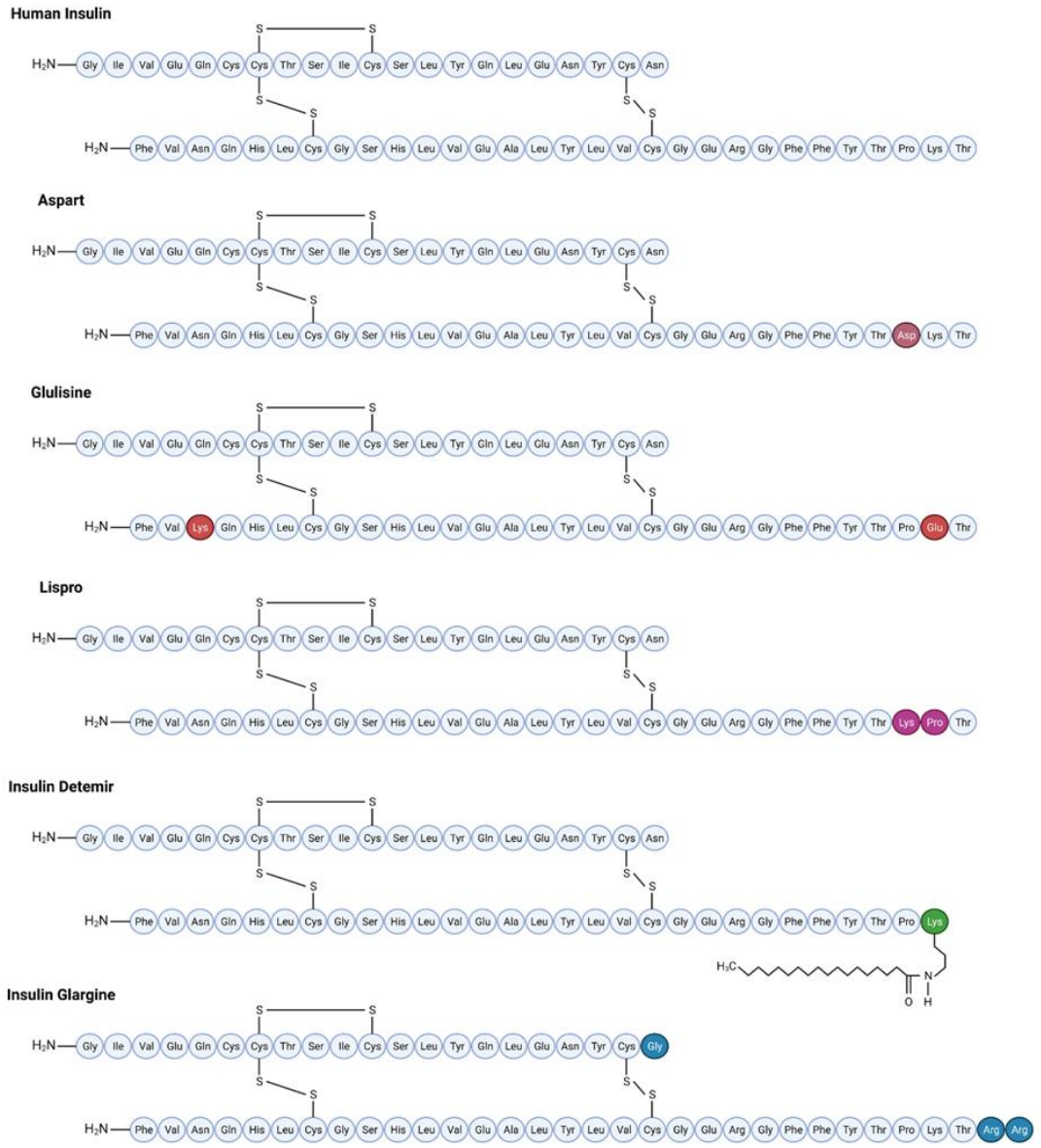

Figure 1-8: Insulin, and its Rapid- and Long-Acting Analogues

Schematic of insulin and analogues: Aspart, Glulisine, Lispro, insulin detemir and insulin glargine, amino acid sequences and disulphide linkages of A- and B-chains. Changes from original insulin residues are shown in colour for each structure. Image adapted from (Agin et al., 2007) and created with BioRender.com.

1.4.2. Insulin-like Growth Factors 1 and 2

Hormones, IGF-1 and IGF-2, sometimes named somatomedins 1 and 2 are involved in several biological activities such as proliferation, mitochondrial protection (Perez et al., 2008), cell survival (Vincent and Feldman, 2002), tissue growth and development (Powell-Braxton et al., 1993; Fowden and Forhead, 2013; Lee, O.H. et al., 2000), anti-inflammatory and antioxidant (Garcia-Fernandez et al., 2003; Garcia-Fernandez et al., 2005), antifibrogenic (Muguerza et al., 2001) and anti-aging (Puche et al., 2008; Garcia-Fernandez et al., 2008).

The IGF-1 and IGF-2 are the cognate ligands for IGF1R and insulin-like growth factor 2 receptor/mannose-6-phosphate receptor (IGF2R/M6PR), though they have also been shown to activate insulin receptors with varying affinities (Massagué and Czech, 1982; Denley et al., 2003). Unlike the IGF1R, IGF2R does not possess any signalling transduction ability, it instead provides cell surface regulation of circulating IGF-2, resulting in degradation of the growth factor (Massagué and Czech, 1982). Insulin and the IGFs share structural and functional similarities; IGFs are composed of a single peptide chain containing four distinct regions (domains A-D), bridged by two inter-domain disulphide bonds and one internal disulphide bond in the A domain. IGF-1 is comprised of 70-amino acids, whereas IGF-2 has 67 (Figure 1-9). IGF-1 shares high sequence identity with human insulin (45-52%) and 67% similarity with IGF-2: in IGF-1, positions 1 through 29 are homologous to insulin B chain and positions 42 to 62 are homologous to insulin A chain (Rinderknecht and Humbel, 1978; Le Roith, 1997). This structural similarity explains how IGFs are able to bind to insulin targets. What is perhaps most

interesting about IGF structure is the inherent design to limit higher affinity binding with the insulin receptor, at the expense of maximizing binding to its cognate receptor. Nature has elected to design a single chain peptide to limit affinity of these species for the insulin receptor. Tseng *et al.* produced a two-chain molecule of IGF-1 A- and B-domains and demonstrated only 10-15% potency for its cognate receptor due to this region (Tseng et al., 1987). Replacement of the IGF-1 C-domain (residues 28-37) with a four-residue glycine bridge displayed a thirty-fold reduction in affinity for the IGF1R – highlighting real importance of this domain in IGF-1 action (Bayne et al., 1989). Bayne *et al.* also deduced that absence of the D-domain had little effect on IGF receptor binding yet increased two-fold for the insulin receptor – also in agreement with Blundell and King who showed that inclusion of the D-region sterically hindered binding to IR (Bayne et al., 1988; Blundell, T.L. et al., 1978; King et al., 1982).

Unlike insulin, IGFs are unable to form dimers. Though the amino acid content of their A- and B-domains are alike, the ordering of this sequence has a large part to play on their inability to self-associate: for insulin, (B23)GFFYTPKT(B30) and IGF-1, (22)GFYFNKPT(29). The inversion of Phe ↔ Tyr residues has minimal effect on receptor affinity or self-association of peptides (Mirmira and Tager, 1991; Shoelson et al., 1992), however the Pro ↔ Lys exchange, while similarly has little effect on binding affinity, appears to dramatically reduce IGF-1 dimerization (DiMarchi et al., 1992). Hexamerisation is largely dependent on coordination to zinc ions. In insulin, histidine imidazole rings are able to coordinate to two zinc ions, forming a nucleus for hexamer formation (section 1.4.1, Figure 1-7). The corresponding residues for IGF-1 are glutamic acids and are unable to chelate zinc, thus

cannot form hexamers in this manner. Instead, they are protected by six different insulin-like growth factor binding proteins (IGFBP I-VI) (Rosenfeld et al., 1999). Binding of these proteins to IGFs have been shown to interact with distinct domains, differing to those involved in binding interactions with receptors – loss of domains C and D did not appear to affect affinity to the former (Cascieri et al., 1988a; Bayne et al., 1988; Cascieri et al., 1989a). These IGFBPs also determine cellular bioavailability, activity and tissue distribution of IGF ligands (Firth and Baxter, 2002).

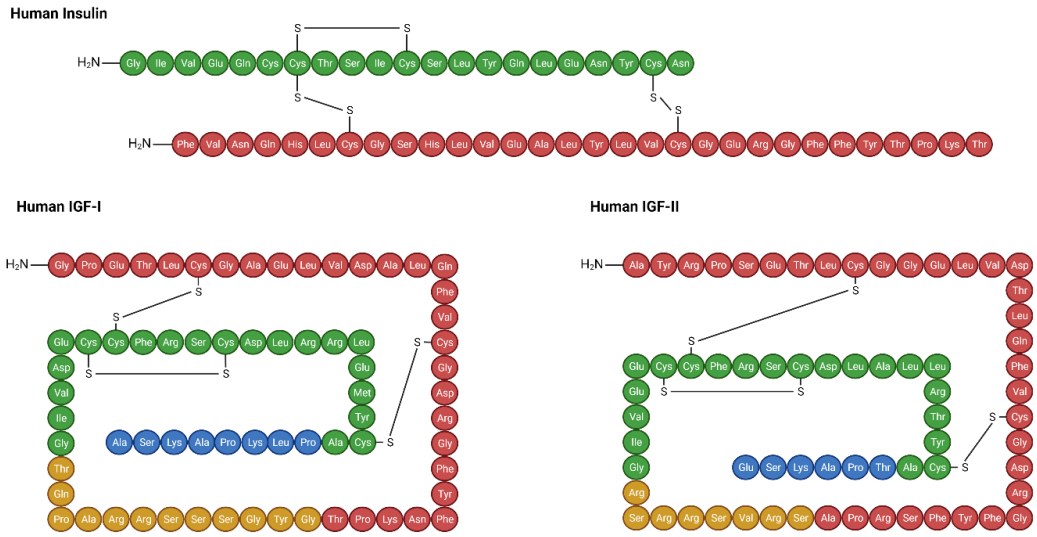

Figure 1-9: Structure of Insulin-like Growth Factors 1 and 2

Schematic of insulin and insulin-like growth factors 1 and 2 amino acid sequences and cysteine disulphide linkages between A- (green), B- (red), C- (yellow) and D-domains (blue). Image of own design, created with BioRender.com.

The main difference between the two ligands lies with their biological activities. IGF-2 is expressed primarily in early embryonic and foetal life such as the placenta; IGF-1 is produced in adult tissues, predominantly in the liver (Laron, 2001; Rinderknecht and Humbel, 1978; Le Roith, 1997; Ohlsson et al., 2009). Post-birth, secretion of IGF-1 is stimulated by growth hormone (GH), resulting in the formation of the GH/IGF-1 axis where GH secretion is activated by growth hormone-releasing hormone (GHRH) and inhibited by somatostatin

(Puche and Castilla Cortazar, 2012). The GH/IGF-1 axis is regulated by IGF-1 itself, inhibiting the *GH1* gene by stimulating expression of somatostatin (Bertherat et al., 1995). Circulating GH exists in both free and complexed states with the growth hormone binding protein (GHBP) enabling activation of hepatic GH receptor and promoting IGF-1 production. IGF-1 is released into circulation and its half-life is enhanced by interacting with IGFBPs, specifically IGFBP-III (90%). Some IGFBPs bind the growth factors with greater affinity than their cognate receptors, preventing activation of these intracellular pathways. Proteases or phosphorylation of IGFBP III, as an example, may reduce affinity of these proteins for IGF-1 allowing the ligand to return to its free, biologically-active state and enter target tissues, assisted by other IGFBPs (Jones and Clemmons, 1995; Ohlsson et al., 2009). Unlike IGF-1, IGF-2 is predominantly synthesized by tissues independently of GH, though some evidence suggests the *Igf2* gene may also be regulated by GH in a promoter-specific manner (Humbel, 1990; Livingstone, 2013; van Horn et al., 2002).

1.5. Protein-Protein Interactions of Class II Receptor Tyrosine Kinases

The insulin receptor, IGF1R and their hybrid receptor are activated with varying affinities through interactions with insulin and insulin-like growth factors (Appendix 20.1, Table 20-1,Table 20-2). Binding sites for these ligands are located in the ECD ‘head’ portion of the receptor, it is also the region of the protein where the highest degree of heterogeneity is present between the homologous receptors. These variances are designed to enable preferential binding of one substrate over another. Changes in structural conformation

enables activation of intracellular tyrosine kinase domains, triggering downstream phosphorylation signalling cascades. This structural rearrangement may also serve to impede certain types of interactions. Both the insulin receptor and the IGF1R display cooperativity characteristics that promote engagement of these ligands, it is interesting to speculate whether these behaviours might also be observed for the IR/IGF1R hybrid receptor species.

1.5.1. The Insulin Receptor and Insulin

The insulin receptor is primed with two distinct binding locations upon each receptor monomer, binding sites 1 and 2 upon the first, and 1’ and 2’ on the opposing structure. Site 1 is composed of one L1 subunit and residues from the α-CT’ helix of the other subunit; site 2 is comprised of residues on FnI’ and FnII’ (Williams et al., 1995; Mynarcik et al., 1997; Whittaker, J. et al., 2001; Whittaker, L. et al., 2008). Specific residues within these regions have been highlighted in studies as particularly pertinent to ligand binding. Schumacher et al. prepared chimeric receptor structures combining domains from both IR and IGF1R (Schumacher et al., 1991; Schumacher et al., 1993). Residue regions 1-137 of L1 and 325-524 of L2/FnI were isolated as important in binding, from these particular studies. In a similar study by Zhang and Roth, chimeras of the aforementioned receptors and IRR were cut together, upon switching the region of 450-601 amino acids (a.a.) on IR with the sequence from IRR saw a reduction in binding affinity for insulin, proving its involvement in receptor binding interactions (Zhang, B. and Roth, 1991). Menting has published structures of insulin complexed with the IR L1-CR domain and an exogenous α-CT peptide respectively, and was able to confirm that all three

structural elements were required to constitute the primary binding site of the IR (Menting et al., 2013; Menting et al., 2014). Upon engagement of insulin to site 1, both the substrate and α-CT undergo substantial conformational changes (Menting et al., 2014). Schaffer produced a series of insulin analogues, where residues A13 and B17 were shown to possess anomalous binding properties (Schaffer, 1994). Both of these amino acids are located on the hexamer-forming surface of insulin, he hypothesized that this site might also be highly important in interactions with receptors; this was corroborated by recent data from Gutmann *et al*. (Gutmann et al., 2020). De Meyts proposed that a single insulin might be able to form a cross-link between site 1 and site 2' – provided they were in anti-parallel symmetry – which would also explain the 1:2 stoichiometry of receptor/substrate ratio and curvilinear Scatchard plot (De Meyts, 1994). Menting also backed the hypothesis of De Meyts. Engagement of a second insulin could bridge across the remaining two sites, upon partial dissociation of the first, but would prevent re-binding and accelerate dissociation of the first. This anti-parallel relationship is also concurrent with crystallographic data from both Tulloch and McKern (Tulloch et al., 1999; McKern et al., 2006).

Advancements in electron microscopy (EM) have provided increasingly comparable resolved protein structures, and in the words of Dr. Muench, "EM structures are moving towards the gold standard of resolution that only crystallographers could obtain" (Muench, 2020). And this has certainly been the case for Gutmann *et al.*, revolutionizing IR structural biology by presenting single-particle EM structures of both insulin-activated and inactive glycosylated, full-length insulin receptors housed within lipid nanodiscs (Gutmann et al., 2018). Prior to this publication, no full-length structure had

been reported in the literature and one of the most interesting aspects was their apparent ability to produce snapshots of receptor conformation both with, and without, insulin: inactivated IR adopted a symmetric Λ-shaped conformation which was concurrent with atomic distance dimensions and the general predicted structure from current sources (Tulloch et al., 1999; McKern et al., 2006; Croll et al., 2016). And perhaps the main finding, was through activation with insulin, IR converts to a T-shaped conformation – drawing the transmembrane fibronectin domains together then enabling autophosphorylation between the TK groups. A main drawback to this technique of protein capture is the introduction of artificial constraint induced by housing monomer units within a confined space and therefore could force an interaction or distortion of conformational structure which would not otherwise be seen in nature. Scapin *et al.* reaffirmed Gutmann's results of the Λ conversion to T-shaped structure, by cryogenic EM of the IR-ECD (Scapin et al., 2018). Site 2 (2') may be important in stabilizing this conformation, by acting as a molecular wedge to prevent L1 folding back to its original orientation, as well as being the location for establishing initial ligand-receptor contact (Gutmann et al., 2020; De Meyts, 2004; Xu et al., 2018).

Specific regions upon both the insulin receptor and IGF-1 may have been designed in nature to prevent interactions between the pair. Bayne *et al.* produced chimera structures of insulin and IGF-1, where exchange of 15Gln-16Phe of IGF-1 for (B16)Tyr-(B17)Leu of insulin resulted in a five- to tenfold increase in affinity of the IGF-1 chimera for IR, without affecting its affinity for its cognate receptor, IGF1R (Bayne et al., 1988). Hoyne *et al.* have hypothesized that a large mobile loop on the CR region, residues 255-263, may have been incorporated into the receptor structure as a means to exclude

IGF-1 from the binding site – while allowing the smaller insulin protein to bind to this location (Hoyne et al., 2000).

1.5.1.1. Negative Cooperativity

Negative cooperativity is an intrinsic property of IR and functions independently of interactions with other proteins or messengers. Scatchard plots for this interaction are curvilinear, which is in line with models containing two distinct binding sites of high- and low-affinities, where upon binding of the first insulin protein to the high-affinity site may enable a second to bind at the low-affinity site (Schaffer, 1994). However this is not observed in practice, kinetics studies determined that the affinity for the receptor would decrease as it became occupied by a first ligand (Ginsberg et al., 1976; Wang, C.-C. et al., 1988; Pang and Shafer, 1983; Pang et al., 1984). In addition, dissociation studies highlight that the rate of dissociation of the prebound ligand may be accelerated by the presence of an unlabelled ligand (De Meyts et al., 1973; De Meyts et al., 1978; De Meyts et al., 1976). These data imply that acceptance of two fully-bound ligands upon the receptor surface would be highly unlikely. Dose-response curves for this accelerated dissociation are bell-shaped and indicative of self-antagonism, observing a slowing in acceleration at concentrations of insulin exceeding 100 nM. Each of these observations were indicative of negative cooperativity behaviour.

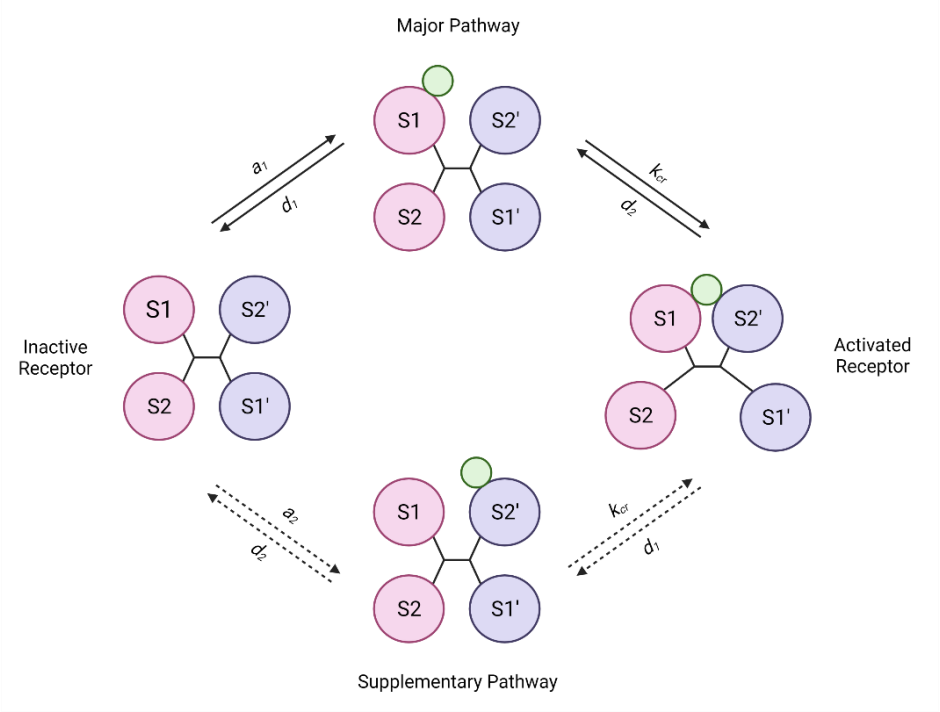

Figure 1-10: Harmonic Oscillator Theory

Simplified reaction scheme of the harmonic oscillator model of insulin receptor binding kinetics. S1 and S2 represents binding sites 1 and 2 (pink, purple), demonstrating activation of the receptor upon binding of insulin (green) to form a cross-link. Image adapted from (Kiselyov et al., 2009) and created with BioRender.com.

Harmonic oscillator theory functions by assumption that the receptor exists in a multitude of different states, where the majority of these conformations would be presented as 'open' to interacting ligands (Kiselyov et al., 2009). This model describes oscillation *via* either the major or supplementary pathways, as singular interaction from ligand to site 1 or site 2', or both, or neither, representing activated or inactive receptors (Figure 1-10). While this model fits kinetic data well, it does not accurately describe the accessibility of sites which are partly obstructed from incoming ligands. As such, two resolutions providing modifications to this theory have been proposed by Xu *et al.* (Xu et al., 2018). The first assumes receptor oscillations exist predominantly in the 'closed' conformation and, where the ligand may access site 1 (or site 2') within the small proportion of receptors in the 'open'

conformation. The second proposes that ligands may bind in an induced fit mechanism, forcing insertion by separating L1 and FnII' domains to reach the binding site. The authors note that these modes of binding are not necessarily mutually exclusive and may both occur under physiological conditions but due to observation of negative cooperativity, it is expected that only one mole of ligand may bind to the receptor at any time.

1.5.1.2. Positive Cooperativity

At low concentrations of insulin, positive cooperativity has been reported. Competitive binding curves for ^{125}I-insulin were indicative of increased affinity binding at low competitive insulin concentrations (Marsh et al., 1984). Positive cooperativity serves to enhance binding of ligand in short supply, a potential and plausible mechanism for this observation is receptor aggregation (Heffetz and Zick, 1986; Kahn et al., 1978). This phenomenon is observed for epidermal growth factor receptors (EGFR), which share structural and kinetic similarities with the insulin receptor family, in fibroblasts and hepatocytes and mediated by anti-receptor antibodies (Schechter et al., 1979). At low levels of EGF or its receptors, EGFR form clusters or aggregates by cross-linking *via* EGF substrates to mediate higher levels of signalling (Wofsy et al., 1992). Due to the observed similarities between receptor types, there is good reason to suggest the same might be possible of IR. The importance of this action cannot be understated, enabling effective intracellular signalling *via* insulin to trigger the required biological response where insulin bioavailability is below physiological levels.

1.5.1.3. Mitogenic Effect of Insulin

Concerns were raised regarding the potential bias of binding affinity of insulin analogue therapies for the more mitogenic IR-A isoform, due to its involvement in cancer and metastatic spread (Vajo et al., 2001; Jensen and De Meyts, 2009). The first and most studied analogue, AspB10 had increased affinity for both IR and IGF1R moieties, leading to enhanced cell proliferation and promotion of mammary tumourigenesis in rat models (Ish-Shalom et al., 1997; De Meyts and Shymko, 2000; Drejer, 1992). It was determined that the high affinity for both IR-A and IGF1R due to prolonged occupancy at binding sites on these receptors may be a contributing factor to the enhanced mitogenic potential of AspB10 (Belfiore et al., 2017). AspB10 was discontinued as a result of these findings.

Today, all synthetic analogues are tested for their mitogenic potential, both *in vitro* and *in vivo* prior to advancing to a clinical setting. Modern 'smart insulin' design aims to maintain effective glucose regulation while ensuring minimal mitogenic potential compared to the native insulin construct. All three short-acting analogues (aspart, lispro and glulisine) have demonstrated comparable binding affinities and dissociation rates as native insulin (Sciacca et al., 2010; Sommerfeld et al., 2010). And in fact, all current short-acting analogues induce phosphorylation at rates comparable to insulin, producing similar cytogenic response. Aspart and lispro, but not glulisine, have demonstrated rapid activation of the MAPK/Erk pathway *via* IR-A – yet all three have shown prolonged Akt activation. Both aspart and lispro possess similar mitogenic potential as native human insulin, however glulisine appears to be slightly more potent, likely due to its ability to activate the IGF1R.

The long-acting analogues (insulin detemir and glargine) vary in their binding characteristics. Both demonstrate a lower affinity for IR-A but dissociate far more slowly, prolonging occupation of receptor binding sites (Sciacca et al., 2010; Sommerfeld et al., 2010; Kurtzhals et al., 2000; Mayer et al., 2008). Insulin detemir also shows low binding affinity for the IR-B isoform (Sciacca et al., 2010; Kurtzhals et al., 2000; Markussen et al., 1996). For these reasons, long-acting analogues affect biological response differently to native insulin and short-acting analogues. Glargine may exert an even stronger mitogenic effect due to a higher affinity for IGF1R (Kurtzhals et al., 2000), inducing preferential activation of the MAPK/Erk pathway (Sciacca et al., 2010; Kurtzhals et al., 2000; Mayer et al., 2008; Staiger et al., 2007; Shukla et al., 2009; Weinstein et al., 2009). Glargine also stimulates increased rates of proliferation in cells overexpressing IR-A (ter Braak et al., 2014; ter Braak et al., 2015), which occurs preferentially *via* IRs due to the slow rate of dissociation from these receptors resulting in extended activation (Sciacca et al., 2010). It is also important to consider the effects of the hybrid receptor isoforms, which have been shown to be upregulated in disease states and so likely to bear impact. Hansen *et al.* did not determine distinct differences between the long-acting analogues and either of the IR isoforms as homo- or heterodimer species, showing comparable phosphorylation and activation of downstream signalling cascades (Hansen et al., 2012). However, binding affinity of glargine for both HR-A and HR-B was three times higher than for human insulin – similar to AspB10. Interestingly by contrast, detemir showed a fourfold decreased affinity for both isoforms, compared to human insulin.

Native human insulin may exert an increased mitogenic effect upon binding to IR-A, the isoform predominantly expressed in many cancers. Comparatively

to insulin, clinical evidence has not attributed a higher degree of risk associated with analogue use and cancer development, where many of these trials focus on glargine due to its aforementioned receptor affinity and mitogenic potential. It has been suggested that mitogenic potency is related to the half-life of the receptor-ligand complex, thus explaining why fast-acting analogues do not possess the same mitogenic risk as long-acting analogues (Hansen et al., 1996). A systematic review of 15 studies in development and progression of breast, colon and prostate cancers determined no causative relationship with use of glargine and detemir, in 13 of these studies (Wu, J.W. et al., 2016).

There is a similar story regarding cardiovascular-associated risk and insulin analogue treatments. There is some evidence, though fairly controversial, that glycaemic control may reduce long-term cardiovascular risk in both T1DM and T2DM (Writing Team for the Diabetes et al., 2003; Monami et al., 2013). The relationship between native insulin and cardiovascular events has been extensively discussed. The Helsinki Policeman study reported an increase in cardiovascular mortality amongst individuals with higher serum insulin levels (Pyorala et al., 2000) and a second, larger study, the Paris Protection Study determined that higher fasting serum insulin levels were an independent risk factor for the development of coronary artery disease (Ducimetiere et al., 1980). Though these seem to point towards a direct link between elevated insulin plasma concentrations and cardiovascular disease, other factors relating to development of insulin resistance are likely responsible for this increased risk (Semenkovich, 2006). As insulin analogues possess different biological activities to native insulin, the risk associated with these may be more significant. However, there may be a further unforeseen advantage to

using analogues: Pierre-Eugene discovered that insulin glargine bound to both HR isoforms with distinctly improved affinities than compared with insulin (sevenfold for HR-A, ninefold for HR-B) – a similar observation was made for lispro which increased threefold and aspart which bound HR-B specifically twofold more. Activation of metabolic signalling by glargine was increased *via* Akt and Erk pathways, which is suspected to be mediated through hybrid receptors; insulin analogues could improve insulin signalling sensitivity in dysfunctional cells (Pierre-Eugene et al., 2012).

Insulin analogues may result in beneficial or detrimental side effects regarding development or progression of cardiovascular disease, independent of their role in lowering of blood glucose levels. A review by Mannucci *et al.* describes a similar ongoing debate as those in cancer research, that a higher incidence of cardiovascular events have been observed in patients using long-acting insulin treatments (glargine and detemir), though clinical trials have failed to pin these observational data as a causative effect of use of the former (Mannucci et al., 2015).

Further trials into current marketed therapies for diabetes are still required to garner concrete evidence of molecular mechanisms linking the observed effects of insulins on cancer and cardiovascular risk.

1.5.2. The Insulin-like Growth Factor 1 Receptor and Insulin-like Growth Factor 1

Due to the high sequence identity between IR and IGF1R, it was supposed that binding interactions with their cognate ligands would occur in a similar manner – which appears to be true, though there are some notable differences. The two ligand binding sites are present in equivalent locations:

site 1 composed of residues from L1 and α-CT' of the opposing monomer and, site 2 comprising of residues on FnI' and FnII' (Williams et al., 1995; Mynarcik et al., 1997; Whittaker, J. et al., 2001; Whittaker, L. et al., 2008).

Several studies have highlighted specific regions important in binding of IGF-1 to the IGF1R, approximating to the region of residues 131-314 (Schumacher et al., 1991; Schumacher et al., 1993; Zhang, W. et al., 1994; Kjeldsen et al., 1991; Gustafson and Rutter, 1990; Schäffer et al., 1993). Andersen *et al.* also described that residues 1-284 possess specificity for IGF-1, over insulin (Andersen et al., 1990). This large sequence was narrowed to r253-266, attributable to a variable loop upon the CR domain by Hoyne *et al.* which has been shown to be specifically involved in high affinity binding interaction of IGF-1 to IGF1R (Hoyne et al., 2000; Li, J. et al., 2019). Additionally, residues 184-279 show a high degree of affinity for both ligands, though notably for insulin (Hoyne et al., 2000). Whitaker *et al.* found 22 amino acids within the α-subunit of the IGF1R that are critical determinants of its function: ten in L1 domain, four in CR and eight in the C-terminus (Whittaker, J. et al., 2001). The N-terminus residues are contained within a β-sheet, forming the wall of the ligand binding cavity. Alanine mutagenesis of α-chain N-terminus subdomain residues (Asp-8, Asn-11, Tyr-28, His-30, Leu-33, Phe-58, Arg-59, Phe-90) showed a 2-10-fold reduction in affinity for IGF-1, each, with the exception of Phe-90 with a 23-fold decrease (Mynarcik et al., 1997; Whittaker, J. et al., 2001). The CR domain residues sit adjacent to the base of the L1 domain and are supposed to interact with Trp-79, located in the loop between the β-sheets and are strongly assumed to form part of the contact site of interacting ligands. Mutation of these residues (Arg-240, Phe-241, Glu-242 and Phe-251) may result in a two-to sixfold loss of affinity (Whittaker, J. et al., 2001). The third

set of residues, located in the C-terminus are presumed to interact through side chains, though this has yet to be confirmed. Mutations of residues at the C-terminus subdomain (Phe-692, Glu-693, Leu-696, His-697, Asn-698, Ile-700, Phe-701) resulted in a loss of IGF-1 affinity up to 6-fold (Mynarcik et al., 1997), four of these (Phe-692, Leu-696, Ile-700, Phe-701) caused significant decreases to the point of being devoid of any binding activity (Whittaker, J. et al., 2001). All aforementioned residues are critical contributors of IGF1R specificity and ultimately, its function.

The IGF-1 ligand is similarly primed, containing regions within its amino acid sequence that serve to enhance its ability to interact with its cognate receptor and associated binding proteins (IGFBPs). Chimeric protein studies, swapping amino acid sequences between IGF-1 and insulin have provided insight into which regions have been designed for function specificity. Bayne deduced that domains B, A and D were not required in the high affinity interactions with the IGF1R (Bayne et al., 1989), hence their inclusion must concern interactions with other receptors and proteins. Residues 1-16 were exchanged for those within the insulin amino acid sequence, observing a highly significant reduction in affinity for the IGF-1 chimera for IGFBPs, and reaffirming that there was no effect on its association to IGF1R (Bayne et al., 1988; Cascieri et al., 1988b; Cascieri et al., 1989b). More specifically, replacement of 15Gln-16Phe of IGF-1 for (B16)Tyr-(B17)Leu of insulin saw a 5- to 10-times increase in affinity for the insulin receptor, while affinity for IGF1R remained consistent (Bayne et al., 1988). This would suggest that inclusion of these particular amino acids in IGF-1 sequence would serve to inhibit interactions from this ligand with the insulin receptor. The lack of determinants in the C region of IGF-1 contributes to the poor affinity for the

insulin receptor (Bayne et al., 1989). Substitutions and deletions within the C domain also provide insight into which residues are highly involved in binding to IGF1R. Deletion of residues 28-37, by replacement of a 4-residue glycine bridge, enabling retention of tertiary structure, saw a 30-fold reduction in affinity for the IGF1R, while retaining the same affinities for IGF2R, IR and IGFBPs (Bayne et al., 1989). Gill *et al.* explained that removal or replacement of this series of amino acids negatively affected the binding free energy to the IGF1R, hindering flexibility of this particular region of the protein and therefore preventing subsequent changes in conformation, which are highly important in receptor-ligand interactions of this nature (Gill et al., 1996). More specifically, studies have shown that Tyr-31 alone contributes greatly to high specificity between these interacting pairs. Alanine substitution at this site proved a tenfold loss of IGF1R binding affinity (Maly and Lüthi, 1988). Cascieri and Bayne have also demonstrated importance of singular residues not contained within the C region. Single-point mutations of Phe-24 to [Leu-24]IGF-1 and [Ser-24]IGF-1 resulted in a reduction in binding affinity to IGF1R of 32- and 16-fold, respectively (Cascieri et al., 1988a; Bayne et al., 1989) and, [Ala-31]IGF-1 and [Leu-60]IGF-1 in a 6- and 20-fold loss (Bayne et al., 1990). Multiple-point mutations of the aforementioned sites resulted in dramatic loss of sensitivity for IGF1R ranging from 240- to over 1200-fold (Bayne et al., 1990). Amino acid residues Tyr-24 (B), Tyr-31 (C) and Tyr-60 (A) contribute highly to the activity of this ligand for its cognate receptor. Zhang *et al.* also deduced that specificity of IGF-1 for IGF1R was influenced by inclusion of positively-charged side chains, where uncharged alanine substitution of arginine in C region and lysine residues in D region saw

reduction of 15- and 10-fold respectively yet increased for IR by 29- and 6-fold (Zhang, W. et al., 1994).

Scatchard plots of the IGF1R-IGF-1 interaction had been variably reported as either linear or curvilinear (Tollefsen et al., 1987) though De Meyts suspected that the presence of IR/IGF1R hybrids were confusing the data (De Meyts, 1994). IGF1R-specific overexpression in a variety of cell lines showed that IGF-1 binding exhibited similar negative cooperativity to the insulin receptor, producing curvilinear Scatchard plots with a 1:2 stoichiometry and accelerated dissociation upon second ligand engagement. The IGF1R may therefore bind a single molecule of IGF-1 with high affinity and has capacity for binding at the lower affinity site upon dissociation of the former (Tollefsen and Thompson, 1988).

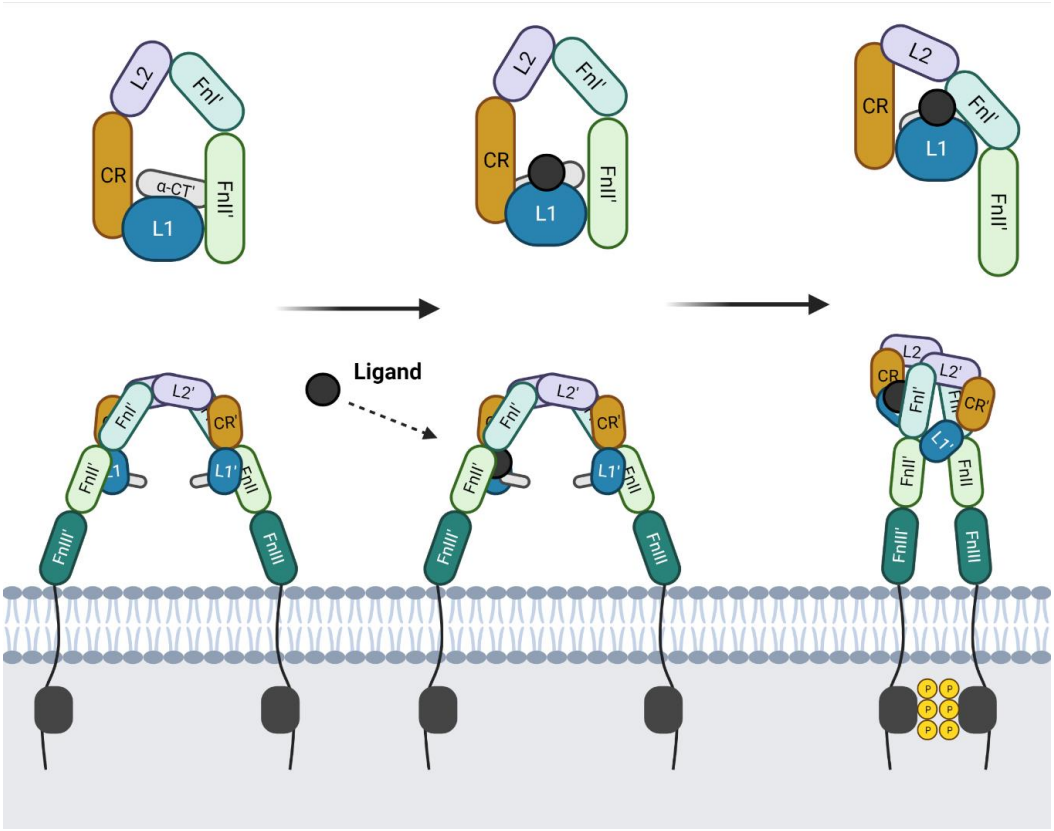

Figure 1-11: Conformational Change of IGF1R upon Engagement of IGF-1

Schematic representation of the mechanism of binding of IGF-1 to the IGF1R. Side view of binding pocket is shown above. In the apo-conformation, IGF1R forms an open inverted Λ-shape, with FnIII legs maintained far apart. Upon engagement of the ligand, a considerable structural rearrangement occurs, forming a Γ-shape with FnIII legs in close proximity enabling autophosphorylation of intracellular tyrosine kinase domains. Based on work by (Li, J. et al., 2019), adapted from (Blyth et al., 2020) and created with BioRender.com.

Xu *et al.* produced crystal structures of apo- and IGF-1-bound forms of IGF1RΔβ ectodomains (Xu et al., 2018; Whitten et al., 2009). The apo-IGF1RΔβ adopted a Λ-shaped assembly, much like structure of the insulin receptor however there are some notable differences: when overlaying the unliganded IGF1RΔβ L1-CR-L2 with the respective domains of the IRΔβ structure, a 26° difference in orientation between L1-CR and L2 in the two receptors and a 17° difference in alignment of the IGF1RΔβ and IRΔβ L1 and FnII' domains of the adjacent monomer were observed (Xu et al., 2018). This difference in alignment has resulted in the α-CT C-terminus residues being

packed against the surface of the adjacent FnII' domain, unlike for IRΔβ where these are completely disordered and directed away from the FnII' domain. The apo- conformation is maintained by autoinhibitory stabilisation interactions between each set of L1 and FnII' domains. However, engagement of a single IGF-1 ligand induces a conformational change disrupting the aforementioned L1-FnII' stabilisation, producing the asymmetric, Γ-shaped structure (Li, J. et al., 2019) (Figure 1-11). The binding site for IGF-1 is composed of the L1 and CR domains of one monomer and the α-CT' and FnI' of the other. The close proximity of both α-CT domains to the FnI' enables the formation of a rigid helical beam, stabilized by disulphide bonds between the two α-CTs and additionally stabilized by the interaction between α-CT and FnI'. The C-domain loop of IGF-1 extends enabling interaction with both the L1 and CR domains (Li, J. et al., 2019), which in the case of IGF-2 or insulin where the C-domain loops are far shorter and cannot reach the CR domain resulting in low binding affinity (Gustafson and Rutter, 1990). In addition, two arginine residues (r36, r37) upon the C-domain loop are integral in enhancing the stabilisation of this interaction by contacting the L2 domain (Zhang, W. et al., 1994; Li, Q. et al., 2019). Engagement of IGF-1 induces conformational rearrangement of the tyrosine kinase 'legs', bringing them together. For IR, the FnIII domain legs are brought together (Weis, F. et al., 2018), however due to the aforementioned differences in alignment of IGF1R domains, the FnIII domains are maintained apart (Xu et al., 2018). In this case, the L1 domains have large, yet distinct roles to play and further enabling this asymmetric conformation. L1, where ligand is present at its binding site, moves upwards towards the top part of the Γ-shape conformation; L1' acts as a 'pseudo-ligand' and forms a crucial stabilizing intra-monomer interaction

with FnII', which draws the TK 'legs' together into close proximity for receptor activation (Li, J. et al., 2019; Kavran et al., 2014). This staggered-like conformation also prevents engagement of a second IGF-1 molecule. The rigid α-CT beam prevents conformational restructuring upon attempts at engagement of a second IGF-1 at the unliganded α-CT as binding at site 2 would disturb this coupling. In addition, disruption of the L1' by weak binding of a second IGF-1 appears to impede receptor function by interruption of the L1'-FnII' stabilizing interaction, leading to a loss of receptor activation (Li, J. et al., 2019; Blanquart et al., 2005). The combination of these effects leads to accelerated dissociation of the first molecule of IGF-1, which explains observed negative cooperativity characteristic of IGF1R-IGF-1 binding (Christoffersen et al., 1994; De Meyts, 1994). Nevertheless, engagement of IGF-1 with L1 and α-CT very closely resembles that of insulin's interaction with the corresponding components of IR (Menting et al., 2013; Menting et al., 2014) and aligns well with the observation of interactions between respective ligands to both types of receptors (Denley et al., 2005).

1.5.3. The Insulin Receptor/Insulin-like Growth Factor 1 Receptor Hybrid Receptor and Interactions Involving Insulin and Insulin-like Growth Factor 1

As IR/IGF1R hybrids are formed of one monomer each, these receptors would therefore possess one set of each receptor type's ligand binding sites: the L1 and α-CT of an insulin receptor and L1' and α-CT' of the IGF1R. These sites are equivalent, in terms of the domain-domain structure of the receptors however, the interacting amino acid residues are not necessarily conserved in these regions. This quite clearly impacts binding interactions as it has been

repeatedly characterised that the hybrid receptor's binding affinity for IGF-1 far exceeds its affinity for insulin (Slaaby et al., 2006; Benyoucef et al., 2007; Pandini et al., 2002). To date, no ectodomain or full-length structure exists for the apo- or complexed IR/IGF1R hybrid receptor. Likewise, much is left to be determined as to the subsequent conformational transformation of the hybrid receptor through its interactions with insulin or IGF-1, notably since it is now known that the IGF1R forms an asymmetric 'Γ'-shape in contrast to the insulin receptor which takes an inverted-'Λ' symmetrical shape and that as a consequence would affect how the TK 'legs' are engaged through this structural rearrangement (Li, J. et al., 2019; Gutmann et al., 2018). Elucidation of this structural information will provide the answers for as to the preferred binding affinity for IGF-1 and differences in tyrosine kinase activation. Menting *et al.* produced a truncated hybrid structure of IR L1-CR construct and IGF1R α-CT peptide (residues 691-706) in complex with IGF-1, which has provided insight into structural interaction at these binding sites (Menting et al., 2015). Engagement of IGF-1 with the aforementioned hybrid construct appeared similar to the insulin-μIR complex (Menting et al., 2014); rearrangement of the α-CT segment was conserved and the insulin B-chain equivalent region of IGF-1 Phe23-Tyr24-Phe25 triplet folded outwards in a similar manner, lying between the IGF1R α-CT and IR L1 β-sheet (Menting et al., 2015). The C-domain of IGF-1 remained disordered, in line with observations of the full-length IGF1R structure (Gustafson and Rutter, 1990; Li, J. et al., 2019), the α-CT threads through a loop formed with respect to the three-helix bundle at the growth factor core. Belfiore (2017) questioned the physiological relevance of this choice of construct as the hybrid primary binding site (IR L1 & IGF1R α-CT) has shown a tenfold lower affinity than the alternate binding site (IGF1R

L1 & IR α-CT) (Belfiore et al., 2017; Kristensen et al., 1999). However, all models of insulin and IR interactions use the IR-A isoform (Ex11-), there remains the question as to whether the observed threading might be possible for IR-B (Ex11+) and subsequently the effect on binding to HR-B. The extended α-CT is hypothesized to interfere with the proposed threading mechanism, as it is less sterically accommodating within the space between the L1 β-sheet and opposing CR domain (Denley et al., 2005; Menting et al., 2015).

There are some reported differences in binding affinity between hybrid receptor isoforms, HR-A and HR-B and so, like the IR isoforms, it may prove important to determine which species is present in abundance when treating conditions like insulin resistance. Fairly unanimously, the affinity for insulin is reported as approximately 100-fold lower in both receptor types though this has been challenged by Pandini *et al.* as they observed a high affinity for insulin in HR-A *versus* HR-B (Benyoucef et al., 2007; Slaaby et al., 2006; Pandini et al., 2002). The former argument later reaffirmed by Slaaby *et al.* adds to the growing data that insulin affinity is greatly reduced, and is generally considered as such across the board in hybrid research (Slaaby, 2015). However overall, HR-A affinity for IGF-1 is increased, with all parties in shared agreement of this notion (Slaaby et al., 2006; Benyoucef et al., 2007; Pandini et al., 2002; Slaaby, 2015). The effect of reduction in insulin sensitivity is profoundly felt in tissues with physiological insulin activity, resulting in aforementioned insulin resistance.

1.6. Insulin Signalling

Signalling of insulin *via* its receptor triggers many different pathways to produce various cellular actions. There are two main pathways: PI3K/Akt and MAPK/Erk (Figure 1-12).

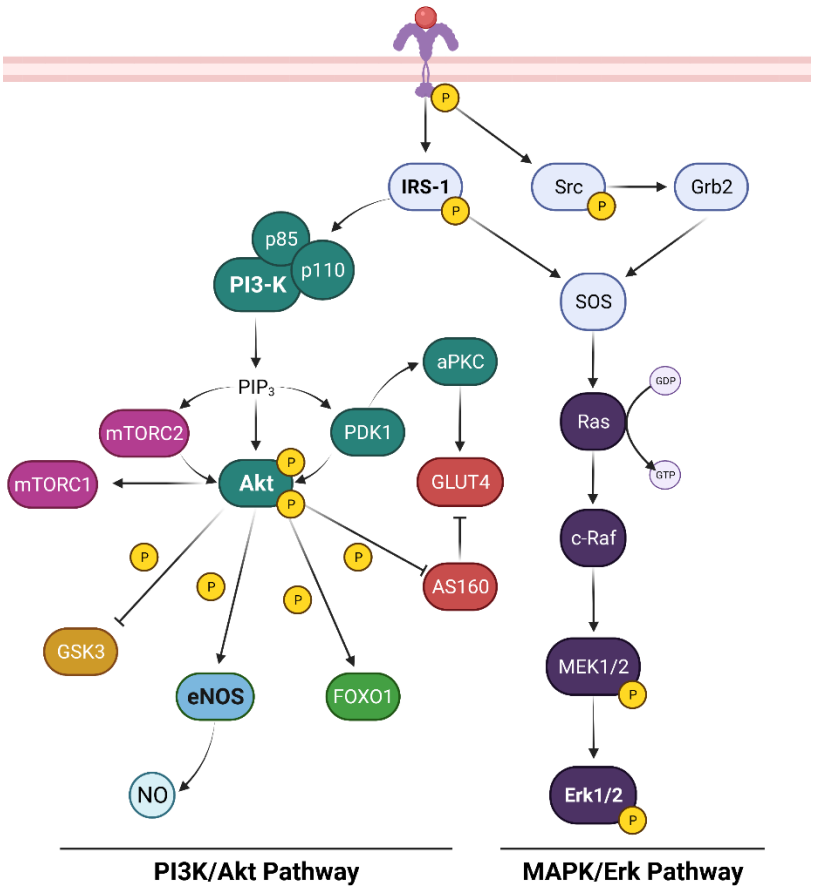

Figure 1-12: Insulin Signalling *via* PI3K/Akt and MAPK/Erk pathways

Schematic of an overview of PI3K/Akt and MAPK signalling pathways, downstream of the insulin receptor. Signalling *via* IR/PI3K/Akt axis triggers metabolic effects, such as glucose uptake through GLUT-4, gluconeogenesis *via* FOXO1 and inhibition of GSK3 to prevent glucose synthesis. Signalling *via* IR/MAPK/Erk axis activates mitogenic effects including cell growth and differentiation, and protein synthesis. Image adapted from (Boucher et al., 2014) and created with BioRender.com

PI3K/Akt signalling occurs exclusively through insulin receptor substrate (IRS) proteins and is responsible for most metabolic effects of insulin. Activation of mammalian target of rapamycin complex 1 (mTORC1) by inhibition of mediating substrates enables regulation of genes controlling metabolism,

protein synthesis and cell growth. When phosphorylated by Akt, glycogen synthase kinase 3 (GSK3) is rendered inactive, which enables glycogen synthase activation and accumulation of glycogen in the liver. Akt has many cell-specific targets, in endothelial cells eNOS is phosphorylated and becomes activated, producing vasodilatory and anti-inflammatory nitric oxide. Forkhead Box O 1 (FOXO1) controls the expression of lipogenic and gluconeogenic genes and becomes inhibited by Akt. AS160 mediates insulin-agonist glucose uptake, becoming inhibited by Akt and allowing translocation of GLUT-4.

The MAPK/Erk pathway is activated independent of the PI3K/Akt pathway and uses both IRS and Shc proteins. MAPK Erk1/2 proteins have a direct role in regulation of mitogenesis, cell differentiation and gene expression.

1.6.1. Signalling *via* the PI3K/Akt Pathway

The PI3K/Akt pathway mediates many cellular functions, however its involvement in modulation of eNOS and subsequent production of NO is the focus of this thesis (Figure 1-13).

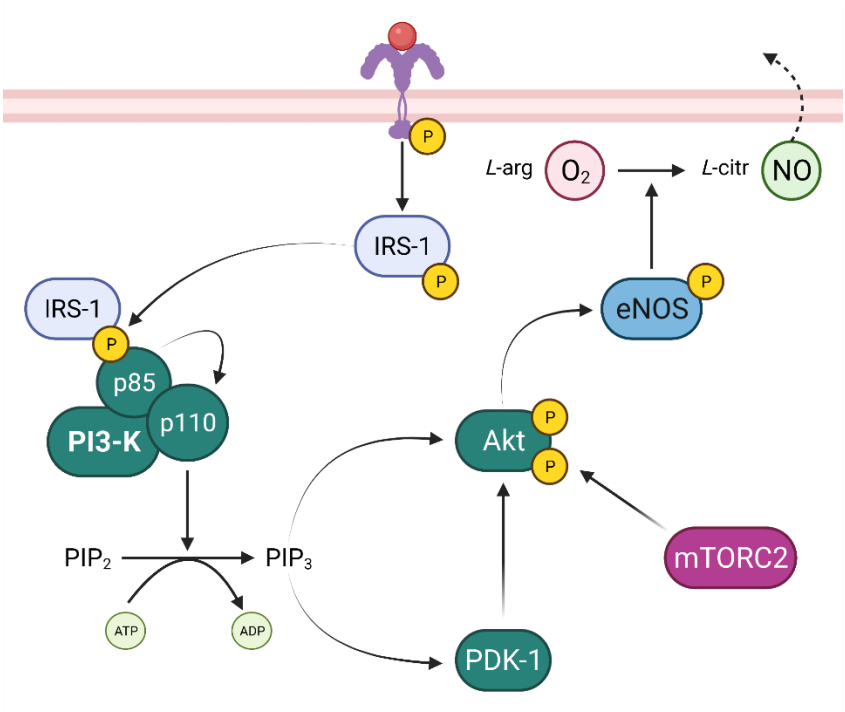

Figure 1-13: Insulin Signalling *via* PI3K/Akt/eNOS Axis in Generation of Nitric Oxide

Schematic of insulin signalling *via* PI3K/Akt/eNOS axis in the generation of nitric oxide. Binding of insulin to its receptor triggers an intracellular phosphorylation cascade between IRS-1, PI3K, Akt and eNOS, which once activated can catalyse the reaction of *L*-arginine and molecular oxygen to *L*-citrulline and NO. Image of own design and created with BioRender.com

Binding of insulin to the ectodomain region of the insulin receptor triggers a conformational change in the structure which results in autophosphorylation of the intracellular tyrosine kinase units. IRS-1 binds the phosphorylated-NPXY motifs present in the juxtamembrane region of the insulin receptor, which in turn phosphorylates the Y612 and Y632 sites of IRS-1 (Backer et al., 1997; Esposito et al., 2001; Gual et al., 2005). Activated IRS-1 associates with the regulatory p85α-subunit of PI3K *via* its SH2 domain. The interaction of IRS-1 stimulates activity of the catalytic p110α-subunit of PI3K which facilitates the conversion of lipid products, PIP_2 to PIP_3 (Esposito et al., 2001). Activated PIP_3 can initiate translocation of proteins containing plekstrin homology (PH)-domains to the plasma membrane, including Akt (Scheid et al., 2002). Once in proximity to the membrane, Akt may be activated at two

different sites, or both for full activation: T308 and S473 (Vivanco and Sawyers, 2002; Sarbassov et al., 2005). Each site can be phosphorylated by phosphoinositide-dependent kinase-1 (PDK-1) and mammalian target of rapamycin complex 2 (mTORC2), respectively. The T308 residue lies within the kinase T-loop, whereas the S473 site is located within a hydrophobic motif in close proximity to the C-terminus. Activation of the T-loop (T308) is necessary and sufficient for Akt activity, whereas phosphorylation of the hydrophobic motif (S473) enhances Akt activity (Baffi et al., 2021).

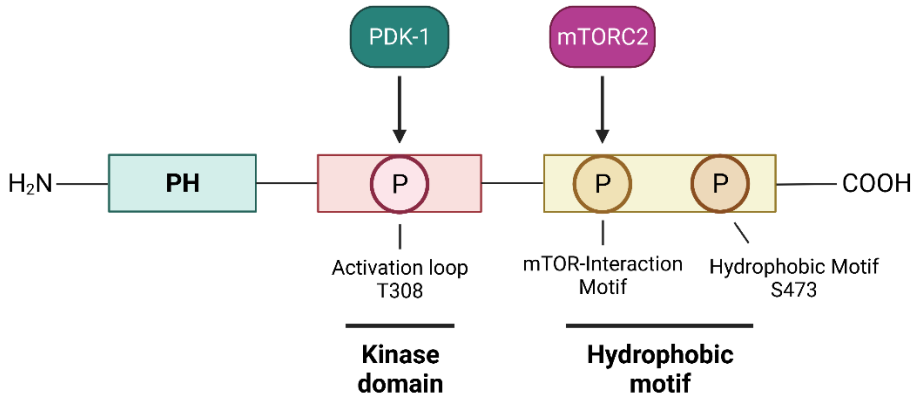

Figure 1-14: Model for Phosphorylation of mTOR-Regulated Akt

Akt is regulated by mTORC2, phosphorylating the TOR-interaction motif at the C-terminus. Phosphorylation of this site facilitates phosphorylation of the activation loop (T308) by PDK-1, which in turn, triggers autophosphorylation of the hydrophobic motif (S473) to leading to complete activation of Akt. Image adapted from (Baffi et al., 2021) and created with BioRender.com.

Membrane localisation of Akt was the primary determinant of S473 phosphorylation (Scheid et al., 2002). However, Scheid *et al.* described that PDK-1 phosphorylation of T308 was primarily dependent upon activation of the S473 site. mTORC2 does not directly phosphorylate S473, instead interacting at a site Baffi *et al.* termed the mTOR Interaction Motif (TIM), triggering autophosphorylation of S473 and facilitating binding of PDK-1 at T308 (Figure 1-14) (Baffi et al., 2021). They confirmed the facilitative nature of mTORC2 through a PDK-1-overexpression model; where in the absence of

mTORC2, exaggerated levels of PDK-1 can rescue phosphorylation of S473, promoted through interactions at T308. Activated Akt, as one of its many actions, can phosphorylate eNOS on its S1177 activatory site, which catalyzes the reaction of *L*-arginine and molecular oxygen to *L*-citrulline and NO, as discussed in depth in section 1.6.2.2 (Dimmeler et al., 1999; Stuehr et al., 2001).

A main feature in T2DM is the loss of insulin sensitivity. Reasons which contribute to endothelial dysfunction and insulin resistance are numerous: from genetic mutation or polymorphism of IR, IRS-1, PI3K and Akt proteins, to inflammation by increased secretion of monocyte attractant protein-1 (MCP-1) contributing to recruitment of leukocytes, oxidative stress leading to enzyme uncoupling and proatherosclerotic signalling between NADPH oxidases and protein tyrosine kinase 2β (PYK2, section 1.6.2.3) and generation of IR/IGF1R hybrid receptors (Boucher et al., 2014; Higashi et al., 2002; Stroes et al., 1996; Viswambharan et al., 2017; Federici et al., 1996). Signalling *via* the PI3K/Akt pathway will be affected as a result of these changes. In a healthy endothelium, signalling occurs as described above, balancing vasodilatory and vasoprotective actions. In insulin-resistant conditions, vasoconstrictive and pro-atherogenic effects take precedence, activating signalling *via* the MAPK/Erk pathway observing a decrease in production of NO and a reciprocal increase in endothelin-1 (ET-1) (Potenza et al., 2009; Avogaro et al., 2006).

1.6.2. Nitric Oxide

Nitric oxide was discovered by Joseph Priestly in 1772, but it wasn't until 1986 that NO became recognized as a signalling molecule of the cardiovascular system, by Furchgott and Zawadzki (Furchgott, 1989). In previous years, they reported that vasodilation involving acetylcholine (ACh) was dependent on the presence of an unknown secondary factor (Furchgott and Zawadzki, 1980). Subsequently, they further determined that ACh relaxation was mediated by endothelium-derived relaxant factor (EDRF) (Furchgott, 1984; Furchgott, 1990). Ignarro *et al.* (Ignarro et al., 1987), in conjunction with Furchgott and Zawadzki (Furchgott, 1988) later deduced that the biological effect of EDRF was also reproducible by NO – which are now believed to be one in the same. NO is synthesized by nitric oxide synthases (NOS), by conversion of *L*-arginine, oxygen, and reduced NADPH co-substrates, resulting in the production of NO and *L*-citrulline.

NO is a small gaseous messenger produced by endothelial cells in the vascular system, in response of vasoconstrictive (Palmer et al., 1987; Hocher et al., 2004; Thomas and Victor, 1997), inflammatory (Radomski et al., 1990; Hogan et al., 1988; Radomski et al., 1987; Sneddon and Vane, 1988; Bhardwaj et al., 1988), proliferative (Nakaki et al., 1990; Garg and Hassid, 1989; Tsihlis et al., 2011; Heller et al., 1999; Cartwright et al., 2000) or thrombotic states (Kubes et al., 1991; Freedman and Loscalzo, 2003). The function of NO as a vasodilator in smooth muscle cells has been most widely investigated. Diffusing through semi-permeable membranes from its point of origin within endothelial cells into adjacent smooth muscle cells, NO activates soluble guanylate-cyclase (sGC), resulting in an increase of cyclic guanosine

monophosphate (cGMP). Activated cGMP downregulates intracellular calcium levels and sensitivity of myosin light chain phosphorylation, which causes relaxation of the smooth muscle and subsequently, vasodilation of the vessel (Somlyo and Somlyo, 1994; Etter et al., 2001). Nitric oxide acts further in an atheroprotective manner by maintaining reduced levels of platelet aggregation and adhesion, LDL oxidation and adhesion molecules (Figure 1-15) (Wang, G.-R. et al., 1998; Lievens and von Hundelshausen, 2011; Goss et al., 1997; Wang, W. et al., 2011; Gao et al., 2017).

In addition, NO has been shown to regulate proliferation and migration of endothelial cells, and angiogenesis involving these aforementioned processes (Ziche et al., 1994; Matsunaga et al., 2002; Cooke and Losordo, 2002).

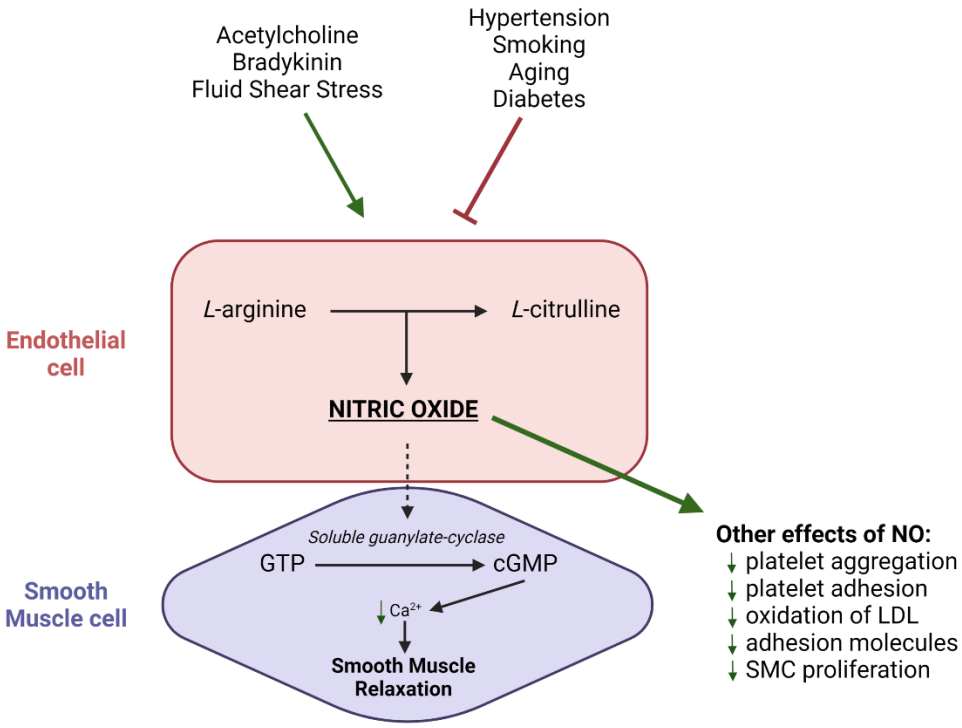

Figure 1-15: Regulation of Nitric Oxide on Smooth Muscle Cell Relaxation

Schematic representing the production of nitric oxide within endothelial cells and its involvement in smooth muscle cell relaxation. Nitric oxide production may be up- or downregulated by various agonists and mechanostressors. Image adapted from (Gaunt, 2018) and created with BioRender.com.

1.6.2.1. Nitric Oxide Synthases

Three isoforms of nitric oxide synthase are produced in mammalian cells: neuronal (nNOS/NOS I), inducible (iNOS/NOS II) and endothelial (eNOS/NOS III) (Forstermann and Sessa, 2012). As the names suggest, nNOS and eNOS were initially discovered in neuronal cells and the endothelium, respectively and, are the constitutive forms of NO synthase, producing low, continuous concentrations of nitric oxide. Inducible NOS however, the transcriptionally regulated form of the enzyme, was first detected in macrophages, acting in a cytostatic and cytotoxic manner. In macrophages, iNOS produces large quantities of NO which may inhibit iron-containing enzymes by binding to the ferrous core and interfere with DNA of target cells, resulting in breakages and fragmentation (Forstermann and Sessa, 2012). However, expression of iNOS may be 'induced' within virtually any cell or tissue by proinflammatory cytokines or endotoxins. Once expressed in cells, iNOS is constitutively active, unaffected by changes in intracellular Ca^{2+}, and may assist in coordination of pathogen-induced T-cell response (Moncada and Higgs, 1993; Schmidt and Walter, 1994; Nathan, 1997; Forstermann and Sessa, 2012). Nitric oxide synthases must be strictly regulated to maintain homeostasis as uncontrolled expression of these proteins may result in low blood pressure or detrimental cytotoxic events. The specificity of NOS isoforms is managed by direct interactions of other proteins and/or phosphorylation, nitration or nitrosylation events (Villanueva and Giulivi, 2010). While both endothelial and smooth muscle cells appear to possess the ability to express the same isoform, this activity is limited to the endothelium. The eNOS promoters within smooth muscle cells are heavily methylated and further silenced methyl-CpG binding proteins preventing the transcription of eNOS and consequently nitric

oxide production in these cells (Chan, Y. et al., 2004). Nitric oxide synthesis while dependent on the cell type is also further influenced by particular conditions that the cell experiences. In cases of patients with septic shock, iNOS is expressed in endothelial cells and promotes a significant increase in NO bioavailability (Lopez et al., 2004; Petros et al., 1994; Moncada, 1999).

Formation of functional NOS is underpinned by the dimerization between identical monomer units containing an N-terminal oxygenase domain – attached sequentially to haem and tetrahydrobiopterin (BH_4) groups – and a reductase domain comprised of two flavin mononucleotide (FMN) domains, flavin adenine dinucleotide (FAD) and NADPH binding sites. The oxygenase and reductase domains are separated by a Ca^{2+}/calmodulin (CaM) domain (Forstermann and Munzel, 2006) (Figure 1-16). An oxygenase and reductase domain of individual monomer units dimerize covalently *via* a flexible 25-residue linker, in a cross-wise manner (Volkmann et al., 2014).

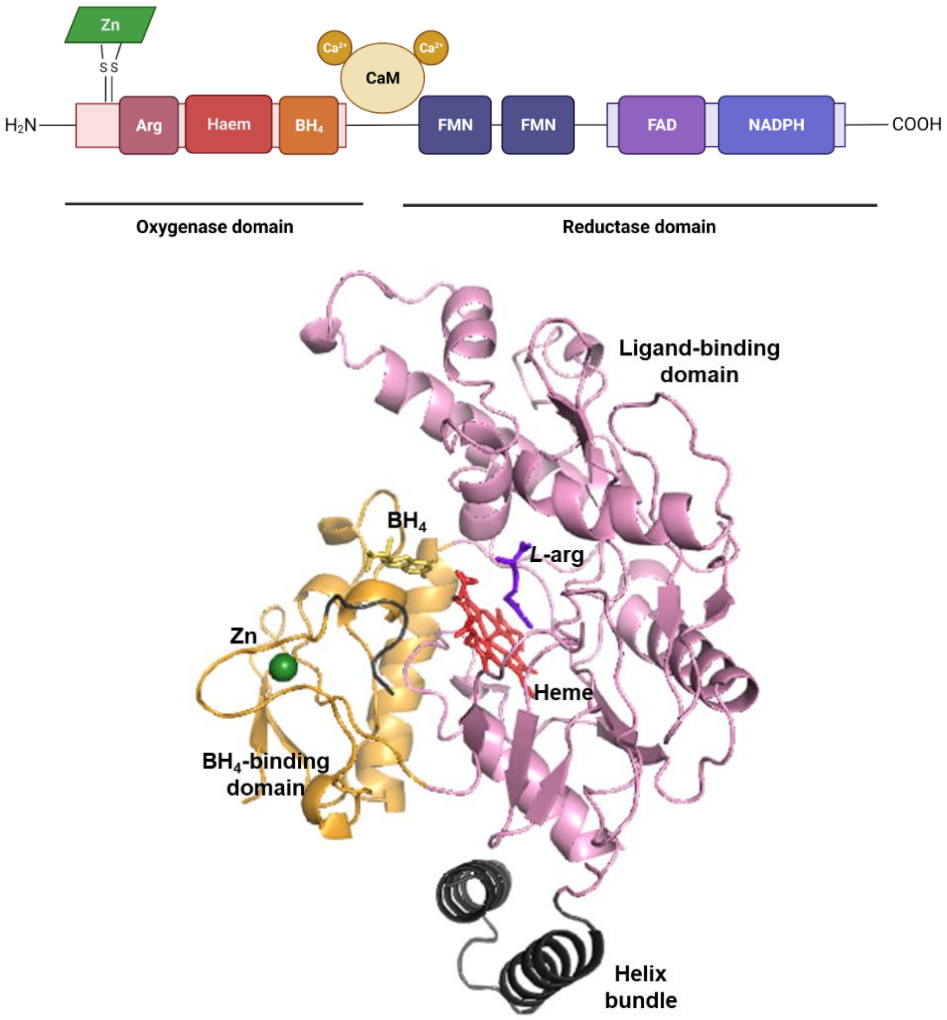

Figure 1-16: Structure of Nitric Oxide Synthases

Top: Schematic of general nitric oxide synthase monomer structure, highlighting individual domains and binding sites within the oxygenase and reductase domains. Image adapted from (Danylovych et al., 2018), created with BioRender.com. **Bottom:** X-ray crystal structure of eNOS oxygenase domain, with *L*-arginine substrate (purple) and highlighting presence of the haem group (red), BH_4 ligand (light orange) and zinc ion (green). Image created using PyMOL Molecular Graphics System, version 2.0 Schrödinger, LLC, using PDB 3NOS published by (Fischmann et al., 1999).

Each aforementioned constituent of the NO synthase structure pertains to a critical aspect tied to its function in the production of nitric oxide. *L*-arginine, molecular oxygen and (*6*-)5,6,7,8-tetrahydrobiopterin interact with NOS at their respective binding sites on the oxygenase domain. Transfer of electrons to haem, originating from NADPH terminus are facilitated by the calmodulin domain which increases the rate of transfer. The electrons at haem are used to reduce O_2 to form activated $2O^-$ radicals. Hydroxylation of *L*-arginine

produces the intermediary species, N^{ω}-hydroxy-*L*-arginine which remains bound to the enzyme, before cycling NOS a second time to oxidize the aforementioned intermediate to form *L*-citrulline and NO (Stuehr et al., 2001) (Figure 1-17). All isoforms of NOS bind calmodulin. In constitutive isoforms, calmodulin is able to bind upon increase of intracellular Ca^{2+} and so regulation of these enzymes is possible by affecting the affinity for calmodulin to NOS. For iNOS, calmodulin is able to bind at concentrations of Ca^{2+} up to ten-fold less than required for constitutive isoforms due to modification in amino acid sequence at this location (Cho et al., 1992; Hemmens and Mayer, 2000). All three isoforms contain a zinc-thiolate cluster, composed of a tetrahedrally-coordinated zinc ion (Zn^{2+}) to two CXXXXC-motifs at the point of contact between the monomer units (Raman et al., 1998). The zinc-thiolate cluster appears to have a structural role rather than being used in catalysis, though the eNOS C99 residue is considered to make a significant contribution to the BH_4 binding site (Hemmens and Mayer, 2000; Martasek et al., 1998). Missense mutation of the homologous nNOS C331A residue results in a loss of binding affinity for BH_4 and is subsequently rendered catalytically incompetent (Martasek et al., 1998).

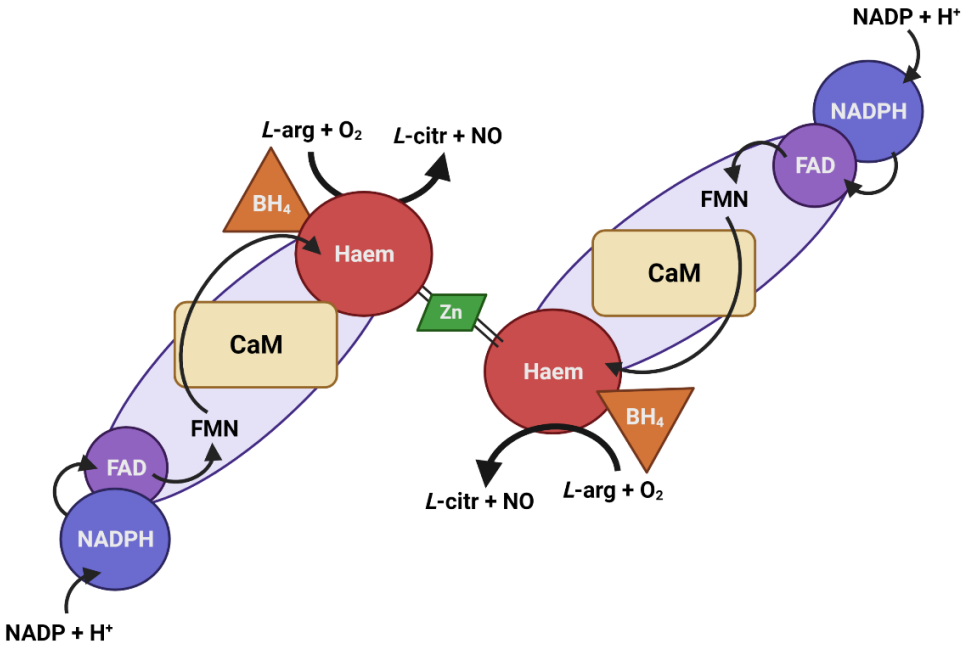

Figure 1-17: Catalysis of *L*-arginine by Nitric Oxide Synthase

Schematic showing the movement of electrons through the nitric oxide synthase domains, enabling molecular oxygen reduction to produce the nitric oxide species. Image adapted from (Gielis et al., 2011) and created with BioRender.com.

1.6.2.2. Endothelial Nitric Oxide Synthase

Endothelial NOS is the focus of this thesis due to its presence within vascular tissues. And while eNOS is considered as the endothelial-specific NOS however in actual fact, it is expressed in various additional locations including the examples of epithelial cells, fibroblasts, hepatocytes, neutrophils and skeletal muscle (Buchwalow et al., 2005; Ricciardolo et al., 2003; McNaughton et al., 2002; Ermert et al., 2002). Expression of eNOS may also become increasingly upregulated under specific conditions such as exercise (Laughlin et al., 2001), oestrogen stimulation (Chambliss and Shaul, 2002), hyperthermia (Harris et al., 2003) and fluid shear stress (Lam et al., 2006; Balligand et al., 2009; Fleming, 2010).

Endothelial NOS is expressed in the Golgi apparatus and plasma-lemmal caveolae, small cavities or folds within the plasma membrane of endothelial

cells (Sessa et al., 1995; Garcia-Cardena et al., 1996). eNOS was classified previously as a Ca^{2+}/CaM-dependent enzyme, active at low concentrations of intracellular calcium (Busse and Mulsch, 1990). Under serum-starved conditions, eNOS forms a complex with caveolin which inhibits eNOS activity - the eNOS-caveolin complex is predominantly present in a perinuclear location awaiting activation (Wang, H. et al., 2009). Increases in intracellular Ca^{2+} concentration and recruitment of heat shock protein-90 (HSP90) causes the interaction between eNOS and caveolin to become disrupted, allowing association of the calmodulin domain for further facilitation of *L*-arginine catalysis (Gratton et al., 2000; Fleming, 2010). Activation by insulin enables phosphorylation of eNOS *via* Akt or AMPK proteins. In a translocation event unique to eNOS, phosphorylated-eNOS complexed with palmitoylated-caveolin are transported to the plasma membrane to facilitate further interactions between the enzyme and its co-localised binding partners (Michel et al., 1997; Sase and Michel, 1997). A proportion of eNOS may remain at the Golgi apparatus, however the enzyme and caveolin are separated into distinct compartments, suggesting that activity in this particular location is not managed by caveolin-1 (Cav-1) (Govers et al., 2002). There is further evidence that caveolin may also serve to further modulate eNOS activity by inhibition of plasma membrane-localised proteins, such as guanosine triphosphate cyclohydrolase I (GTPCH I). Initial evidence from Peterson *et al.* and further investigation by Du and Chen using caveolin-1-deficient and knockout mouse models would suggest that GTPCH may be essential in stabilisation of eNOS by maintaining coupling of BH_4 (Peterson et al., 2009; Du and Chen, 2009; Alkaitis and Crabtree, 2012) (Figure 1-18). Uncoupling of the enzyme results redirection of electron transfer producing ROS superoxide,

O_2^-. Uncoupling is increasingly observed in patients with endothelial dysfunction and diabetes and hypertension (Higashi et al., 2002; Stroes et al., 1996).

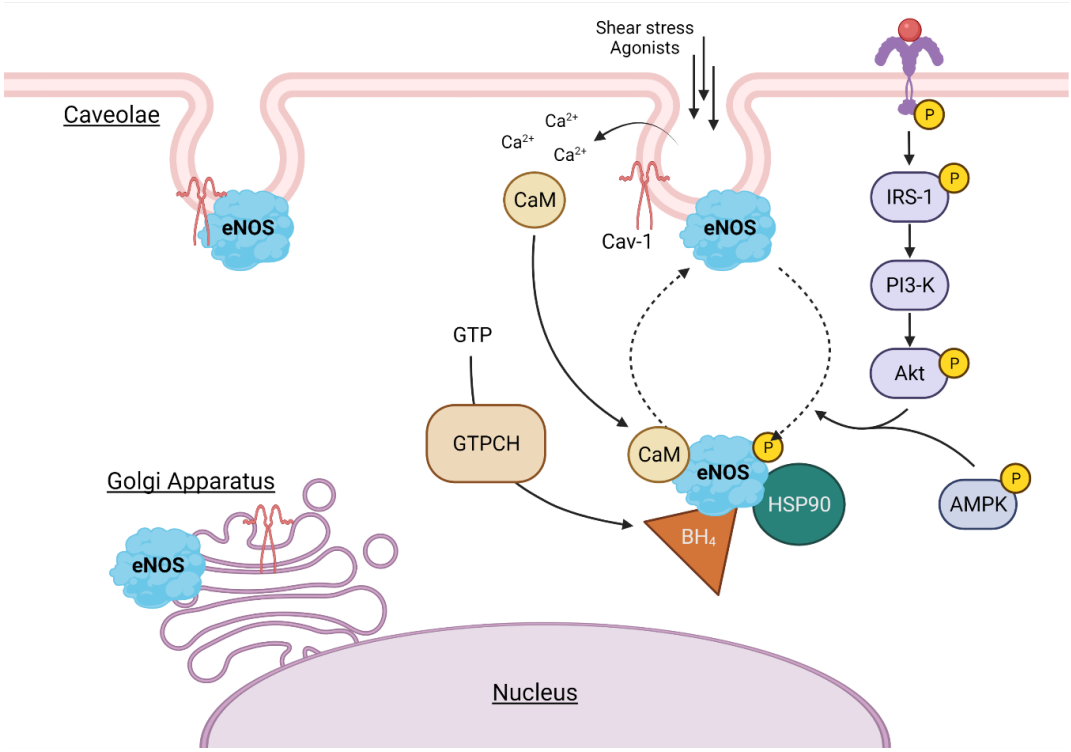

Figure 1-18: Translocation of Endothelial Nitric Oxide Synthase

Endothelial nitric oxide synthases (eNOS) are present near the nucleus and at the cell membrane, for activation in signalling. eNOS may translocate from the cytoplasm to the caveolae upon calcium ion entry, activation by insulin receptors or interactions with localised binding partners, such as heat shock protein 90 (HSP90). Image of own design and created with BioRender.com.

1.6.2.2.1. Phosphorylation Sites of Endothelial Nitric Oxide Synthase

Endothelial NOS may be phosphorylated at multiple sites, each resulting in up- or downregulation in activity of the enzyme (Figure 1-19). Sites at S1177 and Y657 are of notable interest in this thesis, due to their respective activatory and inhibitory effects on eNOS catalysis of NO.

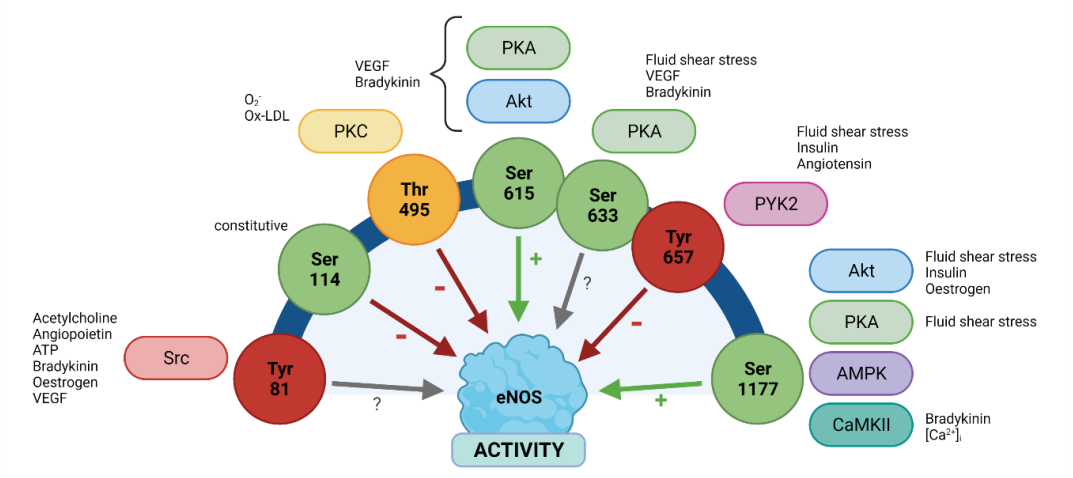

Figure 1-19: Effectors of Endothelial Nitric Oxide Synthase Phosphorylation

Schematic highlighting possible sites for phosphorylation of human endothelial nitric oxide synthase, the effectors of these events and the subsequent effect on enzyme activity. Activation is shown *via* green arrows, inhibition *via* red arrows and the black arrow represents no direct effect on the enzyme activity. Image adapted from (Fleming, 2010) and created with BioRender.com.

1.6.2.2.2. Serine Phosphorylation of eNOS

Phosphorylation of Serine-1177 activates eNOS resulting in an increase in NO production, in the quickest phosphorylation event of all sites discussed in this section. Akt (Hurt et al., 2002), protein kinase A (PKA) (Boo et al., 2002b) and AMPK (Zhang, Y. et al., 2006) may all activate this site, and particularly at higher rates when stimulated by VEGF (Dimmeler et al., 2000), bradykinin (Fleming et al., 2001), fluid shear stress (Dimmeler et al., 1999) or co-association of HSP90 (Bauer et al., 2003).

Serine-633 is located upon one of the auto-inhibitory loops and is considered to be structurally included in such as to sterically impede binding of calmodulin, therefore reducing the rate of catalysis and NO production. It is likely activated *in vivo* by PKA after stimulation by fluid shear stress, VEGF, or bradykinin in a Ca^{2+}-independent manner – however it's true effect overall on eNOS has yet to be confirmed (Boo et al., 2002a; Michell et al., 2002).

The Serine-615 site was initially found by phosphorylation site mapping. It may be phosphorylated by either Akt or PKA, similarly to the S633 site. Bradykinin stimulation is Ca^{2+}-dependent in this particular instance, acting *via* Akt by increasing the calcium sensitivity of calmodulin. VEGF may also induce phosphorylation by acting *via* PKA (Michell et al., 2002), however phosphorylation of S615 has not been shown to directly affect eNOS activity. Instead, it is supposed that it may promote phosphorylation and protein-protein interactions at other sites on the enzyme (Bauer et al., 2003).

Serine-114 is constitutively phosphorylated and is deemed important in agonist-induced NO production (Bauer et al., 2003).

1.6.2.2.3. Threonine Phosphorylation of eNOS

A single threonine residue may be phosphorylated which suppresses eNOS activity: Threonine-495. T-495 is constitutively phosphorylated in endothelial cells and acts by interfering with binding of calmodulin to its binding site (Fleming et al., 2001). Agonists such as bradykinin may elicit a calmodulin-dependent protein kinase II (CaMKII)-independent response to dephosphorylate the enzyme as a means of increasing NO production. Actions of this kind are thought to occur through protein kinase C (PKC) (Davda et al., 1994; Michell et al., 2001).

1.6.2.2.4. Tyrosine Phosphorylation of eNOS

There are several tyrosine residues upon eNOS which are phosphorylatable and certainly the use of tyrosine kinase inhibitors has been shown to diminish NO production highlighting their involvement in regulation of its activity (Ayajiki et al., 1996).

Tyrosine-657 is located within the FMN domain and inhibits the activity of the enzyme. Fisslthaler *et al.* described a shear stress-mediated phosphorylation event *via* PYK2 (Fisslthaler et al., 2008). Mutation of this residue resulted in a complete loss of NO, *L*-citrulline and O_2^- generation, however superoxide species were instead observed (Fisslthaler et al., 2008; Viswambharan et al., 2017). The implications of PYK2 phosphorylation of eNOS will be discussed further in section 1.6.2.3.

Oxidant stress and overexpression of v-Src lead to the phosphorylation of Tyrosine-81, located within the oxygenase domain of eNOS (Fulton et al., 2005). Interestingly, *in vitro* Y81F mutants demonstrated increases in NO production but saw no effect on the maximal activity of the enzyme. Current hypotheses assume that Y81 phosphorylation may modulate the sensitivity of eNOS for Ca^{2+}, altering protein-protein interactions or changing its subcellular location resulting in this observed increase in output. Src-dependent phosphorylation of this site occurs upon stimulation of endothelial cells by acetylcholine, angiopoietin, ATP, bradykinin, oestrogen, and VEGF (Fulton et al., 2005); while this site is acted upon by a large list of agonists, the purpose of this phosphorylation event is yet to be determined.

1.6.2.2.5. Chemical Modulators of Nitric Oxide Synthases

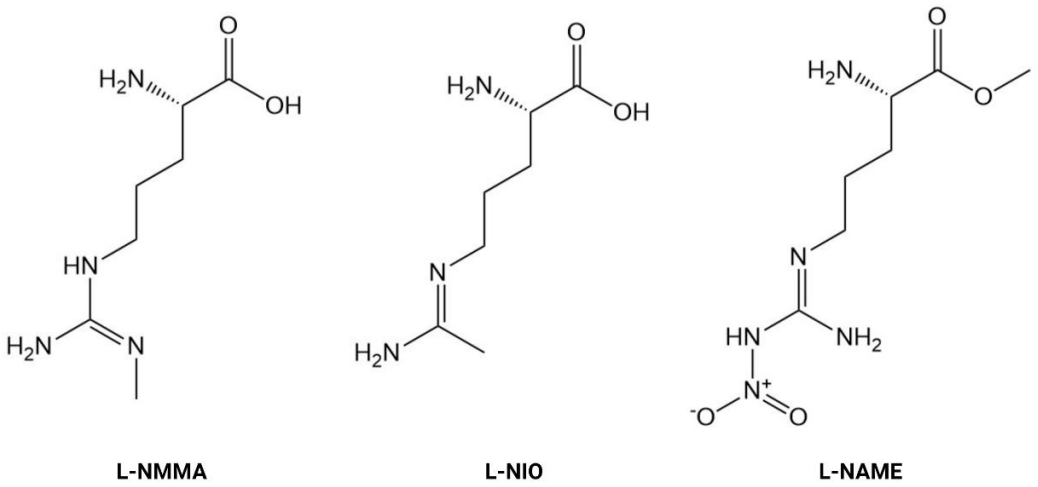

Figure 1-20: Chemical Inhibitors of Nitric Oxide Synthases

Structures of L-NMMA, L-NIO, and L-NAME nitric oxide synthase inhibitors. Structures prepared using PerkinElmer ChemDraw Prime and replicated from (Rees et al., 1990).

In addition to biological modulation of eNOS, regulation of activity by human intervention has also been demonstrated. Three potent chemical inhibitors of all NOS isoforms were reported by Salvador Moncada's group: N^G-monomethyl *L*-arginine (L-NMMA), N^5-(1-iminoethyl)-*L*-ornithine (L-NIO) and N^G-nitro *L*-arginine methyl ester (L-NAME) – synthetic analogues of the *L*-arginine substrate (Figure 1-20) (Palmer et al., 1988; Rees et al., 1990). L-NMMA, the most recognizable species of the trio would inhibit NO production in a dose-dependent manner, resulting in blunted relaxation of rabbit aorta rings. While competitive inhibition at the *L*-arginine binding site has attracted the majority of interest, targeting of BH_4, haem and calmodulin domains have also attracted some focus (Bommel et al., 1998; Wolff et al., 1993).

1.6.2.3. Protein Tyrosine Kinase 2

PYK2 is a redox-sensitive kinase and is one of two members of the focal adhesion kinase (FAK) subfamily of non-receptor tyrosine kinases. PYK2 possesses an important role in many cellular processes, including: cytoskeletal rearrangement, proliferation, migration, inflammatory responses and apoptosis (Shen et al., 2010). It is composed of an N-terminal 4.1 ezrin radixin moesin (FERM) domain, a central catalytic domain and a C-terminus region containing two proline-rich subdomains and a focal adhesion targeting (FAT) domain (Figure 1-21) (Han et al., 2009). The N- and C-terminal lobes are connected by a ‘hinge’ sequence, which partially contains the binding site for ATP and any ATP-competitive inhibitors. The N-terminus also contains an invariant Asp-Phe-Gly (DFG) motif and is a highly important determinant of kinase activity: in ‘DFG-in’ conformation the amino acids are in coordination with the ATP binding site and it is effectively active, however conversely, in ‘DFG-out’ conformation, the kinase does not bind ATP and is inactive.

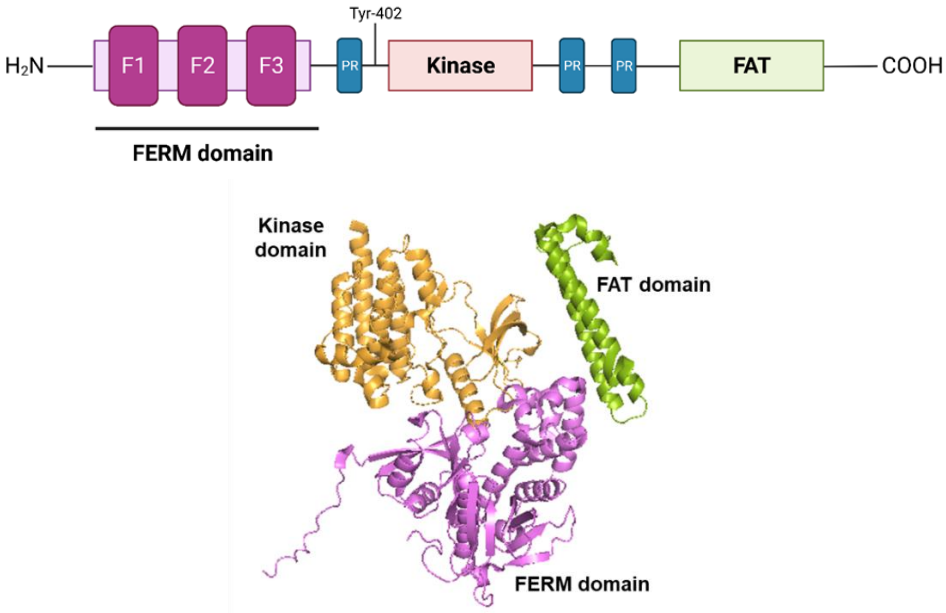

Figure 1-21: Structure of Protein Tyrosine Kinase 2

Top: Schematic of protein tyrosine kinase (PYK2) structure, highlighting individual domains, proline-rich (PR) regions and the Tyr-402 phosphorylation site of interest. Image adapted from (Zhu et al., 2018) and created with BioRender.com. **Bottom:** X-ray crystal structure of PYK2 FERM (purple), kinase (orange) and FAT (green) domains. Image created using manual docking function in PyMOL Molecular Graphics System, version 2.0 Schrödinger, LLC, using PDB 4EKU (Savarimuthu et al., 2012), 3CC6 (Busam et al., 2008) and 4XEK (Vanarotti et al., 2016) respectively, and based upon the predicted PYK2 structure using AlphaFold (Jumper et al., 2021; Varadi et al., 2022).

Whilst PYK2 and its homologue FAK share 48% sequence identity, they have opposing cellular roles. FAK promotes cell cycle progression and survival, however PYK2 tends to inhibit these actions (Naser et al., 2018). Likewise, FAK and PYK2 differ in their distribution of tissues: where FAK is widely expressed, PYK2 is highly localised in areas of the brain, osteoclasts, macrophages, and lymphocytes. However, certain chemical and mechanical stimuli, such as shear and oxidative stress may upregulate expression and activity of PYK2 in other cell and tissue types.

In endothelial cells, a hallmark of PYK2 is its inhibitory effect on eNOS. PYK2 is able to autophosphorylate its Y402 site which phosphorylates the Y657 site of eNOS, in the FMN domain – completely diminishing its activity (Fisslthaler

et al., 2008). The FMN region of eNOS is hypothesized to move in a swinging-like motion, becoming immobilised when phosphorylated at Y657 and remains frozen in an electron-acceptor position, suppressing its activity (Garcin et al., 2004).

PYK2 can be activated by shear stress, in a calcium-dependent manner (Tai et al., 2002) – though in in vitro assays, addition of calcium did not affect PYK2 activity, which was not surprising as PYK2 does not possess any known sequences for Ca^{2+} binding and suggests it is indirectly affected by the influx of ions (Fisslthaler et al., 2008). Production of ROS, both superoxide and hydrogen peroxide (H_2O_2) trigger an influx of Ca^{2+} ions and subsequent autophosphorylation of PYK2 at Y402 (Tai et al., 2002). This observation is interesting as shear stress is known to elicit the activation of eNOS, in endothelial cells and so the contrast of activating a negative regulator to this activity may appear strange at first glance. Shear stress-induced NO production is low, approximately 2-4 times higher than basal levels – significantly lower than agonist-induced stimulation which is over 20-fold higher (Fisslthaler et al., 2008). However, the duration of agonist-induced stimulation lasts for a matter of minutes, whereas shear stress-induced activation will endure so long as the stimulus remains. It is likely that PYK2 is upregulated to maintain low NO output and prevent the possibility of BH_4 depletion which if left unchecked, would cause uncoupling of the enzyme.

ROS production, independent of shear stress, is a hallmark for many cardiovascular diseases and endothelial dysfunction, a precursor to T2DM. ROS, generated by NADPH oxidases, or agents which promote ROS production such as angiotensin II and ET-1 can activate PYK2 Y402

autophosphorylation (Loot et al., 2009; Bibli et al., 2017b). When stimulated by H_2O_2, eNOS undergoes dual phosphorylation by PYK2 at its activatory S1177 site and Y657 inhibitory site. However, the phosphorylation of Y657 maintains dominance over activation of S1177 and the enzyme activity is blocked irrespective of this action (Bibli et al., 2017b). This mechanism is mediated by the PYK2/PI3K/Akt axis, observing recruitment of the PI3K p85 subdomain to PYK2, which are then involved in downstream phosphorylation of Akt. This reaction explains why agents, such as insulin which would otherwise activate the S1177 site *via* the PI3K/Akt signalling pathway, do not increase NO production.

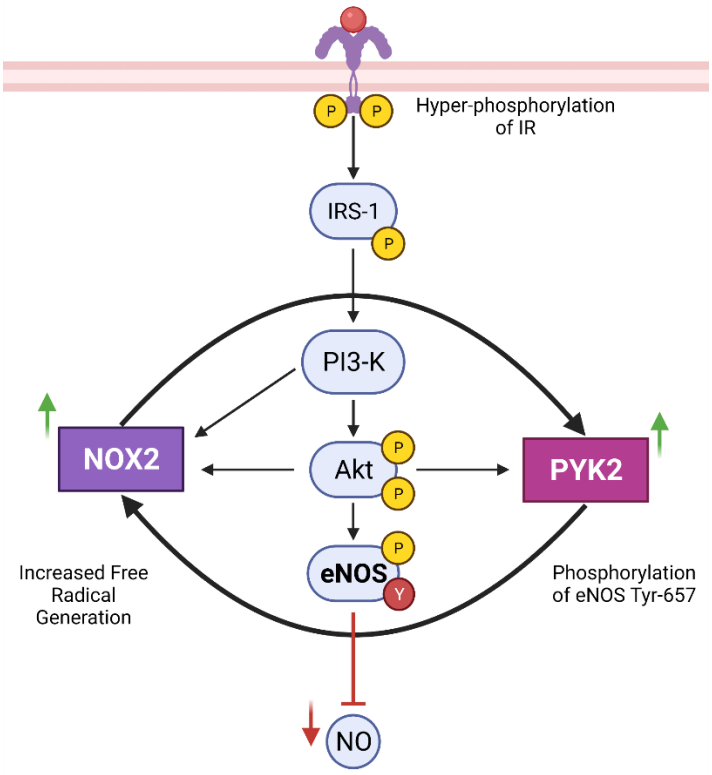

Figure 1-22: Proatherosclerotic Signalling Loop Between PYK2 and NOX2 NADPH oxidase

Proposed mechanism for signalling downstream of the insulin receptor when insulin sensitivity is enhanced, noting a crosstalk loop between NOX2 isoform of NADPH oxidase and PYK2 which results in inhibition of eNOS and subsequent loss of NO bioavailability. Image adapted from (Viswambharan et al., 2017) and created with BioRender.com

In hyperinsulinaemia, a proatherosclerotic signalling loop involving PYK2 has been described in endothelial cells, utilizing an endothelial cell-specific overexpression of the human insulin receptor (hIRECO) mouse model of type-2 diabetes (Viswambharan et al., 2017). The signalling loop was triggered by enhanced insulin action upon the receptor, leading to increases in PYK2 expression, in concert with increased production of superoxide by the NOX2 isoform of NADPH oxidase (Figure 1-22). The effect of mutual upregulation of both species resulted in exaggerated eNOS inhibition and subsequent loss of NO bioavailability. Elevated PYK2 expression feeds back to NOX2, further increasing generation of superoxide and the crosstalk continues, where production of each species bolsters the levels of the other. The reduction in anti-atherogenic products, such as NO, and increase in ROS promotes accelerated progression of atherosclerosis.

As a result of localised upregulation in certain diseases, PYK2 has attracted focus as a novel therapeutic target. Hydrogen sulfide (H_2S) may preserve the function of eNOS by inhibiting PYK2 Y402 activity (Bibli et al., 2017a). H2S acts through post-translational modification of cysteine residues, in a process referred to as sulfhydration, which enhances the production of NO *via* eNOS. Interaction of H_2S in this manner promotes eNOS phosphorylation at the activatory S1177 site and reduces phosphorylation at T495, an inhibitory site. Effect of exposure of H_2O_2 on PYK2 can be effectively reversed by the presence of H_2S. Shear stress may contribute to uncoupling of BH_4 from eNOS, rendering the enzyme catalytically inactive (Yang, Y.M. et al., 2009). H_2S promotes eNOS dimerization and coupling through sulfhydration of C443, restoring its catalytic ability (Bibli et al., 2017a).

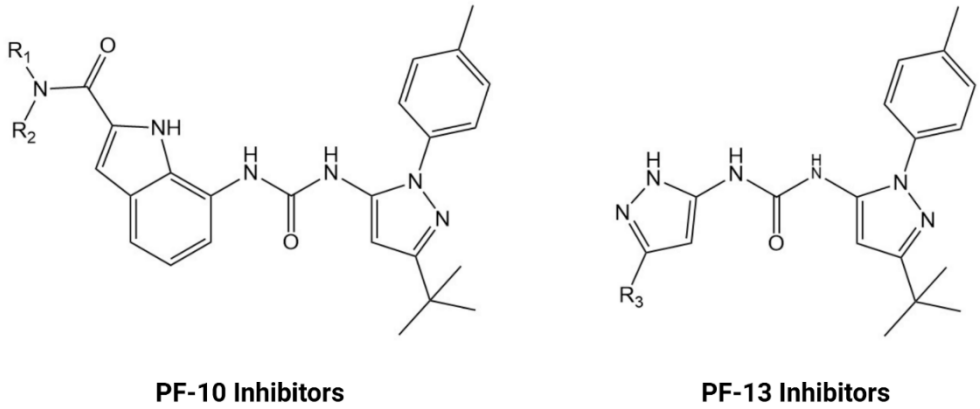

Figure 1-23: Pyrazole and Indole-Urea Based DFG-out PYK2 Inhibitors

Representations of Pfizer (PF) PYK2-selective inhibitor series, disubstituted indole carboxamide ureas (10) and monosubstituted bis-pyrazole ureas (13), where *R* groups indicate points of substitution. Structures prepared using PerkinElmer ChemDraw Prime and based on compounds published in (Bhattacharya et al., 2012).

Due to their structural similarity, it has proven difficult to identify selective PYK2 inhibitors without FAK activity. Bhattacharya *et al.* have designed a series of PYK2-selective (vs. FAK) kinase inhibitors (Figure 1-23) for use as treatment for osteoporosis, as opposed to use of classical inhibitors based on the ATP-binding site which tend to have broader selectivity profiles across kinase panels (Bhattacharya et al., 2012). The novel inhibitors targeted stabilisation of the 'DFG-out' conformation, rendering the protein effectively inactive. Weis *et al.* described a compensatory mechanism involving PYK2 in response to attenuation of FAK expression (Weis, S.M. et al., 2008). FAK is intrinsically involved in angiogenesis, which is a critical factor in the progression of malignant tumours. An inducible EC-specific FAK knockout (*i*-EC-FAK-KO) model showed that where expression of FAK was inhibited, PYK2 expression significantly increased and exhibited a compensatory role in angiogenesis – observing slowed sprouting compared to controls, but a distinct response, nonetheless. Design of an anti-cancer, anti-angiogenic therapeutic would require dual action against both FAK and PYK2.

1.7. Thesis Rationale

Determination of physical and functional interactions between molecular structures is of critical importance to characterise protein-protein complexes and their reaction pathways. In disease, this is paramount to influence or inhibit a dysfunctional system; in human disease, aberrant PPIs are the likely cause of the loss of essential interactions or the formation of a new complex which causes an imbalance to physiological homeostasis. The development of novel therapeutic and selective protein-protein interaction modulators have become increasingly focussed upon, with six therapeutic agents reaching clinical trials as of 2014 (Arkin et al., 2014). Due to the growing prevalence of people with a type-2 diabetes diagnosis, its progressive nature and risk of developing further conditions, such as cardiovascular disease, focus on novel therapeutics in this field is at an all-time high. Current therapies typically target mechanisms promoting a reduction in blood glucose levels, however many patients do not obtain sufficiently adequate glycaemic control using these products, nor observe a particular amelioration of their condition as a consequence (Bailey and Day, 2018). There is a real need for pioneering strategies to alleviate the symptoms of the condition, or restore physiological homeostasis to a healthy normal.

In this thesis, characterisation of two distinct protein-protein interactions were undertaken, each requiring a different approach due to their inherent modes of interaction. Those under focus are the IR/IGF1R hybrid receptor and eNOS-PYK2 interactions, both involved in the insulin signalling pathway of endothelial cells, which is impaired in type-2 diabetes.

The desired outcomes of this thesis were to:

- Characterise the interaction utilizing a minimum of two distinct techniques,
- Identify a small cohort of novel small molecules which have been predicted to inhibit the interaction,
- Determine the subsequent effect of inhibition on cellular function as it relates to type-2 diabetes.

A vast array of techniques across the fields of biochemistry, biophysics and computation were employed to establish understanding of these mechanisms involved in progression of the disease. We hypothesise that targeting these interactions using novel small molecule inhibitors could contribute to restoration of a ‘healthy’ endothelial cell phenotype, alleviation of symptoms associated with type-2 diabetes and subsequent a reduction in risk of developing atherosclerosis.

1.7.1. Insulin Receptor/Insulin-like Growth Factor 1 Receptor Hybrids

Research into IR/IGF1R hybrids has predominantly focussed on their mitogenic effect in human cancers (Pandini et al., 1999; Belfiore et al., 1999). However since the early 1990’s, they have garnered interest regarding their effect on metabolic signalling due to their increased formation and subsequent reduction in available, functional IR and loss of cellular insulin sensitivity in type-2 diabetes (Back and Arnqvist, 2009; Federici et al., 1996; Federici et al., 1997a; Federici et al., 1997b; Federici et al., 1998).

The stimulus which drives formation of these receptors is still unknown, however due to the loss of insulin sensitivity associated with their presence, they directly contribute to endothelial dysfunction and a type-2 diabetes

phenotype. As the structural constituents are desirable to form the native homodimeric receptor proteins, genetic manipulation is not an option and therefore, small molecule modulation presents itself as an ideal solution to promote or inhibit hybrid receptor formation.

Further characterisation of this receptor species could contribute to understanding their role in type-2 diabetes and used as a method to monitor modulation. Design and evaluation of a novel small molecule modulator would not only serve as an investigative tool in research but potentially as a treatment for type-2 diabetes.

1.7.2. Endothelial Nitric Oxide Synthase and Protein Tyrosine Kinase 2β

The interaction between eNOS and PYK2 is largely unexplored, however its involvement in cardiovascular disease has been of great interest to Fleming and colleagues (Dimmeler et al., 1999; Fisslthaler et al., 2008; Loot et al., 2009; Bibli et al., 2017b). In addition, the Kearney group also determined a feedback loop involving eNOS and PYK2, resulting in reduced NO bioavailability in type-2 diabetes (Viswambharan et al., 2017). No target molecule of this interaction exists at present, therefore, a novel eNOS-PYK2 inhibitor could designed as restoring homeostasis may prove beneficial in regenerating phenotypical endothelial cell function, increased NO bioavailability and reduced the risk of atherogenesis.

1.7.3. Molecular Dynamics Simulations

A distinct property of IR/IGF1R hybrid receptors is that they do not bind insulin at physiological concentrations. The structural basis for this loss of sensitivity is unknown. As cryo-EM and x-ray crystallography structures have not been

produced to date, a computational model could be employed to predict which regions are inhibiting association of insulin and, to elucidate why each receptor has a distinct preference for each ligand. Furthermore, as described in section 1.7.1, molecular dynamics could contribute to understanding the role of IR/IGF1R hybrids in disease, in addition to its potential use as a virtual screening tool to identify a new cohort of small molecule modulators.

Methods & Materials

2. Methods

2.1. Endothelial Cell Isolation & Culture

2.1.1. Human Umbilical Vein Endothelial Cells

Pooled donor vials of human umbilical vein endothelial cells (HUVEC) were shipped at passage 'zero' in cryo-medium (PromoCell), on dry ice and stored until use in liquid nitrogen dewars. A single vial was thawed in a water bath at 37°C and its contents were then transferred into 9 mL of full-growth Endothelial Growth Medium 2 (ECGM-2, PromoCell), in a 75 cm^2 tissue culture flask. A full medium change was completed once cells were fully seeded, after several hours but, no later than 24-hours later. HUVEC were expanded into 16 x P2 75 cm^2 tissue culture flasks. Trypsinized, cell suspensions of all flasks were pooled and centrifuged at 400 x g for 8 minutes. The resultant supernatant was discarded, and the cells were resuspended in 8 mL of cryo-medium which was then split sixteen-ways into 1.5 mL cryotubes. All were initially stored at -80°C in a Nalgene® Mr. Frosty™ Cryo Cell Freezing Chamber (Sigma-Aldrich) for 24-hours before being transferred to liquid nitrogen dewars. Each P2 vial was subsequently recovered as required in the same manner as listed above for P0 vials.

HUVEC from passages 2 to 5 were seeded into 75 cm^2 tissue culture flasks and stored in a 5% CO_2, humidified incubator at 37°C. At a minimum of 90% confluence, the cells were washed in Dulbecco Phosphate Buffered Saline (DPBS, PromoCell) before adding 1 mL of 0.05% trypsin (Invitrogen) and placing in the incubator for 3-4 minutes. Cells were resuspended in full growth ECGM-2 and seeded into a fresh tissue culture flask or cell culture plate.

2.1.2. EA.hy926

Dr. Natalie North kindly gifted the use of a single P0 vial of EA.hy926 cells from her liquid nitrogen dewar. The vial was thawed, passaged and seeded as described in section 2.1.1, H, using instead full-growth DMEM (high glucose, pyruvate; 10% FCS, 1% AAS, ThermoFisher).

2.1.3. Outgrowth Endothelial Cells

Dr. Thomas Slater kindly gifted the use of several pre-plated 6-well plates of OECs. The wells were washed in 2 mL of DPBS (PromoCell) and cultured in 2 mL of EGM™-2 (Lonza).

2.1.4. Murine Pulmonary Endothelial Cells

Murine pulmonary tissue was harvested and collected into 5 mL ice-cold Hanks Balanced Salt Solution (HBSS, ThermoFisher). The tissue was then transferred into a petri dish and minced to 1 mm^2 in 100 µL of 1 mg/mL collagenase-HBSS, for 5-7 minutes. Pieces were transferred into 10 mL of collagenase and incubated at 37°C on a rotator for 45 minutes. Tissue aggregates were reduced by pipetting up and down 40 times. The collagenase-tissue mix was then filtered through a 70 µM cell sieve, before centrifuging the filtrate at 300 x g for 5 minutes. The supernatant was discarded, and the pellet was resuspended in 5 mL PBE buffer, repeating the centrifugation step as before. The pellet was resuspended in 200 µL PBE and, transferred to a 1.5 mL Eppendorf. CD146 (LSEC) microbeads (20 µL, Miltenyi Biotec, Germany) were added and incubated at 4°C on a rotator for 20 minutes. Upon completion, the pellet was washed in 1 mL PBE and centrifuged at 4000 RPM for 5 minutes. The pellet was resuspended in 500 µL PBE, then the cell suspension was filtered using a MS Column (Miltenyi

Biotec), washing using 3 x 500 µL PBE. To collect the pulmonary endothelial cells (PEC), the column was placed into a collection tube containing 1 mL PBE and centrifuged at 4000 RPM for 5 minutes. The pellet was resuspended in 500 µL Endothelial Cell Growth Medium MV (ECGM MV, PromoCell) and added to 4 wells of a fibronectin-coated 6-well plate. The medium was replaced with fresh ECGM MV after 2- and 24-hours.

2.1.5. Homogenisation of Murine and Human Tissues

A 3 cm^2 section of tissue was cut and placed in a 2.2 mL round-bottomed tube containing 1 mL lysis buffer and two stainless steel ball bearings (Qiagen). The TissueLyser II (Qiagen) was run at 30 Hz, 5 times for 15 seconds, at 30 second intervals. The tissue lysate was centrifuged twice at 17,000 x g for 10 minutes at 4°C. The supernatant was collected and stored at -80°C until use.

2.1.6. Human Saphenous Vein Endothelial Cells

2.1.6.1. Isolation of SV endothelial cells

Saphenous veins (SV) were obtained from consenting patients undergoing coronary artery bypass graft surgeries at the Leeds General Infirmary (Ethical Approval CA01/040). The donations were stored in-transit in sterile Gibco Medium 199 (M199, Sigma-Aldrich) until the start of the isolation process.

In a sterile laminar flow hood, the vessels were cut longitudinally and pinned open onto a sylgaard-coated petri dish – with the lumen facing upwards. The vessel was then immersed in 5 mL of 1 mg/mL collagenase Type II (Worthington Biomedical)-HBSS and incubated for 10 minutes at 37°C in a 5% CO_2, humidified incubator. The collagenase solution was aspirated dropwise over the tissue several times to dislodge any cells. The collagenase solution was removed from the dish and collected. A 10 mL aliquot of Gibco

DMEM containing 4.5% FCS, 2mM *L*-glutamine and 1% AAS (Sigma-Aldrich) was added in the same manner and the vessel was agitated and collected as before. This step was repeated for a second time and added to the same collection tube. The tube containing the extracted cells was centrifuged at 600 x g, 4°C for 6 minutes. The supernatant was discarded from the pelleted cells and resuspended in a further 25 mL of DMEM and centrifuged as before, for 10 minutes. The supernatant was discarded again, and the pelleted cells were resuspended in 2 mL of Endothelial Cell Growth Medium MV2 containing 10% FCS & 1% AAS (ECGM MV2, PromoCell). The cells were then plated into one well of a six-well plate and incubated at 37°C in a 5% CO_2, humidified incubator. A full medium change occurred after 2 days.

2.1.6.2. Culture of SV endothelial cells

Human saphenous vein endothelial cells (SVEC) were primarily obtained from Dr. Karen Porter's historical liquid nitrogen stocks and kindly granted for use in both hybrid and eNOS-PYK2 projects.

Cells at P2 were recovered from liquid nitrogen and transferred into a 75 cm^2 tissue culture flask containing 16 mL ECGM MV2 (PromoCell). Confluent SVEC at P3-P7 were washed in 2 mL of DPBS and trypsinized in 1 mL of 0.05% trypsin (Invitrogen) for 2-3 minutes at 37°C in a 5% CO_2, humidified incubator. The trypsin was neutralized by addition of 16 mL of ECGM MV2, in small aliquoted amounts. In a 75 cm^2 flask, 8 mL of cell suspension was seeded and topped up with ECGM MV2 medium. The remaining cell suspension was seeded into a single 6-well plate.

2.1.7. Human Adipose Tissue Endothelial Cells

2.1.7.1. Isolation of AT endothelial cells

Human adipose tissues (AT) were obtained from consenting patients undergoing biopsies in pacemaker implant clinics at the Leeds General Infirmary (Ethical Approval 11/YH/0291). The endothelial cells were isolated by Dr. Jason Scragg and Mrs. Jessica Smith. These cells were kindly gifted for use in both hybrid and eNOS-PYK2 projects.

2.1.7.2. Culture of AT endothelial cells

Human adipose tissue endothelial cells (ATEC) obtained were expanded from a single well of a 6-well plate at a ratio of 1:6. Cells were used between passages 2-5. Confluent ATEC were washed in 2 mL of DPBS and trypsinized in 400 µL of 0.05% trypsin (Invitrogen) for 5-6 minutes at 37°C in a 5% CO_2, humidified incubator. The trypsin was neutralized by addition of 1600 µL of ECGM MV and reseeded across a fresh 6-well plate.

2.2. Endothelial Cell Treatment & Transfection

2.2.1. siRNA Transfection

Cells were transfected at 90-95% confluency. A combination of 2 µL of Lipofectamine™ 2000 (Invitrogen) and 400 µL of Opti-MEM I Reduced Serum Media (ThermoFisher) was added to a solution of 2 µL of siRNA (Dharmacon) and 400 µL of Opti-MEM medium, then incubated at ambient temperature for 20 minutes. The transfection media was added to the cells in a six-well plate. The transfection media was left on the cells for 4-hours before reverting to the original growth medium. The cells were then analysed after 48-hours after transfection.

2.2.2. PBS Treatment

Cells were treated at 90-95% confluency. DPBS was diluted in 2 mL ECGM-2 aliquots to produce a 1 µL/mL treatment condition to mimic the volume added in insulin and IGF-1 treatments (section 2.2.4). Each aliquot was added to two wells of a 6-well plate and incubated for 24-hours.

2.2.3. H_2O_2 Treatment

Cells were treated at 90-95% confluency. H_2O_2 (30% w/v, Sigma-Aldrich) was diluted in 4 mL ECGM-2 aliquots to produce 0, 10, 25, 50, 100 and 250 µM treatment conditions. Each aliquot was added to two wells of a 6-well plate and incubated for 24-hours.

2.2.4. Insulin/IGF-1 Treatment

Cells were treated at 90-95% confluency. Plates were serum-starved Gibco M199 containing in 2% FCS, 1% AAS for 16-hours overnight prior to stimulation.

Human insulin (100 mM, Sigma-Aldrich) and IGF-1 stocks (100 mM, Gropep) were both diluted to 100 nM in HEPES buffer. Insulin and IGF-1 were added as 1 µL/mL aliquots directly to each well and incubated at 37°C in a 5% CO_2, humidified incubator for 15-minutes. The reaction was quenched by placing the plate on ice, removing the treated medium and washing in ice-cold DPBS (PromoCell).

2.2.5. Hybrid Inhibitor Compound Treatment Procedure

Cells were treated at 90-95% confluency. An aliquot of compound (10 mM stock solution in DMSO) was diluted in 4 mL of ECGM-2 aliquots (PromoCell) to produce the desired concentration of inhibitor. Control vehicle (DMSO,

Sigma-Aldrich) wells were treated in the same way. Each solution was added to two wells of the six-well plate. Cells were incubated with compound for either short-term (6-hours) or longer-term (24-hours) treatment.

Images of compound treatment condition effects taken using the IncuCyte® ZOOM (Sartorius) system and its proprietary ZOOM 2016A software.

2.2.6. Pfizer PF-10e Compound Treatment

Cells were treated at 90-95% confluency. A 10 µM solution of PF-10e (10 mM stock in DMSO; Pfizer) was added to serum-starved (0.2% FCS) Gibco M199. Cells in five of the six wells were immersed in SSM – three containing 10 µM PF-10e, and the remaining well in full-growth ECGM-2. The plate was incubated at 37°C in a 5% CO_2, humidified incubator for 24-hours.

Prior to the end of the treatment period, 100 nM insulin was added to the medium for 15 minutes at room temperature. To quench the interaction, ice-cold DPBS was added to each well and the cells were lysed as described in section 2.3, Cell Lysis.

2.2.7. Murine Mini-Pump Treatment

Mini-osmotic pumps (#1002, ALZET) were subcutaneously implanted into C57BL/6J mice for a period of two weeks. Pumps contained either 10 µM PF-10e inhibitor or DMSO, in PEG-300 (51.6:48.4% v/v) and released a continuous dose of the aforementioned solutions for the duration of the treatment period.

Murine tissues were harvested upon completion of the experiment by Dr. Nadira Yuldasheva and were stored at -80°C until use. Tissues were

prepared for western blotting as described in section 2.1.5, Homogenisation of Murine and Human Tissues.

2.2.8. Fluid Shear Stress

Cells were selected at 90% confluency. Confluent monolayers of cells in full growth medium were placed onto an orbital rotating platform at 210 RPM, inside a 5% CO_2, humidified incubator at 37°C for the duration of the experimental period. Cells were immediately lysed upon completion of the experiment as described in section 2.3, Cell Lysis.

2.3. Cell Lysis

Cells were cultured in a 6-well plate as described above. Prior to lysis, cells were washed twice in 2 mL of ice-cold phosphate-buffered saline solution (DPBS, PromoCell). A 100 µL aliquot of Cell Extraction Buffer (CEB, Fisher Scientific) containing 1 µL/mL phosphatase and protease inhibitors (Sigma-Aldrich), was added to each well and left on ice for 3 minutes. The cells were scraped, collected, and transferred to the second well where the same process was repeated. The two combined wells' lysates were incubated on ice, with intermittent pipetting or vortexing for 20 minutes. A 15-minute centrifugation step at 4°C and 17,000 x g was performed, and the supernatant collected into fresh Eppendorf tubes. Protein Quantification was performed using the Pierce™ BCA Protein Assay kit (Thermo Scientific) as per manufacturer's protocol. The resultant data were exported into Microsoft Excel for further data transformation.

2.4. Protein Production

2.4.1. Cloning of PYK2 reductase domain gene

A manual PCR reaction was performed by combining 5 µL of 5x Q5 reaction buffer, 0.5 µL of 10 mM dNTPs, 1.25 µL of 10 µM forward primer (1:10), 1.25 µL of 10 µM reverse primer (1:10), 1 µL template DNA (1:100), 0.25 µL Q5 DNA polymerase, 5 µL 5x Q5 high GC enhancer, 10.75 µL nuclease-free water into a single 0.2 mL PCR tube and pipetting two to three times to mix.

The Q5 program on the Veriti Thermal Cycler (ThermoFisher) system was run accordingly:

1 cycle	Initial denaturation	98°C	30 secs
30 cycles	Denaturation	98°C	5 secs
	Annealing	60°C	20 secs
	Elongation	72°C	20 secs per kB
	Final extension	72°C	120 secs
1 cycle	Hold	4°C	∞

The resulting HiFi assembly reaction samples were analysed *via* agarose gel electrophoresis. An agarose gel (1.2% agarose in 1 x TBE buffer, 1:10,000 SYBRSafe, Invitrogen) was loaded with 2 µL 6 x DNA loading dye combined with 5 µL HiFi assembly sample versus 5 µL Quick-load Purple 2-Log DNA ladder (NEB). The gel was run for 40 minutes at 80 V, at constant voltage then imaged upon completion on the G:Box (SynGene). The samples were purified using a QIAquick PCR Purification Kit (Qiagen) according to manufacturer's protocol.

2.4.2. Transformation of pOPIN vectors

The following plasmids were a gift from Ray Owens:

Vector	Tag	ID	Origin
pOPINF	His6-3C-POI	#26042	Addgene
pOPINJ	His6-GST-3C-POI	#26045	Addgene
pOPINM	His6-MBP-3C-POI	#26044	Addgene
pOPINS3C	His6-SUMO-3C-POI	#41115	Addgene

A combination of 7 µL of nuclease-free water, 2 µL of DNA and 1µL of plasmid was incubated at 50°C for 1 hour. Competent 5α cells (NEB) were thawed in a freezer block, where 50 µL was combined with 2 µL of HiFi assembly reaction sample and flicked two to three times to mix. A 30-minute incubation period occurred prior to a heat shock for 45 seconds at 42°C and returned to the freezer block for a further 2 minutes. A 250 µL aliquot of SOC media was added to each sample and incubated at 37°C for 1 hour on a benchtop shaker (StarLab) at 1200 RPM. The final mix was spread across Luria Broth agar plates (LB, 1% w/v Tryptone, 1% w/v NaCl, 0.5% w/v Yeast extract, 1.5% w/v agar) containing 100 µg/mL Ampicillin and 20 µg/mL X-gal, then incubated overnight at 37°C. Using sterile toothpicks, single colonies were selected from the HiFi assembly transformation plate and added to 1 mL of selective LB containing 100 µg/mL, in a 2.2 mL 96-well deep well block. A gas-permeable seal was added and left to grow overnight at 37°C at 220 RPM. The cultures were spun down at 4000xg for 10 minutes, then the media was removed. The samples were processed using the Hamilton MicroLab Star, resulting in a purified plasmid DNA in 96-well PCR plate. The samples were analysed *via* agarose gel electrophoresis (1.2% agarose in 1 x TBE buffer, 1:10,000 SYBRSafe); 10 µL samples were loaded versus 5 µL Quick-load Purple 2-

Log DNA ladder (NEB). The gel was run for 1 hour at 100 V, at constant voltage and imaged on the G:Box (SynGene). The successful clones were selected and sent to Eurofins for sequencing. The samples contained 15 µL of plasmid DNA and 2 µL of pOPIN reverse primer.

2.4.3. Expression of PYK2 reductase domain in *E.coli*

2.4.3.1. Small scale production

Thawed competent cells: DH5α (NEB), Rosetta 2(DE3) (Merck), SHuffle T7 (NEB), BL21(DE3) (NEB) and Lemo21(DE3) (NEB) were transformed separately with 1 µL of each pOPIN plasmid. The tubes were flicked two to three times to mix then returned to the freezer block for a 30-minute incubation period. Proceeding steps were identical to initial transformation protocol detailed in the section 2.4.2.

pOPINM was transformed into competent SHuffle T7, pOPINS into Lemo21 (0 µM *L*-rhamnose) as before. Proceeding steps were followed as in section 2.4.2 using 10 mL of selective LB. The cultures were then centrifuged at 4000 x g, 4°C for 20 minutes. The cells were lysed by resuspending the pellet in 10 mL of lysis buffer (50 mM Tris, pH 7.6; 300 mM NaCl; 20 mM imidazole; 5% v/v glycerol) containing 500 µL of 30 mg/mL lysozyme and incubated on ice for 20 minutes. Using a sonicator, the cells were mixed on ice for 10 seconds, ten times at medium amplitude. The lysate was cleared by centrifuging at 35,000 x g for 40 minutes at 4°C. The cleared lysate was combined with 100 µL of Ni-NTA agarose beads (Qiagen) and incubate at 4°C for 1 hour on a rotator. The unbound lysate was produced by centrifuging at 500 x g for 5 minutes at 4°C, then washed twice with 5 mL of wash buffer (‘lysis buffer’), incubating for 5 minutes. The Ni^{2+} beads were resuspended in

1 mL of each elution buffer (50 mM Tris, pH 7.6; 300 mM NaCl; 40/80/160/240/320 mM imidazole; 5% v/v glycerol), incubate for 15 minutes and centrifuge at 500 x g for 5 minutes at 4°C. The samples were analysed by 4-12% SDS coomassie and western blots.

2.4.3.2. Large-Scale production

A colony from the plate containing SHuffle T7-transformed pOPINM cells was selected and grown in 1 L of starter culture overnight at 37°C, 220 RPM. An aliquot of 150 mL was added to 6 x 1 L of LB in baffled flasks, then left to grow at 37°C, 180 RPM until an OD_{600} reached 0.6. The cultures were induced with 4.6 mL of 0.1 M IPTG and returned to incubate at 18°C, 180 RPM. The cultures were centrifuged at 4000xg, 4°C for 30 minutes, discarding the cleared lysate. The pellets were stored at -20°C until His purification was carried out.

Pellets were resuspended in 40 mL of lysis buffer (50 mM Tris pH 7.6, 0.5 M NaCl, 20 mM imidazole, 5% v/v glycerol, 0.075% β-mercaptoethanol) per litre of original culture stock and added 400 µL of Proteoloc EDTA-free Protease Inhibitor Cocktail (Abcam) per 40 mL of suspension. The lysed samples were centrifuged in the Lynx6000 at 30,000 x g for 45-minutes at 4°C to clear the lysate. The cleared lysate was injected into the ÄKTA Pure liquid chromatography system (Cytiva), containing a 5 mL HisTrap FF column (Cytiva). Wash buffer (50 mM Tris pH 7.6, 0.5 M NaCl, 20 mM imidazole, 5% v/v glycerol, 0.075% β-mercaptoethanol) was flowed through the system and collected as distinct aliquots and stored at 4°C. Immediately following, an elution buffer (50 mM Tris pH 7.6, 0.3 M NaCl, 0.4 M imidazole, 5% v/v glycerol, 0.075% β-mercaptoethanol) was flowed through the system,

designed to remove the protein bound to the Ni^{2+} surface *via* its 6His tag. These elutions were also collected as distinct aliquots and stored at 4°C. The wash buffer and elution aliquots were analysed by 4-12% SDS coomassie gels to locate the elutions containing PYK2-MBP protein.

The elutions containing PYK2-MBP were combined and dialysed overnight in the wash buffer containing a His-tagged 3C protease. Elutions containing PYK2-MBP were pooled and injected into the ÄKTA Pure system, containing the same HisTrap FF column. The His-MBP tag and His-3C should bind the column and the cleaved protein should elute from the column and be collected in the initial fractions. The collected elutions were analysed by 4-12% SDS coomassie gels to locate the specific elutions containing cleaved PYK2 protein.

Elutions containing the cleaved protein were pooled into a 10K MWCO protein concentrator (ThermoFisher) ultrafiltration centrifugal device and centrifuged at 15,000 x g for 10 minutes. The concentrated protein sample and tag cleavage elutions were analysed by 4-12% SDS coomassie gels and western blots.

2.4.4. Expression of PYK2 reductase domain in Sf9-cells

Sf9 insect cells were cultured in Gibco™ Sf-900™ II Serum Free Medium (SFM, Invitrogen) without serum or antibiotics. All cells were grown at 28°C in a 5% CO_2, humidified incubator.

2.4.4.1. Transfection of *flash*BAC™ and PYK2 RD cDNA

The following plasmids were a gift from Ray Owens:

Vector	Tag	ID	Origin
pOPINF	His6-3C-POI	#26042	Addgene
pOPINJ	His6-GST-3C-POI	#26045	Addgene
pOPINM	His6-MBP-3C-POI	#26044	Addgene
pOPINS3C	His6-SUMO-3C-POI	#41115	Addgene
pOPINN-GFP	N-His-GFP-POI	#53541	Addgene

Cells were seeded using Sf-900™ II Serum Free Medium (Invitrogen), 0.5 x 10^5 Sf9 cells per well of a 6-well plate and left to seed for 1 hour in the incubator at 28°C.

The recombinant virus was generated by combining 1 µL of PYK2 RD cDNA with 5 µL of *flash*BAC™ Baculovirus Expression System (Mirus) and 100 µL SFM, and in a separate vessel, 1.2 µL of Cellfectin™ II Reagent (ThermoFisher Scientific) was added to 100 µL SFM. Both vessels were incubated for 5 minutes prior to combination and further incubated for 20 minutes at room temperature. Dropwise, the transfection reagents were added to a single well containing 0.5 x 10^6 cells/mL in 2 mL of SFM and incubated for 7-10 days.

The cells were checked for signs of infection using the pOPINN-GFP control well, taking a grainy, rounded and enlarged appearance, throughout the 7-10 days. These characteristics were observed using an EVOS Auto FL 2 with 4x, 10x, 20x and 40x objectives and phase/red/green/blue. At the end of this period, the baculovirus-infected supernatant was collected by centrifugation at 300 x g for 5 minutes, and stored at 4°C, protected from light.

2.4.4.2. Virus amplification

A maximum of 0.5 mL of virus seed stock (P0) was added to a single Erlenmeyer shake flask containing 2.0 x 10^6 cells/mL in 100 mL SFM and incubated at 28°C, shaking at 130 RPM over 3-4 days. Once infected as in section 2.4.4.1, Transfection of *flashBAC*™ and PYK2 RD cDNA, the virus seed stock was collected by centrifugation at 3,000 RPM for 15 minutes at 4°C. Virus amplification is performed twice (P1 & P2) before use in large scale protein production.

2.4.4.3. Plaque Assay

After collection of both P1 and P2 virus seed stocks, a plaque assay is performed to determine the efficacy of infection and therefore the appropriate point to progress onto protein production.

Serial log dilutions of each virus (10^{-1} to 10^{-7}) were prepared in SFM by transferring 50 µL of undiluted recombinant virus into the first dilution tube and serially transferring 50 µL to the tube in sequence. For each virus, 10 wells in 6-well plates were prepared, containing seeded 0.45 x 10^6 cells/mL in 2 mL of SFM. Prior to the addition of the viral titers, 1.7 mL of medium in each well was discarded and replaced with 100 µL of dilutions 10^{-4} to 10^{-7} or 100 µL SFM media controls. The plates were incubated at room temperature for 1 hour to allow for virus absorption.

At approximately 15 minutes before the end of the incubation period, the LGT agarose was prepared by melting 15 mL aliquots of pre-prepared 2% w/v LGT in a microwave. Once the temperature of the agarose was tolerable to touch (~50°C) and equal volume of SFM was combined. The virus inoculum was quickly removed, and 2 mL agarose mix was pipetted atop the cells carefully

to prevent disturbing the monolayer below. The plates were incubated once more for 15 minutes at room temperature. Once the agarose had solidified, 1 mL of SFM was added to each well as a liquid feed before returning to the 28°C incubator for 4 days.

The following step was not performed, however proceeds as follows:

After the 4 days, a confluent monolayer should be present in each well. The liquid overlay would be removed and replaced with 1 mL diluted Neutral Red stain. The plates would be incubated for 4 hours in the 28°C incubator and at the end of the incubation period, the stain would be removed, and the plates would be inverted before imaging, in the dark.

2.5. *In vitro* Cell Assays

2.5.1. Proliferation

HUVEC were seeded at a density of 20,000 cells per well in a 24-well plate and immersed in 1 mL ECGM-2, containing 100 µM HI-2 or 0.1% v/v DMSO at 37°C in a 5% CO_2, humidified incubator for 24-hours. A 1 µL aliquot of EdU (1:1000) in ECGM-2 was then added to each well and incubated for a further 2 hours. Between each addition, the cells were washed twice in DPBS. The cells were incubated in 1 mL of 4% PFA (ThermoFisher) for 15 minutes at room temperature. To permeabilise the cells, 1 mL of PBS containing 0.5% Triton-X100 (ThermoFisher) was added, and they were further incubated for 20 minutes at room temperature. A 100 µL aliquot of the ClickIT Cocktail was added to each well and incubated for 30 minutes at room temperature, in the dark. A final application with 500 µL propidium iodide was added and incubated for 15 minutes at room temperature, in the dark. The cells were immersed in DPBS during the imaging process.

Four wells per treatment condition were prepared. Images at four distinct locations within each well were sampled using the IncuCyte® ZOOM (Sartorius) system and its proprietary ZOOM 2016A software. Images were analyzed using NIH ImageJ multi-point tool function and exported to Microsoft Excel for further data transformation.

2.5.2. Wound Closure

A 96-well IncuCyte® Imagelock plates (Sartorius) were coated using a 2% bovine gelatin solution in DPBS and placed in a 5% CO_2, humidified incubator to polymerize for 15 minutes. Prior to seeding, the excess gelatin was flushed out by two DPBS washes.

HUVEC at passages 2-5 were trypsinzied for 3-4 minutes in a 5% CO_2, humidified incubator and pelleted by centrifugation at 400 x g for 8 minutes. The cells were then seeded at a density of 200,000 cells/mL and pipetting 200 µL per well – or 200 µL DPBS to any empty wells.

Approximately two days later, once a completely confluent monolayer of cells had formed, a wound was created using the Essen Woundmaker. The 96-well plate was slotted into the device and the scratch was created by utilizing the lever. All wells were carefully washed in 100 µL PBS and checked which wells contained a full scratch using a microscope. Compound treated—ECGM-2 aliquots were added to selected wells before being inserted into the IncuCyte® ZOOM for 24-hour image sampling.

A minimum of three successful scratches per treatment condition were prepared. Images were analyzed using NIH ImageJ freehand selection tool to measure the relative wound density and the resultant data were exported to Microsoft Excel for further data transformation.

2.5.3. Bead Sprouting

Individual 25 cm^2 tissue culture flasks of P3 HUVEC were trypsinized, collected and counted to prepare a cell suspension density of 200,000 cells/mL. The Cytodex-3 beads (Amersham) were combined with 1 mL of cell suspension and transferred to a FAC tube. The beads were then agitated every 20 minutes for a minimum of 4.5 hours. After this period, the beads were transferred to individual 25 cm^2 culture flask in 4 mL ECGM-2 and left in the 5% CO_2, humidified incubator overnight.

On the second day, the beads were gently dislodged from the culture flask and washed in ECGM-2 until suspended in approximately 10 mL of culture media. The beads were then left to settle for 15 minutes and resuspended in 1 mL ECGM-2. The beads were washed thrice more in 1 mL ECGM-2, allowing the beads to settle for 5 minutes each time. After the last wash, the beads were resuspended in a 2 mg/mL fibrinogen master mix containing 37.5 µL aprotinin, 5 ng/mL VEGF and FGF and 100 µM HI-2 or 0.1% v/v DMSO vehicle control. The 24-well plates were prepared by adding 12.5µL thrombin (Sigma-Aldrich) to each well. To trigger clot formation, 500 µL of the bead suspension/fibrinogen mix was combined and spread evenly across the surface. The finished plates were left to sit for 5 minutes in the laminar flow hood before being moved to a 37°C in a 5% CO_2 incubator for 20 minutes to allow clots to solidify. Once clotted, 1 mL ECGM-2 was added dropwise to each well and then incubated for 24-hours before imaging.

Four wells for each treatment condition were prepared. A minimum of ten beads were selected on the basis that their growth was unaffected by adjacent beads or the edges of the dish. The Olympus fluorescence microscope was

set at 10X magnification, with a camera attachment to sample images of individual beads. NIH ImageJ analysis function was used to measure sprout number and length, and the resultant data were exported to Microsoft Excel for further data transformation.

2.5.4. Tube Formation

HUVEC at passage 3 or 4 maximum were seeded in a six-well plate. Once reaching a minimum of 90% confluency, the cells were washed in PBS and treated for 24-hours with 100 µM HI-2 and 0.1% v/v DMSO vehicle control.

On the second day, a 24-well plate was coated with ice-cold Matrigel matrix (GFR LDEV-free, Corning), transferred from the bottle using ice-cold pipette tips. The plate was placed in a 5% CO_2, humidified incubator to polymerize. At the end of the 24-hours, each treatment condition was trypsinized separately for 3-4 minutes in the incubator, before counting the cell number using the Scepter™ 2.0 Cell Counter (ThermoFisher). The cells were then centrifuged at 400 x g for 8 minutes and resuspended in a defined volume of full-growth, compound-treated ECGM-2 such that the concentration of cells was 1 x 10^5 cells/mL. A millilitre of individually-treated cell suspensions were added to a single coated well of the 24-well plate before being returned to the incubator for 4-hours.

Images at five distinct locations within each well were sampled using the IncuCyte® ZOOM (Sartorius) system and its proprietary ZOOM 2016A software. Images were analyzed using NIH ImageJ multi-point tool function and exported to Microsoft Excel for further data transformation.

2.5.5. Proximity Ligation

50,000 cells per well of a µ-Slide 8-well plate (ibidi) were seeded and incubated overnight as per manufacturer's protocol. The cells were washed twice in warm DPBS (PromoCell), fixed using 4% PFA (ThermoFisher) and permeabilized using 0.1% Triton-X100 (ThermoFisher) for 5 minutes. The cells were blocked in DuoLink Blocking Solution (Sigma-Aldrich) for 1 hour then incubated overnight in primary antibodies (eNOS BD 610297 1:100 in DuoLink Antibody Diluent; PYK2 CS 3292 1:100 in DuoLink Antibody Diluent) as before. The cells were washed in Wash buffer A 2 x 5 minutes and incubated with PLUS and MINUS PLA probes (1:5 DuoLink Antibody Diluent) for 1 hour. The cells were washed and were incubated with ligase (1:40 in ligation buffer) for 30 minutes, then further washed as before and incubated with polymerase (1:80 in amplification buffer) for 100 minutes. The cells were washed a final time in Wash buffer B and incubated overnight in Phalloidin-Alexa Fluor 488 (1:100 in PBS) at 4°C. The following morning, cells were washed in PBS then incubated DAPI (1:1000) for 10 minutes. Six drops of ibidi mounting medium were added and then stored at 4°C in the dark until use.

Images were sampled on the Zeiss LSM880 inverted confocal microscope using a 40x/1.4NA Plan Apochromat oil objective and processed by the proprietary ZEN software.

2.5.6. Cell Length Calculations

Changes in cell length and shape observed in HI-2 dose response curves and scratch wound healing at 100 µM over 24-hours, in HUVEC. A single shot of the entire well was sampled using the IncuCyte® ZOOM (Sartorius) system

and its proprietary ZOOM 2016A software. Cell lengths of 20 individual cells per well were analyzed using NIH ImageJ freehand lines tool function and exported to Microsoft Excel for further data transformation.

2.6. Biochemical Assays

2.6.1. Quantitative PCR

Confluent monolayers of HUVEC, SVEC and ATEC were lysed by addition of 0.05% trypsin (Invitrogen) and neutralized using their respective media (ECGM-2, MV, MV2; PromoCell). Two wells of the 6-well plate, sharing the same compound or vehicle-treatment were combined and centrifuged at 1000 x g for 8 minutes at 4°C. The cells were resuspended in DPBS and centrifuged once more under the same conditions. The pelleted cells were dried and stored at -80°C until use.

RNA extraction was performed using the Monarch Total RNA Miniprep Kit (NEB), according to manufacturer's protocol. The frozen pellets were removed from storage and left to equilibrate to room temperature before suspending the cells in 300 µL of RNA Lysis Buffer. The cell suspension was transferred to a gDNA removal column, fitted with a fresh collection tube, and centrifuged at 16,000xg for 30 seconds. The flow-through was combined with 300 µL of ethanol and then transferred to an RNA purification column, fitted with a fresh collection tube, and centrifuged as before. The flow-through was discarded and 500 µL of RNA Wash Buffer was added to the column and centrifuged as before, discarding the flow-through once more. This step was repeated with a second addition of 500 µL RNA Wash Buffer, centrifuged at 16,000xg for 2 minutes. The RNA was collected from the column into a fresh collection tube, by addition of 30-50 µL of Nuclease-free Water, centrifuging the column as

before for 30 seconds. The resultant RNA samples were placed on ice for duration of the experiment.

RNA quantitation was performed using the DS-11 FX+ Spectrophotometer/ Fluorometer (DeNovix) by addition of 2 µL of RNA sample to the crystal plate. Data recorded on the device was collected and exported into Microsoft Excel for further data transformation.

Reverse transcription of RNA to cDNA was performed by combining pre-determined volumes of the RNA samples with the LunaScript™ RT SuperMix (5X) (NEB) in 20 µL aliquots. These were cycled through the following protocol in the PTC-200 Thermal Cycler (MJ Research):

Cycle Step	Temperature (°C)	Time (min)	Cycles
Primer Annealing	25	2	1
cDNA Synthesis	55	10	
Heat Inactivation	95	1	

The cDNA samples were diluted in Nuclease-free water (NEB) to 10 ng/µL, before use in qPCR reactions. The qPCR samples were prepared by combining the cDNA samples with iTaq™ Universal SYBR® Green Supermix (BioRad) and analysed by the LightCycler® 96 system (Roche), using the following protocol:

Cycle Step	Temperature (°C)	Time (s)	Cycles
Preincubation	95	120	1
2-Step Amplification	95	5	45
	60	30	45
Melting	95	10	1
	65	60	1
	97	1	1

Resultant data were analysed using the proprietary LightCycler® Software 4.1 and Microsoft Excel.

2.6.2. Immunoprecipitation

A Magic Mix solution containing 300 µL of binding buffer (0.1 M NaCl; 0.01 M $MgSO_4$; 0.1 M HEPES; 0.025% Tween-20; pH 7.8) containing 2 µL/mL phosphatase and protease inhibitors (Sigma-Aldrich, Merck), and 30 µL of Protein G Agarose beads (Sigma-Aldrich) were combined with 3 µL of primary antibody and the protein sample. Samples were incubated at 4°C overnight (approximately 16-hours), on a medium speed MACs rotator. Upon completion, samples were spun using a centrifuge for one minute at 500 x g, discarding the supernatant. This step was repeated three times using a wash buffer (DPBS; 0.02% Tween-20) containing 2 µL/mL phosphatase and protease inhibitors (Sigma-Aldrich, Merck), discarding the supernatant each time. SDS NuPAGE™ LDS (4X) and Reducing Agent (10X) buffers (Invitrogen) were added to the beads. Samples were stored at -80°C until loading.

Prior to loading, samples were boiled at 95°C for five minutes then spun using a centrifuge for one minute at 1000 x g to pellet the beads. The supernatant can then be pipetted onto the gel for immunoblotting.

2.6.3. Western Blotting

Non-immunoprecipitated protein samples were also combined with SDS NuPAGE™ LDS (4X) and Reducing Agent (10X) buffers and boiled at 95°C for 5 minutes. Samples were placed on ice prior to loading.

Samples were loaded onto NuPAGE™ 4-12% Bis-Tris Protein gels (Invitrogen) against a PageRuler™ Plus Prestained Protein Ladder

(ThermoFisher) and resolved by electrophoresis for 90 minutes at 160-180 V. Samples were transferred onto either a Nitrocellulose or PVDF membrane using the TransBlot® Turbo™ Transfer System (Bio-Rad) for 15 minutes at 20 V. Non-specific sites on the membrane were blocked for 1 hour in 5% milk buffer (5% in TBS-T, 0.02 M Tris pH 7.5; 0.145 M NaCl; 0.05% Tween-20) at room temperature. Target proteins were labelled using their respective primary antibody (1:1000, list in Appendix section 20.1) in 5% Bovine Serum Albumin (5% BSA, Sigma-Aldrich in TBS-T) overnight at 4°C. The following morning, the membrane was further incubated with horse radish peroxidase (HRP) anti-mouse or anti-rabbit secondary antibodies (1:5,000-10,000) in 5% milk buffer for 1 hour at room temperature. The blots were visualized by activating HRP with Millipore™ Western ECL substrate reagents (ThermoFisher) and detecting the signal using the G:Box (SynGene) system and its proprietary GeneSys software.

Blots were stripped of both primary and secondary antibodies to re-probe for a different protein/ Blots were incubated for 15-minutes in stripping buffer (0.2 M glycine, 0.1% SDS, 1% Tween-20) and washed in TBS-T as described above, repeating blocking, primary and secondary antibody incubations for the new probe.

Densitometry of the bands was performed using NIH ImageJ analysis function and exported to Microsoft Excel for further data transformation.

2.6.4. Nitric Oxide Assay

The nitric oxide assay was performed using the Nitric Oxide Assay Kit (Invitrogen), as per manufacturer's protocol with minor modifications. Nitrite and nitrate standards and dilute NADH were prepared fresh at the time of each

assay. After the first run-through, the nitrite assay was omitted completely, analysis resulted from nitrate assays only. Diluted Nitrate Reductase was prepared immediately before plating to ensure use within a 15-minute period. Cell culture supernatant was collected from HUVEC treated with 100 µM HI-2 or 0.1% v/v DMSO vehicle control, after 24-hours. The supernatant samples were diluted 1:1 in 1 x Reagent Diluent and plated directly in the assay, without filtration. In addition to the zero standards, standard dilutions, samples and blanks, sample blanks were added in duplicate to the 96-well plate – omitting the addition of NADH, diluted Nitrate Reductase, Griess I and II reagents and replacing with 1 x Reagent Diluent.

Plates were analysed on an endpoint plate reader, at 540 nm. The resultant data were exported to Microsoft Excel for further data transformation.

2.7. Biophysical Assays

2.7.1. Surface Plasmon Resonance

Protein	Mol. Weight	Conc.	Buffer Composition	Tag	Source
eNOS reductase domain	76 kDa	4 mg/mL	25 mM HEPES, 0.15 M NaCl, 1 mM TCEP; pH 7.5	His, GST	In-house
PYK2 kinase domain	30 kDa	0.18 mg/mL	0.05 M Tris-HCl, 0.5 M NaCl, 5% glycerol, 0.5% SLS; pH 8.0	His	Genscript

Table 2-1: Purified Proteins for Surface Plasmon Resonance

2.7.1.1. Chip Derivatisation

The gold carboxyl-derivatized ‘CM5’ sensor chip consisting of four distinct chambers (Cytiva LifeSciences) was activated by injection of EDC/NHS at 5 µL/min over 7 minutes through each flow cell, using the Biacore 3000 (Cytiva LifeSciences) surface plasmon resonance system. The His/GST Capture Kit

(Cytiva LifeSciences) containing an anti-His or anti-GST antibody were injected at a rate of 5 µL/min for approximately 4 minutes – or until an estimated 7500 relative units (RU) were immobilized onto both reference and test sensor surfaces. The system was continuously flushed with running buffer (HBS-EP, 0.01 M HEPES; pH 7.4, 0.15 M NaCl, 3 mM EDTA, 0.005% v/v P20 surfactant) at a flow rate of 5 µL/min until commencement of ligand immobilisation.

2.7.1.2. Ligand Injection

The protein of interest was injected at a flow rate of 5 µL/min into the test flow cell only to ideally immobilize several hundred RUs of protein to the complementary antibody surface. The unreacted material was eluted from the flow cell by addition of a high-salt solution, 1 M NaCl at a flow rate of 20 µL/min for a couple of minutes. Both immobilisation and unreacted material elution injections were repeated a further time under the same conditions. Unreacted sites were capped using 1 M ethanolamine:HCl at a flow rate of 5 µL/min for 7 minutes to limit analyte interaction with the antibody surface and remove non-covalently bound ligand. The system was continuously flushed with running buffer at a flow rate of 5 µL/min until commencement of analyte injection.

2.7.1.3. Sample Injection

The interacting protein partner at aliquot concentrations increasing in intervals from 1 to 100 nM, were injected at a flow rate of 5 µL/min across both the reference and test flow cells, seeking a comparative change in the sensorgram curve in the test chamber compared with the reference. The antibody surface was regenerated, causing removal of both the ligand and

analyte proteins by injection of regeneration solution (0.1 M $NaHCO_3$, 0.05% Tween-20 v/v).

2.7.1.4. Chip Storage

Immobilized or regenerated chips were flushed with HEPES buffer, containing 0.02% NaN_3 and stored at 4°C until further use.

2.8. Statistical Analyses

GraphPad Prism v9 software was used for data analysis. Averaged data are shown in bar charts as mean ± SEM. Comparisons within groups were made using paired Student *t* tests and, between groups using unpaired Student *t* tests, as appropriate. P values < 0.05 were deemed statistically significant.

2.9. Computational Studies

2.9.1. Molecular Dynamics Simulations

2.9.1.1. Coarse-Grained Simulations

All simulations were performed using the CHARMM-22 forcefield (MacKerell et al., 1998) and GROMACS 5.0 (gromacs.com) (van der Spoel et al., 2005). An elastic network model was applied to all protein backbone atoms within 0.7 nm with a force constraint of 1000 kJ mol^{-1} nm^2. This maintains the secondary and tertiary structure of the proteins. The coordinates of the 4ZXB, 5U8Q and IR/IGF1R homology structures were used in simulations of apo-receptor structures. Any non-protein atoms were removed in the initial stages. Missing unstructured regions were included using Modeller (Webb and Sali, 2016) and was converted to a coarse-grained (CG) system, centred within a 20 x 22 x 22 nm^3 simulation box.

The CG structures were energy-minimized in a vacuum using the steepest decent algorithm embedded within GROMACS. The structures were solvated by random placement of water and NaCl (0.15 M) using CHARMM-GUI (Brooks et al., 2009; Jo et al., 2008; Lee, J. et al., 2016). The systems were further energy-minimized and equilibrated for 2 ns at 323 K with position restraints on the protein backbone constituents. Five independent repeat production simulations for 5 μs were performed for each system, in which there was the same initial position but yielded different starting velocities. During these simulations, a V-rescale thermostat (323 K) and Parrinello-Rahman barostat (1 bar) were employed to maintain the temperature and pressure of the system. The integration time step was 20 fs.

2.9.1.2. Conversion of Coarse-Grained to Atomistic Simulations

The final frames of selected CG simulations were converted to atomistic resolutions, otherwise known as ‘backmapping’. This conversion occurred using the CG2AT protocol (Wassenaar et al., 2014). Backmapping reconstructs the final CG simulation by combining the independent simulations referenced in section 2.9.1.1. The converted structures were energy-minimized and equilibrated for 2 ns. From each backmapped simulation, three distinct replicates were generated with randomized starting velocities.

For the molecular dynamics simulations, the same conditions as the CG simulations were used and performed for 250 ns. This work was undertaken on ARC3, part of the High-Performance Computing facilities at the University of Leeds, UK.

2.9.1.3. Molecular Dynamics Simulation Analyses

All analyses were performed using GROMACS 5.0 (RMSD/C_α, RMSF/C_α and distance). A cut-off distance of 4 Å was defined.

Part I

Insulin Receptor and Insulin-like Growth Factor 1 Receptor Hybrid Receptor

3. Aims and Hypothesis

In people with type-2 diabetes, the literature documents concrete evidence of observations regarding a higher proportion of IR/IGF1R hybrids and as a consequence, fewer IR homodimers present on the surface of endothelial cell membranes. IR/IGF1R hybrids, due to their inherent nature containing a single protein monomer unit of each respective receptor and by extension, half of the homodimer receptor's cognate ligand binding sites, lose the ability to signal for insulin. This combination therefore has a detrimental impact on endothelial cell insulin sensitivity and a subsequent knock-on effect on NO bioavailability. The reduction of available NO results in poor vascular repair and regeneration which are inevitably linked to conditions such as atherosclerosis.

The stimulus driving increased IR/IGF1R hybrid formation is yet unknown. However, what is clear, is that the ability to modulate hybrids themselves could restore of insulin sensitivity in endothelial dysfunction. This presents an interesting target for small molecule modulation, in such a way that the formation of hybrids might be inhibited, while maintaining or improving the potential for functional IR homodimers to form. Immediately, the potential for a small molecule to be used as a therapeutic agent is apparent; most interestingly perhaps, it could be used as an investigative tool – nurturing a deeper understanding into the role of hybrids in endothelial dysfunction and subsequently, pushing advancement in novel care and treatment for type-2 diabetes patients in the future.

Based on these observations, I planned to meet the following objectives in this thesis:

1. To screen a cohort of commercially-available small molecules to determine their efficacy in reducing IR/IGF1R hybrid formation, while maintaining homodimer population levels.

2. To determine the effect of small molecule modulation of IR/IGF1R hybrids on insulin signalling and downstream protein expression.

3. To determine the effect of small molecule modulation of IR/IGF1R on angiogenesis in endothelial cells.

I hypothesized that a small molecule modulator whose mode of action is to inhibit IR/IGF1R hybrid formation, would increase the availability of IR monomers – solely dedicated to form functional IR homodimers. This increase in IR dimers would be associated with an increase in insulin sensitivity which would therefore increase insulin signalling and result in increased NO bioavailability. And by obtaining such results, I predicted that there could be a restorative effect on angiogenesis and a reduction in atherosclerosis.

4. Results

A large library of commercially-available small molecules was screened using virtual docking. Virtual screening is far more cost-effective than high-throughput screening campaigns as millions of different structures can be processed without the requirement to purchase until they are determined to be of interest. There are many commercially-available databases of discovered structures and in addition novel structures, synthesized at the University of Leeds can also be inputted into the search. However prior to commencing the virtual screen, there needs to be a structure of the protein to dock the compounds to. No such EM or X-ray crystal structure of the IR/IGF1R receptor exists in the literature, to date. A homology model of the IR/IGF1R hybrid receptor was prepared based on the IR dimer ectodomain (PDB ID; 2DTG (McKern et al., 2006)). I-TASSER utilizes the IR crystal structure as a template and replaces one monomer with the amino acid sequence of the IGF1R (Zhang, Y., 2008; Roy et al., 2010; Yang, J. et al., 2015). This was possible due to the high sequence identity mentioned above.

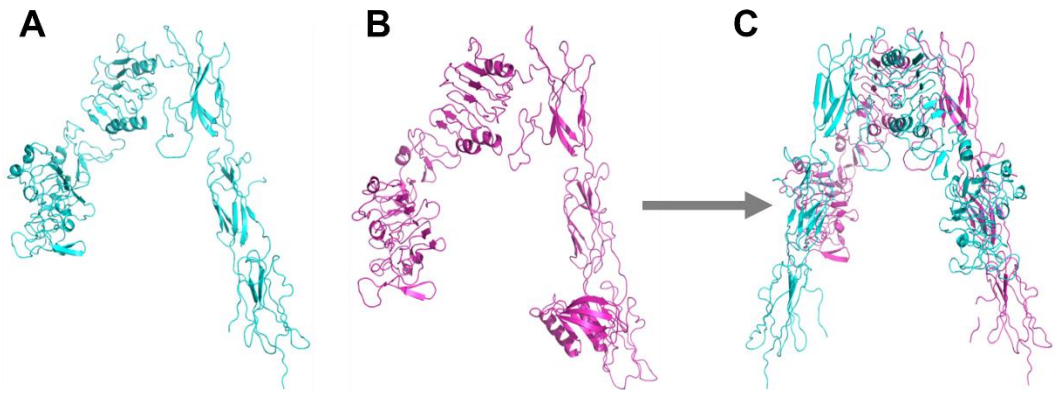

Figure 4-1: Homology model of an IR/IGF1R hybrid receptor

The IR ectodomain crystal structure (**A**), published by McKern *et al.* (2006) and the ITASSER-generated IGF1R ectodomain (**B**) are dimerized to produce the Simmons IR/IGF1R heterodimer homology model (**C**). All images produced by Dr. K. Simmons.

The Maestro graphical user interface (Schrodinger) and Protein Preparation Wizard were used to limit steric clashes between amino acid residues and link the monomer structures *via* disulfide bonds. The hybrid homology model was analysed using the KFC2 PPI hotspot prediction server to locate regions across the structure which could be suitable for compound targeting. The hotspot containing amino acids 400-570 on IR was selected as this sequence had the lowest degree of similarity to the IR and IGF1R homodimer structures, and therefore affording a higher likelihood of selecting a hybrid-selective compound.

A 3D version of the ZINC database of drug-like molecules was generated using OpenEye software - the lowest energy predicted conformer was produced for each molecule. The Glide high throughput screening function was operated using the University of Leeds's ARC3 computing cluster to determine the predicted binding pose of each compound. A proportion of the best scoring entries were rescored using Glide SP and AutoDock Vina, and those that passed additional testing were further assessed using SPROUT, an in-house *de novo* design program which identifies H-bonding, van der Waals and hydrophobic interactions on IR and any subsequent steric clashes with IGF1R. A higher number of these would support the idea that the individual compound might better interfere with dimerization of IGF1R with IR and prevent receptor formation.

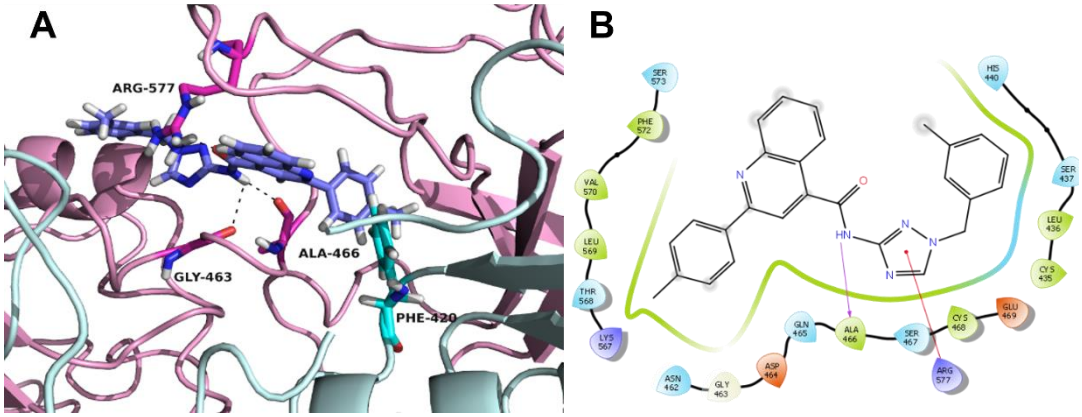

Figure 4-2: *In silico* docking of HI compound series

A. Docking of HI-2 within the IR ectodomain hotspot region, highlighting bonding interactions between residues on the protein structure. **B.** Schematic overview of bonding interactions, steric clashing, and overall fit within the IR ectodomain hotspot region. The green line circling the structure highlights good fit within the pocket. All images produced by Dr. K. Simmons using PyMOL Molecular Graphics System, version 2.0 Schrödinger, LLC and Maestro, Schrödinger, LLC.

A small library of structurally-diverse and synthetically-accessible molecules were purchased and assessed for purity using Liquid Chromatography-Mass Spectrometry (LC-MS) and toxicity *in vitro* by a LIVE-DEAD Cell Viability Assay in HEK293T cells. Acceptable tolerances were set at >95% purity and >80% cell viability, normalized to DMSO-treated cell data.

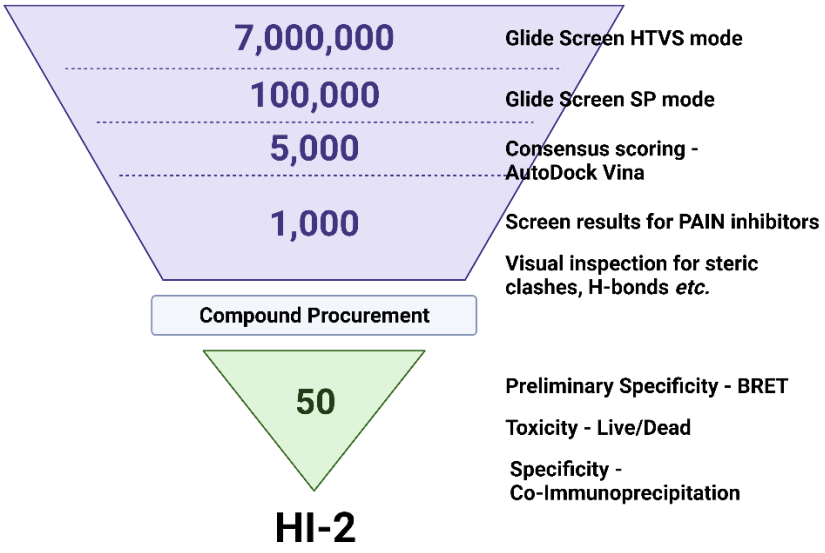

Figure 4-3: Virtual high throughput and *in vitro* screening cascade

Virtual high throughput screening of 3D ZINC database structures docked onto IR ectodomain model and, *in vitro* screening by Bioluminescence Resonance Energy Transfer (BRET), Live/Dead and co-immunoprecipitation assays. Virtual screening, BRET and Live/Dead assays performed by K. Simmons; co-immunoprecipitation assays performed by C. Myers. Image adapted from Dr. K. Simmons (University of Leeds, Leeds, 2020 - unpublished) and created with BioRender.com

Compounds that matched or exceeded those criteria moved to the next assay in the screening cascade - a Bioluminescence Resonance Energy Transfer (BRET) assay. BRET may be used to study the interaction between two partners, where the first partner is fused to *Renilla luciferase* (Rluc) and the second, to a yellow variant of the green fluorescent protein (YFP). The luciferase is excited using coelenterazine, resulting in emission of either one or two signals. Should the two partners not interact, or if the distance between the Rluc and YFP is greater than 100 Å, a single signal may be detected, of emission by the luciferase at 485 nm. However, should the partners interact and the distance between the luminescent donor and acceptor ranges between 10 and 100 Å, an energy transfer occurs between Rluc and YPF. The exchange results in shift of the emission spectrum, as the signal is emitted by YFP at 530 nm. Issad *et al.* designed a chimeric insulin receptor where one

β-subunit is fused to luciferase and the other subunit bound to YFP (Issad et al., 2002). This same methodology has been adapted to incorporate the YFP upon the β-subunit of the IGF1R to monitor the effect of small molecule modulation in cells.

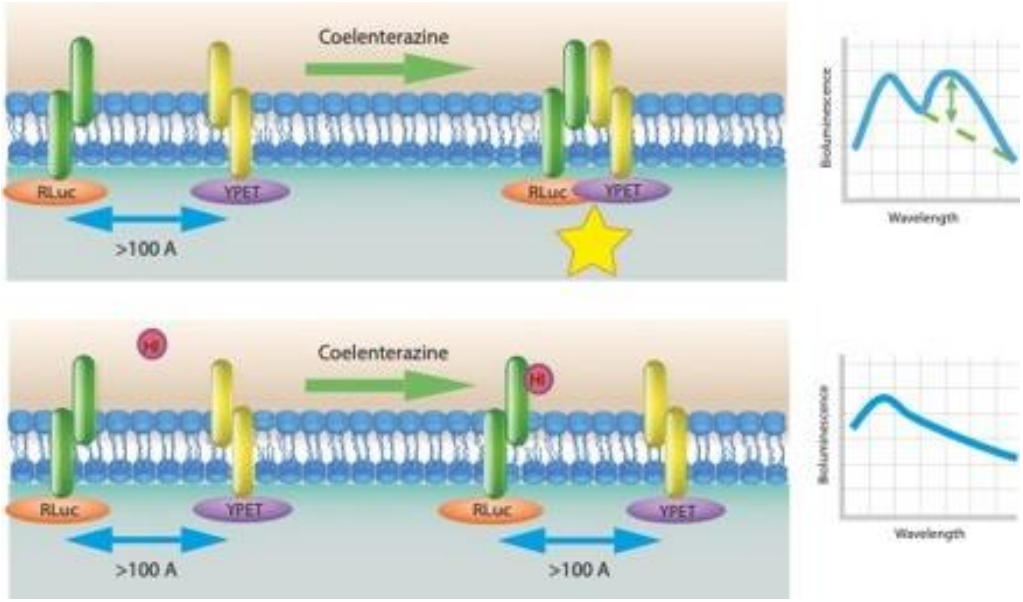

Figure 4-4: Schematic representation of Bioluminescence Resonance Energy Transfer between IR and IGF1R monomers

In vitro coelenterazine-activated dimerization between IR-Rluc and IGF1R-YPET results in a BRET fluorescent BRET signal. Inhibition of IR-Rluc prevents dimerization and the BRET signal is lost. Images produced by Dr. K. Simmons, University of Leeds, Leeds.

The IR-Rluc and IGF1R-YFP cDNA constructs were kindly received from the Issad group at INSERM Institute in Paris. The constructs were co-transfected in HEK293T cells and used as a high-throughput screening system to determine the effect of small molecule modulators on IR/IGF1R hybrid formation. Several compounds were identified through these experiments as hybrid formation inhibitors and were carried forward in further testing.

4.1. Screening of compounds identified using the BRET assay

4.1.1. Compound BTB01314

BTB01314 (BTB) was purchased from Maybridge (ThermoFisher, UK), and was the first prospective hybrid inhibitor to result from BRET and Live/Dead assay testing (Figure 4-5 A). Human umbilical vein endothelial cells (HUVEC) were treated for 6-hours with either 100 μM BTB01314 or volume equivalent, 0.1% v/v of the vehicle control, dimethyl sulfoxide (DMSO) in full-growth ECGM-2 media. A six-hour treatment time had been decided upon due to notable cell death attributable to HI-1 compound in the Live/Dead assay; a shorter compound exposure period would prevent this.

After compound treatment, cells were lysed and analyzed using western blotting (are shown below in Figure 4-5 B and C). In the immunoprecipitation blots, the bands present for IR β represent IR/IGF1R hybrids present in each sample. The IGF1R β antibody selectively pulls-down IGF1R units – and any proteins bound to these structures. This process therefore removes any IR homodimers, as they remain in the supernatant of each sample, while isolating IGF1R homo- and heterodimers.

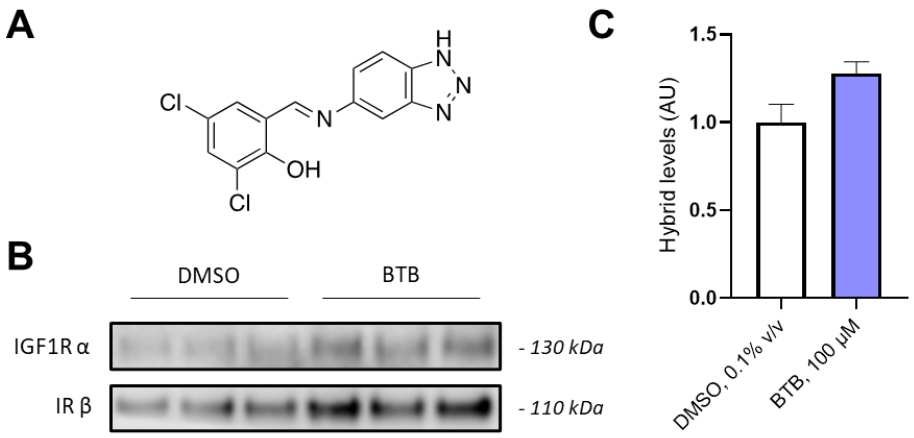

Figure 4-5: Compound BTB01314

A. Structure of BTB01314. Representative co-immunoprecipitation blot (**B**) and graph (**C**) of IR/IGF1R hybrids in volume equivalent DMSO- and 100 µM BTB-treated HUVEC after a 6-hour incubation. Densitometry data have been normalized to respective DMSO averages (+/- SEM) P=0.08 n=6,5.

The data showed a trend towards an increase in IR/IGF1R hybrid formation compared with DMSO controls. While the BRET data suggested BTB would result in a decrease of hybrid formation, the assay is not without its limitations and as a consequence, western blotting is a suitable method to confirm these results. The BRET assay may have generated a lower response due to measurement of a change in conformation of the IR/IGF1R hybrid structure rather than impedance of formation by the BTB small molecule. Testing this hypothesis would require structural information regarding the dimerization of receptors in the presence of the interacting molecule, however for this project, it would not be sufficiently important to discern. As a result of the western blotting data, BTB was not deemed to be suitable as an IR/IGF1R hybrid inhibitor candidate to progress onto further testing.

4.1.2. Compound 56945281

Compound 56945281 (281) was purchased from Chembridge. HUVEC were treated for 6-hours with 100 µM 56945281 or volume equivalent, 0.1% v/v DMSO-vehicle control in full-growth ECGM-2.

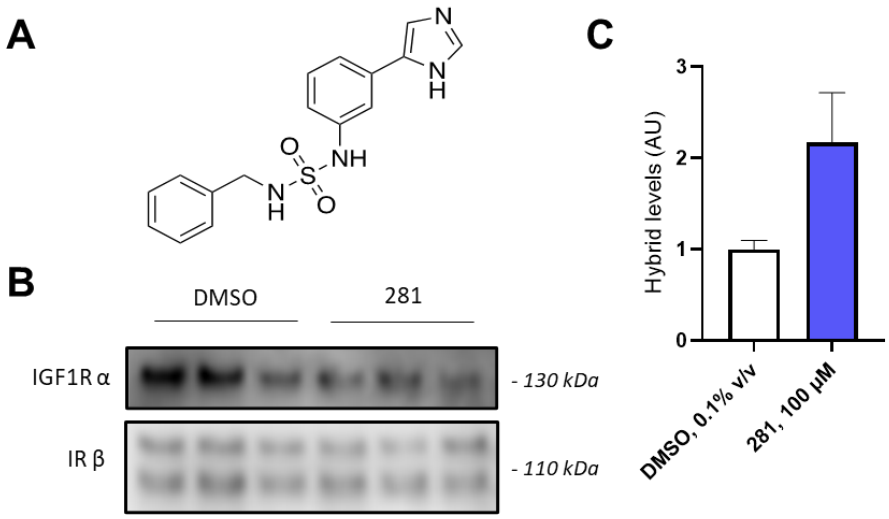

Figure 4-6: Compound 56945281

A. Structure of 56945281. Representative co-immunoprecipitation blot (**B**) and graph (**C**) of IR/IGF1R hybrids in volume equivalent DMSO- and 100 µM 281-treated HUVEC after a 6-hour incubation. Densitometry data have been normalized to respective DMSO averages (+/- SEM) P=0.10 n=3,3.

The immunoprecipitation results assessing the change in IR/IGF1R hybrid levels with 281 are shown in Figure 4-6 B and C. Initial screening of 281 showed a distinct, though non-significant trend towards an increase in hybrid formation compared to DMSO controls. For the same reasons as discussed in section 4.1.1, it is likely that the BRET data interpreted a structural rearrangement of the IR/IGF1R hybrids, rather than 281 small molecule inhibition. As a result of the western blotting data, 281 was not deemed suitable as an IR/IGF1R hybrid inhibitor candidate to progress onto further testing.

4.1.3. Compound 7922787 (HI-1)

HI-1 was purchased from Chembridge (ID 7922787) and was one of the more promising compounds to result from the virtual docking studies, Live/Dead and BRET assays. The compound had previously been analysed using immunoprecipitation and western blotting techniques by Dr. Mughal in Kearney lab and was consistent with reported BRET data, showing a

decrease in hybrid formation after 6h incubation with 100 and 250 μM HI-1 compared with volume equivalent, 0.1% or 0.25% v/v DMSO-vehicle controls. However since the commencement of this work, Chembridge has discontinued the product and so in-house synthesis of a new batch was undertaken by McPhillie lab in the School of Chemistry.

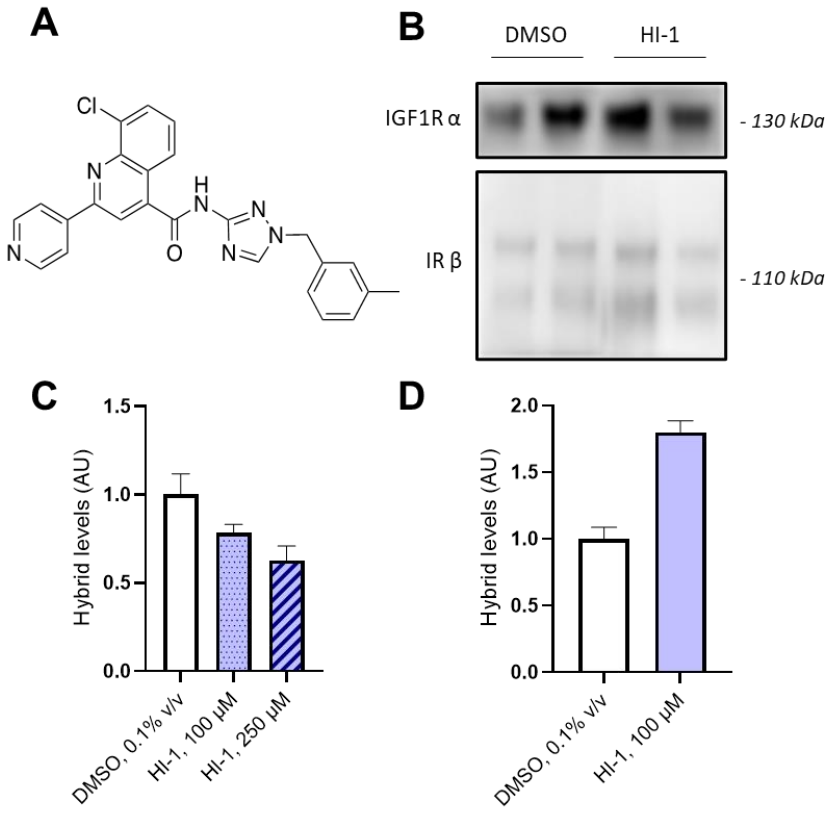

Figure 4-7: Compound HI-1

A. Structure of HI-1. **B.** Representative co-immunoprecipitation blot of IR/IGF1R hybrids in volume equivalent DMSO- and 100 μM in-house synthesised HI-1-treated HUVEC after a 6-hour incubation. **C.** Graph demonstrating decrease in IR/IGF1R IR/IGF1R formation after 6-hour treatment with HI-1, compared to DMSO-vehicle control. Densitometry data have been normalized to DMSO average (+/- SEM) n=2,2,2. Data produced by Dr. R. Mughal (University of Leeds, Leeds, 2018 – unpublished). **D.** Graph demonstrating increase in IR/IGF1R formation after 6-hour treatment with in-house synthesized HI-1, compared to DMSO-vehicle control. Densitometry data have been normalized to respective DMSO averages (+/- SEM) n=2,2.

The immunoprecipitation results pertaining to both the commercial and in-house synthesized compounds are shown in Figure 4-7. Immunoprecipitation data of the new batch of HI-1 showed a marked, though non-significant trend

towards causing an increase in IR/IGF1R hybrid formation compared to DMSO controls. Due to the disparity in effect on IR/IGF1R hybrid formation between different batches of HI-1 by western blotting, and no apparent differences reported by ^{1}H, ^{13}C-NMR or mass spectrometric techniques, it was decided that further testing of HI-1 would not proceed, and it was eliminated from our IR/IGF1R hybrid inhibitor candidate list on this basis.

There are some discrepancies here with our data suggesting the structure of HI-1 *versus* that obtained from Chembridge, as it pertains to the orientation of the triazole group. For this reason, McPhillie lab decided to synthesize a number of analogues of HI-1 to further understand the structure-activity relationship of this series of molecules.

4.1.4. Compound HI-2

To understand the structural requirements for modulation of hybrids, McPhillie lab in the School of Chemistry synthesised a series of HI-1 analogues. Compound HI-2 showed promising inhibition in the BRET assay and no toxicity in subsequent Live/Dead screens.

To understand the initial physiochemical properties of the HI series, HI-1 and HI-2 were evaluated by Shanghai ChemPartner. The purpose of this screening provided insight towards determining their potential suitability for use *in vivo* should the data show HI-2 to be an effective IR/IGF1R hybrid inhibitor (Table 4-1).

Compound ID	FaSSIF sol (pH 7.4) µM	$t_{1/2}$ (min)		CL_{int} (mL/min/kg)	
		human	*mouse*	*human*	*mouse*
HI-1	18.4	5.77	5.93	301.27	920.79
HI-2	1.8	6.97	1.03	249.26	5310.93

Table 4-1: ADME properties of HI-1 and HI-2

ADME screening panel for Fasted state simulated intestinal fluid (FaSSIF), half-life ($t_{1/2}$) and intrinsic clearance (CL_{int}) properties for HI-1 and HI-2. Data obtained from Shanghai ChemPartner.

Neither compound is particularly suitable for *in vivo* studies, each possessing poor metabolic stability represented by low half-lives and high clearance rates. These pharmacological indicators suggest that the drug would metabolize too quickly and would not produce sufficient therapeutic effect. The solubility for HI-1 is moderate but poor for HI-2. Modifications in design of further analogies would require lower LogP values to improve the solubility in aqueous media, however, a fine balance must be met to simultaneously maintain or increase the potency of the compound. All of these characteristics would need to be improved upon for use in mammalian models or continuous dosing using a minipump.

Initial assays treated the cells with potential inhibitors for 6 hours, in the aim of circumventing toxicity. However, the IR turnover rate is approximately every 6.7 hours (Reed and Lane, 1980), and therefore the hybrid inhibitor might have a more profound effect if cells were treated for a longer period. I altered the cell culture treatment method from 6- to 24-hours incubation and assessed the effect of both conditions with HI-2.

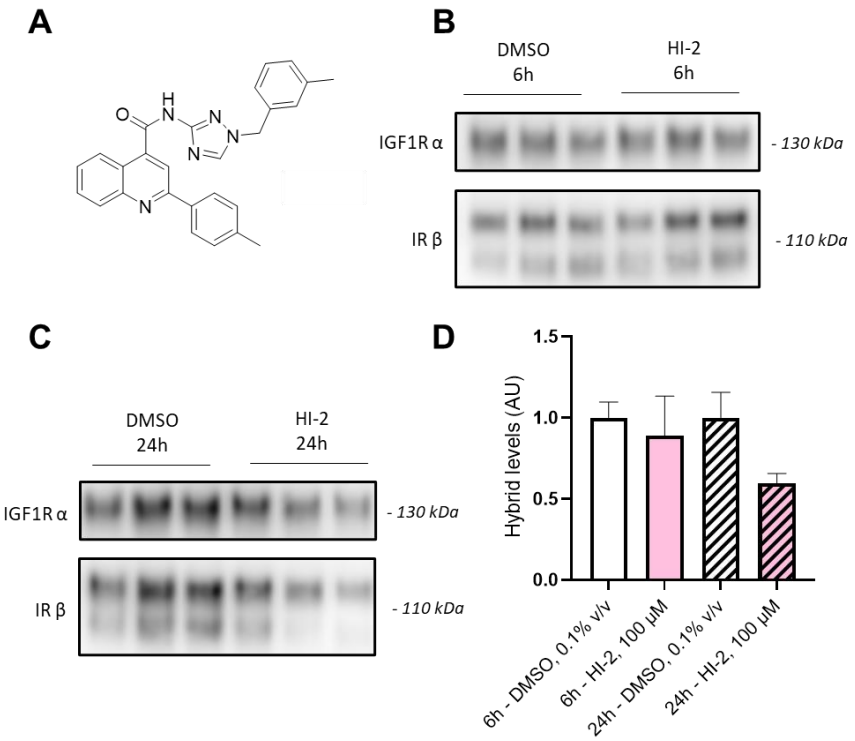

Figure 4-8: Compound HI-2

A. Structure HI-2. Representative co-immunoprecipitation blot of IR/IGF1R hybrids in volume equivalent DMSO- and 100 µM HI-2-treated HUVEC after a 6-hour (**B**) and 24-hour (**C**) incubation. **D.** Graph demonstrating increase in IR/IGF1R formation after 6- and 24-hour treatment with HI-2, compared to respective DMSO-vehicle controls. Densitometry data have been normalized to respective DMSO averages (+/- SEM) 6-hour P=0.43 n=5,6; 24-hour P=0.10 n=3,3.

The immunoprecipitation results of HUVEC incubated for 6- and 24-hours are shown in Figure 4-8. It was immediately clear from Figure 4-8 D that increasing incubation time yielded a more marked reduction in hybrid formation with compound-treatment at the same concentrations compared to respective DMSO controls. Increasing incubation to 24- hours with HI-2 yielded a 40% reduction in hybrids, *versus* 11% after 6-hours. HI-2 was deemed effective as a hybrid formation inhibitor in preliminary screening and carried through to further testing.

And in all subsequent tests by western blotting, cells were consistently treated for 24-hours.

Several commercially available analogues of HI-1 were purchased and characterized using the BRET assay by Dr. Simmons (data not shown). The most promising of these were analysed using western blotting and discussed below.

4.1.5. Compound STK464985

Compound STK464985 (STK985) was purchased from Vitas-M-Labs. HUVEC were treated for 24-hours with 100 µM STK985 or volume equivalent, 0.1% v/v DMSO-vehicle control in full-growth ECGM-2.

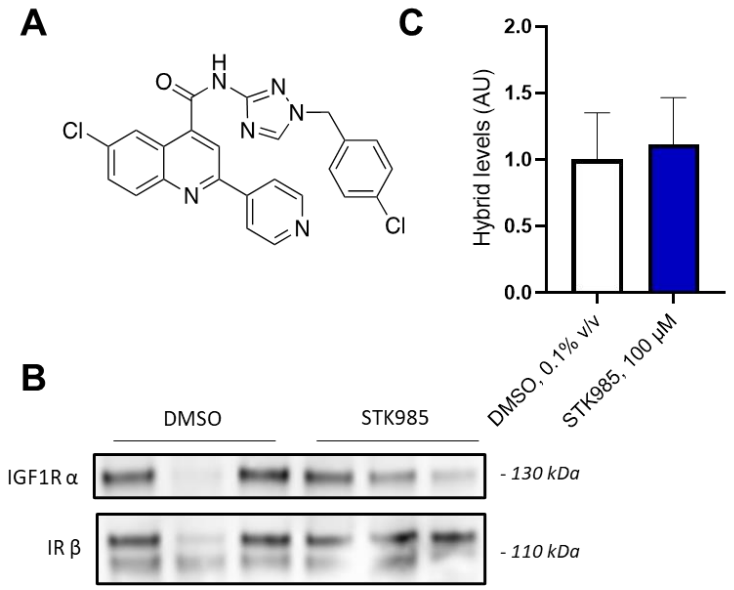

Figure 4-9: STK464985

A. Structure of STK464985. Representative co-immunoprecipitation blot (**B**) and graph (**C**) of IR/IGF1R hybrids in volume equivalent DMSO- and 100 µM STK985-treated HUVEC after a 24-hour incubation. Densitometry data have been normalized to respective DMSO averages (+/- SEM) P>0.9999 n=3,3.

The immunoprecipitation results assessing the change in IR/IGF1R hybrid levels with STK985 are shown in Figure 4-9. Initial screening of STK985 showed no discernible effect on IR/IGF1R hybrid formation with STK985 compared to its respective DMSO controls. STK985 did not demonstrate to

be sufficiently inhibitive of IR/IGF1R hybrid formation and therefore, did not progress onto further testing.

4.1.6. Compound STK446492

Compound STK446492 (STK492) was also purchased from Vitas-M-Labs and was the last of the compounds resulting from the BRET and Live/Dead screening assays. HUVEC were treated for 24-hours with 100 µM STK492 or volume equivalent, 0.1% v/v DMSO-vehicle control in full-growth ECGM-2.

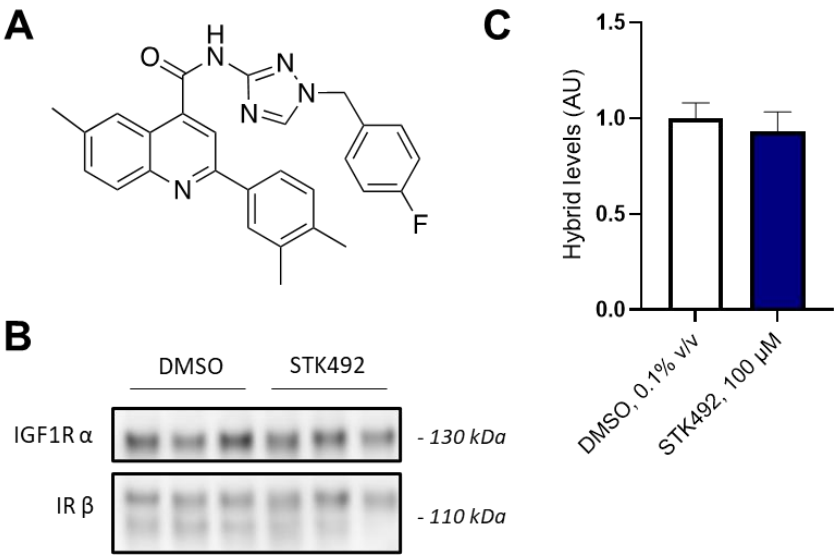

Figure 4-10: Compound STK446492

A. Structure of STK446492. Representative co-immunoprecipitation blot (**B**) and graph (**C**) of IR/IGF1R hybrids in volume equivalent DMSO- and 100 µM STK492-treated HUVEC after a 24-hour incubation. Densitometry data have been normalized to respective DMSO averages (+/- SEM) P>0.9999 n=3,3.

The immunoprecipitation results assessing the change in IR/IGF1R hybrid levels with STK492 are shown in Figure 4-10. Initial screening of STK492 showed no discernible effect on IR/IGF1R hybrid formation with STK492 compared to its respective DMSO controls. STK492 did not demonstrate to be sufficiently inhibitive of IR/IGF1R hybrid formation and as such, did not progress onto further testing.

4.2. Further Evaluation of HI-2 as a Hybrid Inhibitor

4.2.1. Modulation of Insulin Receptor/Insulin-like Growth Factor 1 Receptor Homo- and Heterodimers

The effect of HI-2 was proven in human umbilical vein cells (HUVEC) and showed a marked reduction in IR/IGF1R hybrid formation compared with respective DMSO controls. It was important to determine whether the same effect would be observed in human samples, originating from both 'non-diabetic' (ND) people and people with 'diabetes mellitus' (DM). The opportunity to work with human saphenous vein endothelial cells (SVEC) became available. Human saphenous vein can be obtained from coronary artery bypass grafts as they are easily harvestable and where several grafts are required, a larger sample can be obtained compared to the smaller internal mammary or radial arteries. I felt they would be an appropriate human disease model to elucidate further information regarding the effect of HI-2, as the DM samples demonstrated similar markers associated with diabetes in their signalling and angiogenic properties, as outlined by Roberts *et al.* (Roberts et al., 2015).

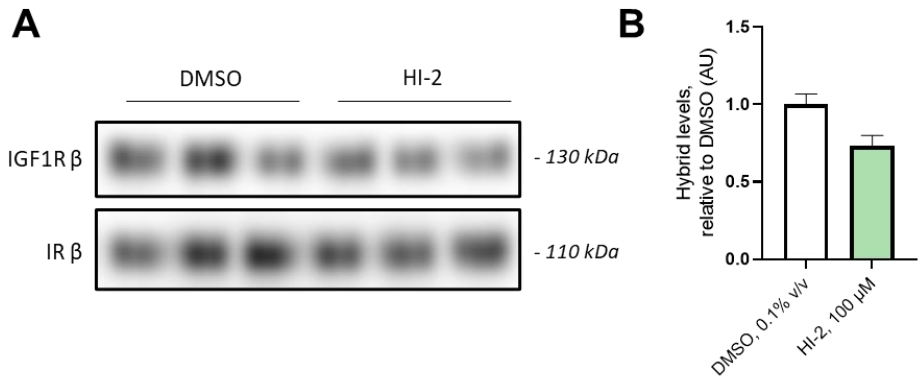

Figure 4-11: Screening the effect of HI-2 in Human Saphenous Vein Endothelial Cells

Representative co-immunoprecipitation blot (**A**) and graph (**B**) of IR/IGF1R hybrids in volume equivalent DMSO- and 100 µM HI-2-treated ND hSVEC after a 24-hour incubation. Densitometry data have been normalized to respective DMSO averages (+/- SEM) N/n=2/2,3.

Saphenous vein samples were no longer being harvested at the Leeds Institute of Cardiovascular and Metabolic Medicine (LICAMM) at the start of this project. Samples were obtained from storage at -80°C, at higher passage numbers; the age and effect of storage limited the proportion of cell samples successfully resurrected for culture and treatment with HI-2. Two non-diabetic samples were obtained for preliminary screening (Figure 4-11). Immunoprecipitation of ND SVEC showed a distinct trend towards reduction in IR/IGF1R hybrid formation in HI-2-treated samples compared to respective DMSO controls, of approximately 27%. The SVEC data complemented results obtained in HUVEC (Section 4.1.4, Figure 4-8).

4.2.2. Characterisation of IR/IGF1R Method Adjustment

A paper published by the groups of Profs. CR Kahn and GL King at Harvard, included a new method of characterizing IR/IGF1R hybrids by immunoprecipitation which offered the opportunity to garner supplementary information from the same single immunoprecipitated sample (Li, Q. et al., 2019). The method included analysis of the supernatant collected from the

immunoprecipitation samples prior to washing, which was otherwise discarded. The bonus to making this change meant that all proteins that do not bind IGF1R β would be present in the supernatant and as such, in this particular instance, $(IR)_2$ homoreceptors would be quantifiable – as opposed to previously being missing from our datasets.

Analysis of the immunoprecipitation supernatant yielded some interesting information regarding the effectiveness of the pull-down of IGF1R, as the supernatant should not contain any IGF1R to consider a completely successful pull-down. And by extension, remaining IR protein in the supernatant blots could be attributed to IR homodimers only. Blots of immunoprecipitation, supernatant, and cell lysate control samples, reported by the method described by Kahn, in HUVECs treated with 100 μM HI-2 and 0.1% v/v DMSO are shown in Figure 4-12.

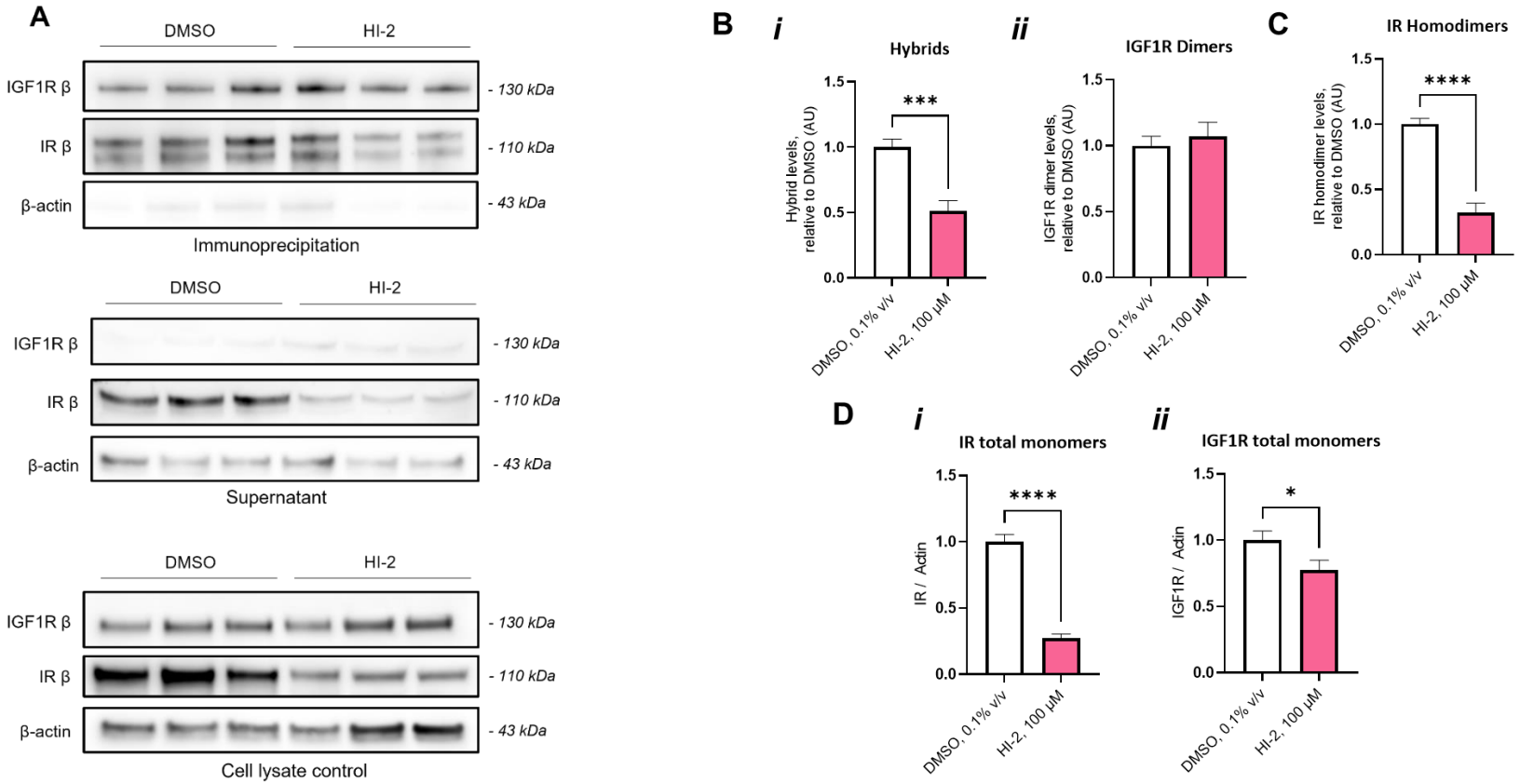

Figure 4-12: Characterisation of IR/IGF1R for HI-2 in Human Umbilical Vein Endothelial Cells using the 'Kahn' method

Representative western blots (**A**) and graphs (**B, C, D**) of immunoprecipitation, supernatant, and cell lysate control samples from non-treated, DMSO- and HI-2-treated HUVEC after 24-hour incubation. **B.** Immunoprecipitation sample graphs reporting change in IR/IGF1R (***i***) and IGF1R dimers (***ii***) after 24-hour treatment with HI-2, compared to respective DMSO-vehicle controls. **C.** Supernatant sample graph reporting change in IR homodimers after 24-hour treatment with HI-2, compared to respective DMSO-vehicle controls. **D.** Cell lysate graphs reporting change in IR (***i***) and IGF1R (***ii***) total monomers after 24-hour treatment with HI-2, compared to DMSO-vehicle controls. Densitometry data have been normalized to respective DMSO averages (+/- SEM). **B*i*** ***P=0.0002 n=12,10; **B*ii*** P=0.67 n=12,10; **C** ****P<0.0001 n=12,10; **D*i*** ****P<0.0001 n=12,9**; D*ii*** *P=0.04 n=12,9.

A significant reduction in IR/IGF1R hybrid formation was observed in the immunoprecipitation blots, of approximately 50% in HI-2 treated HUVEC compared to respective DMSO controls, and IGF1R dimer levels remained consistent across both treatment conditions. In the supernatant blots, there was a distinctively significant reduction in IR homodimer formation with HI-2 treatment compared to respective DMSO controls. In addition, though not analysed for densitometry, IGF1R was detected in the supernatant samples, highlighting that the immunoprecipitation protocol was not sufficiently refined to generate a complete pull-down of IGF1R β. The method for immunoprecipitation of IR/IGF1R hybrids in Kearney lab was for a minimum of 3-hours, this parameter was changed to a minimum of 16-hours, to a maximum of 24-hours, to improve the effectiveness of the pull-down. In cell lysate samples, a significant reduction in IR and IGF1R populations was observed in HI-2-treated cells compared to respective DMSO controls.

4.2.3. Modulation of IR/IGF1R in Diabetic Human Primary Cells with HI-2

The effect of HI-2 was assessed in saphenous vein and adipose tissue endothelial cells (ATEC), in both ND and DM cohorts. Human SVEC harvesting had recommenced in LICAMM with a new team. The method of isolation had considerable complexity and required a few attempts to garner the expertise to carry out the task with speed and finesse. As the tissues collected were not sterile, we had instances where contaminants would become visibly present and was difficult to rescue the cells once this had occurred. As a result, successful isolation attempts were few in number.

ATEC were introduced as an additional human disease model as they were easier to harvest and isolate than SVEC and there was already an established team in place for this work. Additionally, culture of ATEC was simpler compared to SVEC. Once the Covid-19 pandemic lockdown began, SV collection ceased entirely, however sufficient ATEC samples had been banked to produce substantial datasets for subsequent tests and in addition, collection of new tissue recommenced in November 2020 to provide a continuous supply.

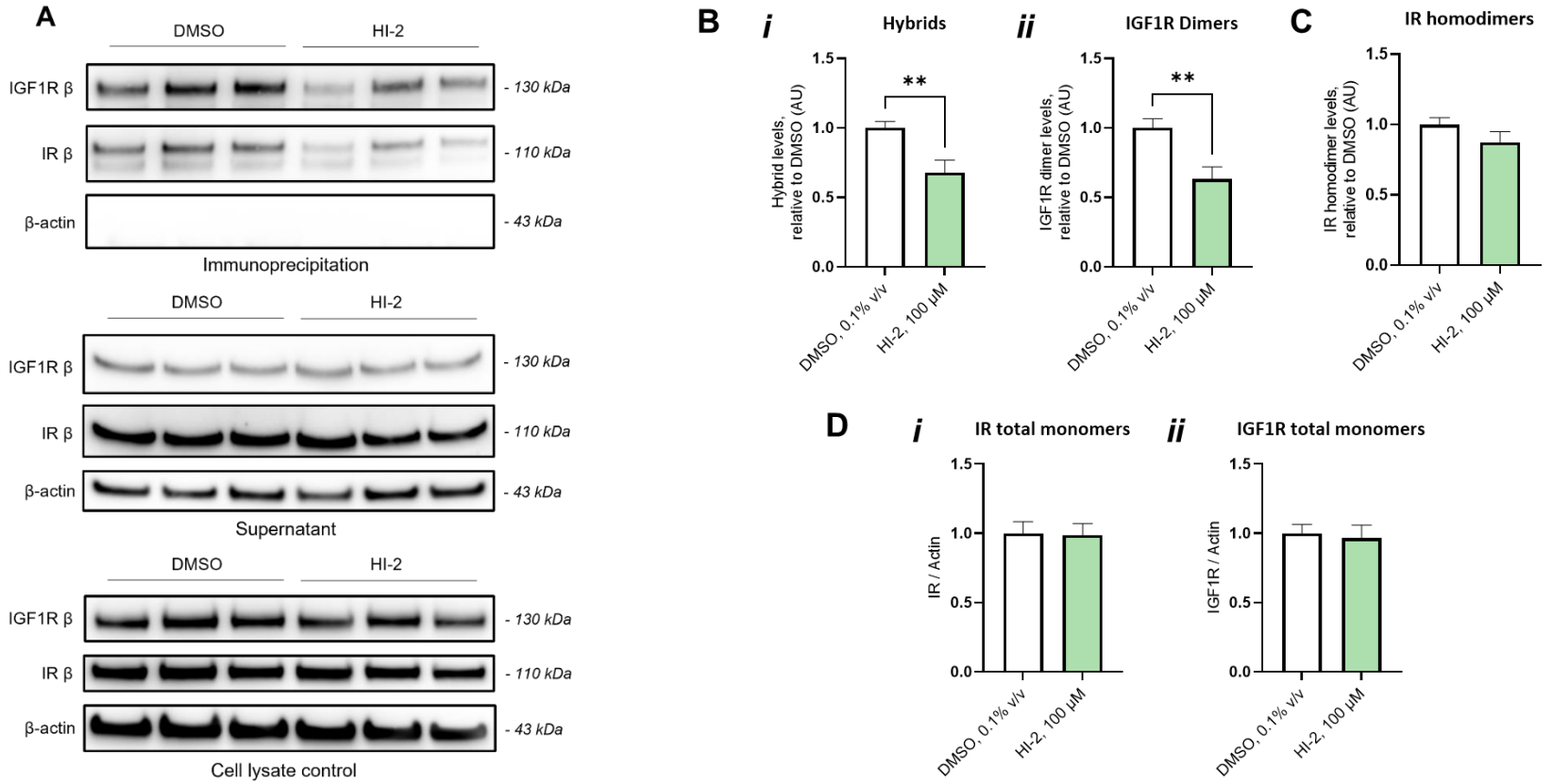

Figure 4-13: Characterisation of IR/IGF1R with HI-2 in Human Saphenous Vein Endothelial Cells

Representative western blots (**A**) and graphs (**B, C, D**) of immunoprecipitation, supernatant, and cell lysate control samples from non-treated, DMSO- and HI-2-treated hSVEC after 24-hour incubation. **B.** Immunoprecipitation sample graphs reporting change in IR/IGF1R (***i***) and IGF1R dimers (***ii***) after 24-hour treatment with HI-2, compared to respective DMSO-vehicle controls. **C.** Supernatant sample graph reporting change in IR homodimers after 24-hour treatment with HI-2, compared to respective DMSO-vehicle controls. **D.** Cell lysate graphs reporting change in IR (***i***) and IGF1R (***ii***) total monomers after 24-hour treatment with HI-2, compared to DMSO-vehicle controls. Densitometry data have been normalized to respective DMSO averages (+/- SEM). ****B*i* **P=0.005 n=11,11; **B*ii* ****P=0.008 n=6,6; **C** P=0.24 n=6,6; **D*i*** P=0.70 n=6,6**; D*ii*** P=0.82 n=6,6.

Blots of immunoprecipitation, supernatant, and cell lysate control samples for SVEC treated with 100 μM HI-2 and 0.1% v/v DMSO are shown in Figure 4-13. As compared with HUVEC data, HI-2 treatment of SVEC showed a significant reduction in IR/IGF1R hybrid formation, maintained at 33%. IGF1R dimers in HI-2 treated cells showed a significant decrease compared to respective DMSO controls. In the supernatant blots, IR homodimer formation was unaffected by HI-2 treatment. However, as IGF1R was still present in the supernatant, it is difficult to draw a conclusion as to the effect of HI-2 in SVEC using this data, since the proportion of IR/IGF1R hybrids and IGF1R dimers cannot be quantified. These immunoprecipitated samples were collected after 3-hours as in the old method using HUVEC, prior to parameter adjustment as in the Kahn method and was to be expected. In the cell lysate control blots, there was no effect of HI-2 on IR or IGF1R total populations. In HUVEC samples, the total population of receptors is significantly affected by treatment of HI-2 (section 4.2.2, Figure 4-12), whereas IR and IGF1R population in SVEC is unaffected. This is likely due to the fact that HUVEC are cultured from multiple, pooled donors whereas SVEC samples originated from singular patients, which will have varying levels of native receptors due to inter-individual expression.

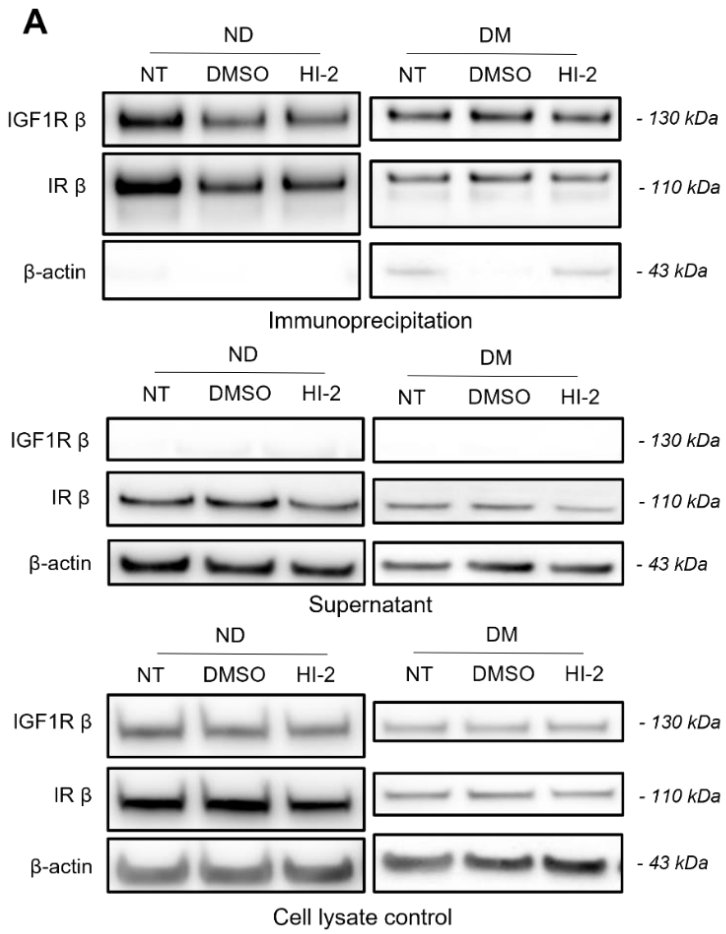

Figure 4-14: Western blots of IR/IGF1R with HI-2 in Non-Diabetic and Diabetic Human Adipose Tissue Endothelial Cells

A. Representative western blot of immunoprecipitation, supernatant, and cell lysate control samples in non-treated, volume equivalent DMSO- and 100 μM HI-2-treated ND/DM hATEC, after 24-hour incubation.

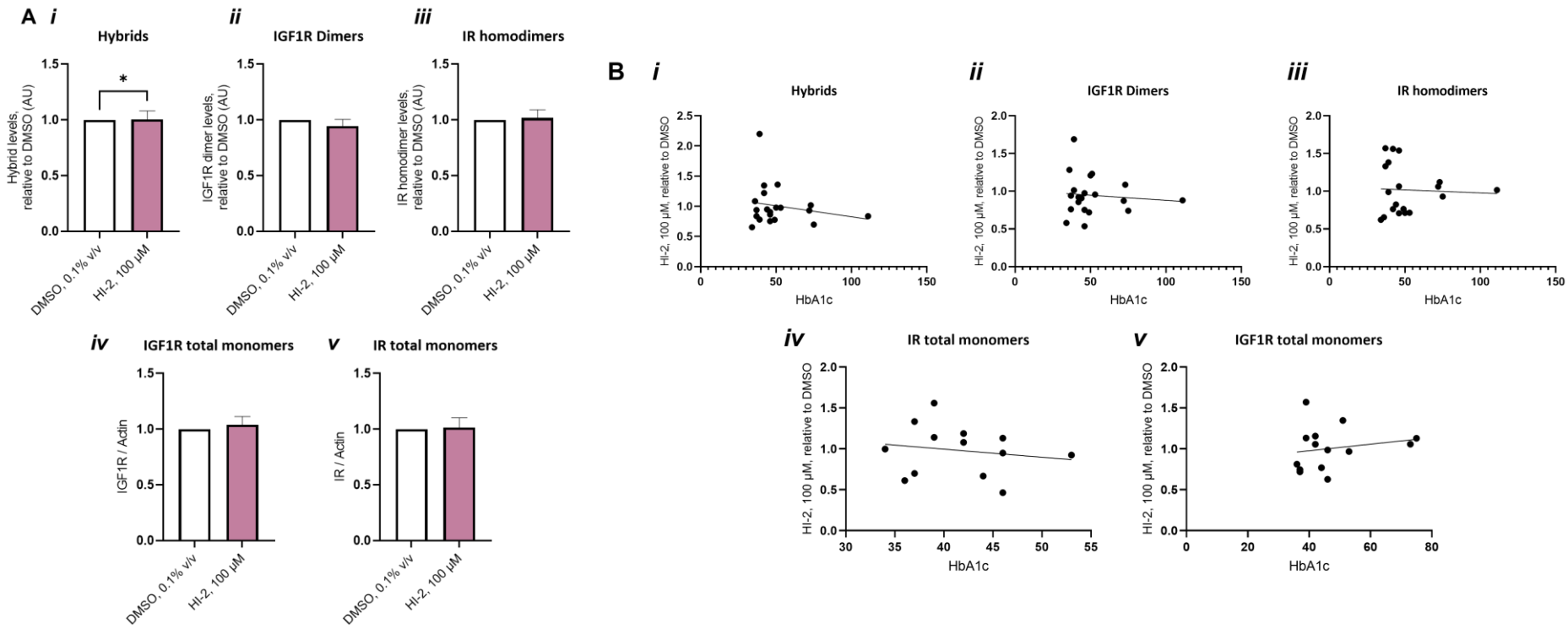

Figure 4-15: Graphs of IR/IGF1R with HI-2 in Non-Diabetic and Diabetic Human Adipose Tissue Endothelial Cells

Immunoprecipitation sample graphs reporting change in IR/IGF1R (**i**), IGF1R dimers (**ii**), IR homodimers (**iii**), IR total monomers (**iv**) and IGF1R total monomers (**v**) after 24-hour treatment with 100 µM HI-2, compared to respective DMSO-vehicle controls (**A**) or respective HbA1c levels (**B**). Densitometry data have been normalized to their respective DMSO replicate (+/- SEM). **A** N=15-20, P>0.; **B** N=13-20, R^2>0.95.

When tissue samples are collected from patients, we obtain some pseudo-anonymized data regarding the patient age, weight and also their HbA1c level. HbA1c figures are an indication of long-term management of blood glucose levels; the readings can be indicative of the presence of pre-diabetes or diabetes. For consideration, diabetes and heart failure patients would likely be suggested to include diet adjustments and various medications which could affect their HbA1c values. Predominantly in patient samples obtained, HbA1c levels, even for some people with diabetes, were recorded around 50 mmol/mol which suggested good blood glucose management and by extension, of their diabetic symptoms. Data regarding IR/IGF1R hybrid formation in ATEC were contrasted against individual patient's HbA1c levels and, further normalized against respective DMSO control samples (Figure 4-15 B). Analysis by previous methods of reporting against DMSO vehicle control found that with increasing *n* numbers, the 'unique' nature of each sample was being lost, noted by virtually identically weighted means between DMSO and HI-2 treated cells (Figure 4-15 A). Analysis reflecting change in receptor numbers with HI-2 treatment, normalized against DMSO vehicle control, compared with their respective HbA1c levels enabled determination of the effect of HI-2 across a range of diabetic severity (Figure 4-15). It is interesting that by inclusion of the HbA1c data, the effect of HI-2 across the receptor types could trend towards being influenced by this level, or the overall diabetic phenotype of the cells. At present, there is no significant relationship between HI-2 treatment and HbA1c for any receptor species. The dataset would benefit from a larger range of samples, notably at higher HbA1c levels (80+).

4.2.4. Dose Response

The working concentration of HI-2 for initial investigative experiments was selected based on the parameters set in the BRET assay prior to my arrival in LICAMM. It was imperative to determine if the inhibitor effect was dose-dependent and therefore if the concentration could be adjusted to modulate the proportion of IR/IGF1R hybrid being formed. Additionally, it could also show whether a lower concentration could achieve the same results as observed previously at 100 μM with a reduction in potentially toxic off-target side-effects.

With increasing HI-2 concentration, across all dimers – IR/IGF1R hybrids, IGF1R dimers and IR homodimers – observed a reduction in formation, and a particularly significant reduction at 250 μM (Figure 4-16). Interestingly, the significant reduction in IR/IGF1R hybrid formation was observed at concentrations greater than, or equal to 100 μM, our current working concentration. Across both IR and IGF1R total populations, there was no significant effect of modulating HI-2 concentration.

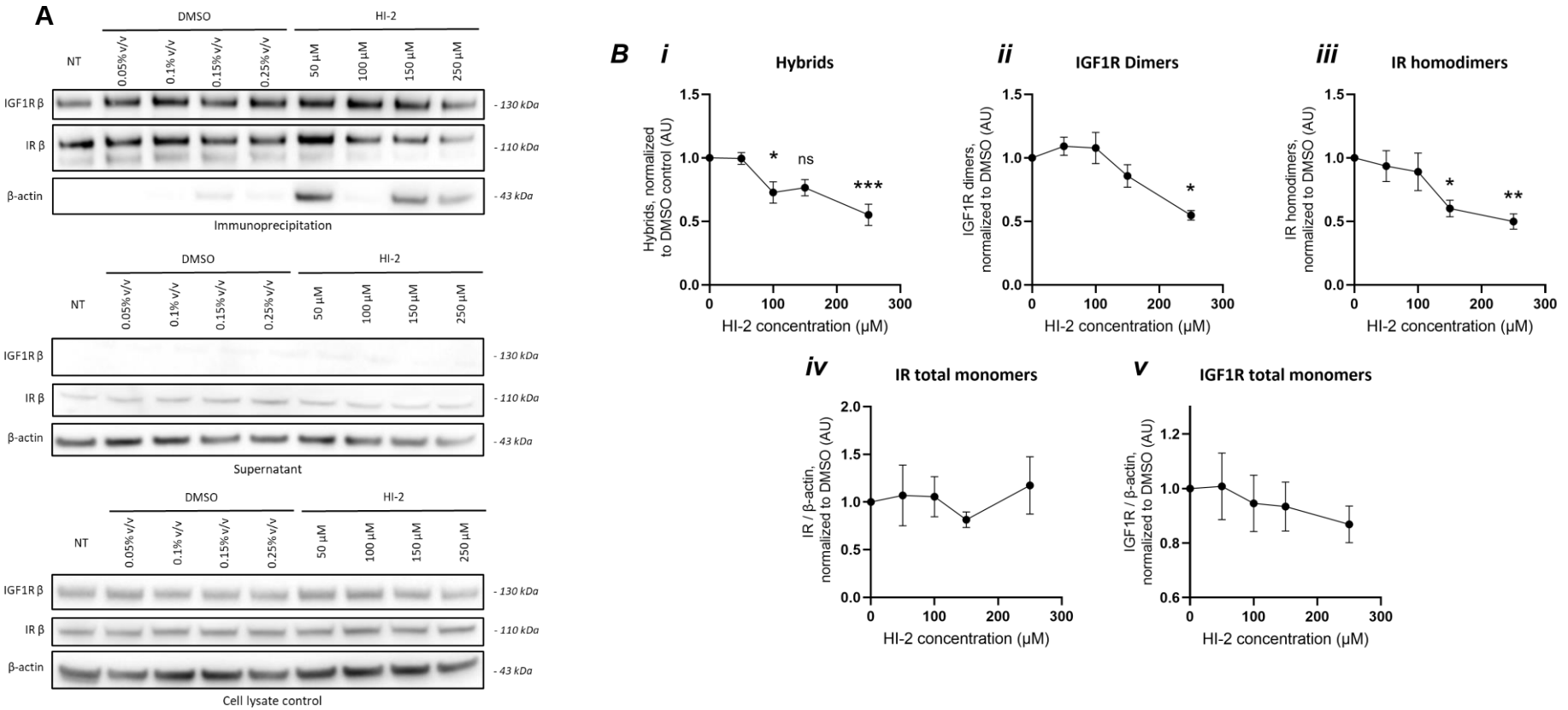

Figure 4-16: Dose-dependent Response of IR/IGF1R Hybrids with HI-2

A. Representative western blot of immunoprecipitation, supernatant, and cell lysate control samples in non-treated, volume equivalent DMSO- and HI-2-treated HUVEC at 0, 50, 100, 150 and 250 µM concentrations, after 24-hour incubation. **B.** Immunoprecipitation sample graphs reporting change in IR/IGF1R (***i***) and IGF1R dimers (***ii***) after 24-hour treatment with HI-2, compared to respective DMSO-vehicle controls. Supernatant sample graph reporting change in IR homodimers (***iii***) after 24-hour treatment with HI-2, compared to respective DMSO-vehicle controls. Cell lysate graphs reporting change in IR (***iv***) and IGF1R (***v***) total monomers after 24-hour treatment with HI-2, compared to DMSO-vehicle controls. Densitometry data have been normalized to their respective DMSO replicate (+/- SEM). N=5-6 **B*i*** *P=0.026, ***P=0.0007; **B*ii*** *P=0.014; **B*iii*** *P=0.019, **P=0.0019.

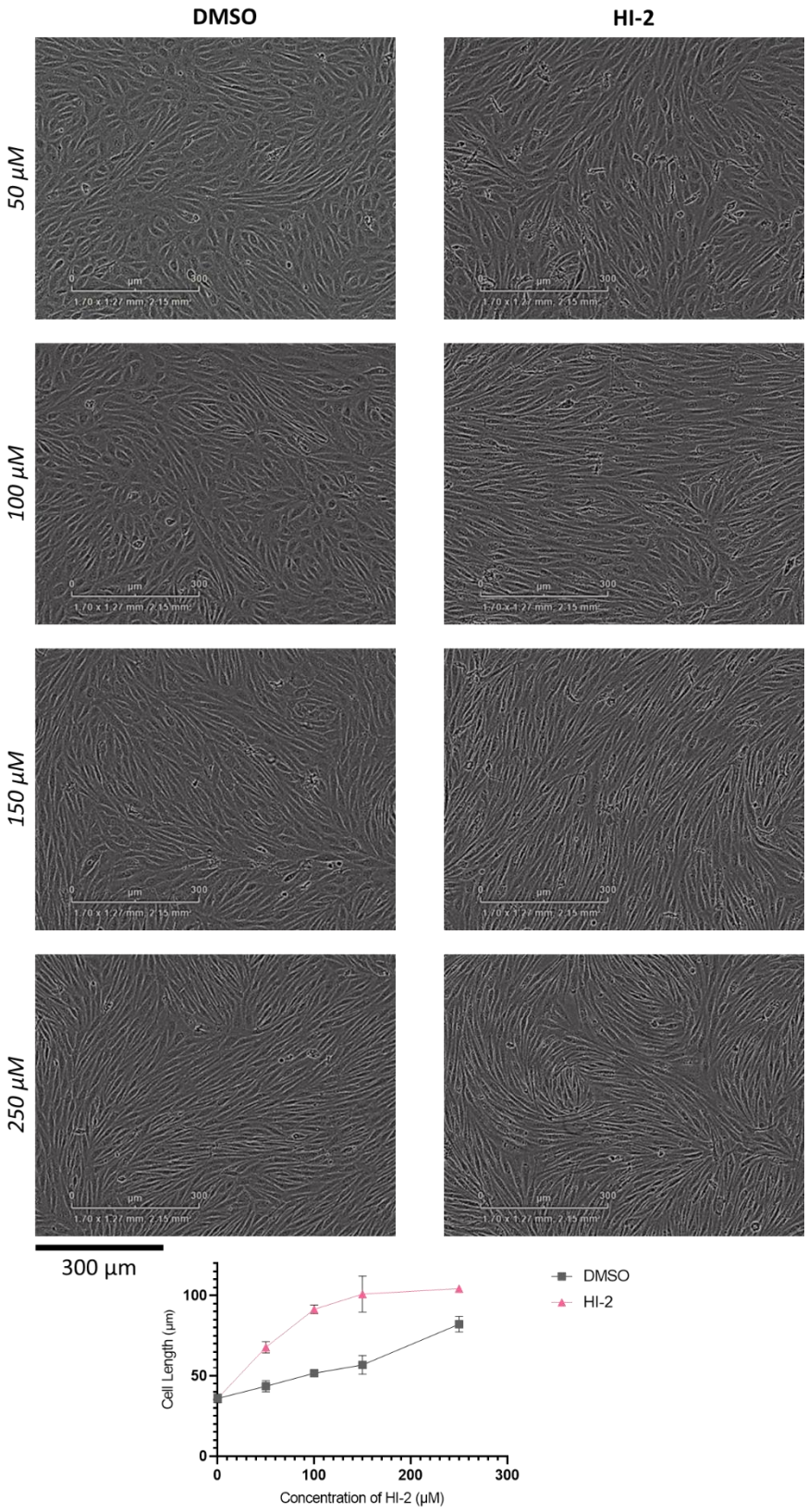

Figure 4-17: Change in Human Umbilical Vein Endothelial Cell Morphology with Increasing HI-2 Concentration

Change in cell morphology with increasing DMSO or HI-2 concentration, at the end of 24-hour compound incubation period. HUVEC change from small, rounded shape to long and needle-like. Scale in lower left corner equates to 300 µm, at 10X optics. N/n=2/2,2.

With increasing concentration of DMSO and HI-2, a notable change in cell morphology was observed (Figure 4-17), and exceptionally distinct at higher concentrations. A typical monolayer of HUVEC demonstrate what is referred as a ‘cobblestone’ pattern, appearing small and rounded in shape. At 100 µM or volume equivalent 0.1% v/v, DMSO and HI-2-treated HUVEC begin to elongate – though morphology was very similar between both treatments at this concentration. Once increased to 150 or 250 µM, the DMSO-treated cells did not change sufficiently in any appreciable manner. However, cells treated with HI-2 at higher concentrations became more significantly elongated and needle-like in shape. The appearance of these cells was similar to cells exposed to a high level of fluid shear stress (Steward et al., 2015). Shear stress can activate the insulin-mediated PI3K/Akt pathway and increase expression and phosphorylation of activatory sites of eNOS and NO bioavailability (Sriram et al., 2016). By reducing the IR/IGF1R hybrid receptor population, a higher proportion of signalling by activation of $(IR)_2$ homoreceptors might occur.

4.3. Effect of HI-2 on Insulin Receptor & Insulin-like Growth Factor 1 Receptor Gene Expression

It was consistently observed that the total population of IR and IGF1R seemed to be decreased in cells treated with HI-2. We had several hypotheses as to why this might be and began at the first possible opportunity for HI-2 to impact IR and IGF1R availability: mRNA transcription.

For any subsequent quantitative PCR testing to be relevant, it was important first and foremost, to determine if mRNA expression of *Insr* and *Igf1r* varied in a diabetic (DM) phenotype, compared to a non-diabetic (ND) phenotype. My

leading hypothesis regarding the favoured production of IR/IGF1R hybrids over IR homodimer receptors suspected that a yet-unknown stimulus was a driving force for this change. Should mRNA transcription of IR and IGF1R protein monomers be increased in diabetic state, a higher abundance of available monomers could explain an increased presence of IR/IGF1R hybrids *in situ*.

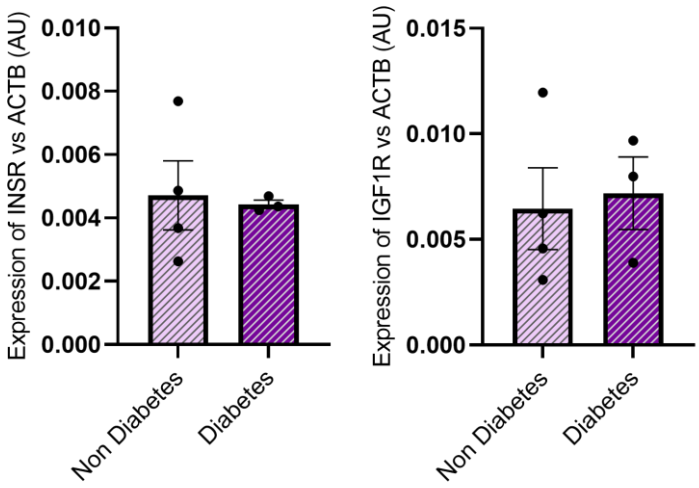

Figure 4-18: Basal *INSR* and *IGF1R* gene expression in Non-Diabetic and Diabetic Human Adipose Tissue Endothelial Cells

Graphs representing no change in *Insr* or *Igf1r* gene expression between non-diabetic or diabetic endothelial cell model. Data have been compared to respective *Actb* housekeeper gene (+/- SEM). INSR P=0.84 n=4,3; IGF1R P=0.80 n=4,3.

A qPCR assay comparing mRNA of *Insr*, *Igf1r* and *Actb* of a small human cohort of basal ND and DM ATECs was performed (Figure 4-18). For both *Insr* and *Igf1r*, compared to *Actb* housekeeper protein, diabetic status does not appear to affect gene expression.

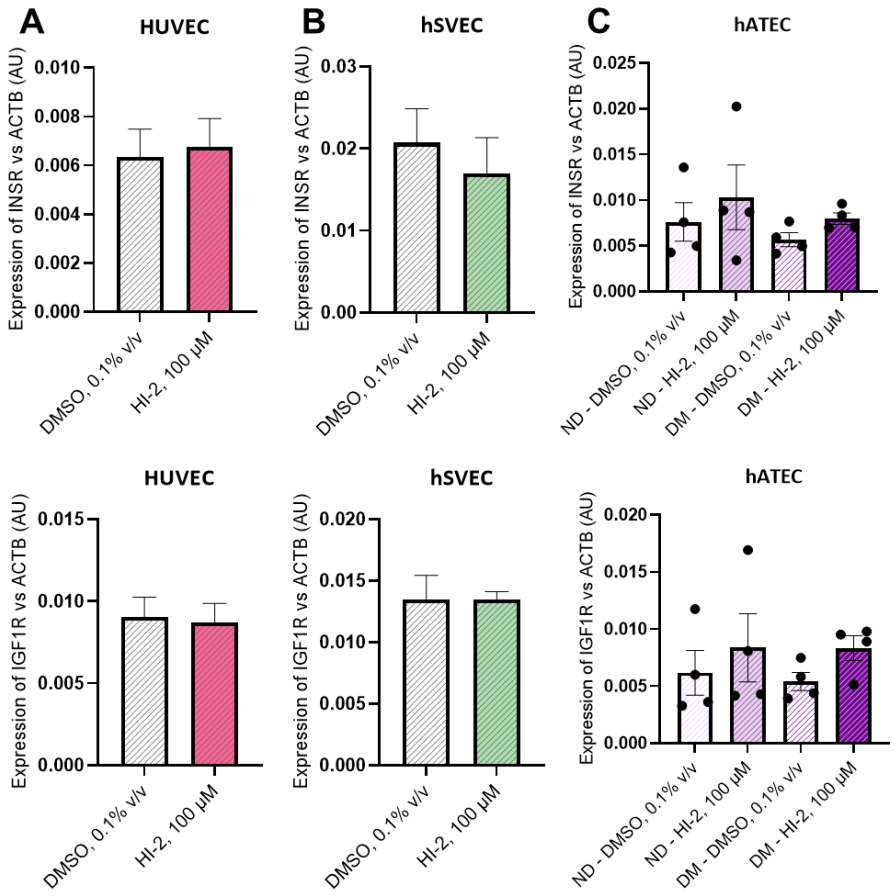

Figure 4-19: Effect of HI-2 on *INSR* and *IGF1R* gene expression in HUVEC, hSVEC and hATEC

Graphs representing no change in *Insr* or *Igf1r* gene expression between volume equivalent DMSO-vehicle control and 100 µM HI-2 in (**A**) HUVEC, (**B**) hSVEC and (**C**) hATEC, after 24-hour incubation. Data have been compared to respective *Actb* housekeeper gene (+/- SEM). HUVEC *Insr* P=0.81 n=5; HUVEC *Igf1r* P=0.84 n=5; hSVEC *Insr* P=0.57 n=1; hSVEC *Igf1r* P=0.99 n=1; ND hATEC *Insr* P=0.54 n=4,4; DM hATEC *Insr* P=0.057 n=4,4; ND hATEC *Igf1r* P=0.56 n=4,4; DM hATEC *Igf1r* P=0.07 n=4,4.

Subsequent qPCR assays comparing mRNA of *Insr*, *Igf1r* and *Actb* after 24-hour treatment with 100 µM HI-2 or 0.1% v/v DMSO in HUVEC, SVEC and ATEC were performed (Figure 4-19). In all cell types tested, HI-2 did not have a significant effect on gene expression of *Insr* or *Igf1r* compared to the *Actb* housekeeper protein. However, in both ND and DM ATEC, treatment with HI-2 suggested a trend towards an increase in gene expression for both *Insr* and *Igf1r* compared to *Actb*.

4.4. Signalling Downstream of the Insulin Receptor

4.4.1. Non-Diabetic Cell Model

The effect of HI-2 was determined across both PI3K/Akt and MAPK pathways in HUVEC (Figure 4-20), probing for p-/eNOS (total, S1177, Y657), PI3K p110α, p110β, p-/p85 (total, Y458), p-/Akt (total, S473, T308) and p-/MAPK proteins. HI-2 treatment significantly increased phosphorylation of Akt at T308 ($P=0.0019$) and eNOS at Y657 ($P=0.0495$). Screening of the remainder of the aforementioned downstream proteins regulation of expression or phosphorylation demonstrated no change with HI-2 treatment.

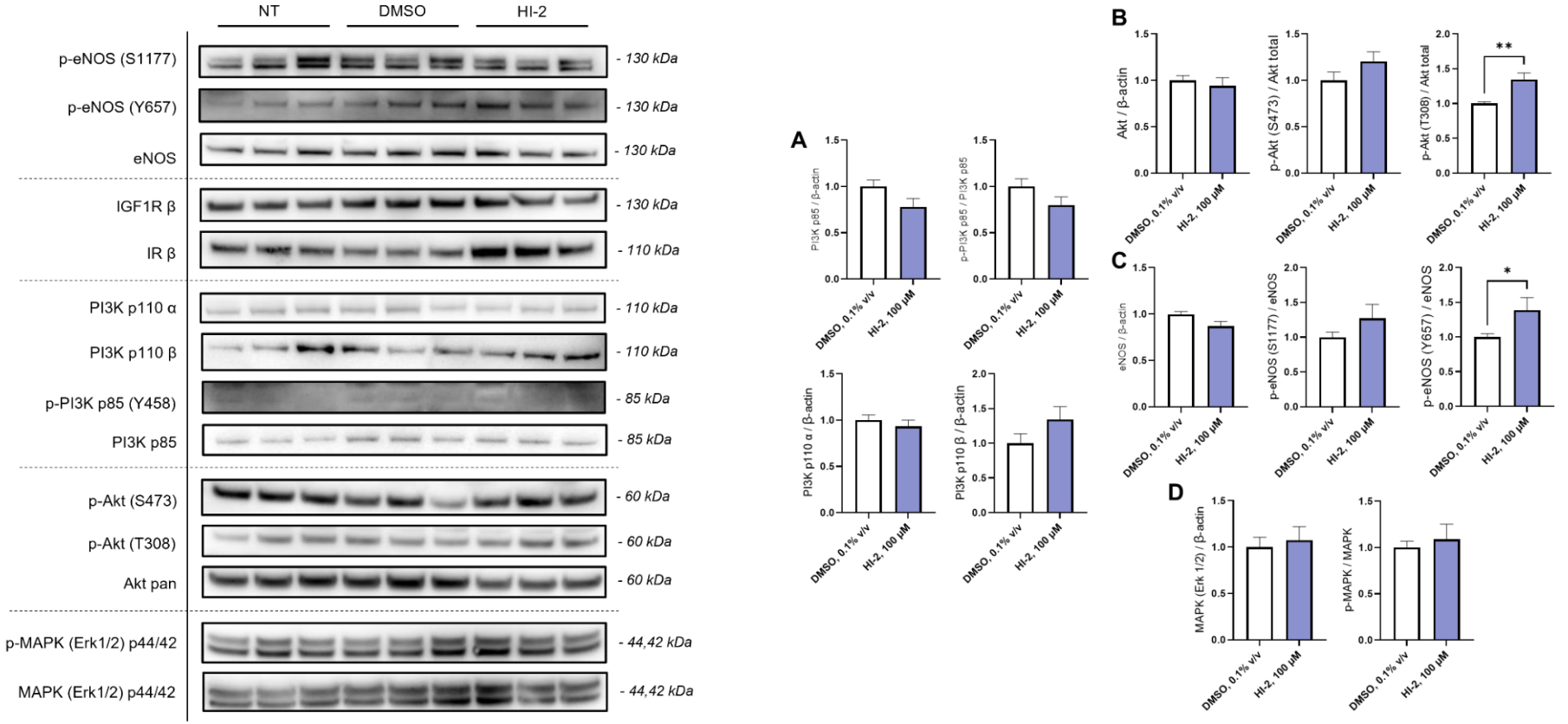

Figure 4-20: Downstream Signalling in Human Umbilical Vein Endothelial Cells

Representative western blot of HUVEC cell lysate samples in non-treated, volume equivalent DMSO- and HI-2-treated HUVEC at 100 µM, after 24-hour incubation. Proteins screened are eNOS total, p-Y657, p-S1177 (**C**); IGF1R; IR; PI3K p110α, 110β, p85 total, p85 p-Y458 (**A**); Akt total, p-T308, pS473 (**B**); MAPK (Erk1/2), p-MAPK (Erk1/2) (**D**). Graphs report a significant increase in Akt p-T308 and eNOS p-Y657. Densitometry data have been normalized to their respective DMSO replicate (+/- SEM). PI3K N=6-12; Akt N=12-17 **P=0.002; eNOS N=10-14 *P=0.05; MAPK N=11-13.

4.4.2. Diabetic Model

The effect of reducing hybrid formation with HI-2 was determined across both PI3K/Akt and MAPK pathways in a human diabetic ATEC cell model (Figure 4-21, Figure 4-22), probing for p-/eNOS (total, S1177, Y657), PI3K p110α, p110β, p-/p85 (total, Y458), p-/Akt (total, S473, T308) and p-/MAPK proteins. Again, as observed in the hATEC panel quantifying inhibition of IR/IGF1R hybrid formation (Section 4.2.3, Figure 4-15 A), representing the data against respective DMSO controls lost the 'unique' nature of each patient's tissue (Figure 4-21). HI-2 data, normalized against respective DMSO controls were plotted against individual patient HbA1c values, and where relevant, HI-2 raw data were paired with respective DMSO raw data (Figure 4-22). As in the HUVEC screening panel (Section 4.4.1, Figure 4-20), the majority of downstream proteins were relatively unaffected by treatment of HI-2, compared to DMSO control and maintained this trend with increasing HbA1c levels. At present, these data do not significantly suggest any trend towards increase or decrease in protein expression or activities. It's possible that across a larger range of HbA1c levels, notably by inclusion of high HbA1c patient samples (80+), that p-eNOS Y657 and p-Akt T308 might complement data obtained from the HUVEC screening panel.

HUVEC are frequently used as they are more robust and easily replicable – however, they often do not represent what occurs *in vivo*. Between batches of HUVEC, there is a very high degree of similarity in their action; protein transcription and signalling events are regulated by genetic modification to consistently perform to the phenotypic standard for the cell type. Primary cells, such as the ATECs derived from human tissues, exhibit normal physiology as

it pertains to that individual, as the cells retain genetic integrity: metabolism, signalling and, aging properties. Therefore, rates of protein expression and phosphorylation will vary from person to person. An additional factor in these studies considers a diabetic phenotype, originating from individual human patients, as opposed to the pooled donor HUVEC we were using. However, the samples from people with a T2DM diagnosis have low HbA1c levels; it would be beneficial to expand the range to higher HbA1c levels to determine the effect of HI-2 at the other extreme. And, a final consideration, some panels, notably for eNOS and its phosphorylation sites, only have four to five replicates. This value needs to be significantly higher to draw more accurate assumptions from these data. Due to these factors, it is likely that the ATEC patient samples vary in proportion of IR:IGF1R:IR/IGF1R hybrid receptors. While it is suspected that people with diabetes should possess higher levels of IR/IGF1R hybrids, due to their low HbA1c level, it may not be significantly different than in people without diabetes.

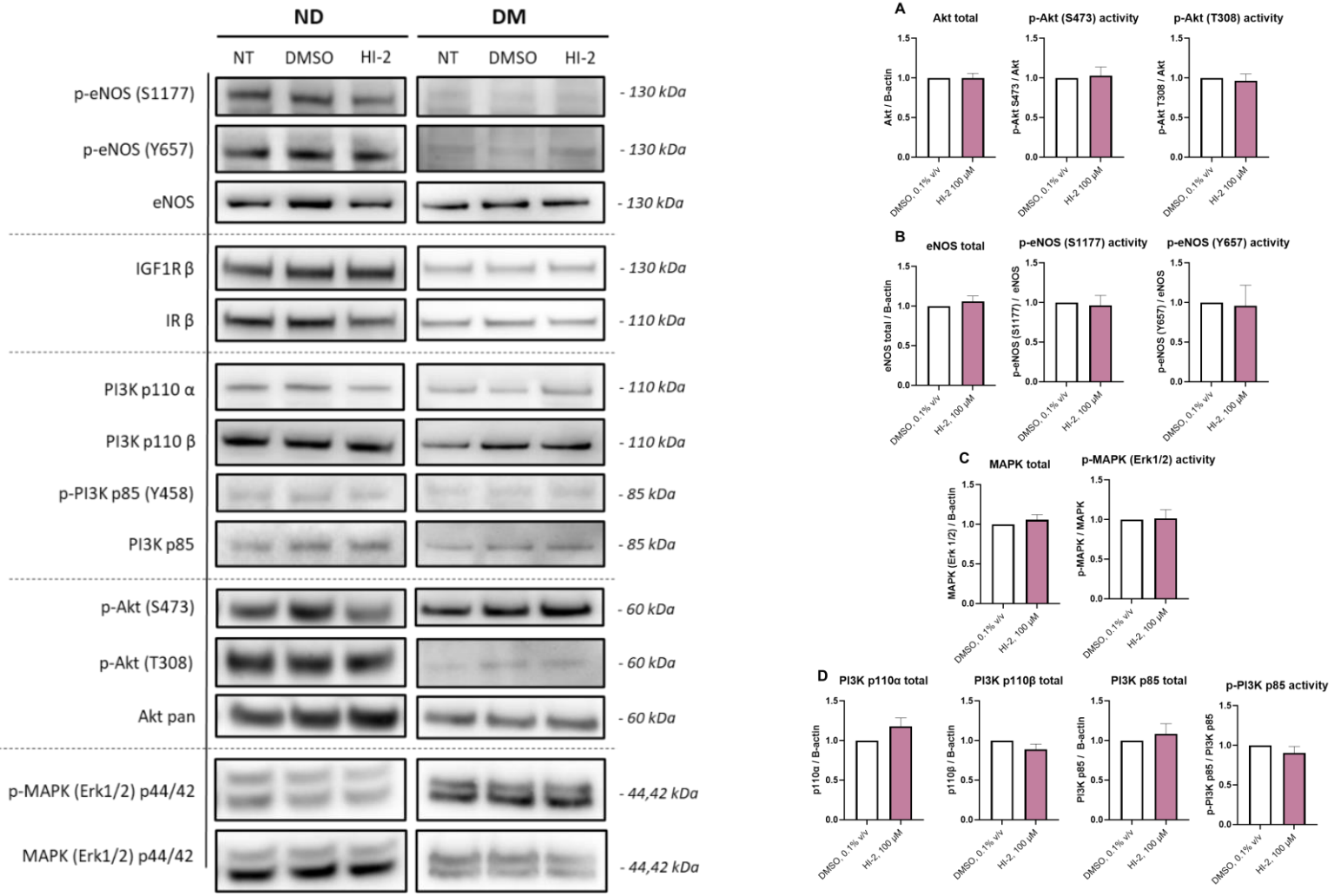

Figure 4-21: Downstream Signalling in Human Adipose Tissue Endothelial Cells Compared with Respective DMSO controls

Left: Representative western blot of human ATEC cell lysate samples in non-treated, DMSO- and HI-2-treated HUVEC at 100 µM, after 24-hour incubation. **Right:** Graphs reported against DMSO controls only do not highlight differences in individual patient samples. Densitometry data have been normalized to their respective DMSO replicate (+/- SEM). Proteins screened are eNOS total, p-Y657, p-S1177 (**B**); IGF1R; IR; PI3K p110α, 110β, p85 total, p85 p-Y458 (**D**); Akt total, p-T308, pS473 (**A**); MAPK (Erk1/2), p-MAPK (Erk1/2) (**C**).

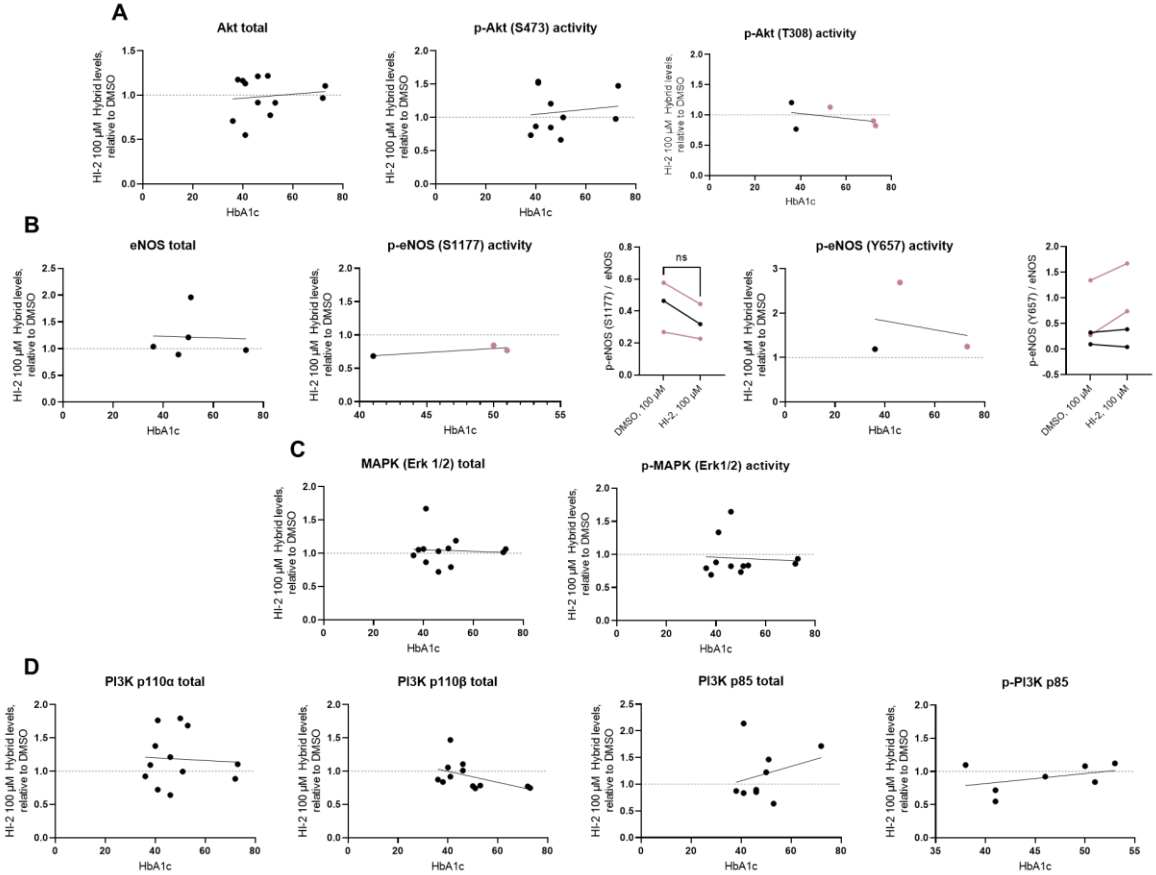

Figure 4-22: Downstream Signalling in Human Adipose Tissue Endothelial Cells Compared with HbA1c Levels

Graphs report a trend towards increases in Akt p-T308, eNOS p-Y657, PI3K p110α, PI3K p85 and decrease in eNOS p-S1177 – with increasing HbA1c levels. Densitometry data have been normalized to their respective DMSO replicate (+/- SEM).(**A**) Akt total N=12; Akt S473 N=10; Akt T308 N=5; (**B**) eNOS total N=5; eNOS S1177 N=3; eNOS Y657 N=3; (**C**) MAPK total N=12; p-MAPK N=11; (**D**) PI3K p110α N=12; PI3K p110β N=12; PI3K p85 total N=9; PI3K p-p85 N=7.

4.4.3. Effect of Reducing Hybrids on Nitric Oxide Bioavailability in Endothelial Cells

Nitric oxide, or NO, is a small radical gas produced in the conversion of *L*-citrulline to *L*-arginine, facilitated by nitric oxide synthase (NOS). NO plays a crucial role in several processes that maintain endothelial equilibrium and an antiatherosclerotic state (Tousoulis et al., 2012). In diabetes, the loss of insulin activation *via* its cognate receptors results in a loss of downstream signalling, including a reduction of NO production *via* downregulation of eNOS.

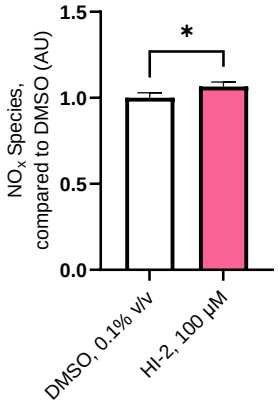

Figure 4-23: Nitric Oxide Quantification in HI-2-treated Human Umbilical Vein Endothelial Cell supernatant

Quantification of combined nitrate and nitrite levels in ECGM-2 supernatant, aspirated from non-treated, volume equivalent DMSO- and 100 µM HI-2-treated HUVEC. Data have been normalized to respective averaged DMSO controls (+/- SEM). *P=0.0436 n=20,20.

Cell culture supernatant was collected immediately at the end of the 24-hour incubation period with HI-2 or vehicle control, stored on ice in the interim and used directly in the assay. Initial experiments utilized whole cell HUVEC lysates, quantifying NO levels by a NO-specific colourimetric assay, however the method was insufficiently sensitive to detect any nitrous species relative to background noise. It was suspected that NO readily diffuses through cell membranes that the bulk of it would be present in the cell culture medium.

Preliminary data of the cell culture supernatant showed no discernible difference detectable by this method between background and samples for nitrite analysis, representing NO_X species from the 'nitrite and nitrate' samples only. Cells treated with HI-2 for 24-hours showed a significant increase of 6% in total NO_X species (P=0.0436) present in cell culture supernatant compared to respective DMSO controls (Figure 4-23).

4.5. Effect of Reducing Hybrids on Angiogenesis in Endothelial Cells

4.5.1. Proliferation

Proliferation involves the balance of newly-forming dividing cells and cell death by apoptosis or differentiation. Measurement of cellular proliferative ability can be assessed by a multitude of various assays, focusing on discrete elements contributing to cell proliferation. The Click-iT EdU Cell Proliferation Kit assay functions by fluorescent labelling of newly-synthesized DNA, distinguishing between proliferating and non-proliferating cells *in vitro*.

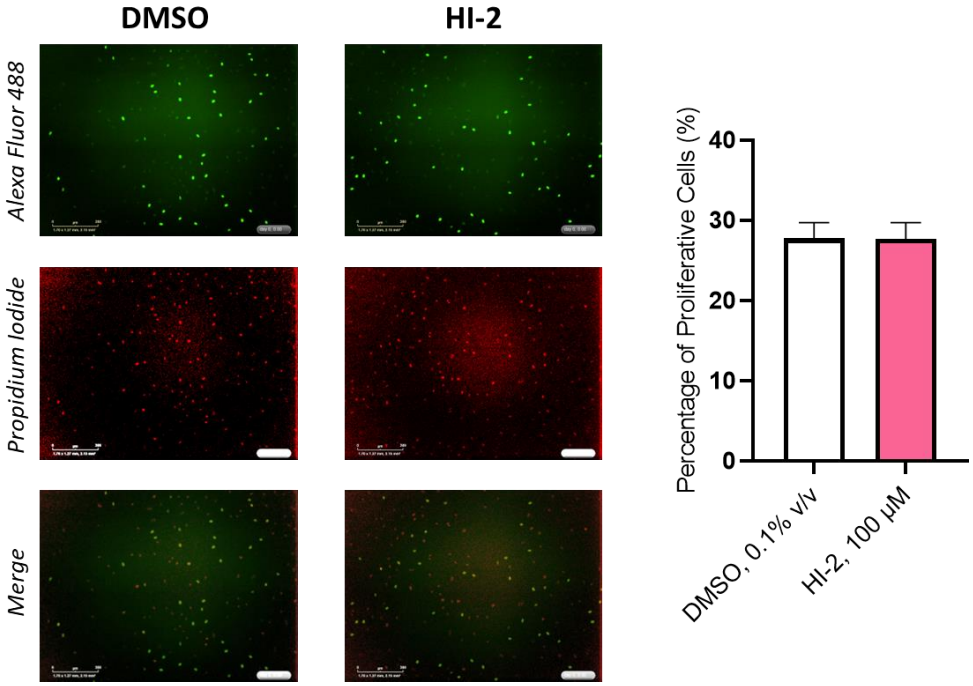

Figure 4-24: Effect of Reducing Hybrids using HI-2 on Cell Proliferation of Human Umbilical Vein Endothelial Cells

Representative images of EdU proliferation assay for volume equivalent DMSO- and 100 µM HI-2-treated HUVEC. Graph demonstrating no change in cell proliferation between DMSO-vehicle and HI-2-treated HUVEC, after 24-hours (+/- SEM). P=0.98 n=12,12.

The ratio of proliferative HUVEC cells to total living cells was assessed using an EdU assay. Seeded cells were treated with either 100 µM HI-2 or 0.1% v/v DMSO-vehicle control for 24-hours. At the end of this period, cells were incubated for two hours with 10 µM 5-ethynyl-2'-deoxyuridine (EdU) nucleotide, in addition to 100 µM HI-2 or 0.1% v/v DMSO, before being fixed and permeabilized to enable labelling of actively-forming DNA with Alexa Fluor 488 dye. Fluorescent images were sampled by the IncuCyte ZOOM® upon completion (Figure 4-24) and the ratio of total cells *versus* proliferative cells in representative samples was quantified. The IncuCyte ZOOM® is live-cell imager possessing phase contrast, green and red channels and can acquire non-invasive, continuous images from inside the cell culture incubator. The ratios of proliferative cells between the two treatment conditions showed that

HI-2 had no effect on proliferation, comparing mean values of 27.8% proliferating cells for DMSO and 27.7% for HI-2.

4.5.2. Wound Closure

Wound repair is highly dependent upon both migration and proliferation of endothelial cells (Ammann et al., 2019). Upon injury of the intimal layer, endothelial cells migrate into the gap; cells at the wound edge then enter a regenerative process involving two distinct phases. In the initial phase, approximately 4-7 columns of ECs located at the border of injury become activated, named the regenerating front, and enter the cell cycle. A small subset of these cells continues to proliferate and conclude regeneration in a second, and final phase (McDonald et al., 2018). A simple and inexpensive method to study this property is to use an *in vitro* scratch wound assay. A precise artificial “scratch” is delivered to a confluent monolayer of endothelial cells and over time, the cells at the edge of the wound move to close the gap (Liang et al., 2007).

Endothelial cell regeneration was assessed *via* the rate of scratch wound recovery of HUVEC treated with 100 µM HI-2 or 0.1% v/v DMSO-vehicle control and was monitored over 24-hours using the IncuCyte ZOOM®. The confluent monolayers were scratched using the Essen Woundmaker device to ensure all scratches were of similar width and length.

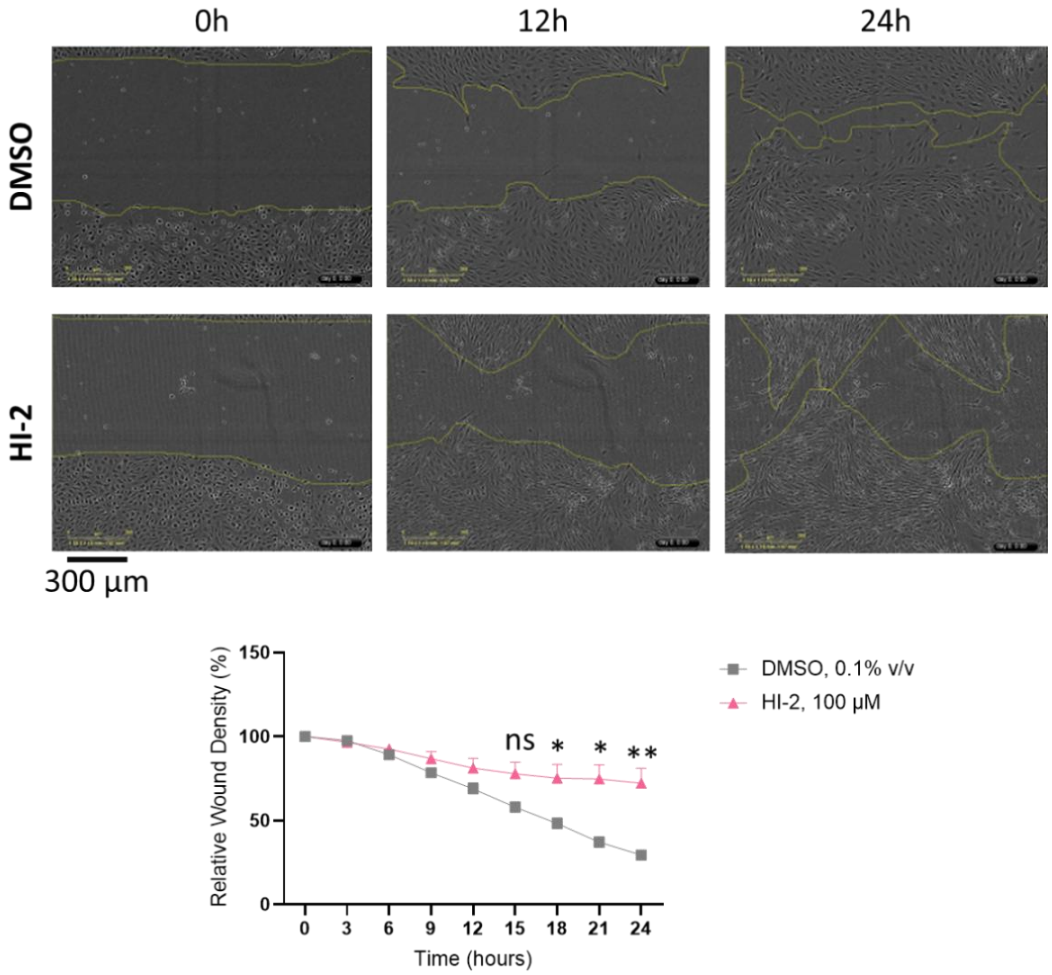

Figure 4-25: Effect of Reducing Hybrids using HI-2 on Wound Healing of Human Umbilical Vein Endothelial Cells

Representative images of scratch wound assay of volume equivalent DMSO- and 100 µM HI-2-treated HUVEC. Graph demonstrating change over 24-hours, observing a significantly reduced ability of wound repair with HI-2-treated HUVEC, from 18h onwards (+/- SEM). Scale bar equates to 300 µm, at 10X optics. N=3; 15h ^{ns}P=0.056; 18h *P=0.037; 21h *P=0.013; 24h **P<0.001.

Over a 24-hour time course, the “non-treated” or basal HUVEC monolayer consistently recovered (Figure 4-25). Comparatively, the average relative wound density of the DMSO-vehicle was approximately 29% at the end of the observation period. This was unsurprising as DMSO, while considered to be the safest solvent for use by the FDA, still has some toxicity effects – the effects of which were tested in the Live/Dead assay prior to this work where some toxicity was reported. DMSO increases cell permeability, facilitating entry of the small molecule into the cell, but in high doses or prolonged

exposure can result in dissolution of cell membranes. McDonald *et al.* detail that endothelial cells retain junctional complexes and remain connected throughout the repair process, therefore maintenance of plasma membrane integrity is of utmost importance (McDonald et al., 2018).

In stark contrast to the DMSO control, HI-2-treated cells were unable to regenerate a confluent monolayer; the average relative wound density of 72%, a 43% difference attributable effect of HI-2 treatment compared to vehicle control. It is possible that migration or proliferation mechanisms of endothelial cells treated with HI-2 have been markedly affected by the reduction in hybrid formation in the process of wound closure. Both IR and IGF1R mediate migration and proliferation *via* the PI3K/Akt pathway (Shrader et al., 2009; Girnita et al., 2014) and therefore, by reducing available IR/IGF1R hybrid receptors which may also mediate signalling of this pathway by activation of its constitutive IGF1R tyrosine kinase domain (Nitert et al., 2005; Li, G. et al., 2005). While the EdU data (Figure 4-24) does not suggest HI-2 treatment affects proliferation overall, it is possible that this process might become impaired upon injury.

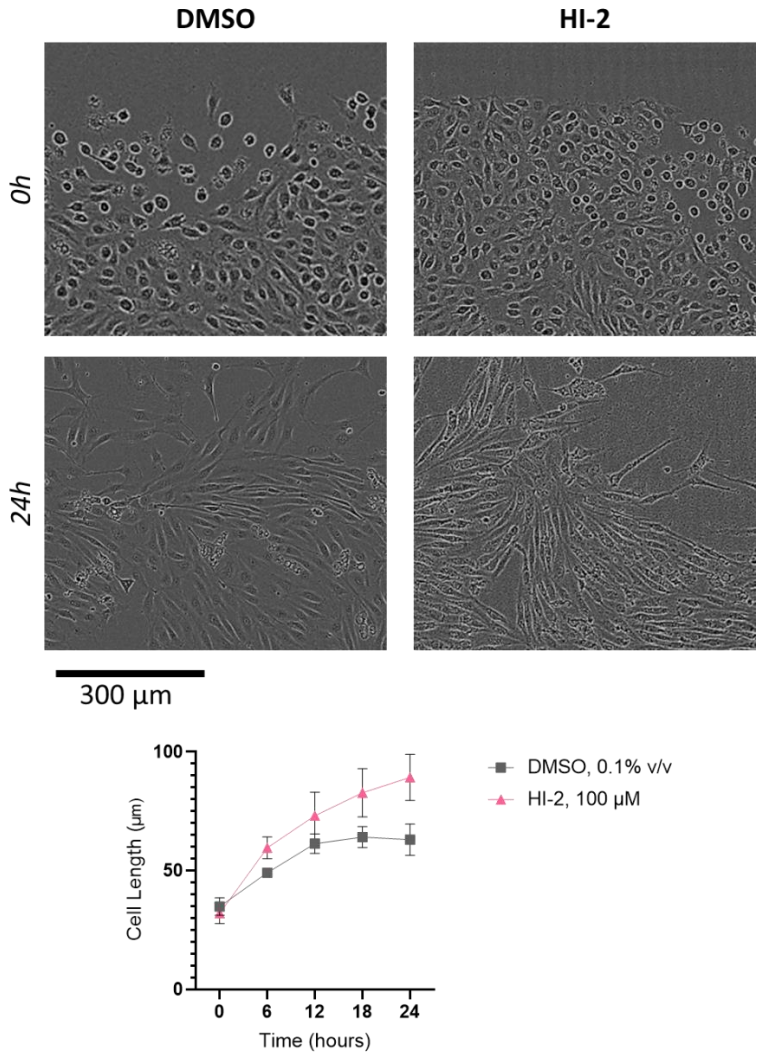

Figure 4-26: Change in Human Umbilical Vein Endothelial Cell Morphology at Wound Edge with 100 µM HI-2 treatment

Localised focus at wound edge on change in cell morphology, from small, rounded shape to long, needle-like with 100 µM HI-2-treatment. Scale bar equates to 300 µm, at 10X optics. N=3, all P>0.05.

The significant difference in loss of wound healing ability was marked by a distinct change in cell morphology observed across the three conditions (Figure 4-26). The cells treated with HI-2 appear more stressed, like those observed under fluid shear, taking a more elongated and narrow shape compared to their phenotypical rounded appearance. Compound solubility issues did arise through the duration of these experiments, as a newly synthesized batch of HI-2 with a slightly different crystal form was precipitating out of DMSO once added to an aqueous medium. It was possible that this

could have had an exaggerated effect on reduced wound regeneration, however we did also observe this needle-like appearance with higher concentrations of HI-2 (Figure 4-17) where issues with precipitation were not occurring.

4.5.3. Sprouting

Bead sprouting is a process within angiogenesis of tip formation and the development of new vessel sprouts. Bead sprouting of cells on Cytodex beads offers the ability to culture vessels in a 3D capacity.

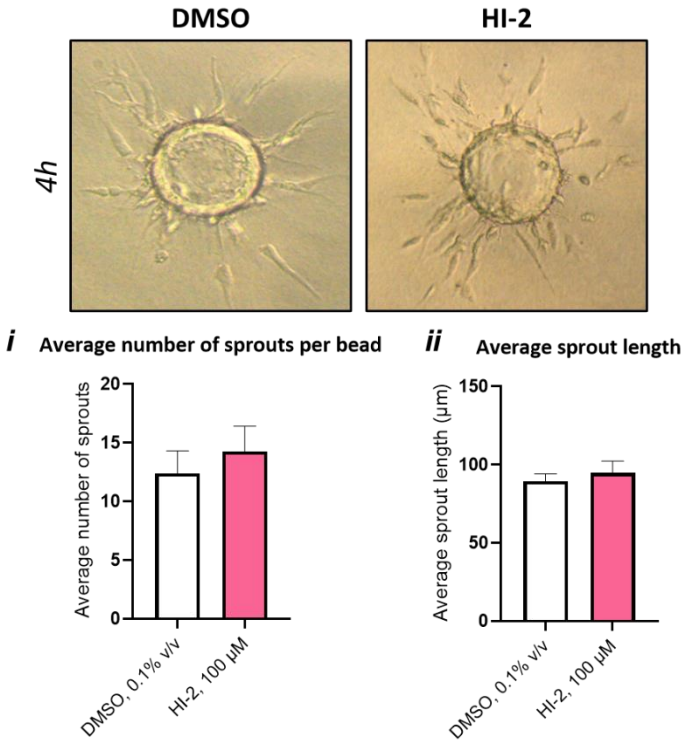

Figure 4-27: Effect of HI-2 on Bead Sprouting of Human Umbilical Vein Endothelial Cells

Representative images of bead sprouting assay for volume equivalent DMSO- and 100 µM HI-2-treated HUVEC, after 4-hours. Graphs demonstrating no significant difference between compound-treated and vehicle control sprout number (***i***) or length (***ii***), however a trend towards an increase in sprout number (***i***) may be observed (+/- SEM). ***i*** P=0.55 n=3,3; ***ii*** P=0.58 n=3,3. Bead sprouts prepared by Ms. E. Clavane (University of Leeds, Leeds, 2020 – unpublished) and imaged by C. Myers.

The HUVEC-coated Cytodex beads were kindly prepared by Eva Clavane in Kearney lab and analyzed by me using an Olympus microscope. Coated beads were suspended in a thrombin clot, containing a fibrinogen solution with either HI-2 or DMSO-vehicle control for 24-hours prior to imaging. Representative bead sprouts and graphs of average sprout number and length comparing DMSO and HI-2 treatments can be observed in Figure 4-27. Across the datasets, there was no significant difference in sprout length or number between the two treatment conditions. However, for sprout number, there was a trend towards an increase with HI-2-treated cells across all replicates. Tip formation in the early stages of sprouting angiogenesis, as shown in this assay, is highly dependent on migration of endothelial cells (Potente et al., 2011). If proliferation is impacted by treatment of HI-2, this may suggest why there is a trend towards an increase in sprout number – reliant upon migration of ECs – rather than length – which would require proliferation of ECs.

4.5.4. Tube Formation

Another property of angiogenesis regards the formation of networks of new vessels. Tube formation on a Matrigel matrix platform enables 2D visualisation of forming vascular networks or tubes.

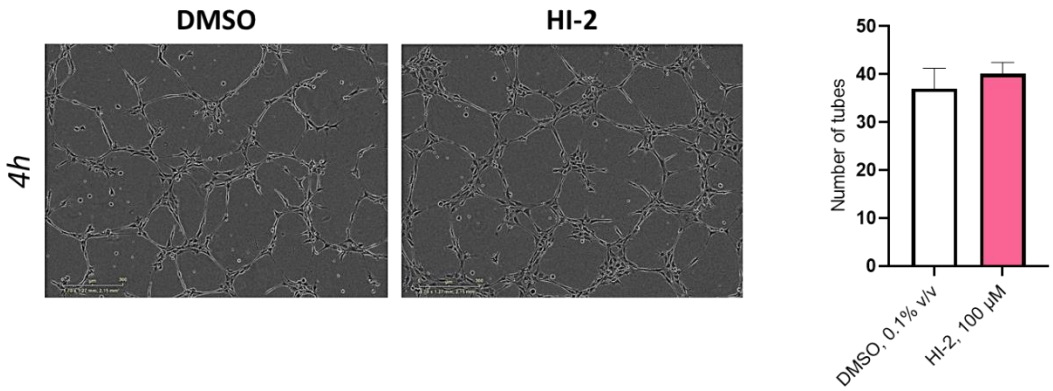

Figure 4-28: Effect of HI-2 on Tube Formation of Human Umbilical Vein Endothelial Cells

Representative images of tube formation assay for non-treated, volume equivalent DMSO- and 100 µM HI-2-treated HUVEC, after 4-hours. Graph demonstrating no significant difference between compound-treated and vehicle control tube formation (+/- SEM). P=0.53 n=4,4.

Tube formation angiogenesis was assessed in HUVECs, treated for 24-hours prior to the start of the assay with 100 µM HI-2 or 0.1% v/v DMSO. Treated cells were seeded onto polymerized endothelial cell matrix containing 100 µM HI-2 or 0.1% v/v DMSO and incubated for 4-hours. Images were sampled at the end of the 4-hour incubation period (Figure 4-28). Between the two conditions, HI-2 treatment did not appear to have significant effect on tube formation. Similarly to the bead sprouting assay (section 4.5.3), tube formation at this stage in the process is highly dependent upon migration of endothelial cells so it could be possible that HI-2 might contribute to upregulation of this process.

5. Conclusion and Discussion

In people with type-2 diabetes, a higher proportion of IR/IGF1R hybrid receptors populate endothelial cell membranes, resulting in formation of fewer IR homodimeric receptors. IR/IGF1R hybrid receptors do not possess comparable signalling ability for either IR- or IGF1R-activated cascades, with respect to their homodimeric receptor counterparts; insulin sensitivity is markedly reduced in endothelial cells. Loss of signalling contributes to a dysfunctional phenotype, as production of NO is attenuated, resulting in a loss of vascular repair and regeneration. While the physiological role and function of hybrid receptors in type-2 diabetes is unknown, the potential to modulate the formation of this receptor species as means to restore insulin sensitivity has presented itself.

5.1. Discovery of Novel IR/IGF1R Hybrid Formation Inhibitor

Modulation of IR/IGF1R hybrids by genetic manipulation is not possible, as changes in IR and IGF1R protein expression would impact the formation of homodimeric receptors and further aggravate the insulin resistant phenotype of these cells, by reduced insulin and IGF-1 signalling. Design and development of a small molecule could produce a target-specific agent to investigate the effects of reducing IR/IGF1R hybrids and mutually increase formation of IR homodimers.

A virtual high-throughput screening method was developed. A homology model of the IR/IGF1R hybrid receptor ectodomain was designed, based on the IR ectodomain crystal structure (PDB ID; 2DTG (McKern et al., 2006)) and replacing the amino acid sequence of one monomer of IR with the complementary sequence of the IGF1R. Small molecule candidates were

docked against a hotspot on the IR which possesses the lowest degree of similarity between homodimer receptors, and measured favourable interactions supporting binding to IR and steric clashes with IGF1R. A set of structurally-diverse inhibitors were purchased and screened for their respective *in vitro* toxicity and specificity for IR/IGF1R hybrids over IR and IGF1R homodimers, using Live/Dead and BRET assays. BRET measures the proximity of the Rluc and YFP; to confirm the results obtained using the BRET assay, co-immunoprecipitation of IGF1R and western blotting for IR were performed. All compounds, with exception of HI-2, were not sufficient to inhibit hybrid receptor formation, in contrast with preliminary BRET data. It is likely that the BRET signal indicated both a change in hybrid conformation upon binding of these compounds and some inhibition of hybrid formation, as opposed to complete impedance of formation of this receptor species. This is in contrast with western blotting methods which can only quantify protein levels present in a sample, and therefore, by using a co-immunoprecipitation method for IGF1R and IR would only extract dimerized hybrid receptors. Structural biology techniques, such as x-ray crystallography and electron microscopy would be required to confirm this hypothesis.

Hybrid inhibitor, HI-2 was identified through the aforementioned screening process, producing an approximate 30% reduction in IR/IGF1R hybrid formation in HUVEC (section 4.2.4, Figure 4-16), 33% in SVEC (section 4.2.3, Figure 4-13) and could trend towards a more profound reduction of these species with increasing HbA1c level in ATEC however the current spread of data does not suggest a significant difference (section 4.2.3, Figure 4-14). Despite presentation as a promising hybrid inhibitor candidate, HI-2 possesses poor metabolic stability, with short half-life and high clearance

rates, and solubility and therefore, HI-2 would not be suitable for use *in vivo* or by continuous administration *via* minipump. However, the identification of HI-2 is an excellent proof of concept and starting point to produce a series of structural analogues with improved solubility and stability characteristics. With improved ADMET characteristics, the hybrid inhibitor could be further used in investigative research surrounding IR/IGF1R hybrids in disease, but also potentially as a therapeutic treatment for type-2 diabetes.

5.2. Method Development of IR/IGF1R Co-Immunoprecipitation and Western Blotting Technique

Preliminary screening of IR/IGF1R hybrid formation consisted solely of co-immunoprecipitation of IGF1R and western blotting of IR (section 4.1) to determine the effect on hybrid formation inhibition. Further screening of the effect of HI-2 on total IR and IGF1R population levels was performed by western blotting of cell lysate. The combination of these methods enabled quantification of hybrids, total IGF1R dimers, and total IR and IGF1R populations; information regarding the IR dimers was absent. The aim of designing novel, selective hybrid formation inhibitor compounds would respectively promote the formation of IR dimers – no longer sequestered within hybrids – to improve insulin sensitivity of endothelial cells. Synchronously, preventing sequestration of IGF1R in hybrid receptors would also increase formation of IGF1R homodimers, which upon activation by IGF-1, can also trigger the corresponding PI3K/Akt pathway and improve NO bioavailability, in a similar manner to the IR-insulin complex.

A publication by Kahn and colleagues included a slight variation of the current IGF1R co-immunoprecipitation method (Li, Q. et al., 2019). Quantification of

the previously discarded supernatant, containing non-pulled down IR dimers, could serve to fill the gap in this method. Characterisation of IR, IGF1R and IR/IGF1R dimers utilizing the 'Kahn' method did indeed allow for quantification of IR dimers, however it also highlighted issues with the previous method, which were otherwise concealed due to missing information. Pull-down of IGF1R was incomplete, noted by its presence in the supernatant. Likewise, there were low-lying levels of β-actin present in the immunoprecipitation blots, suggesting that non-specific binding may be occurring after the washes.

There are several variables to consider when making adjustments to the co-immunoprecipitation method, to resolve the aforementioned issues: type of support surface *i.e.,* magnetic or agarose beads, the type or concentration of protein-specific antibody, duration of protein immobilisation and, number and volume of washes upon completion of the immobilisation period. To improve the efficiency of the pull-down of IGF1R, changes regarding the antibody used or duration of the pull-down can be altered. Increasing antibody concentration would be more cost-inhibitive and the current antibody offers effective specificity of binding to the IGF1R in western blotting experiments, a new antibody would require validation work to ensure continued specificity for IGF1R. Therefore, the simplest and most cost-effective modification would be to increase the immobilisation period of protein to the agarose bead surface; the previous method required a minimum of 3h prior to clean-up, this was re-adjusted to a minimum of 16h, or overnight to improve yield of pulled-down IGF1R. The increase to 16h minimum vastly improved the yield of pulled-down IGF1R, improving accuracy of quantification of IR/IGF1R hybrids and IGF1R total dimer species (section 4.2.4). Likewise, changing the support surface to magnetic beads could reduce non-specific binding however implementing this

apparatus in western blotting would require more extensive validation and be more cost-inhibitive compared to the alternative of increasing the volume and frequency of immunoprecipitated sample washes. The previous method required three, 500 µL washes; the first method implementation decided upon six, 1000 µL washes. Increasing the volume and frequency of washes at the conclusion of co-immunoprecipitation method saw considerable decrease in β-actin in immunoprecipitation blots (section 4.2.4). These slight adjustments have created a more robust and accurate method for quantification of IR/IGF1R hybrids and their counterparts, in addition to monitoring the change in formation levels using hybrid inhibitors.

5.3. Modulation of IR/IGF1R Hybrid Formation in Endothelial Cells

Development of the new IR/IGF1R quantification method allowed for characterisation and determination of modulation of these receptor species in HUVEC (section 4.2.4), SVEC (section 4.2.3) and ATEC (section 4.2.3).

HI-2 inhibited the formation of IR/IGF1R hybrid receptors across all cell types tested, producing an approximate reduction of 32% in HUVEC, 33% SVEC and may trend towards an increasingly effective reduction in ATEC from patients with increasing HbA1c level however further investigation is required. In initial characterisation using HUVEC and SVEC, IR and IGF1R levels were also significantly reduced with HI-2 treatment; HI-2 could increasingly inhibit hybrid formation with increasing HbA1c, in line with the observation of a higher proportion of IR/IGF1R hybrid receptor species present in diabetic endothelial cells (Nitert et al., 2005; Li, G. et al., 2005). HbA1c is an indicator of glycaemic control which could be used as an indicator of the severity of diabetic phenotype and could be suggestive of a higher proportion of IR/IGF1R hybrid

receptors. HI-2 was determined to inhibit IR/IGF1R hybrid receptor formation in a dose-dependent manner, in HUVEC. However, at higher concentrations, at 150 μM for IR and 250 μM for IGF1R, HI-2 became less target-selective, noting significantly affected interaction with IR and IGF1R homodimer receptors. Non-specific binding is linearly proportional to unbound ligand, therefore the excess of available compound would drive binding to IR and IGF1R (Salahudeen and Nishtala, 2017). This assay also highlighted that the selected working concentration of 100 μM was not only sufficient to induce significant inhibition of IR/IGF1R hybrid receptor formation, but also limited non-specific binding.

Due to some observed variation in total IR and IGF1R receptor levels in HUVEC and SVEC western blots, HI-2 was assessed for any off-target effects using PCR (section 4.3). PCR measures the levels of mRNA transcribed for individual proteins; mRNA expression was unaffected in all cell types tested, though there was a trend towards an increase in *Insr* and *Igf1r* in non-diabetic and diabetic ATEC with HI-2 treatment. Further work will be required to determine if HI-2 is interfering in protein translation or degradation.

5.4. Effect of Reduction in IR/IGF1R Hybrid Formation on Downstream Signalling

Quantification of the regulation of downstream signalling proteins of the insulin receptor and IGF1R have been evaluated in HUVEC and human ATEC (section 4.4).

The effect of reducing IR/IGF1R hybrid receptor population in HUVEC by treatment with the hybrid formation inhibitor, HI-2 would decrease binding of available insulin or IGF-1 ligands to this receptor species and increase

availability of the aforementioned ligands in binding and triggering subsequent increased functional signalling *via* the homodimeric IR and IGF1R species. These receptors can signal *via* the PI3K/Akt/eNOS axis, resulting in an increase in Akt T308 phosphorylation, an activatory site of Akt (section 4.4.1, Figure 4-20) and a resultant increase in NO production, as observed by a 6% increase in NO_X species present in HUVEC cell culture supernatant treated with HI-2 (section 4.4.3, Figure 4-23). While this difference is statistically significant, it is unlikely that there would be a significant biological effect associated with this slight increase in NO production. However higher NO production *via* eNOS could trigger a regulatory feedback loop by activation of proteins which inhibit eNOS, as a protective response to prevent enzyme uncoupling, which could explain the increased levels of eNOS Y657 phosphorylation (section 4.4.1, Figure 4-20). Protein tyrosine kinase 2β (PYK2) has been shown to phosphorylate this inhibitory site of eNOS upon stimulation by insulin or angiotensin and fluid shear stress (Fisslthaler et al., 2008; Loot et al., 2009). However, it is also possible that eNOS is inhibited by PYK2 from the offset; the increase in NO production could be a result of upregulation of inducible NOS in response to stress as an adaptive response by the endothelial cells, due to HI-2 treatment (de Assis et al., 2002; Pohlman and Harlan, 2000). The human ATEC data (section 4.4.2, Figure 4-22) may support the results obtained in HUVEC and aforementioned hypotheses with further investigation utilizing a larger range of patient samples, notably with high HbA1c levels.

Confirmation of the involvement of regulatory proteins, such as PYK2 *via* a feedback loop or induction of iNOS would require further work. Treatment of endothelial cells with HI-2 appears to promote signalling *via* PI3K/Akt pathway

and increase NO bioavailability, despite evidence of constitutive NOS-protective interactions inhibiting its catalytic activity. The observation of increased intracellular signalling is promising, as it suggests the potential for improved NO production via the IR/PI3K/Akt/eNOS axis and therefore generation a protective, anti-atherosclerotic state.

5.5. Effect of Reduction in IR/IGF1R Hybrid Formation on Angiogenesis and Regeneration

Regulation of angiogenesis and regenerative processes are impaired in endothelial dysfunction (Carmeliet, 2005). Nitric oxide is a known regulator of proliferation, migration, and angiogenesis (Ziche et al., 1994; Matsunaga et al., 2002; Cooke and Losordo, 2002). Functional signalling *via* IR and IGF1R by activation of insulin and IGF-1 is markedly reduced in cells possessing a high proportion of IR/IGF1R, due to sequestration of the aforementioned receptor species in hybrid receptors and their lack of functional intracellular signalling ability *via* either ligand species (Belfiore et al., 2009; Nitert et al., 2005; Li, G. et al., 2005). Inhibition of IR/IGF1R formation using HI-2 has been shown to increase PI3K/Akt signalling in HUVEC and ATEC (section 4.4) and, NO_X species in HUVEC cell culture supernatant (section 4.4.3).

The effect of HI-2 treatment on endothelial cell regeneration and angiogenesis has been described in HUVEC through use of EdU proliferation assay, scratch wound healing assay, tube formation and tip cell formation angiogenesis assays. Wound closure of endothelial cells is reliant upon both proliferative and migratory mechanisms (Ammann et al., 2019). Regeneration of HUVEC upon receipt of injury has been markedly affected by HI-2 treatment (section 4.5.2, Figure 4-25). Migration of endothelial cells is the dominant factor in this

process, accountable for 95% of wound repair at 4h post-injury while slowly decreasing to 55% at 48h; over time, proliferation of endothelial cells becomes increasingly involved in regeneration of the monolayer, responsible for the reduction in migration (Ammann et al., 2019). This concomitant relationship is in agreement with HUVEC scratch wound healing, where regeneration of the monolayer is sustained until between 6h and 9h, significantly diverging at 18h, compared to DMSO and basal cell controls. This timeframe also aligns with a full cycle of receptor turnover, occurring approximately every 6 hours, which suggests the full effect of HI-2 inhibition of newly forming homodimeric and hybrid receptors can be observed from this point onwards (Reed and Lane, 1980). Proliferating endothelial cells are only activated at the regeneration front, consisting of approximately 4 to 7 columns of cells from the site of injury (McDonald et al., 2018). While the EdU proliferation assay did not detect any changes in proliferation of the cells with HI-2 treatment (section 4.5.1, Figure 4-24), it is possible still that either of these mechanisms could be affected by treatment of HI-2. It is not unexpected to observe a difference between repair and angiogenic mechanisms (Potente et al., 2011; Ammann et al., 2019), sprouting angiogenesis assays, demonstrating the ability of endothelial cells to migrate, appear to trend towards being upregulated with HI-2 treatment. In the bead sprout assay representing the formation of new tip cells (section 4.5.3, Figure 4-27) and tube formation (section 4.5.4, Figure 4-28), both sprout number and tube number could trend towards being increased with HI-2 treatment at higher *n* numbers; sprout length appeared unaffected by HI-2. Sprout length could be limited by impeded proliferation of endothelial cells, whereas sprout and tube number are highly dependent upon migration

(Goodwin, 2007). Therefore, migration could be upregulated with HI-2 treatment, whereas proliferation of endothelial cells could be downregulated.

Compound solubility issues may be exaggerating the response observed in wound healing experiments. Injury can impair endothelial cell growth, notably when the wound is chronic or large in size, resulting in senescence of the cells and further contributing to endothelial dysfunction (Ammann et al., 2019). The response may be impaired due to endoplasmic reticulum or mitochondrial stress or damage of endothelial cells which could explain the observed senescence (Jiang et al., 2020; Kluge et al., 2013). The difference in assay method may also contribute to loss of activation of endothelial cells. In EdU assays, the cells are plated prior to reaching confluency, remaining in a proliferative state however, in the scratch wound healing assay, a complete monolayer is generated prior to inducing injury, where the cells may have reached a stationary phase and would require re-activation upon receipt of injury (Scalera et al., 2001).

Migration of endothelial cells could be upregulated as a result of HI-2 treatment; however, proliferation may be downregulated. Further work is required to isolate the mechanistic cause of impaired wound repair due to HI-2. Impaired wound repair and a lack of significant change across proliferation, tube formation and sprouting angiogenesis assays suggests the reduction in hybrids due to 100 μM HI-2 treatment is not sufficient to induce a favourable change in endothelial cell function and therefore ineffective as a means to restore a ‘healthy’ endothelial cell phenotype for type-2 diabetic patients. It is possible that with further investigation with a more selective and active inhibitor, that this change may be reflected.

6. Future Work

6.1. Localisation of HI-2

The predicted interaction of HI-2 with the IR ectodomain hotspot is based solely upon *in silico* modelling studies. HI-2 should bind to a small hydrophobic pocket within the IR ectodomain, preventing dimerization with IGF1R, but not a complementary IR monomer. However, due to observed variable levels of IR and IGF1R homodimeric receptors in HUVEC and SVEC, off-target binding effects have been suspected to be occurring. Localisation of HI-2 *in situ* would grant some insight into its mechanism of action producing the observed effects on protein levels, intracellular signalling, and function of endothelial cells.

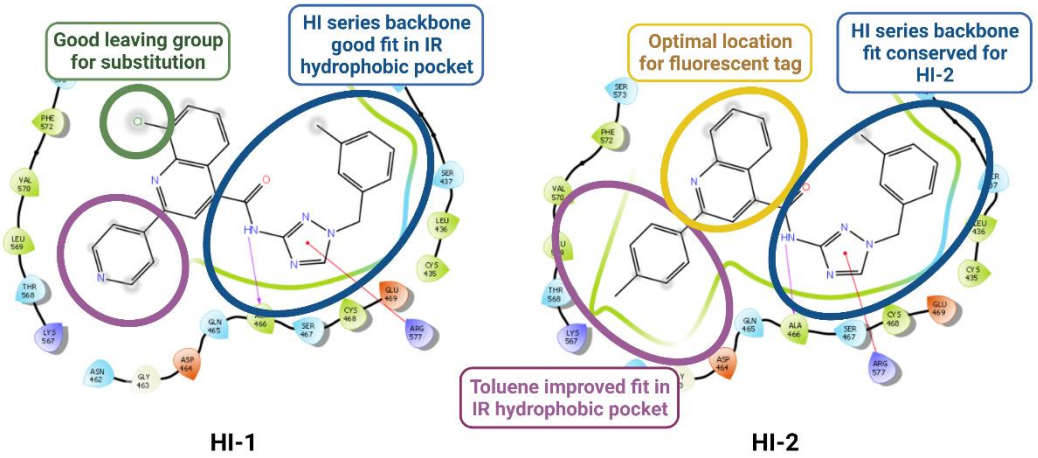

Figure 6-1: Points for Substitution on HI-2

The conserved 2-(3-methylbenzyl)-2H-1,2,3-triazole backbone (blue) of HI-1 and HI-2 is predicted to fit well into the IR ectodomain pocket. Likewise, the inclusion of toluene group in HI-2, as compared to phenyl group in HI-1 observes improved fit in the hydrophobic pocket (purple). The quinoline (yellow) group is not involved in binding or steric interactions with IR or IGF1R and could be an optimal location for substitution, HI-1 possesses a chloride leaving group (green) which can be readily utilized in substitution reactions. Images produced by Dr. K Simmons; descriptive comments created with BioRender.com.

HI-2 is composed of three main groups for potential substitution: 2-(3-methylbenzyl)-2H-1,2,3-triazole, quinoline and toluene groups (Figure 6-1). According to *in silico* modelling data, the benzyl triazole and toluene

groups are essential to binding to the IR ectodomain and sterically impeding binding of IGF1R. The quinoline group could be a potential location for substitution; HI-1 contains a chloride leaving group, removed in design of HI-2, which could be exploited in addition of an organic fluorescent probe.

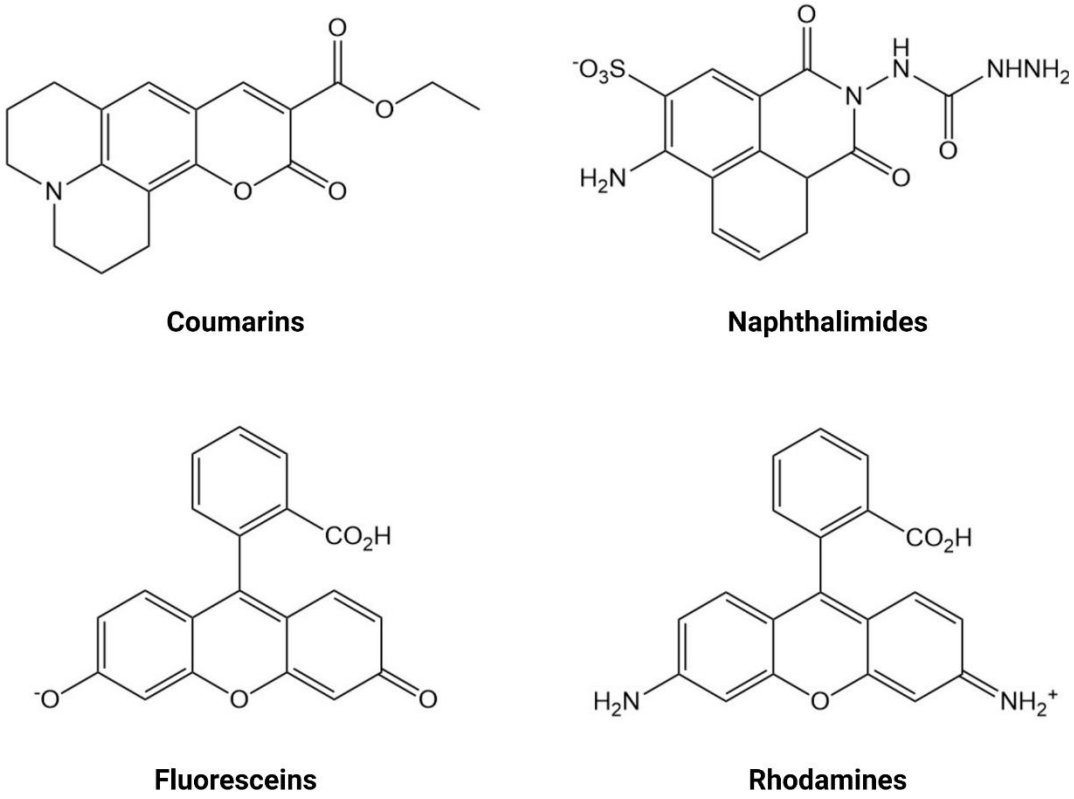

Figure 6-2: Fluorescent Probes

Examples of common fluorophores used in fluorescent probes: structures of Coumarin 314 (top, left), Lucifer Yellow CH naphthalimide (top, right), fluorescein (bottom, left) and rhodamine 123 (bottom, right). Structures prepared in PerkinElmer ChemDraw Prime and based on publication by (Fu and Finney, 2018).

Fluorophores consist of conjugated π-systems, otherwise denoted as a continuous set of unsaturated hydrocarbons in heterocycles and branching chains, which can absorb UV or visible light spectra. Absorbance of UV-vis light causes excitation of an electron from the highest occupied molecular orbital (HOMO) to the lowest unoccupied molecular orbital (LUMO) – relaxation of this electron to ground state re-emits a fluorescent signal. There are many examples of fluorophores however, selection of one which would be

suitable for detection of protein-protein interactions may prove difficult due to size constraints. The conjugated fluorophores are typically large, planar cyclic structures which could interfere in binding of the protein partners; some smaller tags including coumarins, naphthalimides, fluoresceins and rhodamines could be suitable (Figure 6-2) – though coumarins have been shown to be unsuitable for use *in vitro* (Fu and Finney, 2018). Addition of a tag cannot come at the cost of a loss of activity; prior to use of fluorescent tagged-HI-2 in localisation experiments, the HI-2 derivative must be validated for its potential to inhibit hybrid receptor formation, against data obtained for HI-2 in western blotting experiments.

6.2. Insulin, IGF-1 and Hydrogen Peroxide Treatments and, Fluid Shear Stress Experiments

All experiments performed in this project have been under basal conditions – without serum starvation or modulation of insulin or IGF-1 levels. The HUVEC used in this study do not possess a disease-like phenotype, though this may be induced *via* various methods relevant to T2DM, including addition of insulin for hyperinsulinaemia or application of fluid shear stress. Higher levels of insulin and IGF-1 would trigger higher rates of signalling *via* these receptors and may observe subsequent effects downstream, commensurate with doses of these substrates. Similarly, hydrogen peroxide and shear stress may be used to promote oxidative stress mechanisms involving NADPH oxidases and activation of the PI3K/Akt and MAPK/Erk signalling pathways and their subsequent effects on NO bioavailability.

Increasing rates of stress, as observed in cells of people with T2DM, could increase the proportion of hybrid:homoreceptor formation as a model of

endothelial dysfunction. If so, it would result in a more relevant model of T2DM to evaluate the effect of hybrid inhibitors on reducing hybrid formation and to simultaneously determine if restoration of insulin receptor population to basal levels would be possible using these treatments.

6.3. Determine Effects of IR/IGF1R Hybrid Receptor Inhibition in Primary Cells and *In Vivo* Models

The ATEC data presented in this thesis concerns a small proportion of the diabetic population, predominantly comprised of patient data with low HbA1c levels. It would be beneficial to determine the effects of HI-2 on patients with higher HbA1c, suggestive of a more severe diabetic phenotype, to assess if a more profound reduction occurs in larger IR/IGF1R hybrid receptor populations and subsequently, restoration of mechanisms of angiogenesis and insulin signalling. From this data, it could be determined if there is a linear relationship between IR/IGF1R population, and subsequent reduction in formation of the species and restoration of endothelial cell function.

Endothelial cells obtained from high-fat fed diabetic mouse model could be utilized as a next step to determine the effects of IR/IGF1R hybrid inhibitors, and if successful, prior to determination of long-term effects of treatment by continuous dosage in these models. HI-2 does not possess appropriate ADMET properties to be used *via* direct administration or using a continuous release by mini-pump method. An analogue of HI-2 with improved solubility, lower clearance and higher half-life could be administered over a two-week period *via* minipump to assess the effect on development of atherosclerosis and revascularization of ischaemic limb, as models of T2DM.

6.4. Assessment of Potential Off-Target Effects of HI-2

Due to continuous observation that the total population of IR and IGF1R appears reduced in cells treated with HI-2. The effect on mRNA expression was assessed using qPCR in both HUVEC and ATEC non-diabetic and diabetic cells, noting no significant change in levels of *Insr* or *Igf1r* compared to *Actb* mRNA. It is possible that binding of HI-2 to these proteins may lead to aggregation or misfolding, and usually presents as stress of the endoplasmic reticulum (ER).

While it is not possible to determine ER stress directly, proteins associated with various aspects of protein translation may be quantified; unfolded protein response (UPR) is activated by three stress sensors, including protein kinase RNA-activated-like ER kinase (PERK), inositol requiring enzyme (IRE1α) and activating transcription factor 6 (ATF6). PERK, IRE1α and ATF6 are negatively regulated by interaction of an ER chaperone protein under normal conditions, however once stressed, they dissociate from the chaperone protein and become active (Walter et al., 2018). IREα removes an intron from X-box binding protein 1 (XBP1) mRNA – and so monitoring of XBP1 expression is a good marker for IREα activation (Junjappa et al., 2018). Unfolded proteins in ER stimulate PERK oligomerization and autophosphorylation which may be quantified as a marker for this particular mechanism of ER stress (Hu et al., 2018). ATF6 becomes cleaved and activated upon translocation to the Golgi body, induced by ER stress. It forms a complex with ATF/cAMP and ER-stress response elements which bind to promoters of several genes involved in UPR, such as C/EBP-homologous protein (CHOP), glucose regulated protein 78 (GRP78) and XBP1. CHOP,

GRP78 and XBP1 (Hu et al., 2018). Each of these protein mRNAs can be quantified by qPCR to determine any off-target effects of HI-2 on protein translation.

6.5. Design of an Accurate, High-Throughput Downstream Signalling Method

The use of western blotting to quantify changes in downstream signalling protein expression and phosphorylation activities uses affordable consumables and reagents however is extremely time-consuming; the particular method undertaken resulting in gel electrophoresis of the same set of samples in quadruple, sectioning of each membrane by mass and re-labelling with antibodies of each membrane a maximum of five-fold – on the assumption that no issues are encountered at any point in the process. This method would greatly benefit from design of a selective, specific and high-throughput system to quantify a high number of proteins and their respective phosphorylation sites with minimal reagent use, in a time-efficient manner. Use of a multiplexed chemiluminescent immunoassay, such as an ELISA may improve upon the current method in use. Meso Scale Discovery have developed a platform combining sandwich ELISA with electro-chemiluminescence detection, as in western blotting, across a multi-well plate which enables detection of up to ten different species per well in a highly sensitive manner.

Additionally, the colourimetric quantification of nitric oxide species in cell culture supernatant samples, while time-efficient and within limits of easy replicability may not be the optimal method for specificity and quantification at levels below limit of detection of the spectrofluorometer (1 nmol/well).

Siragusa *et al.* (Siragusa et al., 2021) utilized a Nitric Oxide Analyzer (particular model Sievers 280_max, GE Healthcare) which may process the cell culture supernatant for measurement of nitric oxide, nitrite, nitrate and nitrosothiol species, to a minimum detection limit of 1 pg. I predict that use of a dedicated analyzer would be beneficial to specifically quantify changes in nitric oxide production, in addition to improving time-efficiency and replicability with hybrid inhibitor treatment.

6.6. Determine Effect of Selective Reduction of IR/IGF1R Hybrids on Endothelial Cell Proliferation

Cell proliferation is essential in the process of wound closure. The effect of inhibiting IR/IGF1R hybrid formation using HI-2 treatment may result in a reduction of wound repair, as observed in scratch wound healing experiments using HUVEC.

McDonald *et al.* described changes in the transcriptional profile of endothelial cells through the regenerative process (McDonald et al., 2018). *Atf3* was highlighted as an important regulator of regenerative response in arterial endothelium; it is upregulated in response to a range of stress signals. In addition, transcriptional factors associated with junctional complexes such as *FosL2*, a known regulator of endothelial regeneration and downstream effector of the Hippo pathway, *Yaz* and *Tead4* which are triggered in the early stages of regeneration following injury. A set of transcriptional factors known to regulate cell proliferation in sprouting angiogenesis have observed increased expression, namely *Myc*, *FoxM1* and *FoxO1*. Screening of transcriptional factors as described could determine if proliferation of endothelial cells is affected by reduction in IR/IGF1R hybrid formation using

HI-2 treatment. Proliferating cells could also be visualized by combining the EdU proliferation assay with the scratch wound healing method to identify proliferating cells in the regenerating front.

6.7. Generation of Physical Molecular Model of IR/IGF1R Hybrids

Virtual high-throughput screening is limited by assumptions underpinning the insulin receptor/IGF1R homology *in silico* model. Development of cryo-electron microscopy, x-ray crystallography or nuclear magnetic resonance methods to produce the protein structure, as a minimum of the ectodomain 'head' containing ligand binding sites. In addition, computational methods calculate the most likely binding pose of the protein and docked small molecule structure, usually significantly simplified by existing within an aqueous environment with few, to no, ionized or competing structures (gases, peptides, proteins etc.) in solution as present *in vivo*. It would advance understanding of IR/IGF1R hybrid binding kinetics, the resultant loss of insulin signalling ability and therefore subsequent development of therapeutics to overcome these observed effects. In this particular project, production of an accurate docking template for novel HI compounds would allow fine-tuning of selectivity and specificity for binding upon IR and sterically inhibiting IGF1R only.

My colleague, Mr. Samuel Turvey along with Drs. Martin McPhillie and Stephen Muench, are developing a cryo-EM method to selectively image IR/IGF1R hybrid dimers in the Astbury Center, at the University of Leeds. Sam has also developed his own *in silico* homology model, using the IGF1R protein structure and remapping for the amino acid sequence of IR to compare against Dr. Katie Simmons' original homology model. This method is being

used to re-evaluate the compounds from the first round of screening and discover novel compounds which improve upon HI-2.

6.8. Design of *De Novo* and Improved Analogues of HI-2

The reported ADMET properties for the HI compound series are poor when considering conventional (oral tablet, subcutaneous injection) methods for use *in vivo*: poor solubility, low half-life and high clearance. Small functional group substitutions to form novel analogues of HI-2 may improve these factors. However, substantial consideration must be given when selecting these modifications as the molecule must be specific for binding to IR and prevent dimerization of IGF1R – preferably, any changes would also improve this relationship.

Dr. Martin McPhillie's lab in the School of Chemistry has taken the task of designing new compound series and HI analogues with improved solubility properties. Each is also being assessed against the BRET screening assay to determine specificity for hybrids, over homodimer receptors by Samuel Turvey.

6.9. Design of IR/IGF1R Formation-Promoting Compound Series

The focus of small molecule thus far has identified hybrid formation inhibitors to serve to restore signalling function in states of endothelial dysfunction. However, it may prove insightful to determine the effect of inducing endothelial dysfunction by encouraging formation of hybrid receptors – and how the observed higher population of hybrids might occur in T2DM.

Previous rounds of iterative screening by computational and BRET methods have identified compounds which promote hybrid formation and presently, colleagues in the School of Chemistry have committed to producing novel

series of compounds explicitly for this purpose. The basis for my work will be repeated using these hybrid promoter compounds, quantifying changes in hybrid population, effect on signalling downstream of the insulin receptor and the angiogenic phenotype of the endothelial cell model.

7. Concluding Remarks

Modulation of IR/IGF1R hybrid receptors using small molecules is not only possible, but ideal to selectively reduce hybrid receptor species and preferentially promote formation of its homodimeric counterparts.

A virtual high throughput and *in vitro* screening process has been developed to identify novel IR/IGF1R hybrid formation inhibitors. Ideal small molecule candidates will possess strong ADMET properties – good solubility and metabolic stability, low toxicity and be target-selective and specific. Reducing IR/IGF1R formation in this manner could increase expression and activation of downstream proteins and subsequently improve nitric oxide bioavailability. As a consequence, mechanisms of endothelial cell angiogenesis and regeneration could also be restored.

Current candidate, HI-2 selectively inhibits IR/IGF1R hybrid receptor formation up to 100 μM. Reduction in IR/IGF1R hybrid receptors using HI-2 has demonstrated increased signalling *via* the PI3K/Akt signalling pathway, resulting in phosphorylation of Akt activatory site T308 and Y657 inhibitory site of eNOS – which may be a protective response by activation of PYK2. Migration of endothelial cells may be increased with HI-2 treatment, observing a trend towards an increase in forming tip cell and vessel numbers. Proliferation of endothelial cells in wound repair could be impaired, though confirmation through further work is required. Design of a more selective and effective IR/IGF1R hybrid formation inhibitor could be used both as an investigative tool in research and as a therapeutic treatment for type-2 diabetes.

Part II

Endothelial Nitric Oxide Synthase and Protein Tyrosine Kinase 2

8. Aims and Hypothesis

Endothelial NOS activity can be upregulated by activation *via* its Ser-1777 site (Dimmeler et al., 1999; Fleming, 2010) and by the same measure, downregulated by phosphorylation of its Tyr-657 site. Regulation of Tyr-657 phosphorylation is controlled by PYK2 *via* phosphorylation of its Tyr-402 site (Fisslthaler et al., 2008). Typically, regulation of these sites is maintained at equilibrium until a stimulus skews activity in one direction or another. In type-2 diabetes, hyperinsulinaemic insulin resistance causes hyperphosphorylation of the insulin receptor, a proatherosclerotic loop forms between NAPDH NOX2 and PYK2 – in a synergistic relationship where increased superoxide free radical generation promotes increased PYK2 expression, and vice versa. This has a knock on-effect of increased inhibition of eNOS and a subsequent reduction in NO bioavailability.

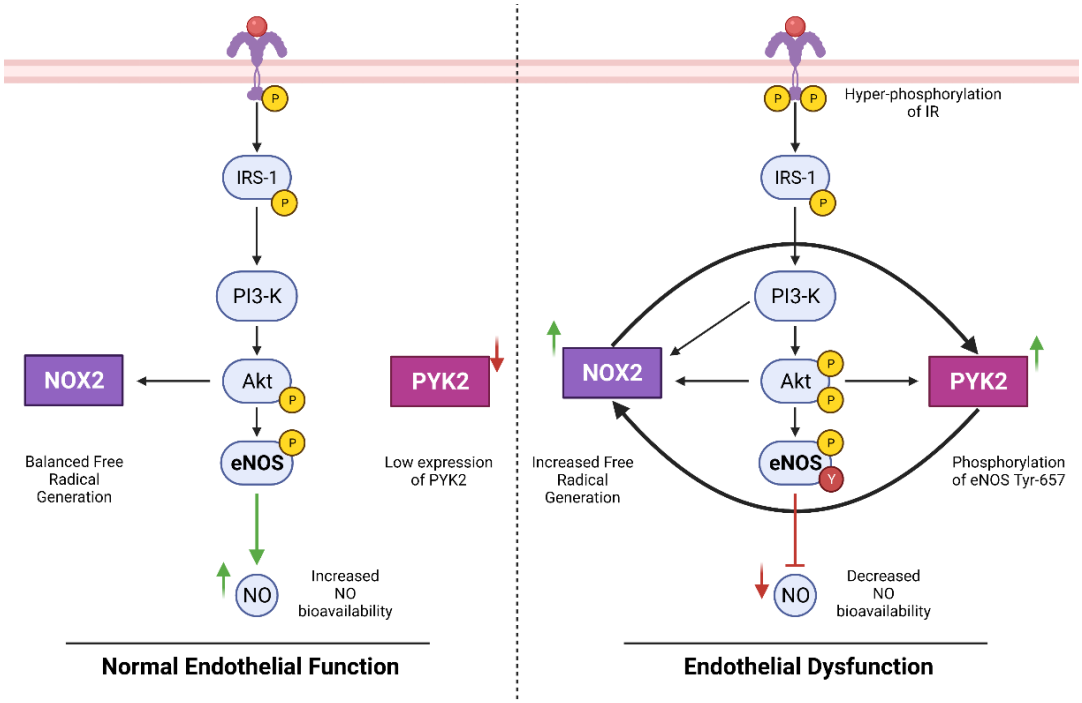

Figure 8-1: Insulin Signalling in Normal and Dysfunctional Endothelial Cells

Changes in endothelial cell signalling *via* the PI3K/Akt pathway from a normal to dysfunctional phenotype. Production of NO *via* eNOS is attenuated due to inhibition of enzyme activity by phosphorylation of its Y657 site by PYK2. A proatherosclerotic signalling loop forms between superoxide generator NADPH NOX2 and PYK2. Image adapted from (Viswambharan et al., 2017) and created with BioRender.com.

PYK2 is involved in many processes within cells, including cell adhesion, migration and inflammation (de Pins et al., 2021). However, this relationship between eNOS and PYK2 in particular is relatively unexplored, particularly when considering this protein-protein interaction (PPI) as a target for small molecule modulation. PPIs of this nature were previously overlooked as therapeutic targets as they were considered to be difficult to target effectively. However, with an increasing number of such PPI inhibitors entering clinical trials, this area of research has become more accessible to the traditional medicinal chemist.

To further understand and characterize the eNOS-PYK2 interaction, I planned on meeting the following objectives in this thesis:

1. To demonstrate the interaction between eNOS and PYK2 in both a diabetic and non-diabetic cell model and, by surface plasmon resonance (SPR) using purified human protein.
2. To determine the effect on angiogenesis and atherosclerosis by reducing PYK2 expression *via* pharmacological and chemical inhibition.
3. To screen a library of small drug-like fragments as potential eNOS-PYK2 modulators, *via* ^{19}Fluorine-Nuclear Magnetic Resonance (^{19}F-NMR) and Surface Plasmon Resonance (SPR).
4. To identify a model compound to proceed with further *in vitro* and *ex vivo* experimental testing.

I hypothesized that breaking the chain in the hyperinsulinaemic proatherosclerotic-signalling loop between PYK2 and NAPDH NOX2 using a small molecule modulator would restore eNOS activity and increase NO bioavailability. I predicted that this would therefore improve angiogenesis and prevent development and progression of atherosclerosis.

9. Results

9.1. Introduction

Characterisation of the eNOS-PYK2 interaction by various methods had been performed in LICAMM prior to the commencement of this thesis work. A homology model of the reductase domain of eNOS (UniProtKB P29474) and the whole of the PYK2 (UniProtKB Q14289) protein (Consortium, 2021) were generated using the I-TASSER homology modelling webserver (Zhang, Y., 2008; Roy et al., 2010; Mukherjee and Zhang, 2011). The HADDOCK webserver was used to predict the binding interaction between the two partner proteins (Dominguez et al., 2003). The predictive model proposed a binding interaction in close proximity of eNOS Y657 (Figure 9-1).

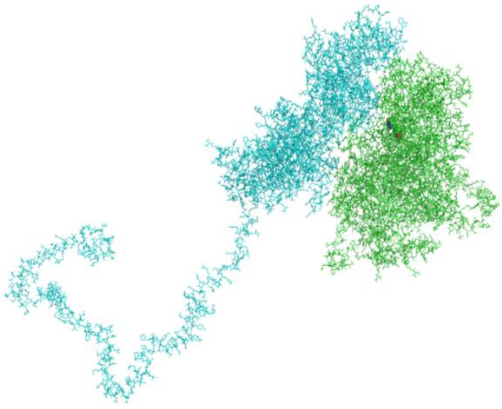

Figure 9-1: Homology Model Prediction of eNOS-PYK2 Interaction

Binding interaction predicted using the HADDOCK webserver. The I-TASSER-generated models demonstrate the eNOS (green) and PYK2 (cyan) binding interaction at eNOS Y657 (green spheres). Image produced by Dr. K. Simmons (University of Leeds, Leeds, 2018 – unpublished).

The interaction between eNOS and PYK2 had also been demonstrated to be present in a series of different human and murine cells (Figure 9-2). Immunoprecipitation of eNOS using the Y657-specific antibody or the PYK2-specific antibody demonstrated a binding interaction by retention of the bound protein partner in these samples.

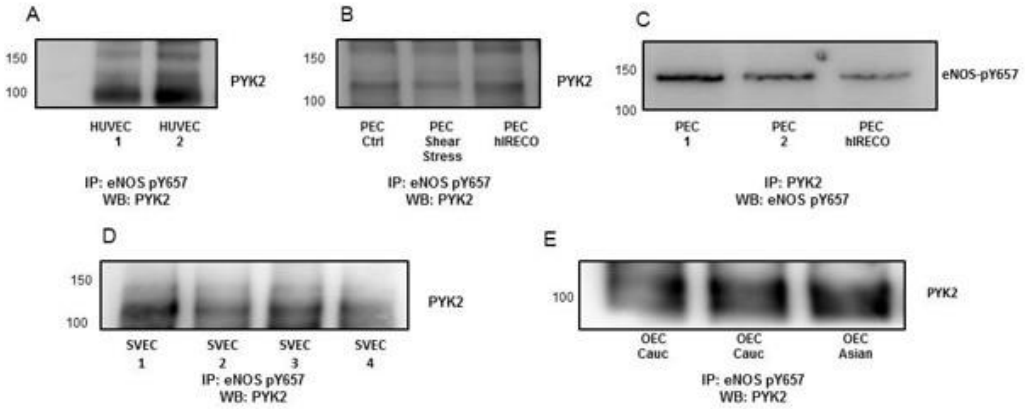

Figure 9-2: Historical Western Blots of eNOS-PYK2 Interaction

Representative western blots demonstrating the eNOS-PYK2 interaction in human umbilical vein endothelial cells (**A**), murine pulmonary endothelial cells of wild-type mice basal or under shear compared with the hIRECO mouse (**B**&**C**), in human saphenous vein endothelial cells (**D**) and human outgrowth endothelial cells from Caucasian and South Asian males (**E**). Blots produced by Dr. H. Viswambharan (University of Leeds, Leeds, 2018 – unpublished).

Fluorescence resonance energy transfer (FRET) was not found to be a suitable method to demonstrate the eNOS-PYK2 interaction. FRET functions by radiation of an energy source stimulating excitation of the fluorescent donor which transfers energy to its respective acceptor. Emission of energy from the acceptor can be detected, determining a change in emission intensity at the wavelength of choice. The energy transfer may only occur once the fluorophores are within a 10 nm distance. FRET and the modified technique of fluorescence lifetime imaging (FLIM) based on the aforementioned limitations and assay design qualities are highly attractive as a method for characterisation of protein-protein interactions (Truong and Ikura, 2001; Margineanu et al., 2016). HEK293T cells were co-transfected with eNOS-mTurquoise2 and PYK2-SYFP2 which enabled biosynthesis of fluorophore-tagged eNOS and PYK2 proteins. Cells were irradiated and the intensities and lifetimes were mapped (Figure 9-3). Co-transfected cells containing both eNOS-mTurq2 and PYK2-SYFP2 showed no significant change in intensity or

lifetimes compared with the singly transfected cells containing eNOS-mTurq2 only.

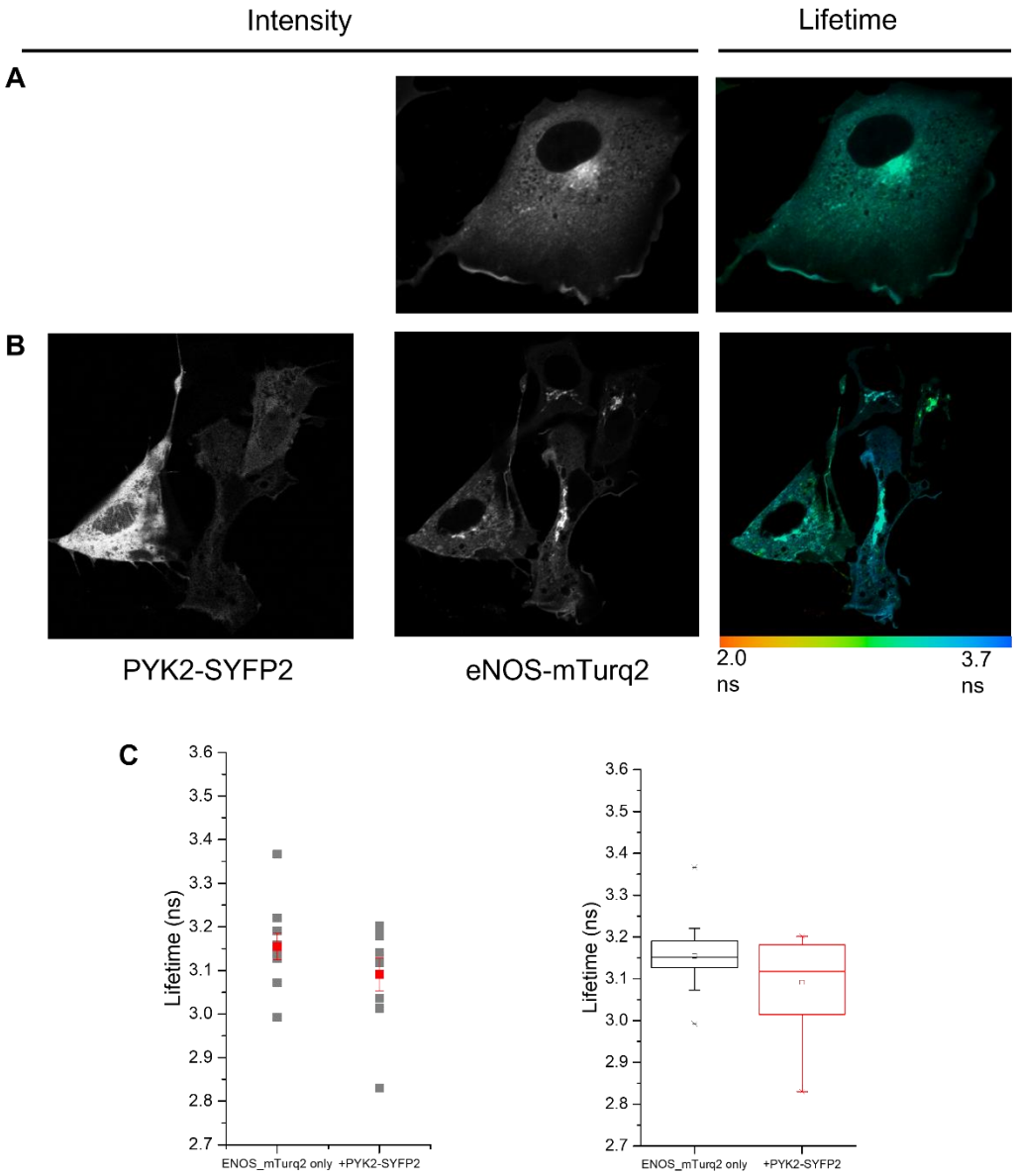

Figure 9-3: Fluorescence Resonance Energy Transfer between eNOS-mTurq2 and PYK2-SYFP2

A. Intensity and lifetime maps were taken of eNOS-mTurq2 in the absence of PYK2-SYFP2 to act as a control. **B.** Intensity and lifetime maps were taken of eNOS-mTurq2 with a co-expression of PYK2-SYFP2. **C.** The distribution of lifetimes for the donor-only image produced a lifetime of approximately 3.15 ns. When eNOS-mTurq2 is co-expressed with PYK2-SYFP2, the range of lifetimes across three independent repeats revealed a range between 2.0-3.7 ns. Images and graphs by Dr. E. Chuntharpursat (University of Leeds, Leeds, 2018 – unpublished).

Upon commencement of the project, I aimed to repeat the immunoprecipitation method in both non-diabetic and diabetic cell models,

prior to genetic manipulation of PYK2 mRNA or small molecule inhibition, to determine the effect of reducing PYK2 expression and activity on the diabetic phenotype and potential recovery of NO production and mechanisms of angiogenesis. In addition to characterizing the eNOS-PYK2 interaction by this method, use of biophysical techniques, such as surface plasmon resonance (SPR) and microscale thermophoresis (MST) were to be employed to further develop understanding of kinetics and thermodynamic properties involved in the interaction.

9.2. Characterisation of the eNOS-PYK2 interaction

9.2.1. Characterisation by Western Blotting

9.2.1.1. *In vitro* Cell Model Screening

Prior to characterizing the interaction between eNOS and PYK2, it was first important to choose a cell model which would be appropriate to perform repeat experiments, easily detect changes in protein levels and be physiologically relevant for the type of study being conducted. Commercially available or primary endothelial cells isolated by technicians in-house were determined as most appropriate as a consistent stream of replicates could be obtained to progress throughout the project.

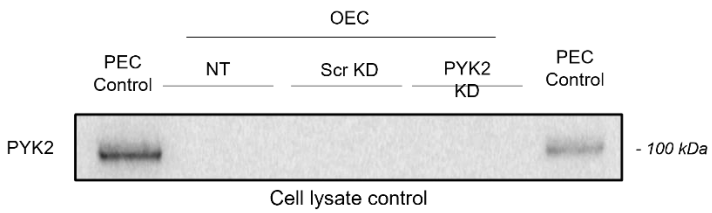

Figure 9-4: Basal Levels of PYK2 in Outgrowth Endothelial Cells

Representative western blots of PYK2 in outgrowth endothelial cells (OEC).

Outgrowth endothelial cells (OEC), derived from circulating endothelial progenitor cells (EPC) in peripheral blood were collected as frequently as

required from staff blood donation in LIGHT. OECs can be obtained from continuous culture of early EPCs; the cells develop into a separately distinct population after approximately seven days, exhibiting the phenotypical ‘cobblestone’ morphology and, expressing highly similar genes and protein signalling patterns as would mature endothelial cells (Ormiston et al., 2015; Ormiston et al., 2010; Toshner et al., 2014). Historically, OECs have been used particularly in endothelial cell dysfunction and cardiovascular disease studies and are recognised widely as a reliable vasculogenesis model (van Beem et al., 2009) due to their primitive use in cell therapies (Paschalaki and Randi, 2018). Basal OEC and murine pulmonary endothelial (PEC) cell lysates were assessed by western blotting, probing for PYK2 (Figure 9-4). It is immediately apparent that PYK2 levels were undetectable by western blotting in OECs, in contrast to the clear bands present in the PEC control lanes. OECs were determined as unsuitable, through repeat testing, as a cell model to investigate the eNOS-PYK2 interaction.

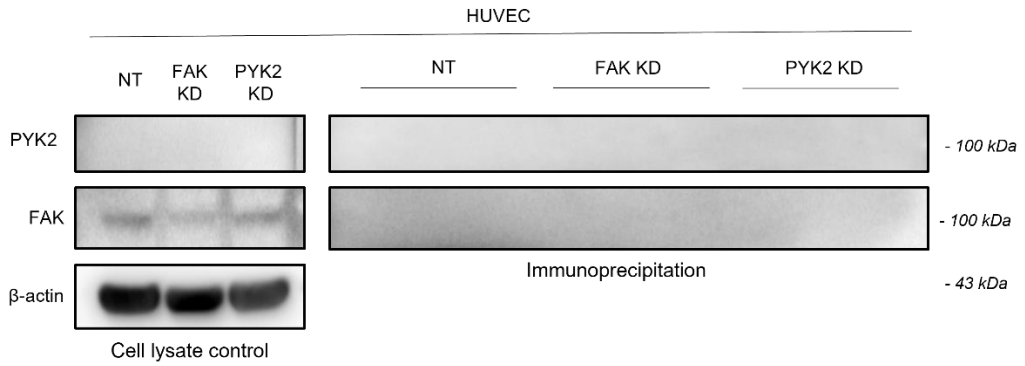

Figure 9-5: Basal Levels of PYK2 in Human Umbilical Vein Endothelial Cells

Representative western blots of PYK2 in human umbilical endothelial cells (HUVEC).

Human umbilical vein endothelial cells (HUVEC) are isolated from umbilical cords, postpartum. They are widely used in endothelial research as they can be characterised by endothelial cell markers, highlighting the possibility to

study pathophysiological mechanisms (Baudin et al., 2007). Additionally, HUVEC are extremely easy to culture and highly reproducible which makes them an ideal model for study of endothelial dysfunction (Medina-Leyte et al., 2020). HUVECs, with no stimulation were assessed by western blotting, probing for PYK2 and FAK (Figure 9-5). Consistently across both immunoprecipitation and cell lysate blots, PYK2 was not detectable under the current conditions in any samples. Bands were however observed in the cell lysate blots for FAK, with a notable decrease with FAK-silencing siRNA knockdown compared to control and PYK2-silencing siRNA knockdown. These suggested that PYK2 knockdown was specific for PYK2, as it had no effect on FAK, a paralogue protein of PYK2. The lack of FAK in the PYK2 pull-down also suggested that the pull-down might be specific for PYK2 as FAK was not observed – though this could not be confirmed as PYK2 was also undetected in these blots. HUVEC were determined as unsuitable as a cell model to characterise the eNOS-PYK2 interaction.

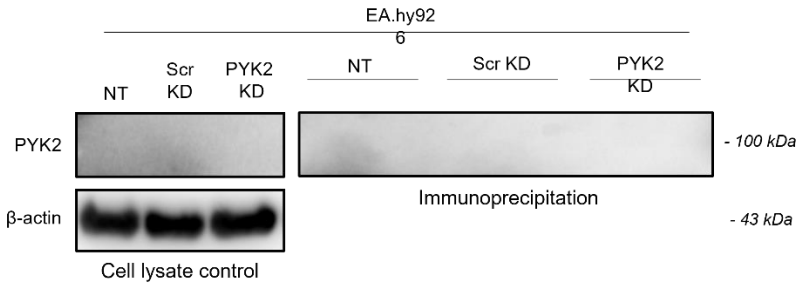

Figure 9-6: Basal Levels of PYK2 in EA.hy926 cells

Representative western blots of PYK2 in EA.hy926 cells.

EA.hy926 cells are an immortalized cell line designed by hybridization of HUVEC and epithelial cell line A549 (Lu et al., 2009). EA.hy926 immunoprecipitation of PYK2 and cell lysates were assessed by western blotting, probing for PYK2 (Figure 9-6). Across both immunoprecipitation and cell lysate blots, PYK2 could not be detected under present conditions in any

samples. EA.hy926 were also deemed unsuitable as a cell line model to characterise the eNOS-PYK2 interaction.

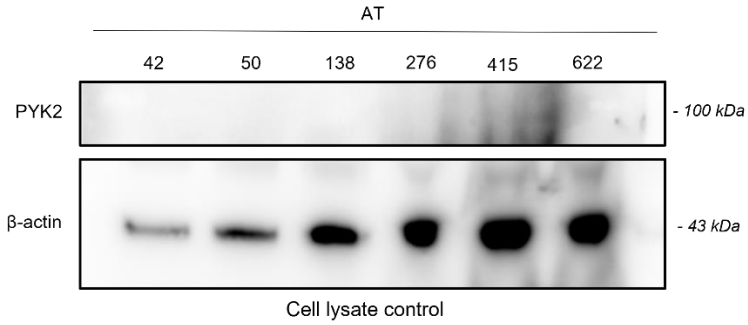

Figure 9-7: Basal Levels of PYK2 in Adipose Tissue

Representative western blots of PYK2 in human adipose tissue (AT).

Adipose tissue (AT) was obtained from consenting patients receiving pacemaker surgery at The Leeds General Infirmary. The tissues were lysed and homogenized, removing the oily fat layer. Adipose tissue was loaded at various increasing concentrations (µg/µL concentrations) from left to right, analysed by western blotting, probing for PYK2 (Figure 9-7). Bands were not observed for PYK2 in any sample, however, were observed for the β-actin housekeeper protein. With increasing concentration of adipose tissue lysate, smearing from oily fat were observed which the impacted β-actin band shape. As endothelial cells were not specifically isolated from the tissue, I hypothesized that the amalgamation of different cells and proteins within the whole tissue sample were diluting the presence of PYK2. Adipose tissue (whole) was deemed unsuitable as a model to characterise the eNOS-PYK2 interaction.

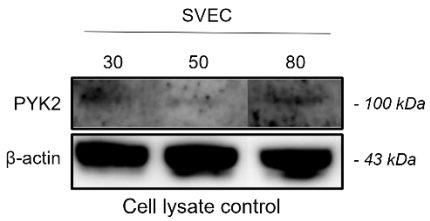

Figure 9-8: Basal Levels of PYK2 in Saphenous Vein Endothelial Cells

Representative western blots of PYK2 in human saphenous vein endothelial cells (SVEC).

Human saphenous vein endothelial cells (SVEC) were isolated previously in-house from coronary artery bypass graft saphenous vein vessels, stored in liquid nitrogen and cultured to confluent endothelial cell monolayers, as required. SVEC cell lysate was loaded at various increasing concentrations (µg/µL concentrations) from left to right and analysed by western blotting, probing for PYK2 (Figure 9-8). Bands were observed of increasing intensity with increasing cell lysate concentration. SVEC were identified as a suitable cell model to characterise the eNOS-PYK2 interaction. However, shortly after this work was carried out, supply of cells was proving difficult – a bias towards cells of a select phenotype were successfully being resurrected from liquid nitrogen after a long period of storage. Collection and isolation of new vessels was underway but was paused once the Covid-19 pandemic began.

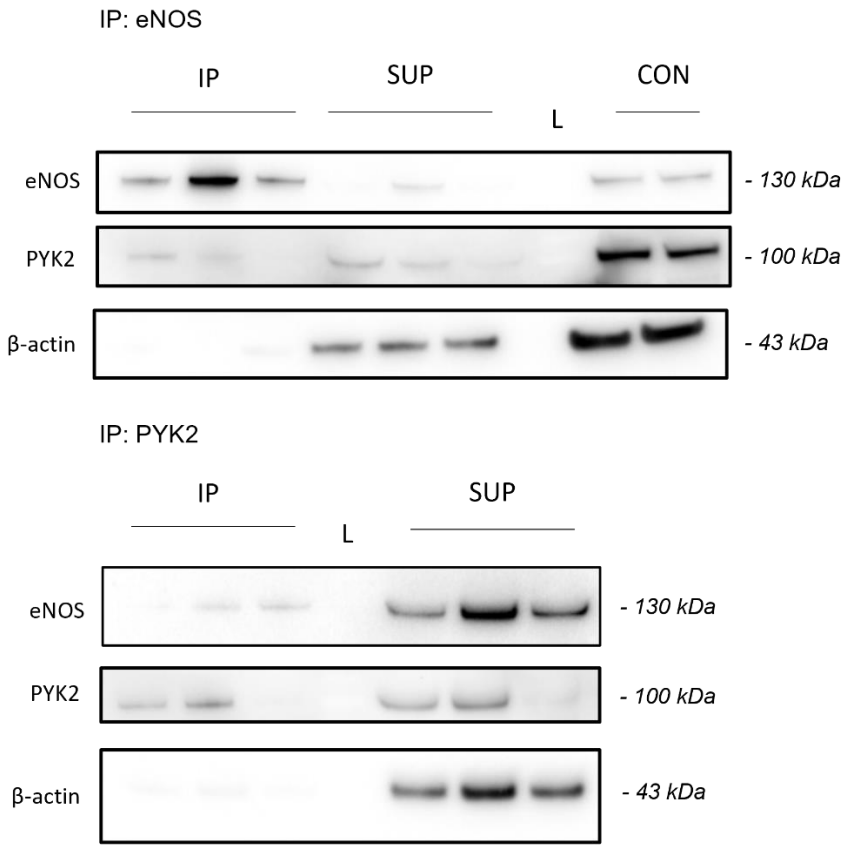

Figure 9-9: Basal Levels of eNOS and PYK2 in Human Adipose Tissue Endothelial Cells

Representative western blots of immunoprecipitation, supernatant and cell lysate samples from human adipose tissue endothelial cells. Immunoprecipitation pull-down by eNOS or PYK2 are both viable options to demonstrate the interaction between eNOS and PYK2, however eNOS pull-down is more complete under the current conditions. PYK2 and eNOS proteins are detectable across all sample types.

Human adipose tissue endothelial cells (ATEC) were isolated in-house from tissues obtained from consenting patients undergoing pacemaker surgery at the LGI and were cultured to confluent monolayers of endothelial cells. The method was adjusted compared to the previous studies: blots probing for anti-PYK2 were incubated for a period of three days prior to imaging as I confirmed that band intensity was better distinguished from background interference. Immunoprecipitation, supernatant and cell lysate ATEC samples were assessed by western blotting, probing for the interaction between eNOS and PYK2. In Figure 9-9, two IPs – each pulling down either eNOS or PYK2 were

performed. In each immunoprecipitation panel, the interacting partner (PYK2 for eNOS and eNOS for PYK2) were detectable in both IPs. The eNOS pull-down appeared ‘cleaner’ under current method conditions, compared to the PYK2 pull-down as significant PYK2 protein was detected in the respective supernatant samples. Non-interacting protein was also detected in supernatant samples, which also aligns with the hypothesis that only a proportion of available eNOS and PYK2 would interact at any time due to the observed transient nature of the interaction. Both proteins were distinctly present in cell lysate samples to measure total levels of protein present in each lysate. ATECs were deemed suitable as a cell model to characterise the eNOS-PYK2 interaction. The interaction between eNOS and PYK2 has also been confirmed by both immunoprecipitation pull-down methods, in ATEC by western blotting.

9.2.1.2. Activation of PYK2 *in vitro by* Cell Stimulation

Several publications have highlighted conditions where PYK2 activation has been up- or downregulated. Production of reactive oxygen species have been shown to induce autophosphorylation of PYK2 Tyr-402, triggered by several different agonists, including insulin (Fisslthaler et al., 2008), IGF-1 (Sekimoto et al., 2005; Shen et al., 2010) and hydrogen peroxide (Bibli et al., 2017b). Hydrogen sulfide can inhibit PYK2 Tyr-402 activity by addition of post-translational modifications of cysteine residues (Bibli et al., 2017a). Stimulation of confluent monolayers of HUVEC was carried out for insulin, IGF-1 and hydrogen peroxide in attempts to upregulate PYK2 expression and activation. Levels of PYK2 in the stimulated HUVEC samples were assessed using western blotting (Figure 9-10). In A, HUVEC were treated with 1 µL/mL

PBS for 24-hours and stimulated with 100 nM human insulin and/or IGF-1 for 15 minutes. Across all insulin/IGF-1 treatment conditions, PYK2 was not detected. In panel C, HUVEC were stimulated with increasing concentrations (μM) of hydrogen peroxide (H_2O_2) from left to right, for 24-hours. With increasing concentrations of H_2O_2, the intensity of bands representing PYK2 in the sample also increased – observing the strongest band at 250 μM H_2O_2, however these bands are still too low-lying compared to the background to be able to obtain quantifiable PYK2 protein levels. It was determined from these experiments that it was possible to promote the expression of PYK2 by H_2O_2 in HUVEC.

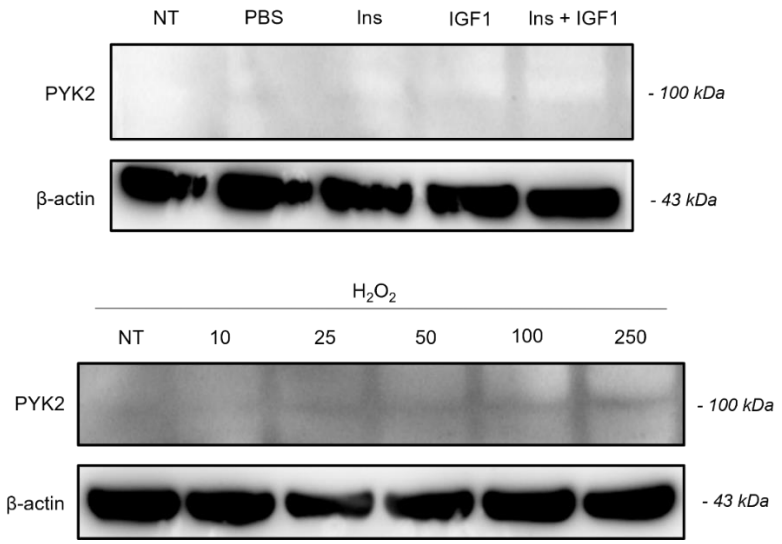

Figure 9-10: Levels of PYK2 in HUVEC stimulated by PBS, Insulin, IGF-1 and Hydrogen Peroxide

Representative western blots of PYK2 in HUVEC stimulated with PBS, insulin and IGF-1 (**A**) and hydrogen peroxide (**B**). Faint bands can be observed in increasing intensity of increasing H_2O_2, however are too low-lying compared to membrane background to obtain quantifiable protein levels.

9.2.1.3. Activation of PYK2 in endothelial cells *via* Fluid Shear Stress

Variation in blood flow through the lumen of vessels can induce changes in pressure experienced by endothelial cells, otherwise known as fluid shear stress (FSS). FSS has been reported (Tai et al., 2002; Fisslthaler et al., 2008) as a mechanism for modulation of endothelial cell function. Of particular interest, FSS has effect of increasing ROS production which results in activation of PYK2. Phosphorylation of Y402 in PYK2 causes increased inhibitory phosphorylation of Y657 in eNOS.

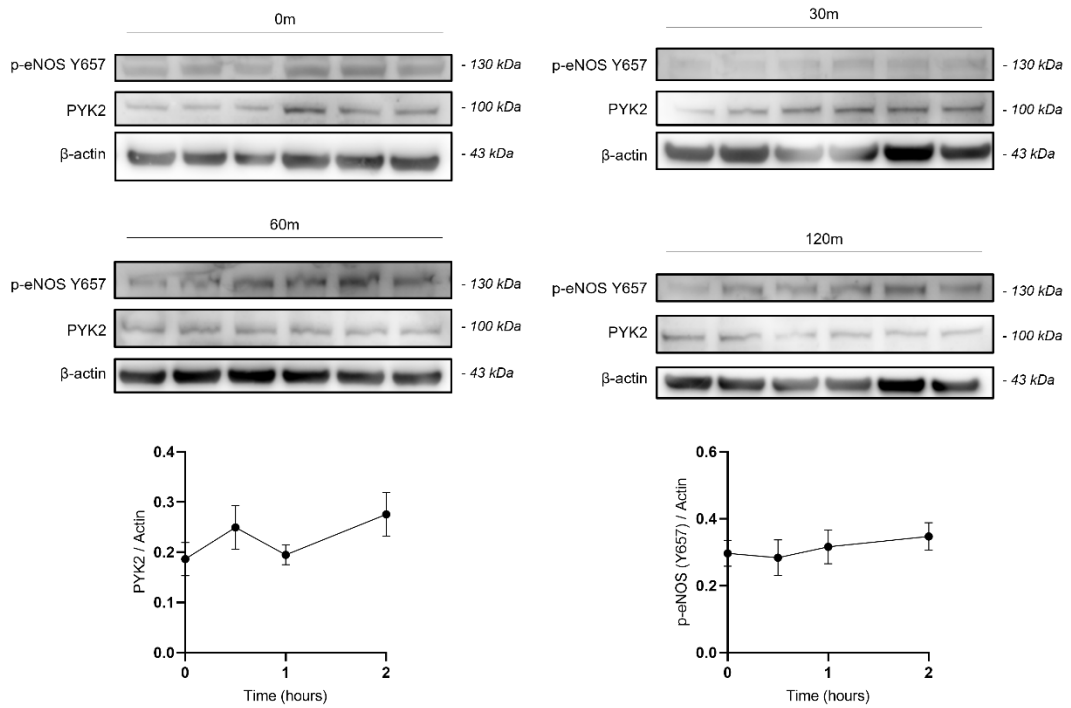

Figure 9-11: Levels of PYK2 in HUVEC under Fluid Shear Stress up to 2-hours

Representative western blots of PYK2 and p-eNOS Y657 in HUVEC after subjection to shear stress for 0, 30, 60 and 120 minutes. Graphs trend towards an increase in PYK2 expression and eNOS Y657 phosphorylation with higher periods of constant stress. N=6.

Short-term shear stress experiments were conducted of increasing duration from 0 to 120 minutes. Confluent monolayers of HUVEC, cultured in six-well plates were placed onto an orbital rotating platform at 210 RPM

(Viswambharan et al., 2017), in a 5% CO_2, 37°C incubator for the duration of the experiment and immediately lysed upon completion. Cell lysates were analysed by western blotting, probing for PYK2, p-eNOS Y657 and β-actin housekeeper protein (Figure 9-11). Bands were detected for PYK2, p-eNOS Y657 and the housekeeper for all timepoints. Densitometry data compared the levels of PYK2 or p-eNOS Y657 against the β-actin housekeeper protein (Figure 9-11). With increasing exposure to fluid shear stress, PYK2 and p-eNOS Y657 trended towards an increase in protein expression and inactivation, respectively.

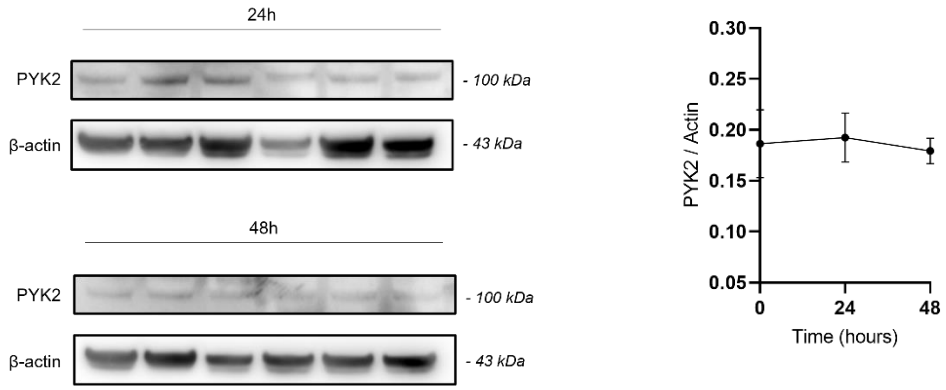

Figure 9-12: Levels of PYK2 in HUVEC under Fluid Shear Stress after 24- and 48-hours

Representative western blots of PYK2 in HUVEC after subjection to shear stress for 24- or 48-hours. Graph shows no change in PYK2 expression between 0- and 48-hours. N=6.

Long-term FSS experiments were subsequently carried out for 24- and 48-hours under the same conditions as above (Figure 9-12). Bands were detected for PYK2 and the housekeeper for both timepoints. Densitometry data compared the levels of PYK2 expression against the housekeeper protein at 0, 24- and 48-hours of fluid shear stress (Figure 9-12). Over a longer period, it was determined that there was no significant difference or particular trend in protein expression of PYK2 between 0, 24- or 48-hours.

9.2.1.4. Effect of Endothelium-specific Inhibition of Insulin Receptor and Endothelial Nitric Oxide Synthase

Mouse models have been employed in study of human disease due to their genetic and physiological similarities. Development of methods creating transgenic, knockout and knock-in mice have proven to be powerful tools in research, particularly when inducing progressive diseases with a high degree of associated mortality (Perlman, 2016). Fleming group developed an eNOS mutant mouse model, replacing the Y656 site of interest (Y657 in humans) with phenylalanine (Y656F), for use in detection of interacting protein partners (Siragusa et al., 2019). In the context of this particular study, inclusion of a Y656F-eNOS mutant would inhibit the inhibitory action of PYK2 Y402. A transgenic mouse model developed by Kearney group, inducing endothelial-specific insulin resistance by overexpression of dominant-negative human mutant insulin receptor (ESMIRO) which possesses modification of tyrosine kinase domains which inhibits insulin activation and downstream signalling, including eNOS and PYK2 (Duncan et al., 2008). A small colony of ESMIRO/Y656F-eNOS wild-type and transgenic mice were bred in-house to determine the effect of this combined genotype on the eNOS-PYK2 interaction. Three mice were transgenic ESMIRO and Y656F-eNOS heterozygous knockout; a fourth mouse was wild-type ESMIRO and Y656F-eNOS heterozygous knockout (Appendix 20.3). Heterozygous knockouts typically display a loss-of-function phenotype, due to their haploinsufficiency.

At the end of the study, PECs were isolated from pulmonary tissues by Dr. H. Viswambharan. Confluent monolayers of PECs were serum-starved for 24-hours and stimulated using insulin at 50, 100 and 150 nM concentrations

for 15-minutes prior to lysis. Immunoprecipitation of PYK2, supernatant and cell lysate samples were assessed using western blotting, probing for the interaction between eNOS and PYK2 and their respective phosphorylation sites at Y656 and Y402 (Figure 9-13). Bands were detected for PYK2, p-PYK2 and the β-actin housekeeper across all three panels for both wild-type and transgenic mice, which showed that the pull-down was successful but not complete due to remaining protein in the supernatant. Bands for total eNOS and eNOS Y656 were not detected after several attempts in any of the immunoprecipitation blots. It is likely that the due to an increased proportion of F656 mutants that fewer eNOS Y656 sites were available for interaction with PYK2 Y402 in conjunction with the transient nature of the interaction between eNOS and PYK2, would observe significantly less association; this is reflected in both mice as they share the same heterozygous and haploinsufficient genotype. In the control blots for transgenic mice, bands pertaining to PYK2 and PYK2 Y402, compared to β-actin showed no significant change in expression or phosphorylation levels with increasing insulin concentration; it is difficult to draw conclusions regarding levels of expression and autophosphorylation of PYK2 in wild-type mice due to low sample population. Detection of eNOS Y656 was not surprising as a proportion of eNOS would possess native Y656 site where phosphorylation by PYK2 would be possible; quantification was not possible due to low-lying exposure compared against blot background. Unfortunately, characterisation of the interaction between eNOS and PYK2 from these murine cell lysates was not successful. The work was paused while waiting for reopening and breeding of the animal models due to closure resulting from Covid-19 pandemic lockdown.

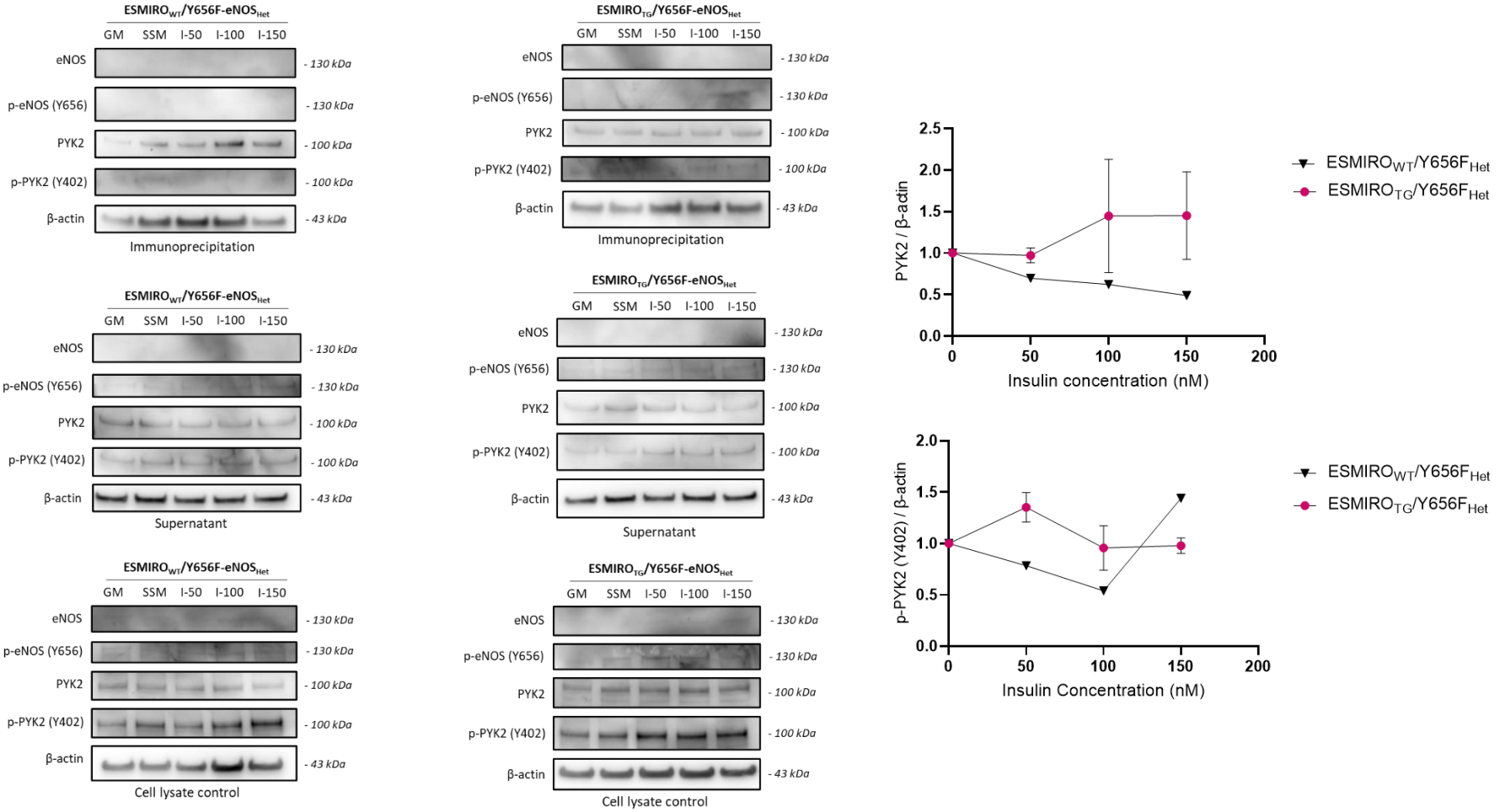

Figure 9-13: Effect of Deleterious Phenotype of ESMIRO/Y656F-eNOS Mice on eNOS-PYK2 Interaction

Representative western blots of immunoprecipitation, supernatant and cell lysate control samples from non-treated and insulin-stimulated WT/Y656F-eNOS (left) and ESMIRO/Y656F-eNOS (center) murine PEC after 15 -minute incubation. Graphs of cell lysate control blots showing the change in total PYK2 expression and PYK2 Y402 phosphorylation with increasing concentrations of insulin. GM; full growth medium, SSM; serum-starved medium, I; insulin. WT/Y656F N=1; ESMIRO/Y656F N=3.

In the interest of obtaining optimal results, characterisation of protein-protein interactions should be performed across various techniques. Proximity ligation, visualizing the interacting proteins *in situ* and biophysical techniques, such as SPR which provides information regarding binding kinetics, are ideal methods to collate data of individual aspects of the interaction.

9.2.2. Characterisation of the eNOS-PYK2 PPI using a Proximity Ligation Assay

Proximity ligation assays (PLA) are a highly sensitive and specific technique which enables *in situ* labelling of proteins to detect interacting partners by inclusion of proximity probes. The DuoLink® Proximity Ligation Assay (Sigma-Aldrich) acts in this particular manner, triggering hybridization of two distinct oligonucleotides bound to the primary antibodies of the target proteins if they are in close proximity.

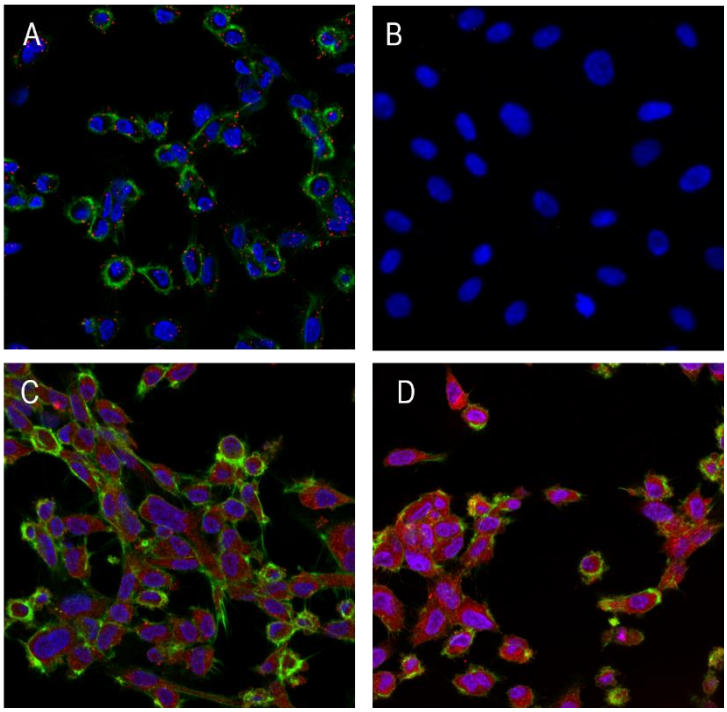

Figure 9-14: Detection of eNOS-PYK2 Interaction by Proximity Ligation

Representative images of the eNOS-PYK2 interaction in EA.hy926 using the DuoLink PLA. **A.** The eNOS-PYK2 interaction (red) is observed in both the nucleus (DAPI stain, blue) and the cytoplasm (F-actin, green). **B.** In the control stain, the interaction cannot be observed when not in the presence of eNOS and PYK2 antibodies. **C**/**D.** Stain demonstrates the singular localisation of PYK2 (**C**, red) and eNOS (**D**, red) in cells, respectively. Cell fixation performed by Dr. K Simmons and imaged by Dr. R. Cubbon (University of Leeds, Leeds, 2019 – unpublished).

The proximity ligation method confirms a close interaction between eNOS and PYK2 in EA.hy926 immortalized cells (Figure 9-14). Vignette A shows localised red immunofluorescence signals throughout the nucleus (blue) and cytoplasm (green) of multiple cells, corresponding to the eNOS and PYK2 proteins in very close proximity to enable oligomerization between the PLA probes. This was confirmed by the control stain in in image B where the protein-specific primary antibodies were not present, and no such signal was observed. In addition, images C and D showed specific localisation of PYK2 (C) and eNOS (D) proteins respectively within nuclei and cytoplasm of cells, confirming their presence as individual entities and in the same location as the PLA signal. The limitation of PLA is that specific interacting domains or

residues cannot be determined. It does not confirm a direct interaction between the proteins, there may still be a chaperone facilitating the interaction.

Characterisation of protein-protein interactions using biophysical methods could prove useful as only the purified proteins are recorded in an isolated environment and can confirm if a chaperone is involved in the interaction.

9.2.3. Characterisation of the eNOS-PYK2 PPI using Surface Plasmon Resonance

Biacore surface plasmon resonance (SPR) measures the molecular weight changes as one protein binds to a surface derivatized with a binding partner of interest. Importantly, SPR allows assessment of the kinetics of association and dissociation of complexes, thus illuminating the dynamics of regulatory networks (Douzi, 2017). The CM5 sensor chip carries a matrix of carboxymethylated dextran, covalently attached to a gold surface. Molecules can be covalently coupled to the sensor surface by exploiting the available amine, thiol, aldehyde, or carboxyl functional groups on the ligand. The CM5 dextran matrix extends about 100 nm from the gold surface, and is flexible, allowing relatively free movement of the attached ligand (Lifesciences, 2021). The binding partner, or analyte can be injected across the ligand surface and any binding interactions can be monitored by tracking the change in refractive index over time. In situations where the binding partners form a complexed species, the change in refractive index is maintained beyond regeneration of the ligand surface; however where transient, the index will re-equilibrate, restoring to baseline levels and the analyte will exit the chamber to waste.

Parameters such as association/dissociation constants from kinetic data may also be obtained from these experiments.

Previous studies using SPR with members of the NOS family of proteins have often focused on the calmodulin (CaM) binding domain (Zoche et al., 1996; Wu, G. et al., 2011). A truncated section of the CaM binding domain from NOS species (eNOS, nNOS and iNOS) was used to determine the binding kinetics of each NOS species to CaM. Similarly, Salerno *et al.* used SPR to characterise the interaction between CaM and MAPK-phosphorylated eNOS at S602 (Salerno et al., 2014). Literature precedent suggested it was possible to study the interactions of eNOS with its binding partners using this technology.

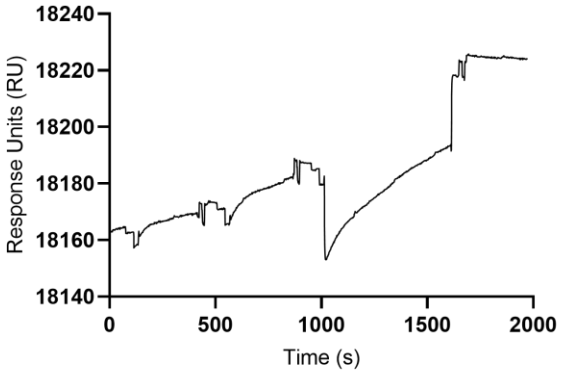

Figure 9-15: Immobilisation of eNOS-GST protein

Amine coupling between anti-GST antibody and GST-tagged eNOS reductase domain protein onto CM5 chip. Sensorgram reveals approximately 100 units of eNOS protein were immobilised onto the surface.

Work on the Biacore 3000 was undertaken with guidance from Dr. Iain Manfield. His/Glutathione-S-Transferase (GST) tagged-eNOS reductase domain (r521-1203) was produced in-house at the Leeds Protein Production Facility whilst the His tagged-PYK2 kinase domain (r360-690) protein was purchased from Abcam. It was decided to attempt to immobilize the first protein *via* amine coupling using a target-specific antibody. Two ligand capture

kits were available for this method, anti-GST and anti-His. As I had proteins with one or both tags, both methods of ligand capture were attempted. eNOS immobilisation *via* its GST tag was observed (Figure 9-15). The baseline rose in response units, signalling that an entity of distinct size had entered the chamber, causing a change in refraction and upon the end of the injection of the ligand at approximately 1600 s, the baseline stabilized at approximately 80 units higher than prior to injection. This change in baseline suggested that approximately 80 units of eNOS had been immobilised onto the CM5 surface.

Surface concentration	$1000\ \mathrm{RU} = 1\ \mathrm{ng/mm^2}$ $1000\ \mathrm{RU} = 10\ \mathrm{mg/ml}$
Ligand concentration	$\mathrm{Conc_{ligand}} = \frac{\mathrm{Response_{ligand}}}{100\ \times\ \mathrm{Mr_{ligand}}}(\mathrm{mol/litre})$

Equation 1: Surface Plasmon Resonance response units' relationship to immobilised ligand concentration

The success of the immobilisation of the eNOS reductase domain *via* anti-GST could be determined from Equation 1 where the relationship between the chip surface concentration and the protein concentration is calculated. The approximate concentration of the eNOS reductase domain (molecular weight ~76 kDa) immobilized was 0.08 ng/mm^2 or 105.3 nmol/L, which is too low to use for any analysis of binding as there would be very few sites available for binding with the PYK2 kinase domain and additionally, some proteins were unlikely to be immobilized in an ideal conformation for binding. Given these limitations and the transient nature of the interaction between the two species, I was unsuccessful in detecting the protein-protein interaction between eNOS and PYK2 using these conditions.

Capture using the anti-His antibody for both eNOS and PYK2 proteins was unsuccessful. Attempts to immobilize a His-tagged maltose binding protein (MBP) control was also unsuccessful, suggesting a problem with the technology. I hypothesized that as the His tag was smaller than GST, it may have been poorly oriented due to shielding neighbouring residues or tertiary structure folding. Coupled with lower than optimal working concentrations and a buffer mismatch, conditions would not have favoured a successful outcome.

Due to limitations regarding laboratory access in the Astbury Center from Covid-19 pandemic restrictions, I was unable to continue this work. However, future work could investigate the use of different sensor chips and methods of immobilisation, such as biotinylation.

9.3. Protein Production

Due to difficulties obtaining the PYK2 kinase domain commercially in high quantities within a buffer solution suitable for SPR, minimizing surfactant levels, in addition to the Protein Production Facility (PPF) located in the Astbury Center at the University of Leeds, it was decided that the PYK2 kinase domain would be produced in-house, just as the eNOS reductase domain had been the year prior. Protocols were followed and adapted from the Leeds PPF Handbook provided by Dr. B. Jackson, *flash*BAC™ Baculovirus Expression Systems and Gibco™ Growth and maintenance of insect cell lines.

9.3.1. Gene Cloning

The Protein Production Facility (PPF) at the University of Leeds offers multiple production systems however the most popular due to its simplicity and high success rate uses *Escherichia coli* (*E. coli*) competent cells. Prior

commencing expression of the PYK2 kinase domain, a vector containing the gene of the protein of interest had to be produced.

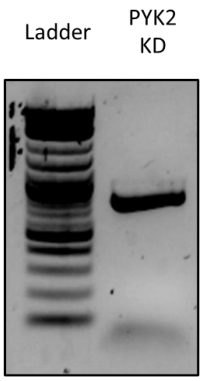

Figure 9-16: Cloning of PYK2 Kinase domain

Representative agarose gel of HiFi assembly reaction sample. Gel confirms reaction was successful at producing a high concentration of PYK2 kinase domain gene copies for vector transformation.

A manual PCR reaction was performed to create an exponential quantity of the PYK2 kinase domain gene (Figure 9-16). As only the genetic material for PYK2 was included in the replication process, the single, strong band in the sample lane must be attributed to the PYK2 kinase domain gene. The lack of additional bands also suggested that the process produced a highly pure sample. Through this process, the PYK2 kinase domain gene was successfully replicated and therefore vector transformation could commence.

9.3.2. Vector Transformation

Plasmids were purchased from Addgene, a non-profit repository. Four distinct plasmids were selected from the pOPIN vector suite: -F, -J, -M (Berrow et al., 2007) and -S3C (Bird, 2011). The pOPIN vectors are suitable for use in both *E. coli* and Baculovirus systems, require a single-step process to insert the gene of interest and most importantly, the ‘fusion’ site, where the protein of interest would attach, is highly precise and allows for a clean cleavage between the two. Each variant provides a different tag or linker to the protein

of interest (POI): F is comprised of His6-3C-POI, J His6-GST-3C-POI, M His6-MBP-3C-POI and S3C His6-SUMO-3C-POI. These tags allow for easier purification of the expressed protein and occasionally can affect the solubility.

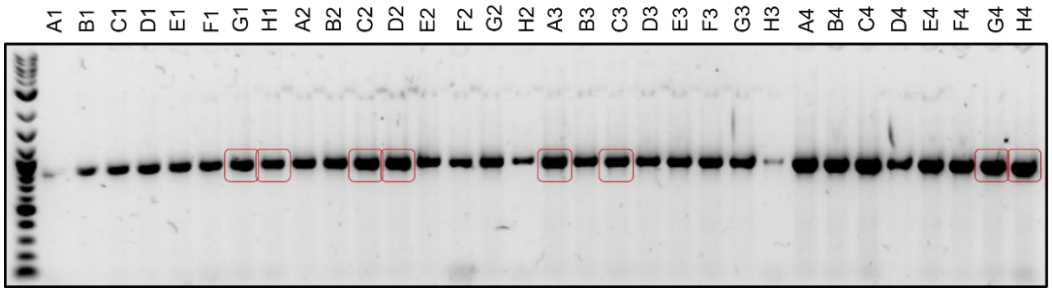

Figure 9-17: pOPIN Vector Transformation

Representative agarose gel of pOPIN vector insertion across individual competent 5α colonies. High levels of gene insertion and replication can be observed for the majority of colonies and all vector types: F(1), J(2), M(3), S3C(4). Colonies from lanes G1, H1, C2, D2, A3, C3, G4 and H4 (highlighted in red) were isolated and dispatched to Eurofins for sequencing.

The pOPIN plasmids containing the PYK2 kinase domain gene were transformed into *E. coli* DH5α competent cells where eight distinct colonies from LB agar plates were selected and subsequently cultured in selective LB containers (Figure 9-17). The coomassie stain contains a strong band in each lane across nearly all selected colonies. This suggests that plasmid transformation into DH5α was successful and therefore the PYK2 kinase domain plasmid could be used in the following processes in protein production. Colonies highlighted in red were isolated and sent to Eurofins for sequencing. Sequencing data confirmed that the PYK2 kinase domain gene had been successfully inserted at the correct position in the amino acid sequence and the strains containing fewest mutations were carried forward into small scale batch testing. These colonies were H1 (F), D2 (J), C3 (M) and G4 (S3C).

9.3.3. Protein Expression in *E. coli* Bacteria

9.3.3.1. Transformation of Plasmids into *E. coli* cells

The four pOPIN constructs were transformed again into BL21(DE3), Rosetta 2(DE3), SHuffle® T7 Express and Lemo21(DE3) competent *E. coli* cell lines. Screening of appropriate competent cell lines was essential to determine which would be the most effective in expression of the PYK2 kinase domain clone. The DE3 and T7 Express cell lines were designed specifically for expression of difficult clones. DH5α is used more frequently for general cloning purposes and so it was worthwhile determining if a different competent cell line would be more suitable for large scale production.

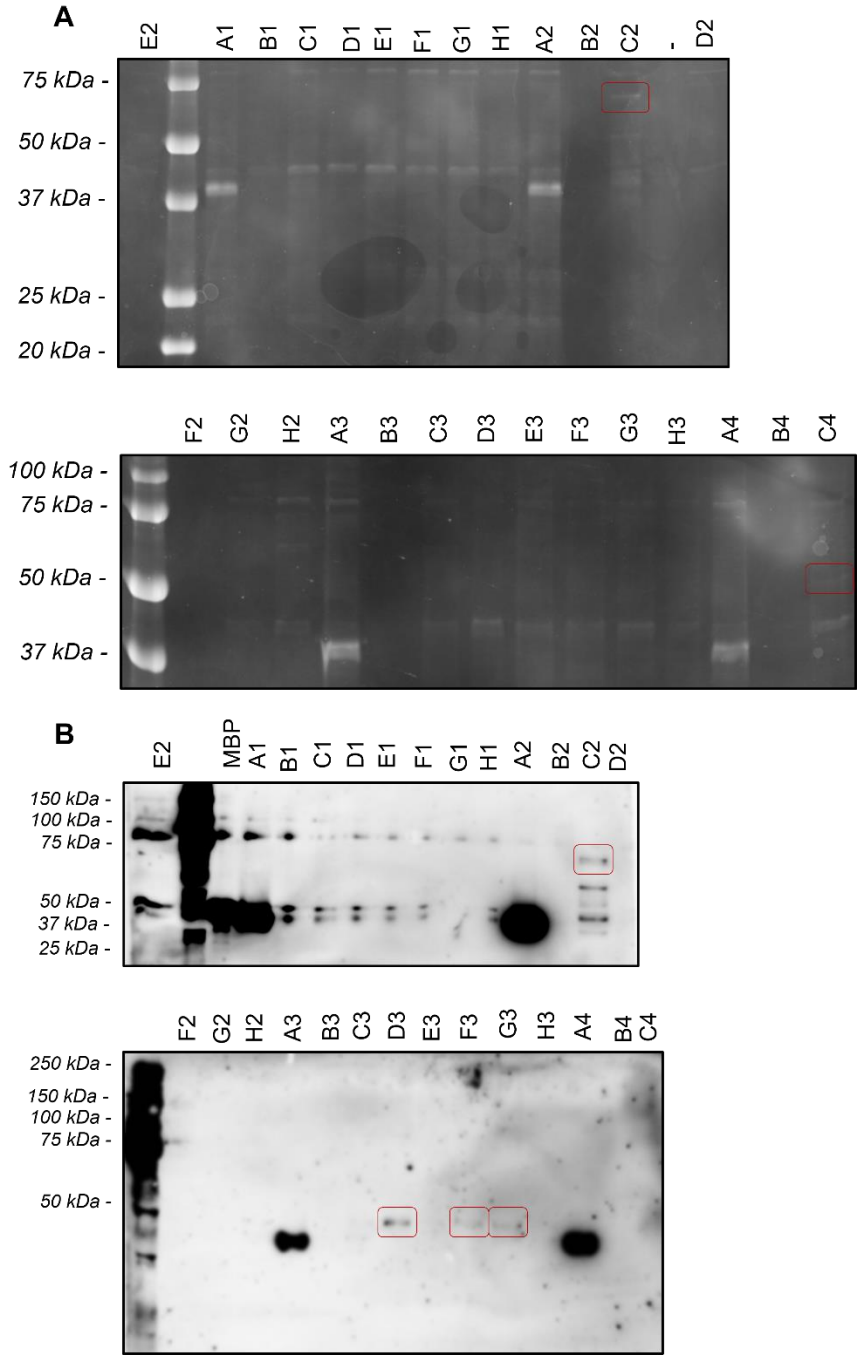

Figure 9-18: Expression of PYK2 Kinase domain in *E. coli* Competent Cell Lines

Representative Coomassie gels (**A**) and western blots (**B**) of PYK2 kinase domain-tagged protein expression in *E. coli* competent cell lines BL21(DE3), Rosetta Gami 2(DE3), SHuffle T7 Express and Lemo21(DE3) (0, 500, 1000, 1500, 2000 µM *L*-rhamnose). Protein expression for each colony occurred in 2 mL volume to deduce which cell line would be most suitable to carry forward in larger scale production. Colonies C2, D3, F3 and G3 were isolated as successes; C2 and D3 produced the most concentrated levels of PYK2 kinase domain – these corresponded to SHuffle T7 containing pOPINM vector, and Lemo21 with pOPINS3C vector, respectively.

Transformation was carried out as before (Section 9.3.2). Coomassie stains are a good indicator for determining if the vector and cell line combination are particularly suited to produce high levels of protein, however this technique identifies all proteins present in the sample. The Coomassie gels (Figure 9-18) contain faint bands for colonies C2 at 72 kinase domain (pOPINM in SHuffle T7) and C4 at approx. 42 kDa (pOPINS3C in SHuffle T7) which were indicative of the presence of the tagged-PYK2 kinase domain. A follow-up set of western blots were prepared (Figure 9-18) to confirm if PYK2 was specifically present in any samples. Exposure of the western blot had to be increased significantly for analysis, any bands detected, excluding the MBP protein control, would contain low levels of protein. Bands were observed in colonies C2 at 72 kDa (pOPINM in SHuffle T7) and D3, F3 and G3 at 42 kDa corresponding to Lemo21 (pOPINS3C) at concentrations of *L*-rhamnose 0 µM, 1000 µM and 1500 µM. The lack of band in the western blot for C4 confirmed that the band seen in the coomassie stain was not attributable to the PYK2 kinase domain.

As the band for Lemo21 was strongest without *L*-rhamnose, this particular construct was selected, alongside pOPINM in SHuffle T7 to advance to small-scale batch testing.

9.3.3.2. Small-Scale Protein Production

Transformation of pOPINS3C into Lemo21 (0 µM *L*-rhamnose) and pOPINM into SHuffle T7 occurred as before and was cultured into a larger volume of 600 mL and 500 mL LB, respectively. The whole culture volume was centrifuged, and at each purification step, the discarded fraction was retained and analysed using Coomassie gels and western blots. Each protein and its associated tag can vary in solubility and as such, will remain solubilized in a

distinct fraction – the purpose of the gels was to determine which should be retained in future for purification in large-scale production. Production of certain proteins does not require progression to large-scale however based on the low density bands detected in Section 9.3.3.1, Figure 9-18, it was established that large volumes of culture would likely be required.

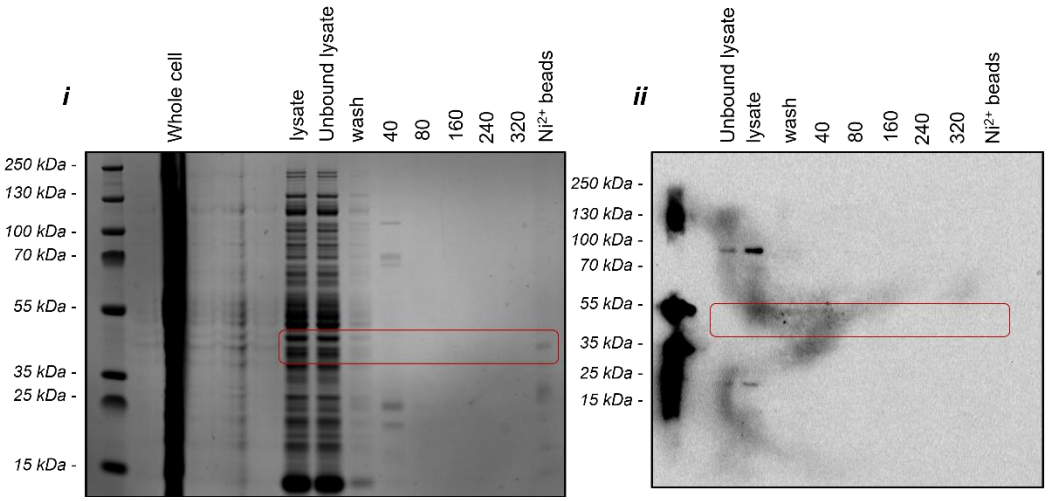

Figure 9-19: Expression of PYK2 kinase domain in Lemo21 Cell Line

Representative Coomassie (***i***) and western blots (***ii***) of PYK2 kinase domain-tagged protein expression in *E. coli* competent cell line, Lemo21. Cells were cultured in 600- and 500-mL volumes, respectively. SUMO-tagged PYK2 kinase domain should appear around 42 kDa, which cannot be observed.

The Coomassie gel and western blot for Lemo21 can be observed in Figure 9-19, highlighting the expected range of 42 kDa, for a band representing PYK2 kinase domain-SUMO protein in red. Several bands in the lysate, unbound lysate, wash and in particular the Ni^{2+} bead fraction were isolated as potentially corresponding to PYK2 kinase domain-SUMO protein. However, when analysing the same fractions by western blotting and probing for PYK2, no bands were detected – even when increasing exposure in analysis. I concluded that Lemo21 (0 µM *L*-rhamnose) containing the pOPINS3C vector were not suitable to produce adequate quantities of the PYK2 kinase domain.

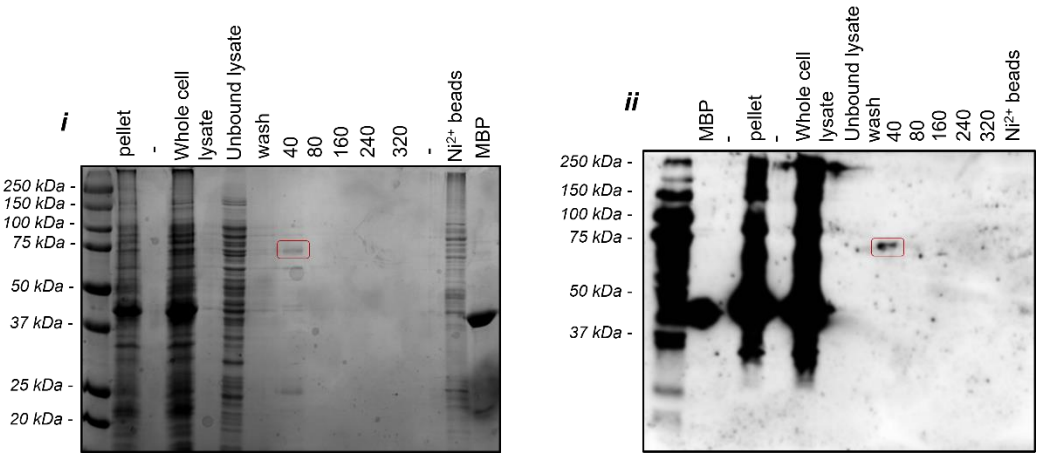

Figure 9-20: Expression of PYK2 kinase domain in SHuffle T7 Cell Line

Representative Coomassie (***i***) and western blots (***ii***) of PYK2 kinase domain-tagged protein expression in *E. coli* competent cell line, SHuffle T7. Cells were cultured in 600- and 500-mL volumes, respectively. A band at 72 kDa can be observed in the 40 µM imidazole buffer elution – which corresponds to MBP-tagged PYK2 kinase domain.

SHuffle T7 representative Coomassie gel and western blot can be observed in Figure 9-20. Bands in the expected range of 72 kDa were detected in the pellet, whole cell, unbound lysate, wash and 40 mM imidazole, 5% v/v glycerol and Ni^{2+} bead fractions. Ideally, to enhance extraction of the PYK2 kinase domain, fewer contaminants was preferable to ensure purity of the protein of interest was as high as possible. A sufficiently strong band was identified in the 40 mM imidazole fraction, containing minimal contaminants using Coomassie gel analysis. The western blot of the same fractions, probing for PYK2, also detected the same band in the 40 mM imidazole fraction. Exposure of the western blot was increased in ImageJ as the MBP protein control was causing over-exposure close to the ladder. The information garnered from both the Coomassie and western data suggested that PYK2 kinase domain-MBP was present, in particular in the 40 mM imidazole fraction with minimal contaminants, in SHuffle T7 transformed by pOPINM. The current levels of protein produced in 500 mL cell culture was insufficient to purify and collect. Large-scale production would be required.

9.3.3.3. Large-Scale Protein Production

A SHuffle T7/pOPINM colony was isolated from the previous experiment and grown in 1 L starter culture and later split across seven separate 1 L flasks of LB. All inoculated flasks were combined and centrifuged as before and through purification, the 40 mM imidazole fraction was retained.

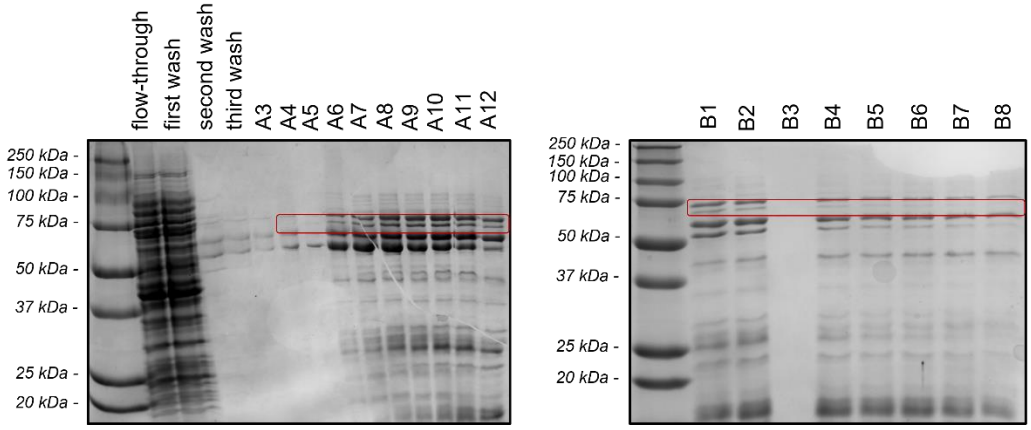

Figure 9-21: His-Tag Purification of PYK2 kinase domain

Representative Coomassie gel of His tag purification to selectively isolate MBP-tagged PYK2 kinase domain protein. Cells were cultured in 7 L volumes. Analysis of Akta elutions suggests that MBP-tagged PYK2 kinase domain (72 kDa) is present in aliquots A4 through B8.

The 40 mM imidazole fraction was eluted through the ÄKTA Pure liquid chromatography system (Cytiva), containing a 5 mL HisTrap FF column (Cytiva). The 6His tag would become selectively immobilized onto Ni^{2+} surface on the column and enabling any contaminants to be flushed through. Coomassie gels of the wash and buffer elutions were analysed to confirm retention of PYK2 kinase domain-MBP onto the column (Figure 9-21). Bands across buffer elutions A3 through B8 were identified at approximately 72 kDa, which were predicted to be attributable to PYK2 kinase domain-MBP. These fractions were combined for intermediate purification.

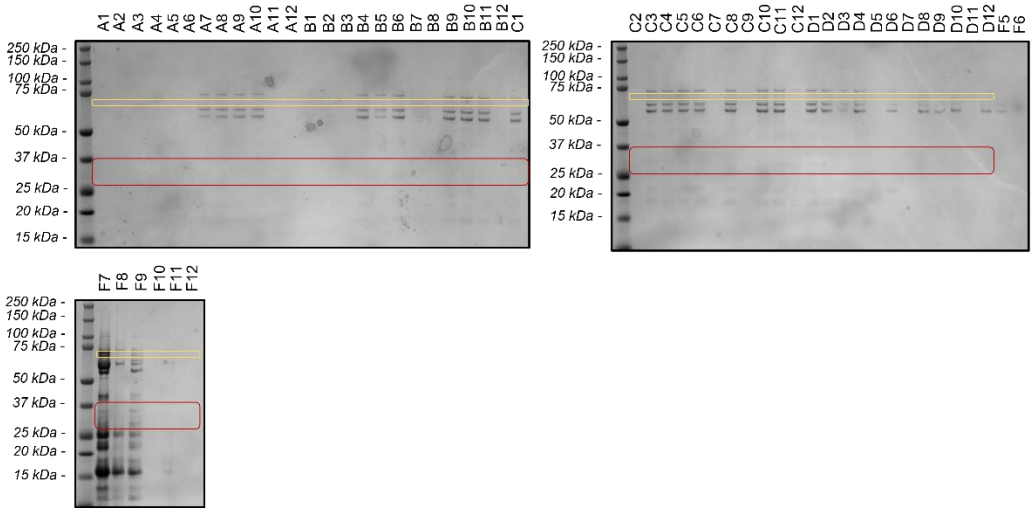

Figure 9-22: Tag Cleavage from PYK2 Kinase domain

Representative Coomassie gel of His/MBP cleavage from PYK2 kinase domain. Cells were cultured in 7 L volumes. Analysis of Akta elutions reveals a loss of the band at approximately 72 kDa (MBP-tagged PYK2 kinase domain) however a resultant band at 30 kDa (untagged PYK2 kinase domain) does not appear in any elution.

To limit interference of the MBP and 6His tags blocking important binding sites and residues between the PYK2 kinase domain and its interaction partner, cleavage of both tags was undertaken using dialysis with His-tagged 3C protease. The dialysed sample was processed through the ÄKTA Pure liquid chromatography system *via* the same HisTrap column. Cleavage of the tag should result in multiple elutions of untagged-PYK2 kinase domain protein. Typically, the cleaved protein would leave the column in elutions A-D however I sampled as far as F to be prudent. Coomassie gels of all elutions were analysed to detect when the untagged protein was eluting from the column and which to retain to concentrate to a pure protein sample (Figure 9-22). The yellow ranges at approximately 72 kDa could comprise of bands relating to MBP-tagged PYK2 kinase domain and red ranges at approximately 30 kDa to untagged-PYK2 kinase domain. However, no bands were detected in either range across any elutions; the results of tag cleavage were inconclusive.

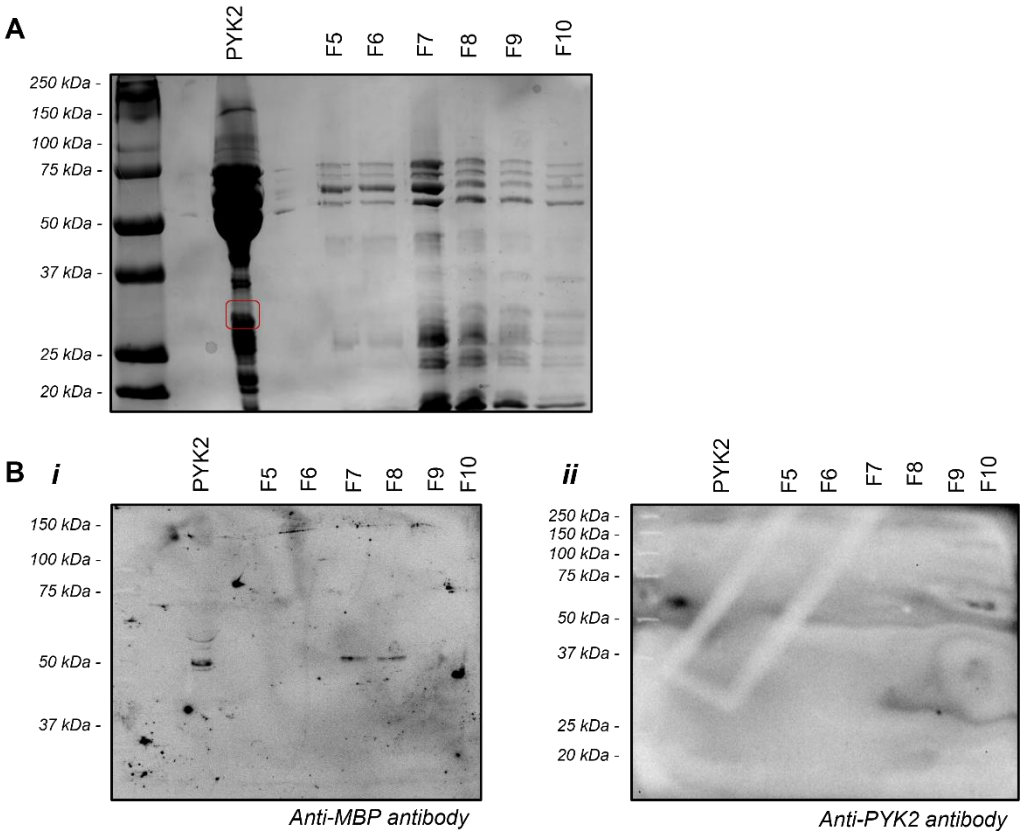

Figure 9-23: Concentration of PYK2 Kinase domain

A. Representative Coomassie gel of concentration of PYK2 kinase domain by centrifugation. **B.** Representative western blots of concentration of PYK2 kinase domain by centrifugation, detection by Anti-MBP (***i***) and Anti-PYK2 (***ii***) probes. Cells were cultured in 7 L volumes. A band in the PYK2 kinase domain concentrated protein elution (highlighted in red) in the Coomassie gel was detected at 30 kDa. However, bands for MBP-tagged PYK2 kinase domain or untagged-PYK2 kinase domain were not observed in either western blot, confirming PYK2 kinase domain was not present in any elution.

To determine if either protein was present, fractions A1-F4 were combined and concentrated into an approximate 200 µL volume and the Coomassie stain was repeated. The Coomassie gel (Figure 9-23) shows the concentrated PYK2 protein and elutions F5-F10. The PYK2 sample is highly impure; multiple bands of differing strength are detectable. Bands between 50 and 75 kDa are most intense and match bands in elutions F5-F10 at the same masses. Additionally, there were bands present around the 30 kDa area in the PYK2 kinase domain sample however the intensity of the band was very low for scale of production carried out. As expression of the protein of interest

occurs in a cellular expression vector, non-specific bands arising from native proteins existing in the cytoplasm and nucleus are also present. As it was difficult to discern for certain by Coomassie, a separate set of western blots, probing for MBP and PYK2 respectively were performed (Figure 9-23). In the MBP western blot, low density bands were detectable in the PYK2, F7 and F8 elutions around 50 kDa, however the molecular mass was too low to pertain to MBP-tagged PYK2 kinase domain, expected at approximately 72 kDa. These could have represented degraded protein tagged with MBP or the cleaved MBP tag (molecular weight ~42 kDa). The PYK2 western blot contains no discernible bands which suggests PYK2 was not present in any elutions. I deduced that the protein was either stuck to the column and therefore lost or, that the production system was not compatible to produce the PYK2 kinase domain protein. The decision was made to discontinue efforts in *E. coli* as discussion of insect and mammalian alternatives were proposed. Insect and mammalian expression systems are more difficult to use since the cells are more fragile, produce significantly less product and can also be more expensive. However, insect and mammalian cells can produce proteins possessing the correct post-translational modifications, including folding, disulfide bonding and *N*-linked glycosylation to provide the native structure. These processes are important to the longevity and function of the protein.

9.3.4. Protein Expression in Sf9 Insect Cells

E. coli expression systems were trialled initially as they are easy to use, growing quickly and readily transfected using methods such as heat shock, however it can be difficult to produce mammalian proteins using bacterial expression systems. Therefore, insect and mammalian cell line protein production became a more viable option. The catalytic domain of PYK2 has previously been produced using the Bac-to-Bac© Baculovirus expression system (Invitrogen) and Sf9 insect cell line for use in crystallographic, surface plasmon resonance and nuclear magnetic resonance studies (Han et al., 2009).

A similar system is used in the PPF, the *flash*BAC™ Baculovirus Expression System (Mirus) which is ideal for production of cytoplasmic and nuclear proteins, in addition to being a highly effective and efficient baculovirus system. The viruses were produced containing the same pOPIN vectors used in *E. coli* production: -F, -J, -M and -S3C. An additional virus was transduced with the pOPINN-GFP plasmid. This plasmid would allow the user to confidently confirm status and follow progression of viral infection.

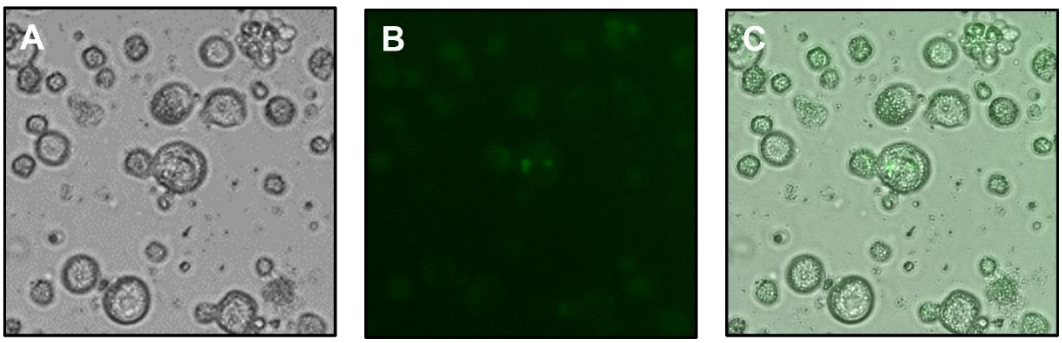

Figure 9-24: Viral Infection of Insect Sf9 Cells

A. Brightfield image of Sf9 cells infected by pOPIN-GFP virus **B.** Green fluorescent light image of Sf9 cells, highlighting three viral replication compartments in an enlarged cell **C.** Overlay of images A. and B.

Phenotypical healthy Sf9 cells are round and comprised of a single nucleus. In the case of infected Sf9 cells, they are enlarged, engorged and appear grainy. In the pOPINN-GFP infected cells, the cells appeared similar to the infected description (Figure 9-24 A). To confirm this, cells were irradiated with a fluorescent signal where small pockets of light became visible in the cytoplasm of individual swollen cells (Figure 9-24 B, C). These green dots corresponded to viral replication compartments which suggested that infection of the host cells had been successful.

Once infection of the host had been established, the virus stock was amplified across three separate passages: P0, P1 and P2. A higher concentration of virus seed stock would be more effective in large scale production. Plaque assays were performed after P1 and P2 passages. Unfortunately, once completing the P1 plaque assay on many separate occasions, during the incubation, the six-well plates would become significantly impacted by external contamination due to factors outside of the project's control, *e.g.,* sharing of media, poor use of tissue culture facilities by others. After several attempts, the project was paused to focus on other areas of research. The impact of laboratory closures due to the Covid-19 pandemic has meant that this work has not resumed upon return to laboratory working at the University.

9.4. Inhibition of the eNOS-PYK2 Interaction

9.4.1. Chemical Inhibition

9.4.1.1. PF-10e

Pfizer published a novel series of PYK2 inhibitors, which possess selectivity for PYK2 over its intra-family isoform focal adhesion kinase (FAK) (Bhattacharya et al., 2012). Broad selectivity across a kinase panel is often difficult to achieve with classical kinase inhibitors, however these inhibitors stabilize the ‘inactive’ DFG-out conformation of PYK2 and are relatively more selective.

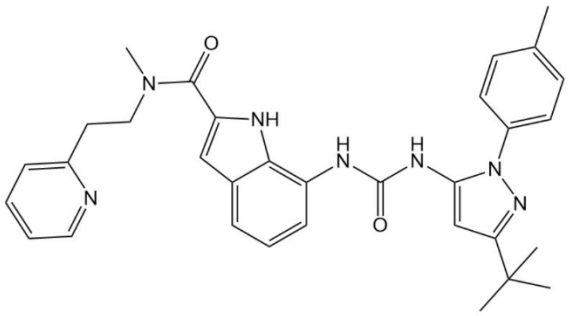

PF-10e

Figure 9-25: Structure of PF-10e PYK2 Inhibitor

Structure of carboxamide urea, PF-10e. Structure prepared using PerkinElmer ChemDraw Prime and based on compounds published in (Bhattacharya et al., 2012).

Two sub-series of the PYK2 inhibitors, an indole carboxamide-urea (such as PF-10e, Figure 9-25) and a pyrazole-urea were identified and found to have different binding interactions at the hinge region of PYK2. These compounds were not pursued as clinical candidates due to their poor pharmacokinetic properties. However, they are suitably interesting as an investigative tool to determine the effect of PYK2 inhibition *in vitro* and *in vivo*. The compounds were procured from Pfizer *via* their compound transfer programme.

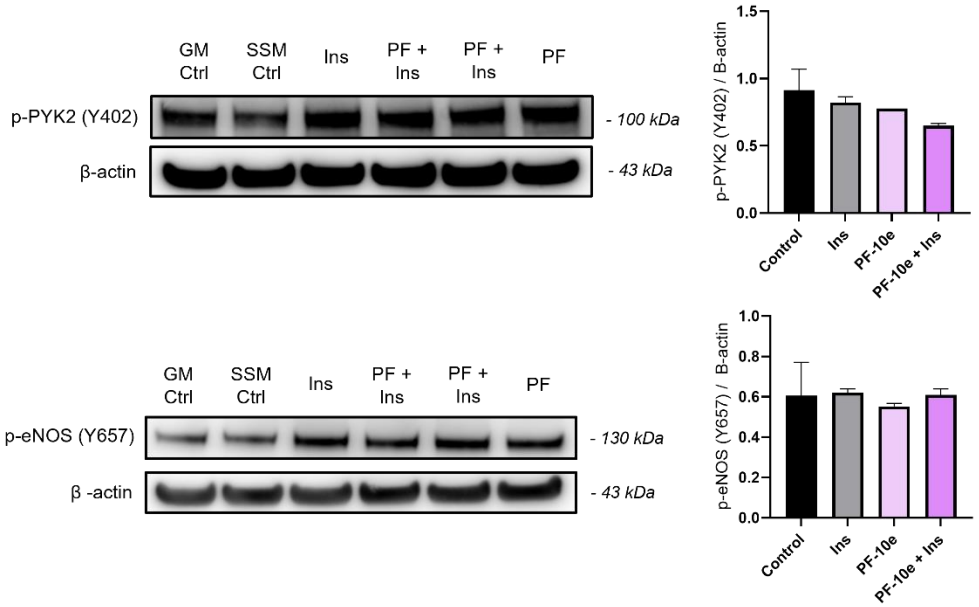

Figure 9-26: Effect of PF-10e Chemical Inhibition on PYK2 and eNOS phosphorylation in Human Saphenous Vein Endothelial Cells

Representative western blots of human SVEC treated with PF-10e and stimulated with insulin. Graphs show no change in PYK2 Y402 and eNOS Y657 phosphorylation with PF-10e, with or without insulin stimulation. N/n=2/2-4.

Confluent monolayers of non-diabetic SVEC were treated for 24-hours with 10 μM of PF-10e and selected samples were stimulated with 100 nM insulin for 15-minutes prior to the end of the treatment period (Figure 9-26). Western blots probed for p-PYK2 Y402 and p-eNOS Y657 levels compared to respective β-actin housekeeper protein. Densitometry data reported no significant difference between cells treated with serum-free medium control and PF-10e with, or without insulin stimulation for either phosphorylated protein. This suggested that PF-10e was not an effective inhibitor of PYK2 phosphorylation on eNOS at position Y657 when analysed using western blotting. Stabilisation of the DFG-out conformation might not be sufficient to inhibit the activity of PYK2 Y402.

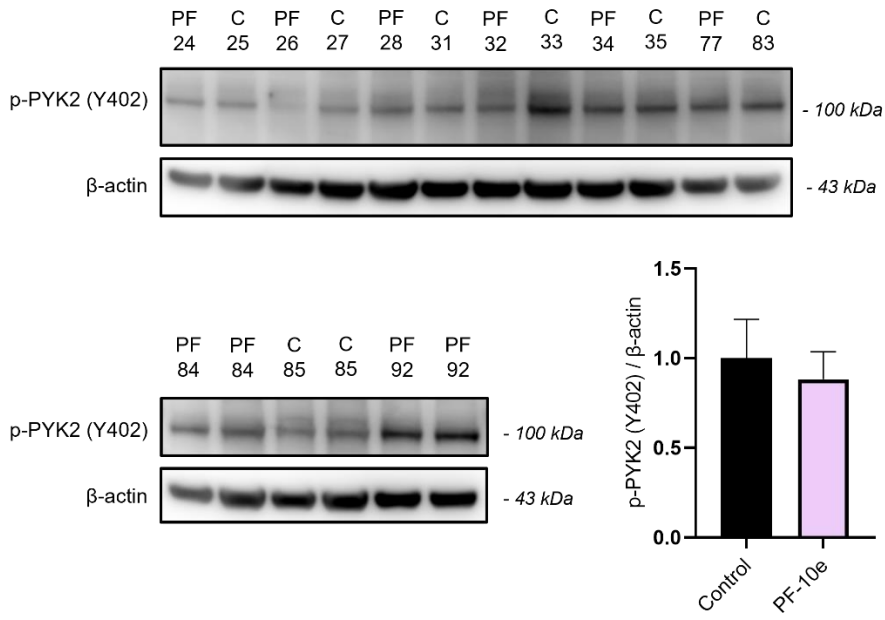

Figure 9-27: Effect of PF-10e Chemical Inhibition on PYK2 phosphorylation in C57BL/6J mice

Representative western blots of murine lung tissues from C57BL/6J mice, attached to minipumps containing 10 μM PF-10e in DMSO for two weeks. Graph shows no change in PYK2 phosphorylation between control and PF-10e cohorts. N=7-8.

In tandem alongside the cell study, to determine the efficacy of PF-10e *in vivo*, an inbred strain of mice, C57BL/6J ('B6' mice, SBS at St James' animal facility) were continually infused with PF-10e for 2.5 weeks using an ALZET osmotic 1000 series minipump. The mice were fitted with minipump containing 51.6 μL of a 10 mM stock solution of PF-10e and 48.4 μL of polyethylene glycol 300 (PEG 300) or, control pumps containing 51.6 μL DMSO and 48.4 μL PEG 300 for a period of approximately 2 weeks while maintaining a standard chow-based diet. Lung, aorta and heart tissues were harvested and lysed to homogenous tissue lysates. Levels of PYK2 and eNOS, and the amount of p-PYK2 Y402 and p-eNOS Y657 were analysed using western blotting (Figure 9-27). Response for proteins were limited for all tissues, excluding p-PYK2 Y402 in lung homogenate – however, there are reports that PYK2 expression is notably higher in lung tissue (Tang et al., 2002) which could explain the marked difference. Densitometry data reported no significant

difference or trend towards reduction in PYK2 phosphorylation of murine tissues upon treatment with PF-10e. The *in vivo* data also suggested that PF-10e was not an effective inhibitor of PYK2 phosphorylation on eNOS Y657, matching the results obtained for our *in vitro* experiments.

It is worth noting that while the cell data shown here would not provide sufficient evidence to ethically support commencement of a mouse study with this compound, preliminary cell data obtained by a first colleague did indicate a reduction in PYK2 activity. The study was repeated by C. Myers after harvest of the B6 mice (Figure 9-26) with significantly different results, which also matched the subsequent murine data analysed by C. Myers (Figure 9-27).

Genetic manipulation using siRNA knockdown is an alternative approach to pharmacological inhibition to regulate expression or activities of proteins.

9.4.2. Inhibition of the eNOS-PYK2 Interaction using siRNA

Gene expression can be manipulated to force up- or downregulation of a singular or family of proteins. Transfection techniques can modulate expression by enabling exogenous nucleic acids such as cDNA and short interfering RNA (siRNA), to enter cells. The former has the ability to promote overexpression and in contrast, the latter may silence a gene of interest – resulting in a gene knockdown or knockout, if expression is completely inhibited.

In this work, gene silencing is of particular interest as removal of one of our interacting partners could affect phosphorylation and activity levels of the other interacting protein, but also have knock-on effect on downstream signalling proteins in the target cell and subsequently on any messengers for

neighbouring cells. The slight alteration may result in a change of phenotype for the cell, causing restoration or dysfunction.

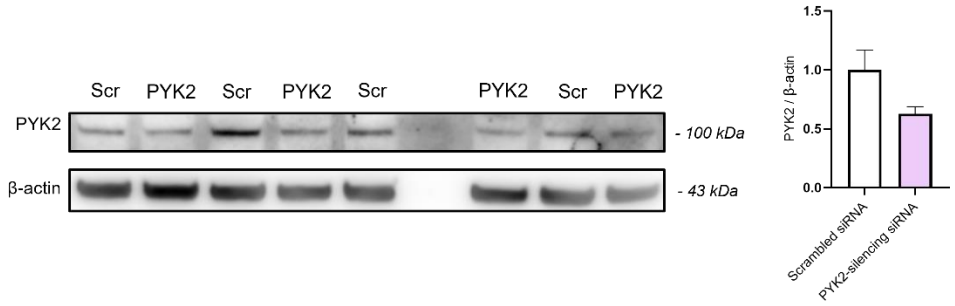

Figure 9-28: Effect of siRNA knockdown on PYK2 in Human Umbilical Vein Endothelial Cells

Representative western blot of HUVEC, where protein expression has been knocked down by scrambled or PYK2-silencing siRNAs. Graph shows trend towards a decrease in PYK2 expression compared to scrambled control, of an approximate 45% reduction. N=4, P=0.20.

Confluent monolayers of HUVEC were transfected with scrambled- (Catalogue ID; D-001810-01-05, Dharmacon) and PYK2-silencing siRNA (SMARTpool, Catalogue ID; L-003165-00-0005, Dharmacon) for a 4-hour period before replacing with full-growth medium for 48-hours. PYK2 levels from cell lysates were analysed using western blotting (Figure 9-28). The blots were incubated with anti-PYK2 antibody for three days to induce a signal for the protein. Densitometry data of PYK2 compared to respective β-actin housekeeper protein showed a trend towards a 45% reduction in PYK2 expression for PYK2-silencing siRNA treatment.

In the future, it would be interesting to determine the effect of this reduction in PYK2 and how it affects the eNOS-PYK2 interaction using techniques such as western blotting or proximity ligation assays.

10. Conclusion and Discussion

Characterisation of the eNOS-PYK2 interaction could provide insight of the functional role of eNOS inhibition in type-2 diabetes and subsequently, how it might be targeted using small molecule modulators to restore enzymatic activity, improving diabetic phenotype of endothelial cells.

10.1. Characterisation of the eNOS-PYK2 Interaction

The eNOS-PYK2 interaction had previously been characterised in HUVEC, PEC, SVEC and OEC using co-immunoprecipitation of either binding partner. Initially, OEC, HUVEC and EA.hy926 cells were selected as they were readily available, easy to culture and are commonly employed as human *in vitro* models for proof of concept experiments (Medina-Leyte et al., 2020). Attempts to confirm the presence of PYK2 in OEC, HUVEC and EA.hy926 cells were not successful. PYK2 has not been shown to be highly expressed in these cell types, unlike in pulmonary cells (Tang et al., 2002) which is reflected in these blots. The opportunity to utilize whole human adipose tissue arose; PYK2 was not visualized in these blots though this is likely due to the fact that whole tissue is composed of several different types of cells which could be diluting the presence of PYK2 in endothelial cells. Human saphenous vein and adipose tissue endothelial cells were obtained from consenting human patients receiving treatment for heart failure and diabetes at the Leeds General Infirmary. These primary cells contain variable levels of protein due to inter-individual expression, including PYK2. PYK2 was observed in these cells which indicated that these cells would be appropriate to use both as a healthy and diseased model in modulation of the eNOS-PYK2 interaction. PYK2 expression has been shown to be upregulated by ROS, such as H_2O_2

generated by exaggerated signalling *via* insulin activation of insulin receptor signalling pathways (Bibli et al., 2017b; Fisslthaler et al., 2008). IGF-1 shares many of the insulin signalling pathways and could also induce increased expression of PYK2 (Adams et al., 2000; Chitnis et al., 2008; Sekimoto et al., 2005). Stimulation of HUVEC to promote expression of PYK2 by treatment of insulin and/or IGF-1 did not prove successful – it is possible that 100 nM was not sufficient to induce hyperinsulinaemic action in these cells. However with H_2O_2 treatment, expression of PYK2 was increased in a dose-dependent manner. These experiments proved that H_2O_2 could be employed to promote the expression of PYK2 in HUVEC. Between experiments for SVEC and ATEC, the western blotting method was reviewed – extending the incubation time of the PYK2 total antibody from overnight to three days which significantly improved visualisation of the protein, as observed in ATEC blots, and subsequent HUVEC blots. Further refinement of the co-immunoprecipitation method is required as the pulled-down protein remains present in the supernatant samples which prevents quantification of the interacting proteins. PYK2 expression has also been reported to be increased under shear as referenced previously (Tai et al., 2002; Fisslthaler et al., 2008). Experiments at a constant speed of 210 RPM (12 dyne cm^{-2}) over 30, 60, 120 minutes and 24 and 48-hours concluded that non-variable shear stress did not significantly increase PYK2 expression.

Preliminary experiments demonstrated that SVEC and ATEC could be ideal *in vitro* model of human diabetes. Method refinement could improve the signals obtained by increasing antibody incubation time, as observed in HUVEC. PYK2 expression can also be promoted using H_2O_2. The eNOS-PYK2 interaction has been demonstrated in ATEC by western blotting,

however method development is required to use this technique to quantify the interacting proteins.

A proximity ligation assay was employed to determine the localisation and potential for interaction between eNOS and PYK2. The assay confirmed mutual localisation of each protein within the nucleus and cytoplasm of EA.hy926 cells and that the supposed interacting partners were within sufficiently close proximity to produce an immunofluorescence signal. Proximity ligation cannot confirm the interaction, nor at which interface or the presence of chaperone proteins, however it does provide plausible evidence that an interaction occurs between eNOS and PYK2.

Use of biophysical techniques such as SPR could provide evidence for involvement of a chaperone protein. Interactions between purified proteins in isolated environments can be recorded if they occur directly between the interacting partners. Two methods of immobilisation were employed yet neither PYK2, eNOS or control protein MBP bound to the sensor surface *via* anti-His. It is likely that due to the short length of the His linker tag, protein folding and incorrect orientation of protein flowing through the cell may have contributed to a non-detectable yield of immobilized protein. Only eNOS possessed a GST tag – which is slightly larger than the His tag – small amounts of eNOS were successfully immobilized onto the surface *via* anti-GST. The amount of eNOS protein immobilized was suboptimal for use in kinetics experiments due to poor concentrations of immobilized protein, in addition to a proportion of the aforementioned protein bound in nonideal conformations for detecting interactions. Protein production of PYK2 kinase domain was started to isolate high concentrations of protein possessing a tag

suitable for SPR experiments and, contained within an ideal buffered solution to match the purchased eNOS reductase domain protein. Issues associated with external contamination and laboratory access due to Covid-19 restrictions prevented completion of this project.

While a SPR method of characterisation has not yet been established for this interaction, the basis for further work to continue to reach success, is present. However, proximity ligation and immunoprecipitation methods have been detailed, which could be used to observe the efficacy of an eNOS-PYK2 small molecule modulator, once identified.

10.2. Modulation of the eNOS-PYK2 Interaction

eNOS activity is modulated by activation of IR. In ESMIRO models, the IR tyrosine kinase domains are impaired and intracellular signalling *via* these receptors is inhibited. This would reflect in a reduction of signalling of the PI3K/Akt/eNOS axis and loss of NO production. Duncan *et al.* reported that activation of eNOS *via* S1177 was unchanged, remaining at low levels in insulin-stimulated ESMIRO aortae, compared to increased activation for WT mice (Duncan et al., 2008). ESMIRO mice had increased ROS generation, *versus* WT mice, by upregulation of NOX2 and NOX4 oxidases – which are known to generate a proatherosclerotic signalling loop with PYK2, increasing its expression and activity. Therefore in transgenic ESMIRO mice, it would be expected that PYK2 expression and activity would be increased irrespective of insulin stimulation as signalling cannot occur *via* PI3K/Akt/eNOS but the increase in ROS species would upregulate and induce autophosphorylation of this kinase. However, due to crossbreeding with the Y656F mutant, PYK2 expression and autophosphorylation levels should remain elevated yet

phosphorylation of eNOS at F656 would not occur, preventing inhibition of the enzyme by this method. A small cohort was used in this study – three transgene and one wild-type – so it is difficult to elucidate an accurate comparison between the two models. In addition, visualisation of eNOS in any panel for both wild-type and transgenic mice was not possible in these samples, when utilizing mouse or rabbit eNOS primary antibodies. Due to the presence of eNOS Y656, though at very low levels, in the supernatant and cell lysate control blots, it would suggest that this absence is due to issues relating to antibody binding. Most importantly, it prevents quantification of the eNOS-PYK2 interaction, if any, in immunoprecipitation blots and total level characterisation to compare against PYK2 levels. From the available information regarding expression and activation of PYK2, there was no observed difference in PYK2 levels with increasing insulin concentration for ESMIRO transgenic mice, unlike the hypothesis that increased ROS generation would promote production of this species. It is likely that as Akt and PI3K activities were not upregulated as observed in states of hyperinsulinaemia (Viswambharan et al., 2017), that the loop between NOX oxidases and PYK2 was not in effect. It would be interesting, in future work, to record the presence of NOx species of each model, to determine if NO bioavailability was affected, in addition to quantification of levels of eNOS expression and activation *in vitro*.

In vitro genetic manipulation was employed to silence PYK2 mRNA expression of localised HUVEC. Proof-of-concept experiment to determine if siRNA knockdown of PYK2 was possible for use in further testing of the angiogenic and atherosclerotic phenotype. Knockdown using scrambled- and

PYK2-specific siRNA saw a trend towards 45% reduction in PYK2 expression compared to the aforementioned controls.

Bhattacharya developed a series of inhibitors of PYK2 to prevent activation of p38 MAPK (Bhattacharya et al., 2012). The novel analogues of imatinib (BIRB-796) targeted a region in close proximity to the Y402 site (Lys457, Glu474, Asp567, Phe568, Met502). Binding to this region is predicted to stabilize a 'DFG' (Asp-Phe-Gly) motif which is highly involved in kinase activity; the 'DFG-out' conformation does not allow binding of ATP and is effectively inactive. One of these structures, PF-10e was screened for its ability to prevent the interaction between eNOS and PYK2 *in vitro* and *in vivo* utilizing a minipump to deliver a continuous dosage to C57BL/6J mice. Phosphorylation of eNOS Y657 and PYK2 Y402 in HUVEC was not affected with treatment of 10 μM PF-10e. Likewise, in B6 murine lung homogenates were also not affected by continuous dosing of PF-10e, over two weeks. These data suggest that stabilisation of the DFG motif is not sufficient to inhibit PYK2 autophosphorylation of Y402 and any subsequent activity at Y657 on eNOS.

Genetic manipulation by crossbreeding of murine models of diabetes and wild-type as controls, knockdown using siRNA or pharmacological inhibition can be employed to measure the effects of modulating the interaction between eNOS and PYK2. Quantification of nitric oxide production, angiogenesis models – such as those utilized in the IR/IGF1R hybrids project, *e.g.,* proliferation and migration of endothelial cells – and atherosclerosis – including the atherosclerosis-prone apolipoprotein E-deficient ($ApoE^{-/-}$) mouse model of atherosclerosis (Lo Sasso et al., 2016).

Identification of a method of genetic manipulation of the eNOS-PYK2 interaction will serve well to characterise the effect of inhibiting the interaction on endothelial cell function, notably when comparing to a small molecule modulator which could be used as a treatment for type-2 diabetes in the future.

11. Future Work

11.1. Refinement of Co-Immunoprecipitation Method for the eNOS-PYK2 Interaction

The co-immunoprecipitation blots for both eNOS and PYK2 pull-downs were not complete, observing the pulled-down protein in the supernatant blots. The eNOS pull-down was notably more effective than the pull-down of PYK2 – most of the eNOS protein pulled-down was present in the immunoprecipitation blots, whereas the majority of PYK2 was not pulled-down and could be observed in the supernatant blots. Based on the current method, the eNOS pull-down would be most suitable to use, with some method refinement. Co-immunoprecipitation of IR/IGF1R hybrid receptors, by IGF1R pull-down was also performed in this thesis (section 4.2.2, Figure 4-12). There are several variables which could improve the yield of eNOS protein, and any interacting protein partners: cell type and concentration of loaded protein, type of support surface – magnetic beads or agarose, duration of protein immobilisation step, number and volume of washes upon completion.

PYK2 is natively expressed at higher levels in specific areas, including the lungs (Tang et al., 2002) as observed by the strong bands in the PEC controls (section 9.2.1, Figure 9-4) in addition to upregulation of its expression in diabetes (Viswambharan et al., 2017). Higher proportion of protein contained within samples will likely result in stronger visualisation of the eNOS-PYK2 interaction by co-immunoprecipitation.

Protein G agarose beads have been used for all experiments in this thesis, however magnetics beads are also a viable option for co-immunoprecipitation. Magnetic beads, while the more expensive option and require associated

consumables, limit non-specific binding and do not require the same preclearing by centrifugation as agarose beads (Sigma-Aldrich, 2022).

In method refinement of IR/IGF1R co-immunoprecipitation (section 4.2.2, Figure 4-12), the duration of the protein immobilisation onto the support surface proved critical in obtaining a complete pull-down of the protein of interest, and its interacting partners. Modifying the length of time of this step may improve the yield of the pulled-down protein. Likewise, the volume and frequency of washes upon completion of immobilisation of the protein of interest reduced non-specific binding, which could be highly important if screening for protein chaperones of the eNOS-PYK2 interaction. In method refinement of IR/IGF1R co-IP, increasing both parameters in the wash phase saw reduced β-actin present in the immunoprecipitation blots.

11.2. Design of Novel ATP-Covalent Linker of eNOS and PYK2 Proteins at Site of Interaction

Characterisation of kinase-substrate interactions are highly challenging due to their transient nature. A covalent method of capture could be employed to freeze these interactions and enable mapping of kinase signalling networks (Wong et al., 2019).

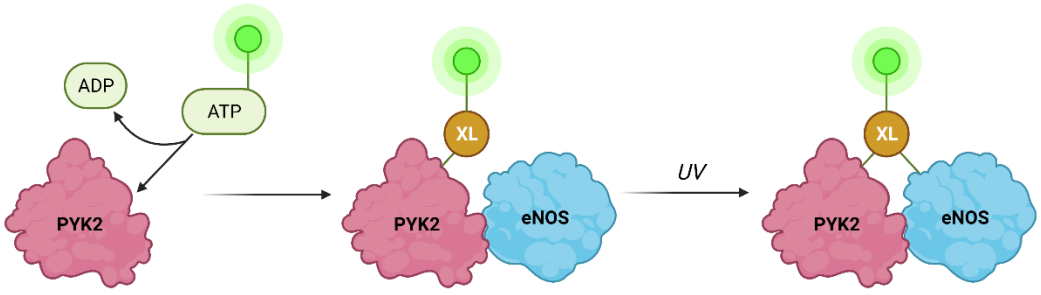

Figure 11-1: Schematic of ATP-Crosslinking

When irradiated by UV light, PYK2 becomes phosphorylated at Y402 by ATP-photocrosslinker (XL) and may form a covalent link with eNOS. Image created with BioRender.com.

Affinity crosslinking using *γ*-phosphate modified ATP analogues have been utilized to capture protein partners of kinase proteins in proteome mapping. The most commonly used have affixed an aryl azide (ATP-ArN_3) or benzophenone (ATP-BP) photocrosslinker (Garre et al., 2014). The kinase becomes phosphorylated by the ATP analogue and when in close proximity to a binding partner, can become covalently linked *via* irradiation of UV light (Figure 11-1). The technique can be carried out both *in vitro* and *in vivo*, used in the latter as means of stabilizing PPIs prior to cell lysis and purification – granting a true snapshot of networks in living cells (Yu and Huang, 2018). Cell lysates may also be used; use of genetic manipulation to induce overexpression of eNOS and PYK2 protein targets may improve the yield of this particular PPI. Reaction products may be separated by SDS-PAGE and characterised using western blotting and quantitative Matrix-Assisted Laser Desorption/Ionization-Time Of Flight (MALDI-TOF) Mass Spectrometry, or LC-MS.

Wong *et al.* employed this technology to capture the interaction between Src, a similar protein tyrosine kinase to PYK2 and its substrate Cortactin by use of an ADP-methacrylate (ADP-MA) linker which demonstrated considerable efficiency over the ATP analogue (Wong et al., 2019). It is possible that a similar method could be used to stabilize the interaction between eNOS and PYK2.

11.3. Identification of Protein Interaction Partners using Quantitative Affinity Purification-Mass Spectrometry

The interaction between eNOS and PYK2 may be facilitated by chaperone proteins. Chaperones, otherwise known as heat shock proteins, classed by their respective molecular weights (*e.g.* heat shock protein 90 kDa, HSP90) and possessing a breadth of functional capabilities (Bascos and Landry, 2019). HSP60 and HSP70 chaperones serve to facilitate protein folding, whereas HSP90 are involved in refinement of protein structures into their functional forms. HSP90 chaperones have been associated with modification of kinases, and as referenced in section 1.6.2.2 is involved in the activation of eNOS by dissociation from caveolin (Gratton et al., 2000).

Affinity purification, combined with mass spectrometry (AP-MS) allows unbiased detection of protein-protein interactions under physiological conditions (Meyer and Selbach, 2015). AP-MS could provide information regarding the interaction interface of eNOS and PYK2, but also any other involved parties which may facilitate binding.

11.4. Biophysical Characterisation of eNOS-PYK2 Interaction

Current endeavours to characterize the eNOS-PYK2 interaction using surface plasmon resonance have encountered issues with sample concentration and buffer composition and, immobilisation technologies.

Proteins used in these studies were of the eNOS reductase domain and PYK2 kinase domain, stabilized in respective buffers containing high levels of surfactants. Surfactants at low levels can minimize non-specific binding of analyte proteins directly to the chip surface, where preventing loss of protein at low concentrations is critical (Schasfoort, 2017). However, in purification of

proteins, surfactants can interfere with protein concentration measurements and may lead to loading of less protein than required to observe an interaction by SPR. In addition, buffer mismatch can also introduce step changes in baseline upon mixing of the two and so it is ideal to have both proteins contained within the same matched buffered solution. The buffer solutions of eNOS and PYK2 were quite different, and where dialysis was used to exchange buffers, resulted in a considerable loss of protein.

Further to the complexities associated with buffer composition and suboptimal protein concentrations, the anti-His technology did not appear to bind either eNOS or PYK2 ligand which introduced further limitations as only eNOS possessed a GST tag for anti-GST immobilisation.

Cytiva also provide a third capture method, using biotinylation. Biotin can be attached onto proteins, by targeting primary amines, sulfhydryl and carboxyl functional groups – these modified proteins can be directly immobilized onto streptavidin sensor chips. Bound biotinylated substrates are almost irreversibly bound to the sensor chip surface; harsher regeneration conditions are required compared to anti-GST or anti-His surfaces which can impact the binding capacity of the ligand in subsequent studies (Hutsell et al., 2010).

As the PYK2 protein was distinctly less concentrated than eNOS (0.18 mg/mL *vs.* 4.0 mg/mL; section 2.7.1, Table 2-1) and the limiting factor in this aspect, we commissioned two PYK2 proteins: FERM+Kinase domains and FAT+Kinase domains to be produced by GenScript. The protein was received during the first Covid-19 lockdown but could still be used in future experiments with eNOS reductase domain, by re-attempting anti-GST or anti-His capture, or the new biotinylation method.

11.5. Screening of Novel eNOS-PYK2 Inhibitors by ^{19}F-NMR

^{19}Fluorine-NMR (^{19}F-NMR) can be employed to screen novel inhibitors of protein-protein interactions.

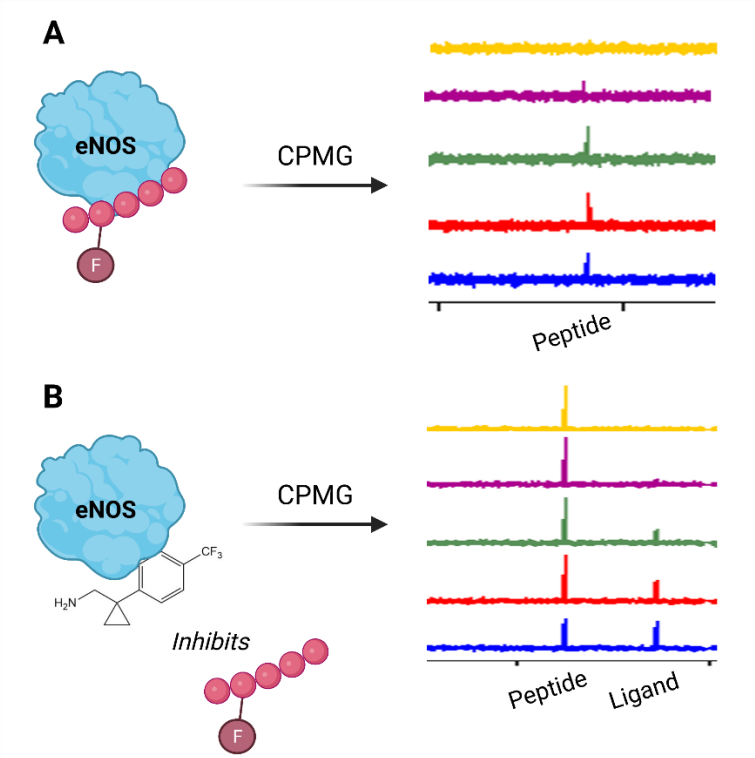

Figure 11-2: ^{19}Fluorine-NMR Screening of eNOS-PYK2 Inhibitors

A. Protein target, eNOS binds to a fluorinated-PYK2 peptide, which can be monitored by Carr-Purcell-Meiboom-Gill (CPMG) ^{19}F-NMR. The fluorine signal is quenched upon binding to the protein, observing a decrease in NMR signal. **B.** A fluorinated small molecule is introduced, binding at the interface between eNOS and PYK2 and displacing the PYK2 peptide. Effective inhibitor binding to its target will observe a reduction in NMR signal, whereas the displaced PYK2 peptide signal should increase. Image adapted from Dr. K. Simmons, University of Leeds, Leeds (2020 - unpublished) and created with BioRender.com.

Dr. Martin McPhillie and Dr. Mark Howard from the School of Chemistry, working with Dr. Katie Simmons have designed a small molecule screening process for targeting of protein-protein interactions. For this particular project, the eNOS reductase domain (produced in-house by the PPF) is bound to a fluorinated, short peptide formulated on the sequence of PYK2 at its autophosphorylation site, Y402. The fluorinated-peptide can be displaced by effective inhibitors of the interaction; these interactions can be monitored by

^{19}F-NMR as binding of a fluorinated species quenches its signal, while observing a systematic increase in signal of the displaced partner (Figure 11-2).

In comparison with virtual screening techniques, ^{19}F-NMR does not produce predicted binding interactions, removing the inherent bias of selecting the binding pose of 3D structures. Dose curves may also be obtained by incorporating defined quantities of protein and inhibitor, which is not possible *via* virtual screening methods. While it is less high-throughput than computational modelling, the team have identified series of inhibitors which can be incorporated into the same screening panel, as each structure possesses a distinct NMR signal from the others.

Use of this technique could identify novel small molecule inhibitors of the eNOS-PYK2 interaction, which could further be used in determining the effects on NO bioavailability and restoration of angiogenesis of diabetic endothelial cells.

11.6. Effect of Modulation of eNOS-PYK2 Interaction

Genetic manipulation of PYK2 expression using siRNA was significantly knocked down, in HUVEC (section 9.4.2, Figure 9-28). While pharmacological inhibition using PF-10e were not effective at preventing the interaction between eNOS and PYK2 (section 9.4.1.1, Figure 9-26 and Figure 9-27), the use of ^{19}F-NMR to screen novel small molecule inhibitors is possible (section 11.5,Figure 11-2). These methods could be employed to reduce or inhibit the eNOS-PYK2 interaction in a diabetic phenotype.

In hyperinsulinaemia, PYK2 expression and activity are increased, observing the knock-on effect of inhibition of eNOS catalysis and production of NO

(Viswambharan et al., 2017). NO is a pro-angiogenic and anti-atherosclerotic signalling radical (Cooke and Losordo, 2002; Wang, G.-R. et al., 1998; Wang, W. et al., 2011; Gao et al., 2017). Therefore by inhibiting PYK2 and subsequently restoring NO bioavailability produced *via* eNOS, endothelial function could be restored and measured by changes in mechanisms of angiogenesis and potentially a reduction in development of atherosclerosis.

12. Concluding Remarks

Collation of data characterising the eNOS-PYK2 interaction through different methods is well-underway. The interaction has been successfully demonstrated by *in silico* modelling, proximity ligation assay in EA.hy926 cells and by co-immunoprecipitation in ATEC. Biophysical techniques such as surface plasmon resonance have commenced however, due to complications regarding sample composition and ligand immobilisation technologies, current effort have not yet yielded results.

Inhibition of PYK2 activity using pharmacological inhibitor, PF-10e *in vitro* and *in vivo* has not been effective; stabilisation of the DFG motif may not be sufficient to prevent PYK2 phosphorylation of eNOS at Y657. Genetic manipulation using siRNA demonstrated a considerable reduction in PYK2 expression which could be used to probe the effects of reducing PYK2 expression and activity on nitric oxide bioavailability and angiogenesis of endothelial cells possessing a diabetic phenotype.

Part III

Molecular Dynamics Simulations of Protein-Protein Interactions

13. Aims and Hypothesis

Computational techniques across all areas of research are quickly becoming recognized as interesting translational tools to pair with more traditional scientific methods. Use of protein modelling and simulations of protein-protein interactions are becoming more prevalent and increasingly accurate against nature – even used as a steppingstone in predicting areas of interactions to be followed up using more conventional techniques (Shin et al., 2017; Macalino et al., 2018).

It is known that IR/IGF1R hybrids do not bind insulin at physiologically-relevant concentrations (Slaaby et al., 2006; Benyoucef et al., 2007; Pandini et al., 2002). However, the structural basis for this is yet unknown. Use of molecular dynamics simulations to investigate binding of insulin and IGF-1 to both homodimeric receptors and hybrid receptors could illuminate the mechanism for insulin-resistance in hybrid receptors.

I planned to meet the following objectives in this thesis:

1. To identify suitable PDB structures of IR, IGF1R, insulin and IGF-1 for use in modelling.
2. To create the dimer ectodomain, insulin and IGF-1 models to prepare larger apo- and complexed structures, suitable for Modeller.
3. To prepare protein simulation boxes through CHARMM-GUI and GROMACS.
4. To generate molecular dynamics simulations on ARC3.
5. To distinguish differences in binding affinity between each dimer ectodomain and ligand.

I hypothesized that the results of the study could grant clearer elucidation of residue-specific differences contributing to the variation in insulin and IGF-1 binding affinity across the three dimer receptors.

14. Results

14.1. Creation of Molecular Dynamics Models

To understand how Class II RTKs interact at an atomistic level with their respective ligands, simulations of the apo-receptor structures were generated using GROMACS 5.0 on the ARC3 high-performance computing (HPC) cluster.

Dr. K. Simmons had previously created a homology model of the IR/IGF1R hybrid receptor ectodomain ('Ward' model) utilizing the insulin receptor homodimer ectodomain crystal structure (PDB 4ZXB, (Croll et al., 2016)). The development of this model is described in detail in section 4. Published structures of the apo IR (PDB ID; 4ZXB (Croll et al., 2016)) and apo IGF1R (PDB ID; 5U8Q (Xu et al., 2018)) were selected as templates. The structures are of sufficiently high resolution (3.30 and 3.27 Å, respectively) and in addition, had good-fit against their individual electron density maps of approximately 85%, where only ~10% residues were missing from the complete amino acid sequence.

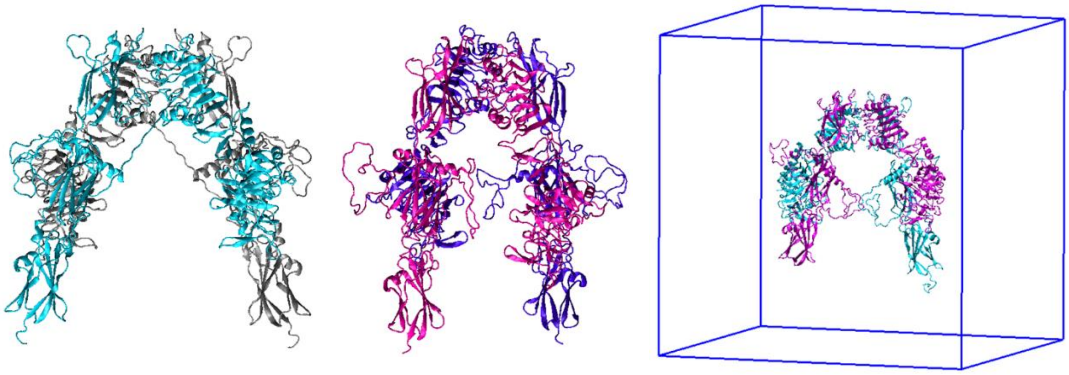

Figure 14-1: Molecular Dynamics Simulations Models of IR, IGF1R and IR/IGF1R Hybrid Apo-Receptors

Molecular dynamics simulations models of the insulin receptor (**Left:** A-cyan, B-silver), IGF1R (**Center:** A-violet, B-magenta) and IR/IGF1R hybrid (**Right:** A-IGF1R, magenta, B-IR, cyan), contained within a simulation box (**C.** dark blue). Models generated using PDB 4ZXB (Croll et al., 2016), 5U8Q (Xu et al., 2018) and Dr. Simmons' IR/IGF1R 'Ward' homology model, visualized using VMD (Humphrey et al., 1996).

The PDB files were firstly cleaned up, retaining only information regarding co-ordinates for each individual atom in the protein structure, using GROMACS 5.0.x (van der Spoel et al., 2005). Each protein contained missing residues, typically occurring in the most flexible regions which are difficult to crystalize, and mutated regions, as a result of inclusion of non-native linker sequences in stabilisation of crystal structures or genetic polymorphism. The protein structures were corrected using Modeller (Webb and Sali, 2016), generating predicted geometries for each missing amino acid residue to produce a complete structure and ensuring no breaks in sequence (Figure 14-1). The complete protein was placed within a simulation box and filled with waters and Na^+ and Cl^- to approximate a cellular environment, using CHARMM-GUI Solution Builder (Figure 14-1.C) (Brooks et al., 2009; Jo et al., 2008; Lee, J. et al., 2016).

The coarse-grained (CG) models were 'backmapped' to an atomistic resolution. Coarse-graining of an atomistic model simplifies the representation of the physical system by reducing the degrees of freedom and therefore

significantly accelerating calculations (Li, W. et al., 2020). Use of a CG system allows larger simulations to run for a longer duration, while still retaining atomistic-detailed information of protein-protein interactions. The simulations were performed for 250 ns on the ARC3, high-performance computer cluster at the University of Leeds.

14.2. Apo-Receptor Analyses

Initial calculations of root-mean-squared deviation (RMSD) and root-mean-squared fluctuation (RMSF) of the trajectory of all carbon-alphas in the protein structure were performed using GROMACS (Figure 14-2) (van der Spoel et al., 2005).

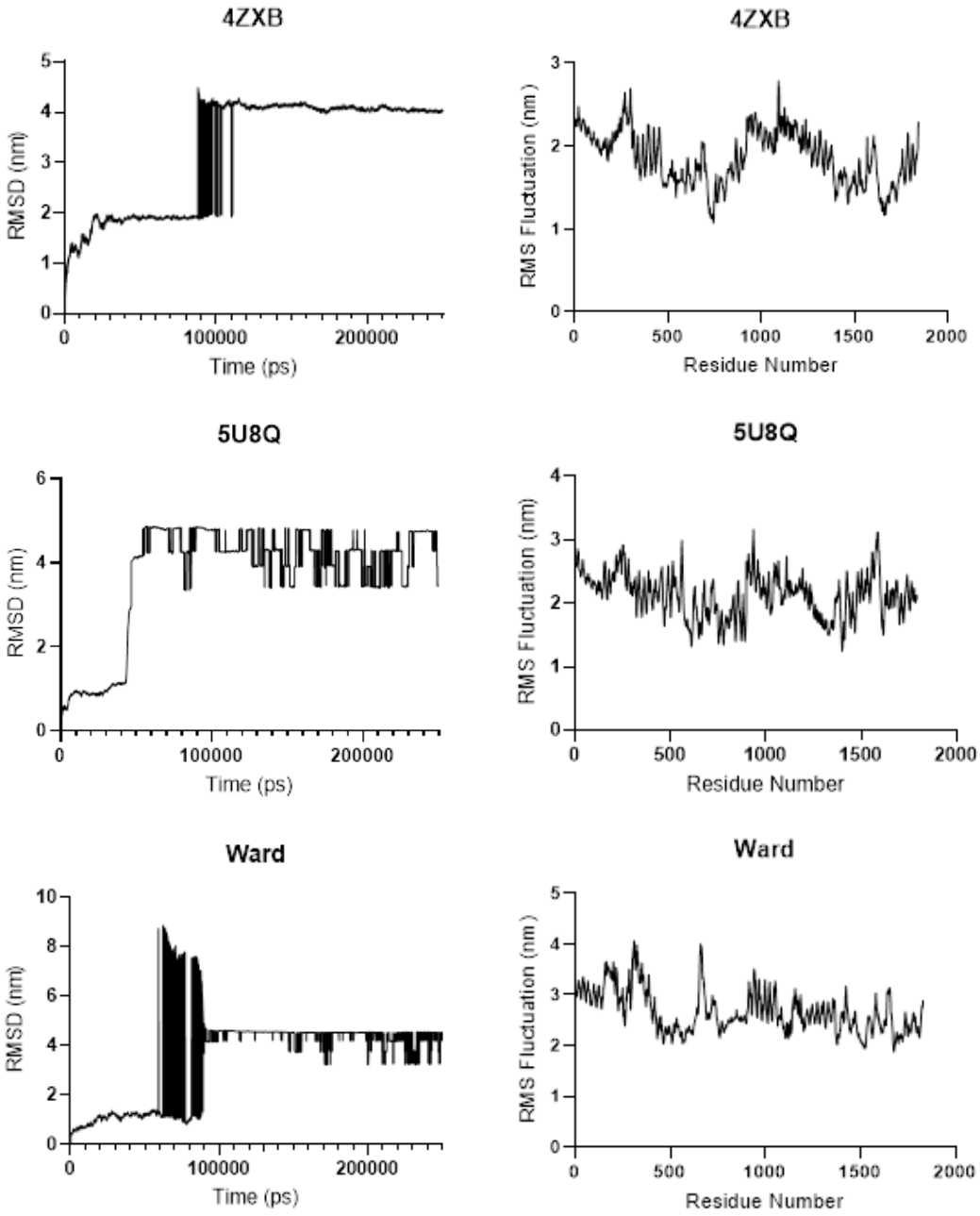

Figure 14-2: RMSD/C_α & RMSF/C_α for IR, IGF1R and IR/IGF1R Hybrid Apo-Receptor Simulations

Root-mean-squared deviation (RMSD/C_α) over 250 ns, and fluctuation (RMSF/C_α) calculations of all amino acid carbon-alphas of the insulin receptor (4ZXB), IGF1R (5U8Q) and IR/IGF1R hybrid ('Ward').

The trajectory files' RMSD calculations highlighted serious errors in the simulations. Across all files, notable step-changes in the curves from 40 ns for 5U8Q, 60 ns for Ward and 90 ns for 4ZXB, continuing throughout the simulation for both 5U8Q and Ward, while ending at approximately 120 ns for 4ZXB though the resting baseline is consistent at 4 nm for the remainder of

the runtime. Step-changes in the baseline in this manner may be indicative of protein wrapping around the simulation box and interacts with itself. Similarly, the RMSF/C_α data were generated around a point of origin of 2-3 nm, as opposed to zero, indicating errors in the simulation.

Limitations associated with working from home, due to Covid-19 pandemic restrictions, prevented analysis using the HPC servers. A maximum of 100 frames, of several thousands, could be downloaded from the server and visually analysed using VMD (Humphrey et al., 1996) to confirm the source of the problem. Preparation and downloading to a local server of shorter trajectory files (~100 frames) took in the region of 4-6 hours per file, dependent on download speed availability. Due to imminent return to a laboratory environment and restrictions regarding use of HPCs, this project was paused.

15. Conclusion and Discussion

Insights into the structural determinants driving IR/IGF1R hybrid receptor binding to insulin and IGF-1 would provide a much-needed template for design of hybrid-specific inhibitors. The basis for this project could offer information regarding involvement of distinct amino acids in binding interactions.

Apo-receptor structures of the insulin receptor (4ZXB), IGF1R (5U8Q) and IR/IGF1R hybrid ('Ward') based on an IR ectodomain homology model have been produced and may be used in molecular dynamics simulations. Issues regarding step-changes in baseline of RMSD/C_α and RMSF/C_α are likely attributed to the periodic boundary conditions (pbc) set when creating the simulation box – this is a known issue and may be overcome by changing the pbc conditions of a new file or, including the '-pbc no jump' when sampling the raw trajectory file, followed by '-pbc whole' which appears to resolve these artifacts.

I have also identified ligated structures for IR and IGF1R which could be used for molecular dynamics simulations to begin to understand the changes in receptor structure upon ligand binding. For IR, two potential structures were identified: 6PXV, a full-length insulin receptor bound to four insulin proteins (Uchikawa et al., 2019) and, 6CE7, an insulin receptor ectodomain in complex with a singular molecule of insulin (Scapin et al., 2018). Both structures were produced using cryo-EM; 6PXV has an excellent resolution at 3.20 Å though 35-41% of the insulin molecules are lacking structural information, in contrast to 6CE7 which has poor resolution at 7.40 Å however, a higher percentage of structural information of both the insulin receptor and insulin molecule chains have been presented. Despite the poor resolution, the 6CE7 structure would

be most compatible to compare against the IGF1R receptor ligand-bound model, in addition to complete information for the 21-amino acid long insulin molecule. The IR/IGF1R hybrid homology model would require design of a second homology structure utilizing this structure.

5U8Q was selected in the first instance as it was published as an IGF1R-IGF-1 complex, where for the apo- structure, the IGF-1 molecule was removed from the original PDB file. The IGF1R-IGF-1 model would be highly compatible for use in the second part of the project.

Design of ligand-receptor structures utilizing the non-cognate ligand, IGF-1 for IR and IR/IGF1R and insulin for IGF1R, would be required. Removal of the original ligand and re-docking with the new peptide could be an option; re-writing the presently-docked molecule would create difficulties as insulin is a dimer protein, whereas IGF-1 is a single-chain peptide.

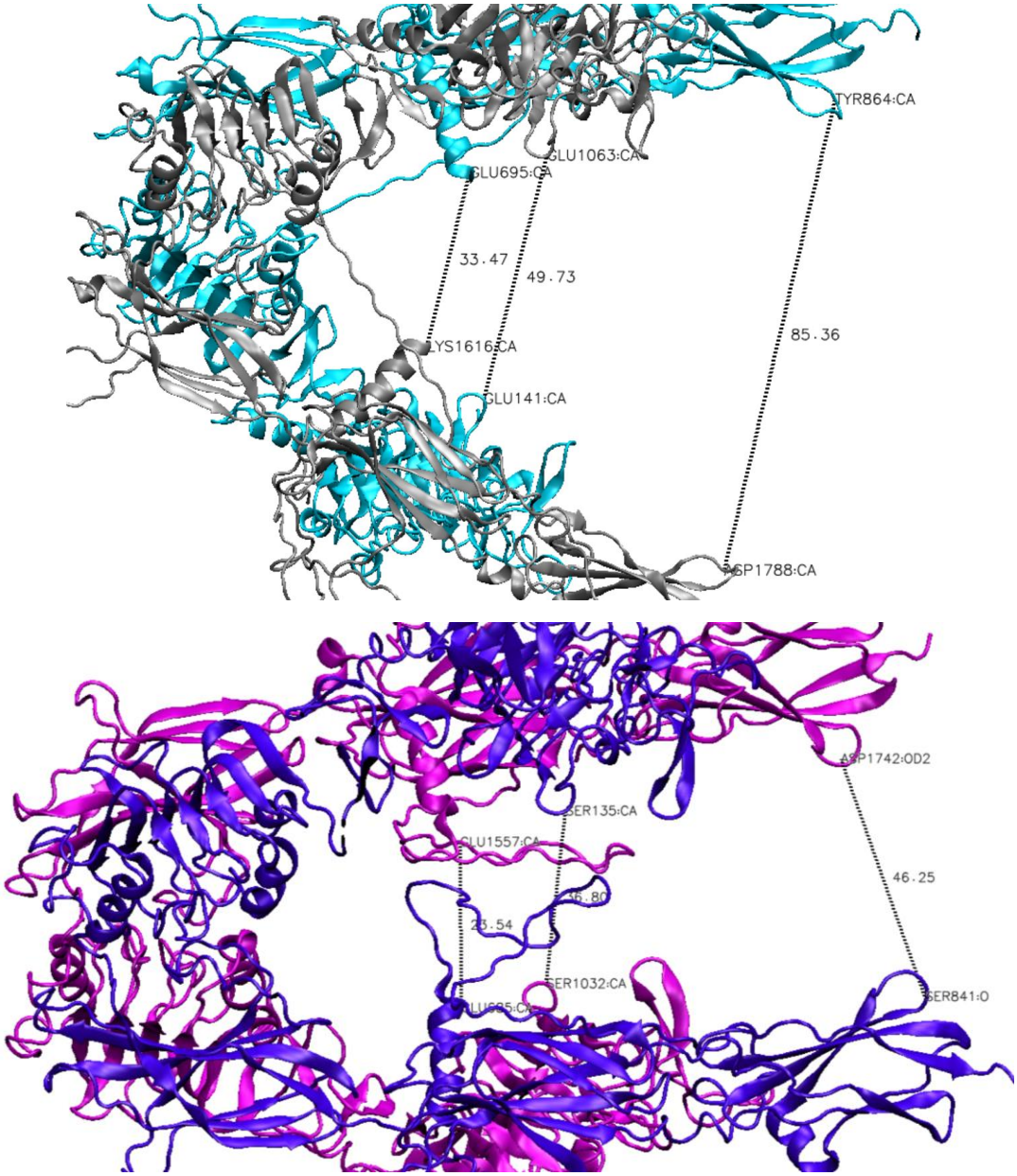

Figure 15-1: Internal diameter of IR and IGF1R FnI-III domains

Internal diameter measurements of the IR (**Top:** A-cyan, B-silver) and IGF1R (**Bottom:** A-violet, B-magenta) at their widest point and at center of mass. IR is 85 Å at its widest and, between 33 and 50 Å at center of mass, dependent on chains compared. IGF1R is 46 Å at its widest and, between 24 and 37 Å at its center of mass. Models were generated using 4ZXB (Croll et al., 2016) and 5U8Q (Xu et al., 2018), visualized using VMD (Humphrey et al., 1996).

Due to the inherent bias introduced by design of an IR/IGF1R homology model based on the IR crystal structure, it is likely that some data may share similarities with IR-insulin/IGF-1 binding. It is highly distinct, particularly when considering the overall protein structure (section 14.1, Figure 14-1) and internal diameter between FnI-III domains (Figure 15-1). The IR ectodomain

is more tapered compared to the IGF1R ectodomain which is straighter, noting a smaller angle moving upwards to the top of the structure. The constraints, in addition to the variation in amino acid sequence at binding regions may have a profound effect on IR/IGF1R binding interaction data obtained. Design of a new homology model based on the IGF1R crystal structure could isolate any commonalities in binding interactions between the two models and may prove insightful to identify regions involved in binding that are conserved in native IR/IGF1R hybrid receptors.

These models could indicate the structural basis for the loss of insulin sensitivity of IR/IGF1R hybrids. The result will contribute to a long-unanswered question which will support understanding of the role of IR/IGF1R hybrids in disease and ideal structure of novel insulin analogues which promote association to these receptor species, improve insulin sensitivity and therefore alleviate symptoms of type-2 diabetes.

16. Future Work

16.1. Completion of IR, IGF1R and IR/IGF1R Hybrid Molecular Dynamics Simulations

Models of the apo IR, IGF1R and IR/IGF1R hybrid receptor have been generated and simulations have been produced using the ARC3 high-performance computing cluster. Issues arising from periodic boundary conditions of the simulation box may be resolved to obtain data for RMSD/C_α, RMSF/C_α and other structural analyses pertinent to protein-protein interactions. Ligand-bound structures of each receptor type have been identified, however will require modelling and simulation on ARC3 prior to use in analysis. The ligand-bound structures can be used to compare against the apo-receptor models to determine changes at atomistic level of individual amino acid residues upon ligand binding. Docking simulations using published structures or use of structural techniques, such as cryo-EM, solution NMR or x-ray crystallography to obtain *de novo* structures of non-cognate ligand-receptor complexes would be required to generate molecular dynamics model templates, as no such structures have been published to-date.

16.2. Generation of a Novel IR/IGF1R Hybrid Homology Model for Molecular Dynamics Simulations

The IR/IGF1R hybrid receptor model has been based on the IR crystal structure and as a result, it is likely that this model will share a high degree of similarity with the IR homodimer model, upon binding of insulin or IGF-1. Design of a new homology model, based on the IGF1R crystal structure could be useful in isolating commonalities in binding interactions between the two

models which may be specifically attributable to the native IR/IGF1R hybrid receptor.

My colleague, Samuel Turvey has designed an IR/IGF1R hybrid homology model using the IGF1R as a template, for use in small molecule docking studies. This model would be suitable as a MD simulation template in design of an alternative IR/IGF1R model to compare with the IR-based IR/IGF1R hybrid receptor MD simulations.

16.3. Generation of IR/IGF1R-Insulin Glargine Model for Molecular Dynamics Simulations

Pierre-Eugene *et al.* identified insulin analogue, glargine bound to both IR/IGF1R hybrid receptor isoforms 7-9-fold higher affinity than native insulin (Pierre-Eugene et al., 2012). They also noted signalling *via* both PI3K/Akt and MAPK/Erk pathways was increased, likely mediated by IR/IGF1R hybrid receptors. Due to loss of insulin sensitivity and subsequently signalling *via* these receptors, use of insulin analogues such as glargine could be used as therapies to improve insulin sensitivity.

Understanding how glargine interfaces with IR/IGF1R hybrid receptors compared to insulin could isolate sequences of amino acids which are crucial to triggering signalling of insulin-mediated pathways. Elucidation of amino acids involved on both binding partners could be identified using molecular dynamics simulations. There are presently no structures of the IR-glargine complex, however there are three high-resolution crystal structures published of the glargine ligand (PDB ID; 4YID (Barba de la Rosa et al., 2014), PDB ID; 4YIF (Barba de la Rosa et al., 2014), PDB ID; 5VIZ (Reyes-Grajeda and Romero, 2017)). Similarly as described in section 16.1, docking of current

templates to this ligand or creation of *de novo* crystal structures could be employed to obtain a model of the IR-glargine complex for use in MD simulations.

16.4. Molecular Dynamics Simulations of eNOS-PYK2 Models

Structural information regarding the eNOS-PYK2 interaction interface is non-existent. It has been well-characterized that activation of PYK2 at its Y402 site, can phosphorylate an inhibitory Y657 residue on eNOS – diminishing its activity (Fisslthaler et al., 2008). Issues using biophysical techniques, such as SPR, were encountered when attempting to characterize this interaction, I hypothesized that molecular dynamics simulations might offer some insight into the surrounding residues involved in binding and any changes in conformation of eNOS upon binding of PYK2.

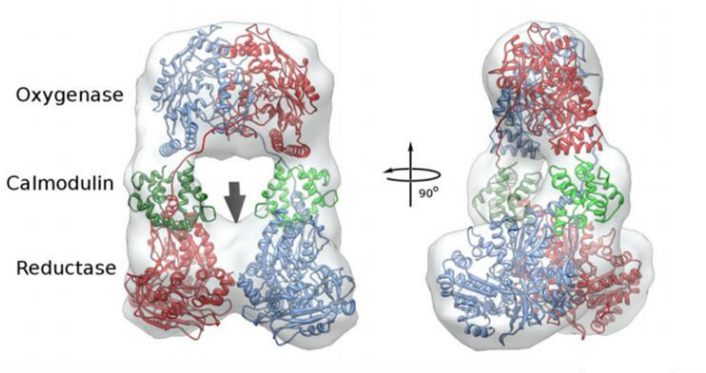

Figure 16-1: Reconstructed eNOS Homology Model

Fitting of reconstruction of eNOS dimer homology model, containing oxygenase (blue), calmodulin (green) and reductase (red) domains in anti-parallel symmetry. Image proprietary of (Volkmann et al., 2014).

Volkmann *et al.* designed an eNOS homology model, based on the crystal structures of the nNOS reductase domain (Garcin et al., 2004) and a CaM-bound iNOS reductase fragment (Xia et al., 2009) to compare the structural conformation both with- and without calmodulin (Figure 16-1) (Volkmann et al., 2014). These same reductase domain structures have been used in

molecular dynamics simulations of eNOS and Akt phosphorylation event, in a similar manner to the proposed simulations between eNOS and PYK2 (Devika et al., 2014). Devika *et al.* reported changes in hydrogen bonding interactions and salt-bridge formation, in addition to marginal structural differences between phosphorylated and phosphomimetic eNOS.

Protein	Source	Domain	PDB ID	Resolution (Å)	Electron Density Good:Poor:Missing (%)
eNOS	Bovine	Haem	1FOO	2.00	A-86:8:6 B-85:8:7
	Human	Oxygenase	**3NOS**	2.40	A-94:0:6 B-94:0:6
iNOS	Human	Reductase, Calmodulin	**3HR4**	2.50	Red A-86:0:14 Red C-83:3:14 CaM B-98:1:1 CaM D-98:1:1
nNOS	Murine	Reductase	**1TLL**	2.30	A-84:8:8 B-78:12:10
PYK2	Human	FERM	**4EKU**	3.25	87:1:11
	Human	Kinase	3FZO	2.20	90:5:5
	Human	Kinase	**3CC6**	1.60	88:8:4
	Human	FAT	3GM3	2.60	83:3:13
	Human	FAT	**4XEK**	1.79	90:9:1

Table 16-1: Published Structures of eNOS and PYK2 Domains

Collection of eNOS and PYK2 domain x-ray crystal structures, suitable for use as molecular dynamics templates. Preferred PDB IDs highlighted in bold. PDB ID: 1FOO (Li, H. et al., 2001), 3NOS (Fischmann et al., 1999), 3HR4 (Xia et al., 2009), 1TLL (Garcin et al., 2004), 4EKU (Savarimuthu et al., 2012), 3FZO (Han et al., 2009), 3CC6 (Busam et al., 2008), 3GM3 (Lulo et al., 2009), 4XEK (Vanarotti et al., 2016).

Oxygenase, calmodulin and reductase domains of eNOS and, FERM, kinase and FAT domains of PYK2 have been identified in preparation of full-length protein models for use in molecular dynamics simulations (Table 16-1). Docking of each domain to form a full-length structure could be modelled as described by Volkmann *et al.* using the HOMER homology modelling server (Volkmann et al., 2014). By employing the same method as Dr. Simmons and Devika *et al.*, the full-length eNOS and PYK2 constructs can then be docked

using HADDOCK before generating MD models using GROMACS as described in this thesis (section 2.9.1) (Devika et al., 2014).

16.5. Implementation in Screening of PPI Inhibitor Compounds

Once the aforementioned protein-protein interaction models have been generated, there would be the possibility to utilize these systems as a means to screen novel PPI inhibitors.

Molecular dynamics simulations offer crucial insights into protein dynamics upon drug binding, whereas techniques such as NMR, x-ray crystallography or static homology modelling may only provide information regarding a single, frozen structure (Durrant and McCammon, 2011; De Vivo et al., 2016). Molecular dynamics also offers the potential to discover novel druggable sites named cryptic binding sites, otherwise obscured when using NMR or EM techniques and, more advanced free-energy calculations.

In combination with information garnered from the initial protein-protein interaction studies between receptor and ligand, or enzyme and kinase, dynamic screening may prove important in the development of a novel series of compound inhibitors for these systems.

17. Concluding Remarks

Molecular dynamics simulations of IR/IGF1R hybrid receptors could provide insight into the mechanism of binding to insulin and IGF-1. Molecular dynamics models of homodimeric and hybrid receptor apo structures have been produced and, ligand complex structures have been identified for continuation of the project. The same procedure of developing models and simulations of hybrids could be extended to characterise the interaction between eNOS and PYK2. All of these models could be integrated into the process of small molecule modulator screening to elucidate protein dynamics of drug binding and identify a more target-selective candidate.

Project Conclusions

18. Project Conclusions

Characterisation of protein-protein interactions involved in disease can grant insight into their role within the larger system of the disease, and provide optimal means to control or reverse its effects. Two distinct protein-protein interactions were characterised utilizing a range of techniques, namely the dimerization of IR/IGF1R hybrid receptors and phosphorylation of eNOS by PYK2.

A virtual high throughput and *in vitro* screening process through BRET and immunoprecipitation methods, has been established to identify novel small molecule modulators of IR/IGF1R hybrid formation. Reduction in forming IR/IGF1R hybrid receptors could result in an increase in the formation of IR homodimeric receptors. This synchronous effect may further trigger the restoration of functional insulin signalling, resulting in increases in expression and activation of proteins downstream and subsequently augment NO bioavailability. In type-2 diabetes, endothelial cell function is reduced, angiogenesis and wound repair mechanisms are impaired compared to functionally, ‘healthy’ cells. Use of an IR/IGF1R specific modulator could also restore this functionality, in addition to providing cardioprotection from conditions such as atherosclerosis.

The current candidate presented in this thesis, HI-2, has been shown to effectively reduce IR/IGF1R hybrid formation in both HUVEC and SVEC, with further work required to determine its effect in ATEC. Signalling downstream of the IR is increased, however no favourable changes in mechanisms of angiogenesis or wound repair were observed at these concentrations of HI-2 in HUVEC. The physicochemical properties of HI-2 are not suitable for use *in*

vivo, however this robust screening process and collaboration from medicinal chemists could generate analogues of HI-2 with improved potency or identify new structures with improved potency and ADMET properties.

Characterisation of the eNOS-PYK2 interaction has provided many challenging due to its fleeting nature. It has been observed using *in silico* modelling, proximity ligation and co-immunoprecipitation techniques; the basis for further characterisation using biophysical methods has been established, however requiring further work to complete, at this time. Modulation of the interaction using an existing PYK2 inhibitor, PF-10e has not been successful. This molecule holds the ATP binding site in the DFG-out conformation, so may not be involved in the interaction between PYK2 and eNOS. A potential inhibitor of the eNOS-PYK2 PPI could be discovered through similar means as in the IR/IGF1R hybrid virtual screen. A genetic knock-down method has been established and could be utilized to probe the effects of modulation of this interaction and subsequent knock-on effects on signalling, NO bioavailability and mechanisms of angiogenesis, through further work. Design of an effective small molecule modulator could improve diabetic phenotype, restore functionality to the cells, in addition to acting in a cardioprotective manner against atherogenesis.

Molecular dynamics simulations of these protein-protein interactions could provide insight into ligand binding kinetics, but also be used in conjunction with docking experiments as a tool in identifying novel small molecule modulators. Models of the IR, IGF1R and IR/IGF1R have been produced and the basis to continue with liganded-structures and eNOS-PYK2 has been established for future work.

While some disruption was encountered due to Covid-19 lockdowns, a good foundation has been provided for future investigators to continue this work, and build upon these results. Small molecule modulation of protein-protein interactions involved in type-2 diabetes could provide much needed treatment for this disease, and its associated co-morbidities.

References & Appendices

19. References

Adams, T.E., Epa, V.C., Garrett, T.P.J. and Ward, C.W. 2000. Structure and function of the type 1 insulin-like growth factor receptor. *Cell. Mol. Life Sci.* **57**, pp.1050–1093.

Agin, A., Jeandidier, N., Gasser, F., Grucker, D. and Sapin, R. 2007. Glargine blood biotransformation: in vitro appraisal with human insulin immunoassay. *Diabetes Metab.* **33**(3), pp.205-212.

Alessi, D.R., Andjelkovic, M., Caudwell, B., Cron, P., Morrice, N., Cohen, P. and Hemmings, B.A. 1996. Mechanism of activation of protein kinase B by insulin and IGF-1. *EMBO J.* **15**(23), pp.6541-6551.

Alkaitis, M.S. and Crabtree, M.J. 2012. Recoupling the cardiac nitric oxide synthases: tetrahydrobiopterin synthesis and recycling. *Curr. Heart Fail. Rep.* **9**(3), pp.200-210.

Ammann, K.R., DeCook, K.J., Li, M. and Slepian, M.J. 2019. Migration versus proliferation as contributor to in vitro wound healing of vascular endothelial and smooth muscle cells. *Exp. Cell Res.* **376**(1), pp.58-66.

Andersen, A.S., Kjeldsen, T., Wiberg, F.C., Christensen, P.M., Rasmussen, J.S., Norris, K., Moller, K.B. and Moller, N.P.H. 1990. Changing the Insulin Receptor To Possess Insulin-like Growth Factor I Ligand Specificity. *Biochemistry.* **29**, pp.7363-7366.

Arkin, M.R., Tang, Y. and Wells, J.A. 2014. Small-molecule inhibitors of protein-protein interactions: progressing toward the reality. *Chem Biol.* **21**(9), pp.1102-1114.

Atkinson, M.A. 2016. Chapter 32 - Type 1 Diabetes Mellitus. In: Melmed, S., et al. eds. *Williams Textbook of Endocrinology (Thirteenth Edition).* Elsevier, pp.1451-1483.

Avogaro, A., Fadini, G.P., Gallo, A., Pagnin, E. and de Kreutzenberg, S. 2006. Endothelial dysfunction in type 2 diabetes mellitus. *Nutr. Metab. Cardiovasc. Dis.* **16 Suppl 1**, pp.S39-45.

Ayajiki, K., Kindermann, M., Hecker, M., Fleming, I. and Busse, R. 1996. Intracellular pH and Tyrosine Phosphorylation but Not Calcium Determine Shear Stress–Induced Nitric Oxide Production in Native Endothelial Cells. *Circ. Res.* **78**(5), pp.750-758.

Back, K. and Arnqvist, H.J. 2009. Changes in insulin and IGF-I receptor expression during differentiation of human preadipocytes. *Growth Horm. IGF Res.* **19**(2), pp.101-111.

Backer, J.M., Wjasow, C. and Zhang, Y. 1997. In vitro binding and phosphorylation of insulin receptor substrate 1 by the insulin receptor: Role of interactions mediated by the phosphotyrosine-binding domain and the pleckstrin-homology domain. *Eur. J. Biochem.* **245**, pp.91-96.

Baffi, T.R., Lorden, G., Wozniak, J.M., Feichtner, A., Yeung, W., Kornev, A.P., King, C.C., Del Rio, J.C., Limaye, A.J., Bogomolovas, J., Gould, C.M., Chen,

J., Kennedy, E.J., Kannan, N., Gonzalez, D.J., Stefan, E., Taylor, S.S. and Newton, A.C. 2021. mTORC2 controls the activity of PKC and Akt by phosphorylating a conserved TOR interaction motif. *Sci. Signal.* **14**(678).

Bailey, C.J. and Day, C. 2018. Treatment of type 2 diabetes: future approaches. *British Medical Bulletin.* **126**, pp.123-137.

Bailyes, E.M., Nave, B.T., Soos, M.A., Orr, S.R., Hayward, A.C. and Siddle, K. 1997. Insulin receptor/IGF-I receptor hybrids are widely distributed in mammalian tissues : quantification of individual receptor species by selective immunoprecipitation and immunoblotting. *Biochem. J.* **327**, pp.209–215.

Baker, E.N., Blundell, T.L., Cutfield, J.F., Cutfield, S.M., Dodson, E.J., Dodson, G.G., Hodgkin, D.M., Hubbard, R.E., Isaacs, N.W., Reynolds, C.D., Sakabe, K., Sakabe, N. and Vijayan, N.M. 1988. The structure of 2Zn pig insulin crystals at 1.5 A resolution. *Philos. Trans. R. Soc. Lond. B. Biol. Sci.* **319**(1195), pp.369-456.

Balakumar, P., Maung, U.K. and Jagadeesh, G. 2016. Prevalence and prevention of cardiovascular disease and diabetes mellitus. *Pharmacol. Res.* **113**(Pt A), pp.600-609.

Balligand, J.L., Feron, O. and Dessy, C. 2009. eNOS activation by physical forces: from short-term regulation of contraction to chronic remodeling of cardiovascular tissues. *Physiol. Rev.* **89**(2), pp.481-534.

Barba de la Rosa, A.P., Lara-Gonzalez, S., Montero-Moran, G.M., Escobedo-Moratilla, A. and Perez-Urizar, J.T. 2014. *Physicochemical and structural analysis of a biosimilar insulin glargine formulation and its reference*. Unpublished.

Bascos, N.A.D. and Landry, S.J. 2019. A History of Molecular Chaperone Structures in the Protein Data Bank. *Int. J. Mol. Sci.* **20**(24).

Baudin, B., Bruneel, A., Bosselut, N. and Vaubourdolle, M. 2007. A protocol for isolation and culture of human umbilical vein endothelial cells. *Nat. Protoc.* **2**(3), pp.481-485.

Bauer, P.M., Fulton, D., Boo, Y.C., Sorescu, G.P., Kemp, B.E., Jo, H. and Sessa, W.C. 2003. Compensatory phosphorylation and protein-protein interactions revealed by loss of function and gain of function mutants of multiple serine phosphorylation sites in endothelial nitric-oxide synthase. *J. Biol. Chem.* **278**(17), pp.14841-14849.

Bayne, M.L., Applebaum, J., Chicchi, G.G., Hayes, N.S., Green, B.G. and Cascieri, M.A. 1988. Structural analogs of human insulin-like growth factor I with reduced affinity for serum binding proteins and the type 2 insulin-like growth factor receptor. *J. Biol. Chem.* **263**(13), pp.6233-6239.

Bayne, M.L., Applebaum, J., Chicchi, G.G., Miller, R.E. and Cascieri, M.A. 1990. The roles of tyrosines 24, 31, and 60 in the high affinity binding of insulin-like growth factor-I to the type 1 insulin-like growth factor receptor. *J. Biol. Chem.* **265**(26), pp.15648-15652.

Bayne, M.L., Applebaum, J., Underwood, D., Chicchi, G.G., Green, B.G., Hayes, N.S. and Cascieri, M.A. 1989. The C Region of Human Insulin-like

Growth Factor (IGF) I Is Required for High Affinity Binding to the Type 1 IGF Receptor. *J. Biol. Chem.* **264**(19), pp.11004-11008.

Belfiore, A., Frasca, F., Pandini, G., Sciacca, L. and Vigneri, R. 2009. Insulin receptor isoforms and insulin receptor/insulin-like growth factor receptor hybrids in physiology and disease. *Endocr. Rev.* **30**(6), pp.586-623.

Belfiore, A., Malaguarnera, R., Vella, V., Lawrence, M.C., Sciacca, L., Frasca, F., Morrione, A. and Vigneri, R. 2017. Insulin Receptor Isoforms in Physiology and Disease: An Updated View. *Endocr. Rev.* **38**(5), pp.379-431.

Belfiore, A., Pandini, G., Vella, V., Squatrito, S. and Vigneri, R. 1999. Insulin/IGF-I hybrid receptors play a major role in IGF-I signaling in thyroid cancer. *Biochimie.* **81**, p403−407.

Benyoucef, S., Surinya, K.H., Hadaschik, D. and Siddle, K. 2007. Characterization of insulin/IGF hybrid receptors: contributions of the insulin receptor L2 and Fn1 domains and the alternatively spliced exon 11 sequence to ligand binding and receptor activation. *Biochem. J.* **403**(3), pp.603-613.

Berrow, N.S., Alderton, D., Sainsbury, S., Nettleship, J., Assenberg, R., Rahman, N., Stuart, D.I. and Owens, R.J. 2007. A versatile ligation-independent cloning method suitable for high-throughput expression screening applications. *Nucleic Acids Res.* **35**(6), pe45.

Bertherat, J., Bluet-Pajot, M.T. and Epelbaum, J. 1995. Neuroendocrine regulation of growth hormone. *Eur. J. Endocrinol.* **132**, pp.12-24.

Bhardwaj, R., Page, C.P., May, G.R. and Moore, P.K. 1988. Endothelium-derived relaxing factor inhibits platelet aggregation in human whole blood in vitro and in the rat in vivo. *Eur. J. Pharmacol.* **157**, pp.83-91.

Bhattacharya, S.K., Aspnes, G.E., Bagley, S.W., Boehm, M., Brosius, A.D., Buckbinder, L., Chang, J.S., Dibrino, J., Eng, H., Frederick, K.S., Griffith, D.A., Griffor, M.C., Guimaraes, C.R., Guzman-Perez, A., Han, S., Kalgutkar, A.S., Klug-McLeod, J., Garcia-Irizarry, C., Li, J., Lippa, B., Price, D.A., Southers, J.A., Walker, D.P., Wei, L., Xiao, J., Zawistoski, M.P. and Zhao, X. 2012. Identification of novel series of pyrazole and indole-urea based DFG-out PYK2 inhibitors. *Bioorg. Med. Chem. Lett.* **22**(24), pp.7523-7529.

Bhaumick, B., Bala, R.M. and Hollenburg, M.D. 1981. Somatomedin receptor of human placenta: Solubilization, photolabeling, partial purification, and comparison with insulin receptor. *PNAS.* **78**(7), pp.4279-4283.

Bibli, S.I., Szabo, C., Chatzianastasiou, A., Luck, B., Zukunft, S., Fleming, I. and Papapetropoulos, A. 2017a. Hydrogen Sulfide Preserves Endothelial Nitric Oxide Synthase Function by Inhibiting Proline-Rich Kinase 2: Implications for Cardiomyocyte Survival and Cardioprotection. *Mol. Pharmacol.* **92**(6), pp.718-730.

Bibli, S.I., Zhou, Z., Zukunft, S., Fisslthaler, B., Andreadou, I., Szabo, C., Brouckaert, P., Fleming, I. and Papapetropoulos, A. 2017b. Tyrosine phosphorylation of eNOS regulates myocardial survival after an ischaemic insult: role of PYK2. *Cardiovasc. Res.* **113**(8), pp.926-937.

Bird, L.E. 2011. High throughput construction and small scale expression screening of multi-tag vectors in Escherichia coli. *Methods.* **55**(1), pp.29-37.

Blanquart, C., Boute, N., Lacasa, D. and Issad, T. 2005. Monitoring the activation state of the insulin-like growth factor-1 receptor and its interaction with protein tyrosine phosphatase 1B using bioluminescence resonance energy transfer. *Mol. Pharmacol.* **68**(3), pp.885-894.

Blundell, T., Dodson, G.G., Hodgkin, D. and Mercola, D. 1972. Insulin: The structure in the crystal and its reflection in chemistry and biology. *Adv. Protein Chem.* **26**, pp.279-402.

Blundell, T.L., Bedarkar, S., Rinderknecht, E. and Humbel, R.E. 1978. Insulin-like growth factor: A model for tertiary structure accounting for immunoreactivity and receptor binding. *PNAS.* **75**(1), pp.180-184.

Blyth, A.J., Kirk, N.S. and Forbes, B.E. 2020. Understanding IGF-II Action through Insights into Receptor Binding and Activation. *Cells.* **9**(10).

Bommel, H.M., Reif, A., Frohlich, L.G., Frey, A., Hofmann, H., Marecak, D.M., Groehn, V., Kotsonis, P., La, M., Koster, S., Meinecke, M., Bernhardt, M., Weeger, M., Ghisla, S., Prestwich, G.D., Pfleiderer, W. and Schmidt, H.H. 1998. Anti-pterins as tools to characterize the function of tetrahydrobiopterin in NO synthase. *J. Biol. Chem.* **273**(50), pp.33142-33149.

Boo, Y.C., Hwang, J., Sykes, M., Michell, B.J., Kemp, B.E., Lum, H. and Jo, H. 2002a. Shear stress stimulates phosphorylation of eNOS at Ser635 by a protein kinase A-dependent mechanism. *Am. J. Physiol. Heart Circ. Physiol.* **283**, pp.H1819-H1828.

Boo, Y.C., Sorescu, G., Boyd, N., Shiojima, I., Walsh, K., Du, J. and Jo, H. 2002b. Shear stress stimulates phosphorylation of endothelial nitric-oxide synthase at Ser1179 by Akt-independent mechanisms: role of protein kinase A. *J. Biol. Chem.* **277**(5), pp.3388-3396.

Boucher, J., Kleinridders, A. and Kahn, C.R. 2014. Insulin receptor signaling in normal and insulin-resistant states. *Cold Spring Harb. Perspect. Biol.* **6**(1).

Brooks, B.R., Brooks, C.L., 3rd, Mackerell, A.D., Jr., Nilsson, L., Petrella, R.J., Roux, B., Won, Y., Archontis, G., Bartels, C., Boresch, S., Caflisch, A., Caves, L., Cui, Q., Dinner, A.R., Feig, M., Fischer, S., Gao, J., Hodoscek, M., Im, W., Kuczera, K., Lazaridis, T., Ma, J., Ovchinnikov, V., Paci, E., Pastor, R.W., Post, C.B., Pu, J.Z., Schaefer, M., Tidor, B., Venable, R.M., Woodcock, H.L., Wu, X., Yang, W., York, D.M. and Karplus, M. 2009. CHARMM: the biomolecular simulation program. *J. Comput. Chem.* **30**(10), pp.1545-1614.

Buchwalow, I.B., Minin, E.A., Samoilova, V.E., Boecker, W., Wellner, M., Schmitz, W., Neumann, J. and Punkt, K. 2005. Compartmentalization of NO signaling cascade in skeletal muscles. *Biochem. Biophys. Res. Commun.* **330**(2), pp.615-621.

Burke-Gaffney, A., Brooks, A.V.S. and Bogle, R.G. 2002. Regulation of chemokine expression in atherosclerosis. *Vasc. Pharmacol.* **38**, pp.283-292.

Busam, R.D., Lehtio, L., Karlberg, T., Arrowsmith, C.H., Bountra, C., Collins, R., Dahlgren, L.G., Edwards, A.M., Flodin, S., Flores, A., Graslund, S.,

Hammarstrom, M., Helleday, T., Herman, M.D., Johansson, A., Johansson, I., Kallas, A., Kotenyova, T., Moche, A.G., Tresaugues, L., Van den Berg, S., Weigelt, J., Welin, M. and Berglund, H. 2008. *Structure of Protein Tyrosine Kinase 2 Beta (PTK2B) Kinase domain*. Unpublished.

Busse, R. and Mulsch, A. 1990. Calcium-dependent nitric oxide synthesis in endothelial cytosol is mediated by calmodulin. *FEBS Lett.* **265**(1,2), pp.133-136.

Cabail, M.Z., Li, S., Lemmon, E., Bowen, M.E., Hubbard, S.R. and Miller, W.T. 2015. The insulin and IGF1 receptor kinase domains are functional dimers in the activated state. *Nat. Commun.* **6**, p6406.

Carmeliet, P. 2000. Mechanisms of angiogenesis and arteriogenesis. *Nat. Med.* **6**(3), pp.389-395.

Carmeliet, P. 2003. Angiogenesis in health and disease. *Nat. Med.* **9**(6), pp.653-660.

Carmeliet, P. 2005. Angiogenesis in life, disease and medicine. *Nature.* **438**(7070), pp.932-936.

Carpenter, M.C. and Wilcox, D.E. 2014. Thermodynamics of formation of the insulin hexamer: metal-stabilized proton-coupled assembly of quaternary structure. *Biochemistry.* **53**(8), pp.1296-1301.

Cartwright, J.E., Johnstone, A.P. and Whitley, G.S. 2000. Endogenously produced nitric oxide inhibits endothelial cell growth as demonstrated using novel antisense cell lines. *Br. J. Pharamcol.* **131**, p131 ± 137.

Cascieri, M.A., Chicchi, G.G., Applebaum, J., Green, B.G., Hayes, N.S. and Bayne, M.L. 1989a. Structural Analogs of Human Insulin-like Growth Factor (IGF) I with Altered Affinity for Type 2 IGF Receptors. *J. Biol. Chem.* **264**(4), pp.2199-2202.

Cascieri, M.A., Chicchi, G.G., Applebaum, J., Hayes, N.S., Green, B.G. and Bayne, M.L. 1988a. Mutants of Human Insulin-like Growth Factor I with Reduced Affinity for the Type 1

Insulin-like Growth Factor Receptor. *Biochemistry.* **27**, pp.3229-3233.

Cascieri, M.A., Hayes, N.S. and Bayne, M.L. 1989b. Characterization of the Increased Biological Potency in BALB/C 313 Cells of Two Analogs of Human lnsulinlike Growth Factor 1 Which Have Reduced Affinity for the 28 K CellDerived Binding Protein. *J. Cell Physiol.* **139**, pp.181-188.

Cascieri, M.A., Hayes, N.S., Kelder, B., Kopchick, J.J., Chicchi, G.G., Slater, E.E. and Bayne, M.L. 1988b. Inability of a Mouse Cell Line Transformed to Produce Biologically Active Recombinant Human Insulin-Like Growth Factor I (IGF-I) to Respond to Exogenously Added IGF-I. *Endocrinology.* **122**(4), pp.1314-1320.

Chambliss, K.L. and Shaul, P.W. 2002. Estrogen modulation of endothelial nitric oxide synthase. *Endocr. Rev.* **23**(5), pp.665-686.

Chan, S.J. and Steiner, D.F. 2000. Insulin Through the Ages: Phylogeny of a Growth Promoting and Metabolic Regulatory Hormone. *Amer. Zool.* **40**, pp.213–222.

Chan, Y., Fish, J.E., D'Abreo, C., Lin, S., Robb, G.B., Teichert, A.M., Karantzoulis-Fegaras, F., Keightley, A., Steer, B.M. and Marsden, P.A. 2004. The cell-specific expression of endothelial nitric-oxide synthase: a role for DNA methylation. *J. Biol. Chem.* **279**(33), pp.35087-35100.

Chen, H.X. and Sharon, E. 2013. IGF1R as an anti-cancer target-trials and tribulations. *Chin. J. Cancer.* **32**(5), pp.242-252.

Chernausek, S.D., Jacobs, S. and van Wyk, J.J. 1981. Structural Similarities between Human Receptors for Somatomedin C and Insulin: Analysis by Affinity Labeling. *Biochemistry.* **20**, pp.7345-7350.

Chiefari, E., Tanyolac, S., Paonessa, F., Pullinger, C.R., Capula, C., Iiritano, S., Mazza, T., Forlin, M., Fusco, A., Durlach, V., Durlach, A., Malloy, M.J., Kane, J.P., Goldfine, I.D. and Brunetti, A. 2011. Functional Variants of the HMGA1 Gene and Type 2 Diabetes Mellitus. *JAMA.* **305**(9), pp.903-912.

Chisalita, S.I. and Arnqvist, H.J. 2005. Expression and function of receptors for insulin-like growth factor-I and insulin in human coronary artery smooth muscle cells. *Diabetologia.* **48**(10), pp.2155-2161.

Chiti, F. and Dobson, C.M. 2006. Protein misfolding, functional amyloid, and human disease. *Annu. Rev. Biochem.* **75**, pp.333-366.

Chitnis, M.M., Yuen, J.S.P., Protheroe, A.S., Pollak, M. and Macaulay, V.M. 2008. The Type 1 Insulin-Like Growth Factor Receptor Pathway. *Clin. Cancer Res.* **14**(20), pp.6364-6370.

Cho, H.J., Xie, Q., Calaycay, J., Mumford, R.A., Swiderek, K.M., Lee, T.D. and Nathan, C. 1992. Calmodullin Is a Subunit of Nitric Oxide Synthase from Macrophages. *J. Exp. Med.* **176**, pp.599-604.

Chothia, C., Lesk, A.M., Dodson, G.G. and Hodgkin, D.C. 1983. Transmission of conformational change in insulin. *Nature.* **307**, pp.500-505.

Christoffersen, C.T., Bornfeldt, K.E., Rotella, C.M., Gonzales, N., Vissing, H., Shymko, R.M., ten Hoeve, J., Groffen, J., Heisterkamp, N. and De Meyts, P. 1994. Negative cooperativity in the insulin-like growth factor-I receptor and a chimeric IGF-I/insulin receptor. *Endocrinology.* **135**(1), pp.472-475.

Collaboration, T.E.R.F. 2010. Diabetes mellitus, fasting blood glucose concentration, and risk of vascular disease: a collaborative meta-analysis of 102 prospective studies. *Lancet.* **375**, pp.2215–2222.

Conlon, J.M. 2001. Evolution of the insulin molecule: insights into structure-activity and phylogenetic relationships. *Peptides.* **22**, pp.1183–1193.

UniProt: the universal protein knowledgebase in 2021. 2021. [Online database].

Cooke, J.P. and Losordo, D.W. 2002. Nitric oxide and angiogenesis. *Circulation.* **105**(18), pp.2133-2135.

Croll, T.I., Smith, B.J., Margetts, M.B., Whittaker, J., Weiss, M.A., Ward, C.W. and Lawrence, M.C. 2016. Higher-Resolution Structure of the Human Insulin Receptor Ectodomain: Multi-Modal Inclusion of the Insert Domain. *Structure.* **24**(3), pp.469-476.

Danylovych, G.V., Bohach, T.V. and Danylovych, Y.V. 2018. The biosynthesis of nitric oxide from L-arginine. Nitric oxide formation features and its functional role in mitochondria. *Ukr. Biochem. J.* **90**(1), pp.3-24.

Davda, R.K., Chandler, L.J. and Guzman, N.J. 1994. Protein kinase C modulates receptor-independent activation of endothelial nitric oxide synthase. *Eur. J. Pharmacol.* **266**, pp.237-244.

de Assis, M.C., Plotkowski, M.C., Fierro, I.M., Barja-Fidalgo, C. and de Frietas, M.S. 2002. Expression of inducible nitric oxide synthase in human umbilical vein endothelial cells during primary culture. *Nitric Oxide.* **7**, pp.254-261.

De Meyts, P. 1994. The structural basis of insulin and insulin-like growth factor-I receptor binding and negative co-operativity, and its relevance to mitogenic versus metabolic signalling. *Diabetologia.* **37**, pp.S135-S148.

De Meyts, P. 2004. Insulin and its receptor: structure, function and evolution. *Bioessays.* **26**(12), pp.1351-1362.

De Meyts, P. 2016. The Insulin Receptor and Its Signal Transduction Network. In: Feingold, K.R., et al. eds. *Endotext.* South Dartmouth, MA: MD.text.com, Inc.

De Meyts, P., Bainco, A.R. and Roth, J. 1976. Site-site interactions among insulin receptors. Characterization of the negative cooperativity. *J. Biol. Chem.* **251**(7), pp.1877-1888.

De Meyts, P., Obberghen, E.V. and Roth, J. 1978. Mapping of the residues responsible for the negative cooperativity of the receptor-binding region of insulin. *Nature.* **273**, pp.504-509.

De Meyts, P., Roth, J., Neville, D.M.J., Gavin, J.R.I. and Lesniak, M.A. 1973. INSULIN INTERACTIONS WITH ITS RECEPTORS: EXPERIMENTAL EVIDENCE FOR NEGATIVE COOPERATIVITY. *Biochem. Biophys. Res. Commun.* **55**(1), pp.154-161.

Insulin and IGF-I Receptor Structure and Binding Mechanism. 2013. [Online database]. Austin, TX: Landes Bioscience.

De Meyts, P. and Shymko, R.M. 2000. Timing-dependent modulation of insulin mitogenic versus metabolic signalling. *Novartis Found. Symp.* **227**, pp.46-57.

De Meyts, P. and Whittaker, J. 2002. Structural biology of insulin and IGF1 receptors: implications for drug design. *Nat. Rev. Drug Discov.* **1**(10), pp.769-783.

de Pins, B., Mendes, T., Giralt, A. and Girault, J.A. 2021. The Non-receptor Tyrosine Kinase Pyk2 in Brain Function and Neurological and Psychiatric Diseases. *Front. Synaptic Neurosci.* **13**, p749001.

De Vivo, M., Masetti, M., Bottegoni, G. and Cavalli, A. 2016. Role of Molecular Dynamics and Related Methods in Drug Discovery. *J. Med. Chem.* **59**(9), pp.4035-4061.

Denley, A., Cosgrove, L.J., Booker, G.W., Wallace, J.C. and Forbes, B.E. 2005. Molecular interactions of the IGF system. *Cytokine Growth Factor Rev.* **16**(4-5), pp.421-439.

Denley, A., Wallace, J.C., Cosgrove, L.J. and Forbes, B.E. 2003. The Insulin Receptor Isoform Exon 11- (IR-A) in Cancer and Other Diseases: A Review. *Horm. Metab. Res.* **35**(11/12), pp.778-785.

Devika, N.T., Amresh, P., Hassan, M.I. and Ali, B.M. 2014. Molecular modeling and simulation of the human eNOS reductase domain, an enzyme involved in the release of vascular nitric oxide. *J. Mol. Model.* **20**(10), p2470.

Dhananjayan, R., Koundinya, K.S., Malati, T. and Kutala, V.K. 2016. Endothelial Dysfunction in Type 2 Diabetes Mellitus. *Indian J. Clin. Biochem.* **31**(4), pp.372-379.

DiMarchi, R.D., Mayer, J.P., Fan, L., Long, H., Sundell, K., Slieker, L.J., Shaw, W.N., Howey, D., Frank, B.H., Shields, J.E. and Chance, R.E. 1992. *Peptides: Chemistry and Biology.* Leiden, Netherlands: Esco Science Publishers.

Dimmeler, S., Dernbach, E. and Zeiher, A.M. 2000. Phosphorylation of the endothelial nitric oxide synthase at Ser-1177 is required for VEGF-induced endothelial cell migration. *FEBS Lett.* **477**, pp.258-262.

Dimmeler, S., Fleming, I., Fisslthaler, B., Hermann, C., Busse, R. and Zeiher, A.M. 1999. Activation of nitric oxide synthase in endothelial cells by Akt-dependent phosphorylation. *Nature.* **399**, pp.601-605.

Dominguez, C., Boelens, R. and Bonvin, A.M.J.J. 2003. HADDOCK: A Protein-Protein Docking Approach Based on

Biochemical or Biophysical Information. *J. Am. Chem. Soc.* **125**, pp.1731-1737.

Douzi, B. 2017. Protein-Protein Interactions: Surface Plasmon Resonance. In: Journet, L. and Cascales, E. eds. *Bacterial Protein Secretion Systems. Methods in Molecular Biology.* New York, NY: Humana Press.

Drejer, K. 1992. The bioactivity of insulin analogues from in vitro receptor binding to in vivo glucose uptake. *Diabetes Metab. Rev.* **8**(3), pp.259-285.

Du, Y.H. and Chen, A.F. 2009. A new role for caveolin-1: regulation of guanosine triphosphate cyclohydrolase I and tetrahydrobiopterin in endothelial cells. *Hypertension.* **53**(2), pp.115-117.

Ducimetiere, P., Eschwege, E., Papoz, L., Richard, J.L., Claude, J.R. and Rosselin, G. 1980. Relationship of Plasma Insulin Levels to the Incidence of Myocardial Infarction and Coronary Heart Disease Mortality in a Middle-aged Population. *Diabetologia.* **19**, pp.205-210.

Duncan, E.R., Crossey, P.A., Walker, S., Anilkumar, N., Poston, L., Douglas, G., Ezzat, V.A., Wheatcroft, S.B., Shah, A.M. and Kearney, M.T. 2008. Effect

of endothelium-specific insulin resistance on endothelial function in vivo. *Diabetes.* **57**(12), pp.3307-3314.

Durrant, J.D. and McCammon, J.A. 2011. Molecular dynamics simulations and drug discovery. *BMC Biology.* **9**(71), pp.1-9.

Ebina, Y., Ellis, L., Jarnagin, K., Edery, M., Graf, L., Clauser, E., Ou, J., Massiarz, F., Kan, Y.W., Goldfine, I.D., Roth, R.A. and Rutter, W.J. 1985. The human insulin receptor cDNA: the structural basis for hormone-activated transmembrane signalling. *Cell.* **40**, pp.747-758.

Ermert, M., Ruppert, C., Gunther, A., Duncker, H.-R., Seeger, W. and Ermert, L. 2002. Cell-Specific Nitric Oxide Synthase-Isoenzyme Expression and Regulation in Response to Endotoxin in Intact Rat Lungs. *Lab Invest.* **82**(4), pp.425-441.

Esposito, D.L., Li, Y., Cama, A. and Quon, M.J. 2001. Tyr612 and Tyr632 in Human Insulin Receptor Substrate-1 Are Important for Full Activation of Insulin-Stimulated Phosphatidylinositol 3-Kinase Activity and Translocation of GLUT4 in Adipose Cells. *Endocrinology.* **142**(7), pp.2833–2840.

Etter, E.F., Eto, M., Wardle, R.L., Brautigan, D.L. and Murphy, R.A. 2001. Activation of myosin light chain phosphatase in intact arterial smooth muscle during nitric oxide-induced relaxation. *J. Biol. Chem.* **276**(37), pp.34681-34685.

Federici, M., Porzio, O., Lauro, D., Borboni, P., Giovannone, B., Zucaro, L., Hribal, M.L. and Sesti, G. 1998. Increased Abundance of Insulin/Insulin-Like Growth Factor-I Hybrid Receptors in Skeletal Muscle of Obese Subjects Is Correlated with In Vivo Insulin Sensitivity. *Mol. Cell Endocrinol.* **83**(3), pp.2911–2915.

Federici, M., Porzio, O., Zucaro, L., Fusco, A., Borboni, P., Lauro, D. and Sesti, G. 1997a. Distribution of insulin/insulin-like growth factor-I hybrid receptors in human tissues. *Mol. Cell Endocrinol.* **129**, pp.121-126.

Federici, M., Porzio, O., Zucaro, L., Giovannone, B., Borboni, P., Marini, M.A., Lauro, D. and Sesti, G. 1997b. Increased abundance of insulin/IGF-I hybrid receptors in adipose tissue from NIDDM patients. *Mol. Cell Endocrinol.* **135**, pp.41–47.

Federici, M., Zucaro, L., Porzio, O., Massoud, R., Borboni, P., Lauro, D. and Sesti, G. 1996. Increased Expression of Insulin/Insulin-like Growth Factor-I Hybrid Receptors in Skeletal Muscle of Noninsulin-dependent Diabetes Mellitus Subjects. *J. Clin. Invest.* **98**, pp.2887–2893.

Fernandez, A.M., Kim, J.K., Yakar, S., Dupont, J., Hernandez-Sanchez, C., Castle, A.L., Filmore, J., Shulman, G.I. and Le Roith, D. 2001. Functional inactivation of the IGF-I and insulin receptors in skeletal muscle causes type 2 diabetes. *Genes Dev.* **15**(15), pp.1926-1934.

Ferrara, N., Houck, K., Jakeman, L. and Leung, D.W. 1992. Molecular and Biological Properties of the Vascular Endothelial Growth Factor Family of Proteins. *Endocr. Rev.* **13**(1), pp.18-32.

Firth, S.M. and Baxter, R.C. 2002. Cellular Actions of the Insulin-Like Growth Factor Binding Proteins. *Endocr. Rev.* **23**(6), pp.824-854.

Fischmann, T.O., Hruza, A., Niu, X.D., Fossetta, J.D., Lunn, C.A., Dolphin, E., Prongay, A.J., Reichert, P., Lundell, D.J., Narula, S.K. and Weber, P.C. 1999. Structural characterization of nitric oxide synthase isoforms reveals striking active-site conservation. *Nat. Struct. Biol.* **6**(3), pp.233-242.

Fisher, E.A. 2016. Regression of Atherosclerosis: The Journey From the Liver to the Plaque and Back. *Arterioscler. Thromb. Vasc. Biol.* **36**(2), pp.226-235.

Fisslthaler, B., Loot, A.E., Mohamed, A., Busse, R. and Fleming, I. 2008. Inhibition of endothelial nitric oxide synthase activity by proline-rich tyrosine kinase 2 in response to fluid shear stress and insulin. *Circ. Res.* **102**(12), pp.1520-1528.

Fleming, I. 2010. Molecular mechanisms underlying the activation of eNOS. *Pflugers Arch.* **459**(6), pp.793-806.

Fleming, I., Fisslthaler, B., Dimmeler, S., Kemp, B.E. and Busse, R. 2001. Phosphorylation of Thr495 Regulates Ca2+/Calmodulin-Dependent Endothelial Nitric Oxide Synthase Activity. *Circ. Res.* **88**(11), pp.e68-e75.

Forstermann, U. and Munzel, T. 2006. Endothelial nitric oxide synthase in vascular disease: from marvel to menace. *Circulation.* **113**(13), pp.1708-1714.

Forstermann, U. and Sessa, W.C. 2012. Nitric oxide synthases: regulation and function. *Eur. Heart J.* **33**(7), pp.829-837, 837a-837d.

Fowden, A.L. and Forhead, A.J. 2013. Endocrine Interactions in the Control of Fetal Growth. In: Bhatia, J., et al. eds. *Maternal and Child Nutrition: The First 1,000 Days.* Basel: Nestle Nutr Inst Workshop Ser., pp.91-102.

Frasca, F., Pandini, G., Scalia, P., Sciacca, L., Mineo, R., Constantino, A., Goldfine, I.D., Belfiore, A. and Vigneri, R. 1999. Insulin Receptor Isoform A, a Newly Recognized, High-Affinity Insulin-Like Growth Factor II Receptor in Fetal and Cancer Cells. *Mol. Cell Biol.* **19**(5), pp.3278–3288.

Freedman, J.E. and Loscalzo, J. 2003. Nitric oxide and its relationship to thrombotic disorders. *J. Thromb. Haemost.* **1**, pp.1183-1188.

Fu, Y. and Finney, N.S. 2018. Small-molecule fluorescent probes and their design. *RSC Advances.* **8**(51), pp.29051-29061.

Fulton, D., Church, J.E., Ruan, L., Li, C., Sood, S.G., Kemp, B.E., Jennings, I.G. and Venema, R.C. 2005. Src kinase activates endothelial nitric-oxide synthase by phosphorylating Tyr-83. *J. Biol. Chem.* **280**(43), pp.35943-35952.

Fulzele, K., DiGirolamo, D.J., Liu, Z., Xu, J., Messina, J.L. and Clemens, T.L. 2007. Disruption of the insulin-like growth factor type 1 receptor in osteoblasts enhances insulin signaling and action. *J. Biol. Chem.* **282**(35), pp.25649-25658.

Furchgott, R.F. 1984. The Role of Endothelium in the Responses of Vascular Smooth Muscle to Drugs. *Ann. Rev. Pharmacol. Toxicol.* **24**(1), pp.175-197.

Furchgott, R.F. 1988. *Studies on relaxation of rabbit aorta by sodium nitrite: the basis for the proposal that the acid-activatable inhibitory factor from retractor penis is inorganic nitrite and the endothelium-derived relaxing factor is nitric oxide.* Raven Press.

Furchgott, R.F. 1989. Endothelium-Dependent Vasodilation and the Nature of the Endothelium-Derived Relaxing Factor. In: Catravas, J.D., et al. eds. *Vascular Endothelium.* Boston, MA: Springer.

Furchgott, R.F. 1990. Studies on endothelium-dependent vasodilation and the endothelium-derived relaxing factor. *Acta Physiol. Scand.* **139**, pp.257-270.

Furchgott, R.F. and Zawadzki, J.V. 1980. The obligatory role of endothelial cells in the relaxation of arterial smooth muscle by acetylcholine. *Nature.* **288**, pp.373-376.

Furman, B.L. 2017. Glargine Insulin. *Reference Module in Biomedical Sciences.* Elsevier.

Gao, F., Lucke-Wold, B.P., Li, X., Logsdon, A.F., Xu, L.C., Xu, S., LaPenna, K.B., Wang, H., Talukder, M.A.H., Siedlecki, C.A., Huber, J.D., Rosen, C.L. and He, P. 2017. Reduction of Endothelial Nitric Oxide Increases the Adhesiveness of Constitutive Endothelial Membrane ICAM-1 through Src-Mediated Phosphorylation. *Front. Physiol.* **8**, p1124.

Garcia-Cardena, G., Oh, P., Liu, J., Schnitzer, J.E. and Sessa, W.C. 1996. Targeting of nitric oxide synthase to endothelial cell caveolae via palmitoylation: Implications for nitric oxide signaling. *Proc. Natl. Acad. Sci.* **93**, pp.6448-6453.

Garcia-Fernandez, M., Castilla-Cortazar, I., Diaz-Sanchez, M., Caballero, F.D., Castilla, A., Casares, A.D., Varela-Nieto, I. and Gonzalez-Baron, S. 2003. Effect of IGF-I on total serum antioxidant status in cirrhotic rats. *J. Physiol. Biochem.* **59**(2), pp.145-146.

Garcia-Fernandez, M., Castilla-Cortazar, I., Diaz-Sanchez, M., Navarro, I., Puche, J.E., Castilla, A., Casares, A.D., Clavijo, E. and Gonzalez-Baron, S. 2005. Antioxidant effects of insulin-like growth factor-I (IGF-I) in rats with advanced liver cirrhosis. *BMC Gastroenterol.* **5**, p7.

Garcia-Fernandez, M., Delgado, G., Puche, J.E., Gonzalez-Baron, S. and Castilla Cortazar, I. 2008. Low doses of insulin-like growth factor I improve insulin resistance, lipid metabolism, and oxidative damage in aging rats. *Endocrinology.* **149**(5), pp.2433-2442.

Garcin, E.D., Bruns, C.M., Lloyd, S.J., Hosfield, D.J., Tiso, M., Gachhui, R., Stuehr, D.J., Tainer, J.A. and Getzoff, E.D. 2004. Structural basis for isozyme-specific regulation of electron transfer in nitric-oxide synthase. *J. Biol. Chem.* **279**(36), pp.37918-37927.

Garg, U.C. and Hassid, A. 1989. Nitric Oxide-generating Vasodilators and 8-Bromo-Cyclic Guanosine Monophosphate Inhibit Mitogenesis and Proliferation of Cultured Rat Vascular Smooth Muscle Cells. *J. Clin. Invest.* **83**, pp.1774-1777.

Garre, S., Senevirathne, C. and Pflum, M.K. 2014. A comparative study of ATP analogs for phosphorylation-dependent kinase-substrate crosslinking. *Bioorg. Med. Chem.* **22**(5), pp.1620-1625.

Garrett, T.P.J., McKern, N.M., Lou, M.Z., Frenkel, M.J., Bentley, J.D., Lovrecz, G.O., Elleman, T.C., Cosgrove, L.J. and Ward, C.W. 1998. Crystal structure of the first three domains of the type-1 insulin-like growth factor receptor. *Nature.* **394**, pp.395-399.

Gaunt, H.J. 2018. *Hannah Jane Gaunt Thesis*. PhD thesis, University of Leeds.

VEGF and Endothelial Guidance in Angiogenic Sprouting. 2000-2013. [Online database]. Austin, TX: Landes Bioscience.

Giabicani, E., Chantot-Bastaraud, S., Bonnard, A., Rachid, M., Whalen, S., Netchine, I. and Brioude, F. 2019. Roles of Type 1 Insulin-Like Growth Factor (IGF) Receptor and IGF-II in Growth Regulation: Evidence From a Patient Carrying Both an 11p Paternal Duplication and 15q Deletion. *Front. Endocrinol.* **10**, p263.

Gielis, J.F., Lin, J.Y., Wingler, K., Van Schil, P.E., Schmidt, H.H. and Moens, A.L. 2011. Pathogenetic role of eNOS uncoupling in cardiopulmonary disorders. *Free Radic. Biol. Med.* **50**(7), pp.765-776.

Gill, R., Wallach, B., Verma, C., Urso, B., De Wolf, E., Grotzinger, J., Murray-Rust, J., Pitts, J., Wollmer, A., De Meyts, P. and Wood, S. 1996. Engineering the C-region of human insulin-like growth factor-1: implications for receptor binding. *Protein Eng.* **9**(11), pp.1011-1019.

Ginsberg, B.H., Kahn, C.R. and Roth, J. 1976. THE INSULIN RECEPTOR OF THE TURKEY ERYTHROCYTE CHARACTERIZATION OF THE MEMBRANE-BOUND RECEPTOR. *Biochim. Biophys. Acta.* **443**, pp.227-242.

Girnita, L., Worrall, C., Takahashi, S., Seregard, S. and Girnita, A. 2014. Something old, something new and something borrowed: emerging paradigm of insulin-like growth factor type 1 receptor (IGF-1R) signaling regulation. *Cell Mol. Life Sci.* **71**(13), pp.2403-2427.

Gkourogianni, A., Andrade, A.C., Jonsson, B.A., Segerlund, E., Werner-Sperker, A., Horemuzova, E., Dahlgren, J., Burstedt, M. and Nilsson, O. 2020. Pre- and postnatal growth failure with microcephaly due to two novel heterozygous IGF1R mutations and response to growth hormone treatment. *Acta Paediatr.* **109**(10), pp.2067-2074.

Gomez-Hernandez, A., Escribano, O., Perdomo, L., Otero, Y.F., Garcia-Gomez, G., Fernandez, S., Beneit, N. and Benito, M. 2013. Implication of insulin receptor A isoform and IRA/IGF-IR hybrid receptors in the aortic vascular smooth muscle cell proliferation: role of TNF-alpha and IGF-II. *Endocrinology.* **154**(7), pp.2352-2364.

Goodwin, A.M. 2007. In vitro assays of angiogenesis for assessment of angiogenic and anti-angiogenic agents. *Microvasc. Res.* **74**(2-3), pp.172-183.

Goss, S.P., Hogg, N. and Kalyanaraman, B. 1997. The effect of nitric oxide release rates on the oxidation of human low density lipoprotein. *J. Biol. Chem.* **272**(34), pp.21647-21653.

Govers, R., Bevers, L., de Bree, P. and Rabelink, T.J. 2002. Endothelial nitric oxide synthase activity is linked to its presence at cell–cell contacts. *Biochem. J.* **361**, pp.193-201.

Gratton, J.P., Fontana, J., O'Connor, D.S., Garcia-Cardena, G., McCabe, T.J. and Sessa, W.C. 2000. Reconstitution of an endothelial nitric-oxide synthase (eNOS), hsp90, and caveolin-1 complex in vitro. Evidence that hsp90 facilitates calmodulin stimulated displacement of eNOS from caveolin-1. *J. Biol. Chem.* **275**(29), pp.22268-22272.

Gual, P., Le Marchand-Brustel, Y. and Tanti, J.F. 2005. Positive and negative regulation of insulin signaling through IRS-1 phosphorylation. *Biochimie.* **87**(1), pp.99-109.

Gustafson, T.A. and Rutter, W.J. 1990. The cysteine-rich domains of the insulin and insulin-like growth factor I receptors are primary determinants of hormone binding specificity. Evidence from receptor chimeras. *J. Biol. Chem.* **265**(30), pp.18663-18667.

Gutmann, T., Kim, K.H., Grzybek, M., Walz, T. and Coskun, U. 2018. Visualization of ligand-induced transmembrane signaling in the full-length human insulin receptor. *J. Cell Biol.* **217**(5), pp.1643-1649.

Gutmann, T., Schafer, I.B., Poojari, C., Brankatschk, B., Vattulainen, I., Strauss, M. and Coskun, U. 2020. Cryo-EM structure of the complete and ligand-saturated insulin receptor ectodomain. *J. Cell Biol.* **219**(1).

Han, S., Mistry, A., Chang, J.S., Cunningham, D., Griffor, M., Bonnette, P.C., Wang, H., Chrunyk, B.A., Aspnes, G.E., Walker, D.P., Brosius, A.D. and Buckbinder, L. 2009. Structural characterization of proline-rich tyrosine kinase 2 (PYK2) reveals a unique (DFG-out) conformation and enables inhibitor design. *J. Biol. Chem.* **284**(19), pp.13193-13201.

Hancock, M.L., Meyer, R.C., Mistry, M., Khetani, R.S., Wagschal, A., Shin, T., Ho Sui, S.J., Naar, A.M. and Flanagan, J.G. 2019. Insulin Receptor Associates with Promoters Genome-wide and Regulates Gene Expression. *Cell.* **177**(3), pp.722-736 e722.

Hanke, S. and Mann, M. 2009. The phosphotyrosine interactome of the insulin receptor family and its substrates IRS-1 and IRS-2. *Mol. Cell Proteom.* **8**(3), pp.519-534.

Hansen, B.F., Danielsen, G.M., Drejer, K., Sorensen, A.R., Wiberg, F.C., Klein, H.H. and Lundemose, A.G. 1996. Sustained signalling from the insulin receptor after stimulation with insulin analogues exhibiting increased mitogenic potency. *Biochem. J.* **315**, pp.271–279.

Hansen, B.F., Glendorf, T., Hegelund, A.C., Lundby, A., Lutzen, A., Slaaby, R. and Stidsen, C.E. 2012. Molecular characterisation of long-acting insulin analogues in comparison with human insulin, IGF-1 and insulin X10. *PLoS One.* **7**(5), pe34274.

Harris, M.B., Blackstone, M.A., Ju, H., Venema, V.J. and Venema, R.C. 2003. Heat-induced increases in endothelial NO synthase expression and activity and endothelial NO release. *Am. J. Physiol. Heart Circ. Physiol.* **285**, pp.H333–H340.

Havelund, S., Plum, A., Ribel, U., Jonassen, I., Volund, A., Markussen, J. and Kurtzhals, P. 2004. The Mechanism of Protraction of Insulin Detemir, a Long-acting, Acylated Analog of Human Insulin. *Pharm. Res.* **21**(8), pp.1498-1504.

Heffetz, D. and Zick, Y. 1986. Receptor aggregation is necessary for activation of the soluble insulin receptor kinase. *J. Biol. Chem.* **261**(2), pp.889-894.

Heller, R., Polack, T., Grabner, R. and Till, U. 1999. Nitric oxide inhibits proliferation of human endothelial cells via a mechanism independent of cGMP. *Atherosclerosis.* **144**, pp.49-57.

Hemmens, B. and Mayer, B. 2000. Enzymology of nitric oxide synthases. *Methods Mol. Biol.* **100**, pp.1-32.

Hex, N., Bartlett, C., Wright, D., Taylor, M. and Varley, D. 2012. Estimating the current and future costs of Type 1 and Type 2 diabetes in the UK, including direct health costs and indirect societal and productivity costs. *Diabet. Med.* **29**(7), pp.855-862.

Higashi, Y., Sasaki, S., Nakagawa, K., Fukuda, Y., Matsuura, H., Oshima, T. and Chayama, K. 2002. Tetrahydrobiopterin Enhances Forearm Vascular Response to Acetylcholine in Both Normotensive and Hypertensive Individuals. *Am. J. Hypertens.* **15**, pp.326-332.

Hill, C.P., Dauter, Z., Dodson, E.J., Dodson, G.G. and Dunn, M.F. 1990. X-ray Structure of an Unusual Ca2+ Site and the Roles of Zn2+ and Ca2+ in the Assembly, Stability, and Storage of the Insulin Hexamer. *Biochemistry.* **30**, pp.917-924.

Hirsch, I.B. and Vega, C.P. 2005. Optimal initiation of insulin in type 2 diabetes. *Med. Gen. Med.* **7**(4), p49.

Hocher, B., Schwarz, A., Slowinski, T., Bachmann, S., Pfeilschifter, J., Neumayer, H.H. and Bauer, C. 2004. In-vivo interaction of nitric oxide and endothelin. *J. Hypertens.* **22**(1), pp.111-119.

Hogan, J.C., Lewis, M.J. and Henderson, A.H. 1988. In vivo EDRF activity influences platelet function. *Br. J. Pharmacol.* **94**, pp.1020-1022.

Howell, K., Costello, C.M., Sands, M., Dooley, I. and McLoughlin, P. 2009. L-Arginine promotes angiogenesis in the chronically hypoxic lung: a novel mechanism ameliorating pulmonary hypertension. *Am. J. Physiol. Lung Cell Mol. Physiol.* **296**(6), pp.L1042-1050.

Hoyne, P.A., Elleman, T.C., Adams, T.E., Richards, K.M. and Ward, C.W. 2000. Properties of an insulin receptor with an IGF-1 receptor loop exchange in the cysteine-rich region. *FEBS Lett.* **469**, pp.57-60.

Hsu, S.Y.T. 2003. New insights into the evolution of the relaxin–LGR signaling system. *Trends Endocrinol. Metabol.* **14**(7), pp.303-309.

Hsu, S.Y.T., Nakabayashi, K., Nishi, S., Kumagai, J., Kudo, M., Bathgate, R.A.D., Sherwood, O.D. and Hsueh, A.J.W. 2003. Relaxin signaling in reproductive tissues. *Mol. Cell. Endocrinol.* **202**(1-2), pp.165-170.

Hu, H., Tian, M., Ding, C. and Yu, S. 2018. The C/EBP Homologous Protein (CHOP) Transcription Factor Functions in Endoplasmic Reticulum Stress-Induced Apoptosis and Microbial Infection. *Front. Immunol.* **9**, p3083.

Hua, Q.X., Shoelson, S.E., Kochoyan, M. and Weiss, M.A. 1991. Receptor binding redefined by a structural switch in a mutant human insulin. *Nature.* **354**, pp.238-241.

Hubbard, S.R. 1997. Crystal structure of the activated insulin receptor tyrosine kinase in complex with peptide substrate and ATP analog. *EMBO J.* **16**(18), pp.5573–5581.

Hubbard, S.R., Wei, L., Ellis, L. and Hendrickson, W.A. 1994. Crystal structure of the tyrosine kinase domain of the human insulin receptor. *Nature.* **372**, pp.746-754.

Humbel, R.E. 1990. Insulin-like growth factors I and I1. *Eur. J. Biochem.* **190**, pp.445 -462.

Humphrey, W., Dalke, A. and Schulten, K. 1996. VMD - Visual Molecular Dynamics. *J Molec. Graphics.* **14**, pp.33-38.

Hurt, K.J., Musicki, B., Palese, M.A., Crone, J.K., Becker, R.E., Moriarty, J.L., Snyder, S.H. and Burnett, A.L. 2002. Akt-dependent phosphorylation of endothelial nitric-oxide synthase mediates penile erection. *PNAS.* **99**(6), pp.4061-4066.

Hutsell, S.Q., Kimple, R.J., Siderovski, D.P., Willard, F.S. and Kimple, A.J. 2010. High-affinity immobilization of proteins using biotin- and GST-based coupling strategies. *Methods Mol. Biol.* **627**, pp.75-90.

Ignarro, L.J., Buga, G.M., Wood, K.S., Byrns, R.E. and Chaudhuri, G. 1987. Endothelium-derived relaxing factor produced and released from artery and vein is nitric oxide. *Proc. Natl. Acad. Sci.* **84**, pp.9265-9269.

Ish-Shalom, D., Christoffersen, C.T., Vorwerk, P., Sacerdoti-Sierra, N., Shymko, R.M., Naor, D. and De Meyts, P. 1997. Mitogenic properties of insulin and insulin analogues mediated by the insulin receptor. *Diabetologia.* **40 Suppl 2**, pp.S25-31.

Issad, T., Boute, N. and Pernet, K. 2002. A homogenous assay to monitor the activity of the insulin receptor using Bioluminescence Resonance Energy Transfer. *Biochem. Pharmacol.* **64**(5-6), pp.813-817.

Jensen, M. and De Meyts, P. 2009. Molecular Mechanisms of Differential Intracellular Signaling From the Insulin Receptor. *Vitamins & Hormones.* Academic Press, pp.51-75.

Jiang, M., Wang, H., Liu, Z., Lin, L., Wang, L., Xie, M., Li, D., Zhang, J. and Zhang, R. 2020. Endoplasmic reticulum stress-dependent activation of iNOS/NO-NF-kappaB signaling and NLRP3 inflammasome contributes to endothelial inflammation and apoptosis associated with microgravity. *FASEB J.* **34**(8), pp.10835-10849.

Jo, S., Kim, T., Iyer, V.G. and Im, W. 2008. CHARMM-GUI: a web-based graphical user interface for CHARMM. *J. Comput. Chem.* **29**(11), pp.1859-1865.

Jones, J.I. and Clemmons, D.R. 1995. Insulin-Like Growth Factors and Their Binding Proteins: Biological Actions*. *Endocr. Rev.* **16**(1), pp.3-34.

Jorgensen, A.M.M., Kristensen, S.M., Led, J.J. and Balschmidt, P. 1992. Three-dimensional Solution Structure of an Insulin Dimer A Study of the B9(Asp) Mutant of Human Insulin Using Nuclear Magnetic Resonance, Distance Geometry and Restrained Molecular Dynamics. *J. Mol. Biol.* **227**, pp.1146-1163.

Jorgensen, A.M.M., Olsen, H.B., Balschmidt, P. and Led, J.J. 1996. Solution Structure of the Superactive Monomeric Des-[Phe(B25)] Human Insulin Mutant: Elucidation of the Structural Basis for the Monomerization of Des-[Phe(B25)] Insulin and the Dimerization of Native Insulin. *J. Mol. Biol.* **257**, pp.684–699.

Juanes, M., Guercio, G., Marino, R., Berensztein, E., Warman, D.M., Ciaccio, M., Gil, S., Bailez, M., Rivarola, M.A. and Belgorosky, A. 2015. Three novel IGF1R mutations in microcephalic patients with prenatal and postnatal growth impairment. *Clin. Endocrinol.* **82**(5), pp.704-711.

Jui, H.Y., Suzuki, Y., Accili, D. and Taylor, S.I. 1994. Expression of a cDNA encoding the human insulin receptor-related receptor. *J. Biol. Chem.* **269**(35), pp.22446-22452.

Jumper, J., Evans, R., Pritzel, A., Green, T., Figurnov, M., Ronneberger, O., Tunyasuvunakool, K., Bates, R., Zidek, A., Potapenko, A., Bridgland, A., Meyer, C., Kohl, S.A.A., Ballard, A.J., Cowie, A., Romera-Paredes, B., Nikolov, S., Jain, R., Adler, J., Back, T., Petersen, S., Reiman, D., Clancy, E., Zielinski, M., Steinegger, M., Pacholska, M., Berghammer, T., Bodenstein, S., Silver, D., Vinyals, O., Senior, A.W., Kavukcuoglu, K., Kohli, P. and Hassabis, D. 2021. Highly accurate protein structure prediction with AlphaFold. *Nature.* **596**(7873), pp.583-589.

Junjappa, R.P., Patil, P., Bhattarai, K.R., Kim, H.R. and Chae, H.J. 2018. IRE1alpha Implications in Endoplasmic Reticulum Stress-Mediated Development and Pathogenesis of Autoimmune Diseases. *Front. Immunol.* **9**, p1289.

Kaarsholm, N.C., Havelund, S. and Hourgaard, P. 1990. Ionization Behavior of Native and Mutant Insulins: pK Perturbation of B13-Glu in Aggregated Species. *Arch. Biochem. Biophys.* **283**(2), pp.496-502.

Kahn, C.R., Baird, K.L., Jarrett, D.B. and Flier, J.S. 1978. Direct demonstration that receptor crosslinking or aggregation is important in insulin action. *Biochemistry.* **75**(9), pp.4209-4213.

Kasuga, M., Fujita-Yamaguchi, Y., Blithe, D.L., White, M.F. and Kahn, C.R. 1983. Characterization of the insulin receptor kinase purified from human placental membranes. *J. Biol. Chem.* **258**(18), pp.10973-10980.

Kasuga, M., Van Obberghen, E., Nissley, S.P. and Rechler, M.M. 1981. Demonstration of two subtypes of insulin-like growth factor receptors by affinity cross-linking. *J. Biol. Chem.* **256**(11), pp.5305-5308.

Kasuga, M., Zick, Y., Blithe, D.L., Crettaz, M. and Kahn, C.R. 1982. Insulin stimulates tyrosine phosphorylation of the insulin receptor in a cell-free system. *Nature.* **298**, pp.667-669.

Kavran, J.M., McCabe, J.M., Byrne, P.O., Connacher, M.K., Wang, Z., Ramek, A., Sarabipour, S., Shan, Y., Shaw, D.E., Hristova, K., Cole, P.A. and Leahy, D.J. 2014. How IGF-1 activates its receptor. *Elife.* **3**.

Kellerer, M., Lammers, R., Ermel, B., Tippmer, S., Vogt, B., Obermaier-Kusser, B., Ullrich, A. and Haring, H.-U. 1992. Distinct a-Subunit Structures of Human Insulin Receptor A and B Variants Determine Differences in Tyrosine Kinase Activities. *Biochemistry.* **31**, pp.4588-4596.

King, G.L., Kahn, C.R., Samuels, B., Danho, W., Bullesbach, E.E. and Gattner, H.G. 1982. Synthesis and characterization of molecular hybrids of insulin and insulin-like growth factor I. The role of the A-chain extension peptide. *J. Biol. Chem.* **257**(18), pp.10869-10873.

Kiselyov, V.V., Versteyhe, S., Gauguin, L. and De Meyts, P. 2009. Harmonic oscillator model of the insulin and IGF1 receptors' allosteric binding and activation. *Mol. Syst. Biol.* **5**, p243.

Kjeldsen, T., Andersen, A.S., Wiberg, F.C., Rasmussen, J.S., Schaffer, L., Balschmidt, P., Moller, K.B. and Moller, N.P.H. 1991. The ligand specificities of the insulin receptor and the insulin-like growth factor I receptor reside in different regions of a common binding site. *PNAS.* **88**, pp.4404-4408.

Kluge, M.A., Fetterman, J.L. and Vita, J.A. 2013. Mitochondria and endothelial function. *Circ. Res.* **112**(8), pp.1171-1188.

Kristensen, C., Wiberg, F.C. and Andersen, A.S. 1999. Specificity of insulin and insulin-like growth factor I receptors investigated using chimeric mini-receptors. Role of C-terminal of receptor alpha subunit. *J. Biol. Chem.* **274**(52), pp.37351-37356.

Kubes, P., Suzuki, M. and Granger, D.N. 1991. Nitric oxide: An endogenous modulator of leukocyte adhesion. *Proc. Nail. Acad. Sci.* **88**, pp.4651-4655.

Kull, F.C., Jacobs, S., Su, Y.F., Svoboda, M.E., Van Wyk, J.J. and Cuatrecasas, P. 1983. Monoclonal antibodies to receptors for insulin and somatomedin-C. *J. Biol. Chem.* **258**(10), pp.6561-6566.

Kume, N., Cybulsky, M.I. and Gimbrone, M.A.J. 1992. Lysophosphatidylcholine, a Component of Atherogenic Lipoproteins, Induces Mononuclear Leukocyte Adhesion Molecules in Cultured Human and Rabbit Arterial Endothelial Cells. *J. Clin. Invest.* **90**, pp.1138-1144.

Kurtzhals, P., Schaffer, L., Sorensen, A.R., Kristensen, C., Jonassen, I., Schmid, C. and Trub, T. 2000. Correlations of Receptor Binding and Metabolic and Mitogenic Potencies of Insulin Analogs Designed for Clinical Use. *Diabetes.* **49**, pp.999–1005.

Lam, C.F., Peterson, T.E., Richardson, D.M., Croatt, A.J., d'Uscio, L.V., Nath, K.A. and Katusic, Z.S. 2006. Increased blood flow causes coordinated upregulation of arterial eNOS and biosynthesis of tetrahydrobiopterin. *Am. J. Physiol. Heart Circ. Physiol.* **290**(2), pp.H786-793.

Laron, Z. 2001. Insulin-like growth factor 1 (IGF-1): a growth hormone. *J. Clin. Pathol: Mol. Pathol.* **54**, pp.311–316.

Larsen, W.J. 1998. *Essentials of Human Embryology.* 2nd ed. New York: Churchill Livingstone.

Laughlin, M.H., Pollock, J.S., Amann, J.F., Hollis, M.L., Woodman, C.R. and Price, E.M. 2001. Training induces nonuniform increases in eNOS content along the coronary arterial tree. *J. Appl. Physiol.* **90**, pp.501-510.

Le Roith, D. 1997. INSULIN - LIKE GROWTH FACTORS. *N. Engl. J. Med.* **336**(9), pp.633-640.

Lee, J., Cheng, X., Swails, J.M., Yeom, M.S., Eastman, P.K., Lemkul, J.A., Wei, S., Buckner, J., Jeong, J.C., Qi, Y., Jo, S., Pande, V.S., Case, D.A., Brooks, C.L., 3rd, MacKerell, A.D., Jr., Klauda, J.B. and Im, W. 2016. CHARMM-GUI Input Generator for NAMD, GROMACS, AMBER, OpenMM, and CHARMM/OpenMM Simulations Using the CHARMM36 Additive Force Field. *J. Chem. Theory Comput.* **12**(1), pp.405-413.

Lee, O.H., Bae, S.K., Bae, M.H., Lee, Y.M., Moon, E.J., Cha, H.J., Kwon, Y.G. and Kim, K.W. 2000. Identification of angiogenic properties of insulin-like growth factor II in in vitro angiogenesis models. *Br. J. Cancer.* **82**(2), pp.385-391.

Leon, B.M. and Maddox, T.M. 2015. Diabetes and cardiovascular disease: Epidemiology, biological mechanisms, treatment recommendations and future research. *World J. Diabetes.* **6**(13), pp.1246-1258.

Li, G., Barrett, E.J., Wang, H., Chai, W. and Liu, Z. 2005. Insulin at physiological concentrations selectively activates insulin but not insulin-like growth factor I (IGF-I) or insulin/IGF-I hybrid receptors in endothelial cells. *Endocrinology.* **146**(11), pp.4690-4696.

Li, H., Raman, C.S., Martasek, P., Masters, B.S.S. and Poulos, T.L. 2001. Crystallographic Studies on Endothelial Nitric Oxide Synthase Complexed with Nitric Oxide and Mechanism-Based Inhibitors. *Biochemistry.* **40**, pp.5399-5406.

Li, J., Choi, E., Yu, H. and Bai, X.C. 2019. Structural basis of the activation of type 1 insulin-like growth factor receptor. *Nat. Commun.* **10**(1), p4567.

Li, Q., Fu, J., Xia, Y., Qi, W., Ishikado, A., Park, K., Yokomizo, H., Huang, Q., Cai, W., Rask-Madsen, C., Kahn, C.R. and King, G.L. 2019. Homozygous receptors for insulin and not IGF-1 accelerate intimal hyperplasia in insulin resistance and diabetes. *Nat. Commun.* **10**(1), p4427.

Li, Q., Wong, Y.L. and Kang, C. 2014. Solution structure of the transmembrane domain of the insulin receptor in detergent micelles. *Biochim. Biophys. Acta.* **1838**(5), pp.1313-1321.

Li, W., Burkhart, C., Polinska, P., Harmandaris, V. and Doxastakis, M. 2020. Backmapping coarse-grained macromolecules: An efficient and versatile machine learning approach. *J. Chem. Phys.* **153**(4), p041101.

Liang, C.C., Park, A.Y. and Guan, J.L. 2007. In vitro scratch assay: a convenient and inexpensive method for analysis of cell migration in vitro. *Nat. Protoc.* **2**(2), pp.329-333.

Libby, P. 2002. Inflammation in Atherosclerosis. *Nature.* **420**, pp.868-874.

Libby, P., Buring, J.E., Badimon, L., Hansson, G.K., Deanfield, J., Bittencourt, M.S., Tokgozoglu, L. and Lewis, E.F. 2019. Atherosclerosis. *Nat. Rev. Dis. Primers.* **5**(1), p56.

Lievens, D. and von Hundelshausen, P. 2011. Platelets in atherosclerosis. *Thromb. Haemost.* **106**(5), pp.827-838.

Lifesciences, C. 2021. *Sensor Chip CM5.* [Online]. Available from: https://www.cytivalifesciences.com/en/us/shop/protein-analysis/spr-label-free-analysis/spr-consumables/sensor-chips/sensor-chip-cm5-p-05858

Lipska, K.J., Ross, J.S., Van Houten, H.K., Beran, D., Yudkin, J.S. and Shah, N.D. 2014. Use and Out-of-Pocket Costs of Insulin for Type 2 Diabetes Mellitus From 2000 Through 2010. *JAMA.* **311**(22), pp.2331-2333.

Lisi, G.P., Png, C.Y. and Wilcox, D.E. 2014. Thermodynamic contributions to the stability of the insulin hexamer. *Biochemistry.* **53**(22), pp.3576-3584.

Livingstone, C. 2013. IGF2 and cancer. *Endocr. Relat. Cancer.* **20**(6), pp.R321-339.

Lo Sasso, G., Schlage, W.K., Boue, S., Veljkovic, E., Peitsch, M.C. and Hoeng, J. 2016. The Apoe(-/-) mouse model: a suitable model to study cardiovascular and respiratory diseases in the context of cigarette smoke exposure and harm reduction. *J. Transl. Med.* **14**(1), p146.

Loot, A.E., Schreiber, J.G., Fisslthaler, B. and Fleming, I. 2009. Angiotensin II impairs endothelial function via tyrosine phosphorylation of the endothelial nitric oxide synthase. *J. Exp. Med.* **206**(13), pp.2889-2896.

Lopez, A., Lorente, J.A., Steingrub, J., Bakker, J., McLuckie, A., Willatts, S., Brockway, M., Anzueto, A., Holzapfel, L., Breen, D., Silverman, M.S., Takala, J., Donaldson, J., Arneson, C., Grove, G., Grossman, S. and Grover, R. 2004. Multiple-center, randomized, placebo-controlled, double-blind study of the nitric oxide synthase inhibitor 546C88: effect on survival in patients with septic shock. *Crit. Care Med.* **32**(1), pp.21-30.

Lou, M.Z., Garrett, T.P.J., McKern, N.M., Hoyne, P.A., Epa, V.C., Bentley, J.D., Lovrecz, G.O., Cosgrove, L.J., Frenkel, M.J. and Ward, C.W. 2006. The first three domains of the insulin receptor differ structurally from the insulin-like growth factor 1 receptor in the regions governing ligand specificity. *PNAS.* **103**(33), pp.12429–12434.

Lu, Z.J., Ren, Y.Q., Wang, G.P., Song, Q., Li, M., Jiang, S.S., Ning, T., Guan, Y.S., Yang, J.L. and Luo, F. 2009. Biological behaviors and proteomics analysis of hybrid cell line EAhy926 and its parent cell line A549. *J. Exp. Clin. Cancer Res.* **28**, p16.

Lulo, J., Yuzawa, S. and Schlessinger, J. 2009. Crystal structures of free and ligand-bound focal adhesion targeting domain of Pyk2. *Biochem. Biophys. Res. Commun.* **383**(3), pp.347-352.

Macalino, S.J.Y., Basith, S., Clavio, N.A.B., Chang, H., Kang, S. and Choi, S. 2018. Evolution of In Silico Strategies for Protein-Protein Interaction Drug Discovery. *Molecules.* **23**(8).

MacKerell, A.D., Jr., Bashford, D., Bellott, M., Dunbrack, R.L., Jr., Evanseck, J.D., Field, M.J., Fischer, S., Gao, J., Ha, S., Joesph-McCarthy, D., Kuchnir, L., Kuczera, K., Lau, F.T.K., Mattos, C., Michnick, S., Ngo, T., Nguyen, D.T., Prodhom, B., Reiher, W.E., III., Roux, B., Schlenkrich, M., Smith, J.C., Stote, R., Straub, J., Wantanabe, M., Wiorkiewicz-Kuczera, J., Yin, D. and Karplus, M. 1998. All-Atom Empirical Potential for Molecular Modeling and Dynamics Studies of Proteins. *J. Phys. Chem. B.* **102**, pp.3586-3616.

Maly, P. and Lüthi, C. 1988. The binding sites of insulin-like growth factor I (IGF I) to type I IGF receptor and to a monoclonal antibody. Mapping by chemical modification of tyrosine residues. *J. Biol. Chem.* **263**(15), pp.7068-7072.

Mannucci, E., Giannini, S. and Dicembrini, I. 2015. Cardiovascular effects of basal insulins. *Drug Healthc. Patient Saf.* **7**, pp.113-120.

Margineanu, A., Chan, J.J., Kelly, D.J., Warren, S.C., Flatters, D., Kumar, S., Katan, M., Dunsby, C.W. and French, P.M. 2016. Screening for protein-protein interactions using Forster resonance energy transfer (FRET) and fluorescence lifetime imaging microscopy (FLIM). *Sci. Rep.* **6**, p28186.

Markussen, J., Havelund, S., Kurtzhals, P., Andersen, A.S., Halstrom, J., Hasselager, E., Larsen, U.D., Ribel, U., Schaffer, L. and Jonassen, I. 1996. Soluble, fatty acid acylated insulins bind to albumin and show protracted action in pigs. *Diabetologia.* **39**, pp.281-288.

Marsh, J.W., Westley, J. and Steiner, D.F. 1984. Insulin-receptor interactions. Presence of a positive cooperative effect. *J. Biol. Chem.* **259**(10), pp.6641-6649.

Martasek, P., Miller, R.T., Liu, Q., Roman, L.J., Salerno, J.C., Migita, C.T., Raman, C.S., Gross, S.S., Ikeda-Saito, M. and Masters, B.S. 1998. The C331A mutant of neuronal nitric-oxide synthase is defective in arginine binding. *J. Biol. Chem.* **273**(52), pp.34799-34805.

Massagué, J. and Czech, M.P. 1982. The subunit structures of two distinct receptors for insulin-like growth factors I and II and their relationship to the insulin receptor. *J. Biol. Chem.* **257**(9), pp.5038-5045.

Matsunaga, T., Weihrauch, D.W., Moniz, M.C., Tessmer, J., Warltier, D.C. and Chilian, W.M. 2002. Angiostatin inhibits coronary angiogenesis during impaired production of nitric oxide. *Circulation.* **105**(18), pp.2185-2191.

Mayer, D., Shukla, A. and Enzmann, H. 2008. Proliferative effects of insulin analogues on mammary epithelial cells. *Arch. Physiol. Biochem.* **114**(1), pp.38-44.

Mc Namara, K., Alzubaidi, H. and Jackson, J.K. 2019. Cardiovascular disease as a leading cause of death: how are pharmacists getting involved? *Integr. Pharm. Res. Pract.* **8**, pp.1-11.

McClain, D.A. 1991. Different Ligand Affinities of the Two Human Insulin Receptor Splice Variants Are Reflected in Parallel Changes in Sensitivity for Insulin Action. *Mol. Endocrinol.* **5**, pp.734-739.

McDonald, A.I., Shirali, A.S., Aragon, R., Ma, F., Hernandez, G., Vaughn, D.A., Mack, J.J., Lim, T.Y., Sunshine, H., Zhao, P., Kalinichenko, V., Hai, T., Pelegrini, M., Ardehali, R. and Iruela-Arispe, M.L. 2018. Endothelial Regeneration of Large Vessels Is a Biphasic Process Driven by Local Cells with Distinct Proliferative Capacities. *Cell Stem Cell.* **23**(2), pp.210-225 e216.

McKern, N.M., Lawrence, M.C., Streltsov, V.A., Lou, M.Z., Adams, T.E., Lovrecz, G.O., Elleman, T.C., Richards, K.M., Bentley, J.D., Pilling, P.A., Hoyne, P.A., Cartledge, K.A., Pham, T.M., Lewis, J.L., Sankovich, S.E., Stoichevska, V., Da Silva, E., Robinson, C.P., Frenkel, M.J., Sparrow, L.G., Fernley, R.T., Epa, V.C. and Ward, C.W. 2006. Structure of the insulin receptor ectodomain reveals a folded-over conformation. *Nature.* **443**(7108), pp.218-221.

McNaughton, L., Puttagunta, L., Martinez-Cuesta, M.A., Kneteman, N., Mayers, I., Moqbel, R., Hamid, Q. and Radomski, M.W. 2002. Distribution of nitric oxide synthase in normal and cirrhotic human liver. *PNAS.* **99**(26), pp.17161-17166.

Medina-Leyte, D.J., Domínguez-Pérez, M., Mercado, I., Villarreal-Molina, M.T. and Jacobo-Albavera, L. 2020. Use of Human Umbilical Vein Endothelial Cells (HUVEC) as a Model to Study Cardiovascular Disease: A Review. *Appl.* **10**(3).

Menting, J.G., Lawrence, C.F., Kong, G.K., Margetts, M.B., Ward, C.W. and Lawrence, M.C. 2015. Structural Congruency of Ligand Binding to the Insulin and Insulin/Type 1 Insulin-like Growth Factor Hybrid Receptors. *Structure.* **23**(7), pp.1271-1282.

Menting, J.G., Ward, C.W., Margetts, M.B. and Lawrence, M.C. 2009. A thermodynamic study of ligand binding to the first three domains of the human insulin receptor: relationship between the receptor alpha-chain C-terminal peptide and the site 1 insulin mimetic peptides. *Biochemistry.* **48**(23), pp.5492-5500.

Menting, J.G., Whittaker, J., Margetts, M.B., Whittaker, L.J., Kong, G.K., Smith, B.J., Watson, C.J., Zakova, L., Kletvikova, E., Jiracek, J., Chan, S.J., Steiner, D.F., Dodson, G.G., Brzozowski, A.M., Weiss, M.A., Ward, C.W. and Lawrence, M.C. 2013. How insulin engages its primary binding site on the insulin receptor. *Nature.* **493**(7431), pp.241-245.

Menting, J.G., Yang, Y., Chan, S.J., Phillips, N.B., Smith, B.J., Whittaker, J., Wickramasinghe, N.P., Whittaker, L.J., Pandyarajan, V., Wan, Z.L., Yadav, S.P., Carroll, J.M., Strokes, N., Roberts, C.T., Jr., Ismail-Beigi, F., Milewski, W., Steiner, D.F., Chauhan, V.S., Ward, C.W., Weiss, M.A. and Lawrence, M.C. 2014. Protective hinge in insulin opens to enable its receptor engagement. *Proc. Natl. Acad. Sci.* **111**(33), pp.E3395-3404.

Meyer, K. and Selbach, M. 2015. Quantitative affinity purification mass spectrometry: a versatile technology to study protein-protein interactions. *Front. Genet.* **6**, p237.

Michel, J.B., Feron, O., Sacks, D. and Michel, T. 1997. Reciprocal regulation of endothelial nitric-oxide synthase by Ca2+-calmodulin and caveolin. *J. Biol. Chem.* **272**(25), pp.15583-15586.

Michell, B.J., Chen, Z., Tiganis, T., Stapleton, D., Katsis, F., Power, D.A., Sim, A.T. and Kemp, B.E. 2001. Coordinated control of endothelial nitric-oxide synthase phosphorylation by protein kinase C and the cAMP-dependent protein kinase. *J. Biol. Chem.* **276**(21), pp.17625-17628.

Michell, B.J., Harris, M.B., Chen, Z.P., Ju, H., Venema, V.J., Blackstone, M.A., Huang, W., Venema, R.C. and Kemp, B.E. 2002. Identification of regulatory sites of phosphorylation of the bovine endothelial nitric-oxide synthase at serine 617 and serine 635. *J. Biol. Chem.* **277**(44), pp.42344-42351.

Mirmira, R.G. and Tager, H.S. 1991. Disposition of the Phenylalanine B25 Side Chain during Insulin-Receptor and Insulin-Insulin Interactions1. *Biochemistry.* **30**, pp.8222-8229.

Monami, M., Adalsteinsson, J.E., Desideri, C.M., Ragghianti, B., Dicembrini, I. and Mannucci, E. 2013. Fasting and post-prandial glucose and diabetic complication. A meta-analysis. *Nutr. Metab. Cardiovasc. Dis.* **23**(7), pp.591-598.

Moncada, S. 1999. Nitric oxide: discovery and impact on clinical medicine. *J. R. Soc. Med.* **92**, pp.164-169.

Moncada, S. and Higgs, E.A. 1993. The L-Arginine-Nitric Oxide Pathway. *N. Engl. J. Med.* **329**, pp.2002-2012.

Mosthaf, L., Grako, K., Dull, T.J., Coussens, L., Ullrich, A. and McClain, D.A. 1990. Functionally distinct insulin receptors generated by tissue-specific alternative splicing. *EMBO J.* **9**(8), pp.2409-2413.

Mozaffarian, D. 2016. Dietary and Policy Priorities for Cardiovascular Disease, Diabetes, and Obesity: A Comprehensive Review. *Circulation.* **133**(2), pp.187-225.

Muench, S.P. 2020. In: *DTSD Seminar, University of Leeds*.

Mughal, R.S., Bridge, K., Buza, I., Slaaby, R., Worm, J., Klitgaard-Povlsen, G., Hvid, H., Schiodt, M., Cubbon, R., Yuldasheva, N., Skromna, A., Makava, N., Skytte-Olsen, G. and Kearney, M.T. 2019. Effects of obesity on insulin: insulin-like growth factor 1 hybrid receptor expression and Akt phosphorylation in conduit and resistance arteries. *Diab. Vasc. Dis. Res.* **16**(2), pp.160-170.

Muguerza, B., Castilla-Cortazar, I., Garcia, M., Quiroga, J., Santidrian, S. and Prieto, J. 2001. Antifibrogenic effect in vivo of low doses of insulin-like growth factor-I in cirrhotic rats. *Biochim. Biophys. Acta.* **1536**, pp.185-195.

Mukherjee, S. and Zhang, Y. 2011. Protein-protein complex structure predictions by multimeric threading and template recombination. *Structure.* **19**(7), pp.955-966.

Murohara, T., Asahara, T., Silver, M., Bauters, C., Masuda, H., Kalka, C., Kearney, M., Chen, D., Chen, D., Symes, J.F., Fishman, M.C., Huang, P.L. and Isner, J.M. 1998. Nitric Oxide Synthase Modulates Angiogenesis in Response to Tissue Ischemia. *J. Clin. Invest.* **101**, pp.2567–2578.

Mynarcik, D.C., Williams, P.F., Schaffer, L., Yu, G.Q. and Whittaker, J. 1997. Identification of common ligand binding determinants of the insulin and insulin-like growth factor 1 receptors. Insights into mechanisms of ligand binding. *J. Biol. Chem.* **272**(30), pp.18650-18655.

Nakaki, T., Nakayama, M. and Kato, R. 1990. Inhibition by nitric oxide end nitric oxide-producing vasodilators of DNA synthesis in vascular smooth muscle cells. *Eur. J. Pharmacol.* **189**, pp.347-353.

Naser, R., Aldehaiman, A., Diaz-Galicia, E. and Arold, S.T. 2018. Endogenous Control Mechanisms of FAK and PYK2 and Their Relevance to Cancer Development. *Cancers.* **10**(6).

Nathan, C. 1997. Perspectives Series: Nitric Oxide and Nitric Oxide Synthases. *J. Clin. Invest.* **100**, pp.2417-2423.

Nitert, M.D., Chisalita, S.I., Olsson, K., Bornfeldt, K.E. and Arnqvist, H.J. 2005. IGF-I/insulin hybrid receptors in human endothelial cells. *Mol. Cell Endocrinol.* **229**(1-2), pp.31-37.

Niu, G. and Chen, X. 2010. Vascular Endothelial Growth Factor as an Anti-angiogenic Target for Cancer Therapy. *Curr. Drug Targets.* **11**(8), pp.1000–1017.

O'Donoghue, S.I., Chang, Q., Abseher, R., Nilges, M. and Led, J.J. 2000. Unraveling the symmetry ambiguity in a hexamer: Calculation of the R6 human insulin structure. *J. Biomol. NMR.* **16**, pp.93-108.

Ohlsson, C., Mohan, S., Sjogren, K., Tivesten, A., Isgaard, J., Isaksson, O., Jansson, J.O. and Svensson, J. 2009. The role of liver-derived insulin-like growth factor-I. *Endocr. Rev.* **30**(5), pp.494-535.

Ojamaa, K., Hedo, J.A., Roberts, C.T., Moncada, V.Y., Gorden, P., Ullrich, A. and Taylor, S.I. 1988. Defects in Human Insulin Receptor Gene Expression. *Mol. Endocrinol.* **2**, pp.242-247.

Ormiston, M.L., Deng, Y., Stewart, D.J. and Courtman, D.W. 2010. Innate immunity in the therapeutic actions of endothelial progenitor cells in pulmonary hypertension. *Am. J. Respir. Cell Mol. Biol.* **43**(5), pp.546-554.

Ormiston, M.L., Toshner, M.R., Kiskin, F.N., Huang, C.J., Groves, E., Morrell, N.W. and Rana, A.A. 2015. Generation and Culture of Blood Outgrowth Endothelial Cells from Human Peripheral Blood. *J. Vis. Exp.* (106), pe53384.

Palmer, R.M.J., Ferrige, A.G. and Moncada, S. 1987. Nitric oxide release accounts for the biological activity of endothelium-derived relaxing factor. *Nature.* **327**, pp.524-526.

Palmer, R.M.J., Rees, D.D., Ashton, D.S. and Moncada, S. 1988. L-ARGININE IS THE PHYSIOLOGICAL PRECURSOR FOR THE FORMATION OF NITRIC OXIDE IN ENDOTHELIUM-DEPENDENT RELAXATION. *Biochem. Biophys. Res. Commun.* **153**(3), pp.1251-1256.

Pandini, G., Frasca, F., Mineo, R., Sciacca, L., Vigneri, R. and Belfiore, A. 2002. Insulin/insulin-like growth factor I hybrid receptors have different biological characteristics depending on the insulin receptor isoform involved. *J. Biol. Chem.* **277**(42), pp.39684-39695.

Pandini, G., Genua, M., Frasca, F., Squatrito, S., Vigneri, R. and Belfiore, A. 2007a. 17beta-estradiol up-regulates the insulin-like growth factor receptor through a nongenotropic pathway in prostate cancer cells. *Cancer Res.* **67**(18), pp.8932-8941.

Pandini, G., Mineo, R., Frasca, F., Roberts, C.T., Marcelli, M., Vigneri, R. and Belfiore, A. 2005. Androgens Up-regulate the Insulin-like Growth Factor-I Receptor in Prostate Cancer Cells. *Cancer Res.* **65**(5), pp.1849-1857.

Pandini, G., Vigneri, R., Constantino, A., Frasca, F., Ippolito, A., Fujita-Yamaguchi, Y., Siddle, K., Goldfine, I.D. and Belfiore, A. 1999. Insulin and Insulin-like Growth Factor-I (IGF-I) Receptor Overexpression in Breast Cancers Leads to Insulin/IGF-I Hybrid Receptor Overexpression: Evidence for a Second Mechanism of IGF-I Signaling. *Clin. Cancer Res.* **5**, pp.1935–1944.

Pandini, G., Wurch, T., Akla, B., Corvaia, N., Belfiore, A. and Goetsch, L. 2007b. Functional responses and in vivo anti-tumour activity of h7C10: a humanised monoclonal antibody with neutralising activity against the insulin-like growth factor-1 (IGF-1) receptor and insulin/IGF-1 hybrid receptors. *Eur. J. Cancer.* **43**(8), pp.1318-1327.

Pang, D.T., Lewis, S.D., Sharma, B.R. and Shafer, J.A. 1984. Relationship between the Subunit Structure of Insulin Receptor and Its Competence to Bind Insulin and Undergo Phosphotylation. *Arch. Biochem. Biophys.* **234**(2), pp.629-638.

Pang, D.T. and Shafer, J.A. 1983. Stoichiometry for the binding of insulin to insulin receptors in adipocyte membranes. *J. Biol. Chem.* **258**(4), pp.2514-2518.

Paschalaki, K.E. and Randi, A.M. 2018. Recent Advances in Endothelial Colony Forming Cells Toward Their Use in Clinical Translation. *Front Med (Lausanne).* **5**, p295.

Perez, R., Garcia-Fernandez, M., Diaz-Sanchez, M., Puche, J.E., Delgado, G., Conchillo, M., Muntane, J. and Castilla-Cortazar, I. 2008. Mitochondrial protection by low doses of insulin-like growth factor- I in experimental cirrhosis. *World J. Gastroenterol.* **14**(17), pp.2731-2739.

Perlman, R.L. 2016. Mouse models of human disease: An evolutionary perspective. *Evol. Med. Public Health.* **2016**(1), pp.170-176.

Peterson, T.E., d'Uscio, L.V., Cao, S., Wang, X.L. and Katusic, Z.S. 2009. Guanosine triphosphate cyclohydrolase I expression and enzymatic activity are present in caveolae of endothelial cells. *Hypertension.* **53**(2), pp.189-195.

Petros, A., Lamb, G., Leone, A., Moncada, S., Bennett, D. and Vallance, P. 1994. Effects of a nitric oxide synthase inhibitor in humans with septic shock. *Cardiovasc. Res.* **28**, pp.34-39.

Petruzzelli, L.M., Ganguly, S., Smith, C.J., Cobb, M.H., Rubin, C.S. and Rosen, O.M. 1982. Insulin activates a tyrosine-specific protein kinase in extracts of 3T3-LI adipocytes and human placenta. *PNAS.* **79**, pp.6792-6796.

Phillips, J.-C. and Scheen, A. 2006. Insulin detemir in the treatment of type 1 and type 2 diabetes. *Vasc. Health Risk Manag.* **2**(3), pp.277–283.

Pierre-Eugene, C., Pagesy, P., Nguyen, T.T., Neuille, M., Tschank, G., Tennagels, N., Hampe, C. and Issad, T. 2012. Effect of insulin analogues on insulin/IGF1 hybrid receptors: increased activation by glargine but not by its metabolites M1 and M2. *PLoS One.* **7**(7), pe41992.

Pohlman, T.H. and Harlan, J.M. 2000. Adaptive responses of the endothelium to stress. *J. Surg. Res.* **89**(1), pp.85-119.

Potente, M., Gerhardt, H. and Carmeliet, P. 2011. Basic and therapeutic aspects of angiogenesis. *Cell.* **146**(6), pp.873-887.

Potenza, M.A., Addabbo, F. and Montagnani, M. 2009. Vascular actions of insulin with implications for endothelial dysfunction. *Am. J. Physiol. Endocrinol. Metab.* **297**(3), pp.E568-577.

Powell-Braxton, L., Hollingshead, P., Warburton, C., Dowd, M., Pitts-Meek, S., Dalton, D., Gillett, N. and Stewart, T.A. 1993. IGF-I is required for normal embryonic growth in mice. *Genes Dev.* **7**, pp.2609-2617.

PubChem. 2021a. *Compound Summary for CID 16132438, Insulin lispro.* [Online]. [Accessed 25 October]. Available from: https://pubchem.ncbi.nlm.nih.gov/compound/Insulin-lispro

PubChem. 2021b. *Compound Summary for CID 16136701, Apidra.* [Online]. [Accessed 25 October]. Available from: https://pubchem.ncbi.nlm.nih.gov/compound/Apidra

PubChem. 2021c. *Compound Summary for CID 16137271, Insulin detemir.* [Online]. [Accessed 25 October]. Available from: https://pubchem.ncbi.nlm.nih.gov/compound/Insulin-detemir

PubChem. 2021d. *Compound Summary for CID 118984445, Insulin aspart.* [Online]. [Accessed 25 October]. Available from: https://pubchem.ncbi.nlm.nih.gov/compound/Insulin-aspart

PubChem. 2021e. *Compound Summary for CID 118984454, Insulin glargine.* [Online]. [Accessed 25 October]. Available from: https://pubchem.ncbi.nlm.nih.gov/compound/Insulin-glargine

Puche, J.E. and Castilla Cortazar, I. 2012. Human conditions of insulin-like growth factor-I (IGF-I) deficiency. *J. Trans. Med.* **10**(224), pp.1-29.

Puche, J.E., Garcia-Fernandez, M., Muntane, J., Rioja, J., Gonzalez-Baron, S. and Castilla Cortazar, I. 2008. Low doses of insulin-like growth factor-I induce mitochondrial protection in aging rats. *Endocrinology.* **149**(5), pp.2620-2627.

Pyorala, M., Laakso, M., Miettinen, H. and Pyorala, K. 2000. Plasma Insulin and All-Cause, Cardiovascular, and Noncardiovascular Mortality. *Diabetes Care.* **23**, pp.1097–1102.

Radomski, M.W., Palmer, R.M.J. and Moncada, S. 1987. THE ROLE OF NITRIC OXIDE AND cGMP IN PLATELET ADHESION TO VASCULAR ENDOTHELIUM. *Biochem. Biophys. Res. Commun.* **148**, pp.1482-1489.

Radomski, M.W., Palmer, R.M.J. and Moncada, S. 1990. An L-arginine/nitric oxide pathway present in human platelets regulates aggregation. *Proc. Natl. Acad. Sci.* **87**, pp.5193-5197.

Rajapaksha, H. and Forbes, B.E. 2015. Ligand-Binding Affinity at the Insulin Receptor Isoform-A and Subsequent IR-A Tyrosine Phosphorylation Kinetics are Important Determinants of Mitogenic Biological Outcomes. *Front. Endocrinol.* **6**, p107.

Raman, C.S., Li, H., Martasek, P., Kral, V., Masters, B.S.S. and Poulos, T.L. 1998. Crystal Structure of Constitutive Endothelial Nitric Oxide Synthase: A Paradigm for Pterin Function Involving a Novel Metal Center. *Cell.* **95**, pp.939-950.

Reed, B.C. and Lane, M.D. 1980. Insulin receptor synthesis and turnover in differentiating 3T3-L1 preadipocytes. *Biochemistry.* **77**(1), pp.285-289.

Rees, D.D., Palmer, R.M.J., Schulz, R., Hodson, H.F. and Moncada, S. 1990. Characterization of three inhibitors of endothelial nitric oxide synthase in vitro and in vivo. *Br. J. Pharamcol.* **101**, pp.746-752.

Reyes-Grajeda, J.P. and Romero, A. 2017. *5VIZ: X-ray structure of Insulin Glargine*. Unpublished.

Ricciardolo, F.L.M., Sterk, P.J., Gaston, B. and Folkerts, G. 2003. Nitric Oxide in Health and Disease of the Respiratory System. *Physiol. Rev.* **84**, pp.731-765.

Rinderknecht, E. and Humbel, R.E. 1978. The amino acid sequence of human insulin-like growth factor I and its structural homology with proinsulin. *J. Biol. Chem.* **253**(8), pp.2769-2776.

Risau, W. and Flamme, I. 1995. VASCULOGENESIS. *Annu. Rev. Cell Dev. Biol.* **11**, pp.73-91.

Roberts, A.C., Gohil, J., Hudson, L., Connolly, K., Warburton, P., Suman, R., O'Toole, P., O'Regan, D.J., Turner, N.A., Riches, K. and Porter, K.E. 2015. Aberrant phenotype in human endothelial cells of diabetic origin: implications for saphenous vein graft failure? *J. Diabetes Res.* **2015**, p409432.

Rosenfeld, R.G., Hwa, V., Wilson, L., Lopez-Bermejo, A., Buckway, C., Burren, C., Choi, W.K., Devi, G., Ingermann, A., Graham, D., Minniti, G., Spagnoli, A. and Oh, Y. 1999. The Insulin-like Growth Factor Binding Protein Superfamily: New Perspectives. *Pediatrics.* **104**, pp.1018-1020.

Rosenfeld, R.G. and Roberts, C.T. 1999. *The IGF System: molecular biology, physiology and clinical applications.* Totowa (NJ): Humana Press.

Ross, R. 1999. ATHEROSCLEROSIS — AN INFLAMMATORY DISEASE. *N. Engl. J. Med.* **340**, pp.115-126.

Rossant, J. and Howard, L. 2002. Signaling pathways in vascular development. *Annu. Rev. Cell Dev. Biol.* **18**, pp.541-573.

Roy, A., Kucukural, A. and Zhang, Y. 2010. I-TASSER: a unified platform for automated protein structure and function prediction. *Nat. Protoc.* **5**(4), pp.725-738.

Ruel, M., Beanlands, R.S., Lortie, M., Chan, V., Camack, N., deKemp, R.A., Suuronen, E.J., Rubens, F.D., DaSilva, J.N., Sellke, F.W., Stewart, D.J. and Mesana, T.G. 2008. Concomitant treatment with oral L-arginine improves the efficacy of surgical angiogenesis in patients with severe diffuse coronary artery disease: the Endothelial Modulation in Angiogenic Therapy randomized controlled trial. *J. Thorac. Cardiovasc. Surg.* **135**(4), pp.762-770, 770 e761.

Salahudeen, M.S. and Nishtala, P.S. 2017. An overview of pharmacodynamic modelling, ligand-binding approach and its application in clinical practice. *Saudi Pharm. J.* **25**(2), pp.165-175.

Salerno, J.C., Ghosh, D.K., Razdan, R., Helms, K.A., Brown, C.C., McMurry, J.L., Rye, E.A. and Chrestensen, C.A. 2014. Endothelial nitric oxide synthase is regulated by ERK phosphorylation at Ser602. *Biosci. Rep.* **34**(5).

Sarbassov, D.D., Guertin, D.A., Ali, S.M. and Sabatini, D.M. 2005. Phosphorylation and Regulation of Akt/PKB by the Rictor-mTOR Complex. *Science.* **307**(5712), pp.1098-1101.

Sase, K. and Michel, T. 1997. Expression and Regulation of Endothelial Nitric Oxide Synthase. *Trends Cardiovasc. Med.* **7**(1), pp.28-37.

Savarimuthu, B., Li, R. and Wang, Y. 2012. *Crystal Structure of the Ferm Domain of Proline-rich Tyrosine Kinase 2*. Unpublished.

Scalera, F., Schlembach, D. and Beinder, E. 2001. Production of vasoactive substances by human umbilical vein endothelial cells after incubation with serum from preeclamptic patients. *Eur. J. Obstet. Gynecol.* **99**(2), pp.172-178.

Scapin, G., Dandey, V.P., Zhang, Z., Prosise, W., Hruza, A., Kelly, T., Mayhood, T., Strickland, C., Potter, C.S. and Carragher, B. 2018. Structure of the insulin receptor-insulin complex by single-particle cryo-EM analysis. *Nature.* **556**(7699), pp.122-125.

Schaffer, L. 1994. A model for insulin binding to the insulin receptor. *Eur. J. Biochem.* **221**, pp.1127-1132.

Schaffer, L. and Ljungqvist, L. 1992. Identification of a Disulfide Bridge Connecting the a-Subunits of the Extracellular Domain of the Insulin Receptor. *Biochem. Biophys. Res. Commun.* **189**(2), pp.650-653.

Schasfoort, R.B.M. 2017. Chapter 1. Introduction to Surface Plasmon Resonance. *Handbook of Surface Plasmon Resonance.* pp.1-26.

Schechter, Y., Hernaez, L., Schlessinger, J. and Cuatrecasas, P. 1979. Local aggregation of hormone-receptor complexes is required for activation by epidermal growth factor. *Nature.* **278**, pp.835-838.

Scheid, M.P., Marignani, P.A. and Woodgett, J.R. 2002. Multiple phosphoinositide 3-kinase-dependent steps in activation of protein kinase B. *Mol. Cell Biol.* **22**(17), pp.6247-6260.

Schmidt, H.H.W. and Walter, U. 1994. NO at Work. *Cell.* **78**, pp.919-925.

Schumacher, R., Mosthaf, L., Schlessinger, J., Brandenburg, D. and Ullrich, A. 1991. Insulin and insulin-like growth factor-1 binding specificity is determined by distinct regions of their cognate receptors. *J. Biol. Chem.* **266**(29), pp.19288-19295.

Schumacher, R., Soos, M.A., Schlessinger, J., Brandenburg, D., Siddle, K. and Ullrich, A. 1993. Signaling-competent receptor chimeras allow mapping of major insulin receptor binding domain determinants. *J. Biol. Chem.* **268**(2), pp.1087-1094.

Schäffer, L., Kjeldsen, T., Andersen, A.S., Wiberg, F.C., Larsen, U.D., Cara, J.F., Mirmira, R.G., Nakagawa, S.H. and Tager, H.S. 1993. Interactions of a hybrid insulin/insulin-like growth factor-I analog with chimeric insulin/type I insulin-like growth factor receptors. *J. Biol. Chem.* **268**(5), pp.3044-3047.

Sciacca, L., Cassarino, M.F., Genua, M., Pandini, G., Le Moli, R., Squatrito, S. and Vigneri, R. 2010. Insulin analogues differently activate insulin receptor isoforms and post-receptor signalling. *Diabetologia.* **53**(8), pp.1743-1753.

Scott, D.A. and Fisher, A.M. 1938. THE INSULIN AND THE ZINC CONTENT OF NORMAL AND DIABETIC PANCREAS. *J. Clin. Invest.* **6**, pp.725-728.

Seino, S. and Bell, G.I. 1989. Alternative Splicing of Human Insulin Receptor Messenger RNA. *Biochem. Biophys. Res. Commun.* **159**(1), pp.312-316.

Seino, S., Seino, M., Nishi, S. and Bell, G.I. 1989. Structure of the human insulin receptor gene and characterization of its promoter. *PNAS.* **86**, pp.114-118.

Sekimoto, H., Eipper-Mains, J., Pond-Tor, S. and Boney, C.M. 2005. (alpha)v(beta)3 integrins and Pyk2 mediate insulin-like growth factor I activation of Src and mitogen-activated protein kinase in 3T3-L1 cells. *Mol. Endocrinol.* **19**(7), pp.1859-1867.

Semenkovich, C.F. 2006. Insulin resistance and atherosclerosis. *J. Clin. Invest.* **116**(7), pp.1813-1822.

Sessa, W.C., Garcia-Cardena, G., Liu, J., Keh, A., Pollock, J.S., Bradley, J., Thiru, S., Braverman, I.M. and Desai, K.M. 1995. The Golgi association of endothelial nitric oxide synthase is necessary for the efficient synthesis of nitric oxide. *J. Biol. Chem.* **270**(30), pp.17641-17644.

Shen, X., Xi, G., Radhakrishnan, Y. and Clemmons, D.R. 2010. Recruitment of Pyk2 to SHPS-1 signaling complex is required for IGF-I-dependent mitogenic signaling in vascular smooth muscle cells. *Cell Mol. Life Sci.* **67**(22), pp.3893-3903.

Shin, W.H., Christoffer, C.W. and Kihara, D. 2017. In silico structure-based approaches to discover protein-protein interaction-targeting drugs. *Methods.* **131**, pp.22-32.

Shoelson, S.E., Lu, Z.-X., Parlautan, L., Lynch, C.S. and Weiss, M.A. 1992. Mutations at the Dimer, Hexamer, and Receptor-Binding Surfaces of Insulin Independently Affect Insulin-Insulin and Insulin-Receptor Interactions1. *Biochemistry.* **31**, pp.1757-1767.

Shrader, C.D., Bailey, K.M., Konat, G.W., Cilento, E.V. and Reilly, F.D. 2009. Insulin enhances proliferation and viability of human umbilical vein endothelial cells. *Arch. Dermatol. Res.* **301**(2), pp.159-166.

Shukla, A., Grisouard, J., Ehemann, V., Hermani, A., Enzmann, H. and Mayer, D. 2009. Analysis of signaling pathways related to cell proliferation stimulated by insulin analogs in human mammary epithelial cell lines. *Endocr. Relat. Cancer.* **16**(2), pp.429-441.

Sigma-Aldrich. 2022. *Agarose Beads Vs. Magnetic Beads in ChIP.* [Online]. Available from: https://www.sigmaaldrich.com/GB/en/technical-documents/technical-article/protein-biology/protein-pulldown/agarose-beads-vs-magnetic-beads-in-chip

Simons, M. 2005. Angiogenesis: where do we stand now? *Circulation.* **111**(12), pp.1556-1566.

Siragusa, M., Oliveira Justo, A.F., Malacarne, P.F., Strano, A., Buch, A., Withers, B., Peters, K.G. and Fleming, I. 2021. VE-PTP inhibition elicits eNOS phosphorylation to blunt endothelial dysfunction and hypertension in diabetes. *Cardiovasc. Res.* **117**(6), pp.1546-1556.

Siragusa, M., Thole, J., Bibli, S.I., Luck, B., Loot, A.E., de Silva, K., Wittig, I., Heidler, J., Stingl, H., Randriamboavonjy, V., Kohlstedt, K., Brune, B., Weigert, A., Fisslthaler, B. and Fleming, I. 2019. Nitric oxide maintains endothelial redox homeostasis through PKM2 inhibition. *EMBO J.* **38**(17), pe100938.

Slaaby, R. 2015. Specific insulin/IGF1 hybrid receptor activation assay reveals IGF1 as a more potent ligand than insulin. *Sci. Rep.* **5**, p7911.

Slaaby, R., Schaffer, L., Lautrup-Larsen, I., Andersen, A.S., Shaw, A.C., Mathiasen, I.S. and Brandt, J. 2006. Hybrid receptors formed by insulin receptor (IR) and insulin-like growth factor I receptor (IGF-IR) have low insulin and high IGF-1 affinity irrespective of the IR splice variant. *J. Biol. Chem.* **281**(36), pp.25869-25874.

Sneddon, J.M. and Vane, J.R. 1988. Endothelium-derived relaxing factor reduces platelet adhesion to bovine endothelial cells. *Proc. Nati. Acad. Sci.* **85**, pp.2800-2804.

Somlyo, A.P. and Somlyo, A.V. 1994. Signal transduction and regulation in smooth muscle. *Nature.* **372**, pp.231-236.

Sommerfeld, M.R., Muller, G., Tschank, G., Seipke, G., Habermann, P., Kurrle, R. and Tennagels, N. 2010. In vitro metabolic and mitogenic signaling of insulin glargine and its metabolites. *PLoS One.* **5**(3), pe9540.

Soos, M.A., Field, C.E. and Siddle, K. 1993. Purified hybrid insulin/insulin-like growth factor-I receptors bind insulin-like growth factor-I, but not insulin, with high affinity. *Biochem. J.* **290**, pp.419-426.

Soos, M.A. and Siddle, K. 1989. Immunological relationships between receptors for insulin and insulin-like growth factor I. *Biochem. J.* **263**, pp.553-563.

Soos, M.A., Whittaker, J., Lammers, R., Ullrich, A. and Siddle, K. 1990. Receptors for insulin and insulin-like growth factor-I can form hybrid dimers. *Biochem. J.* **270**, pp.383-390.

Spampinato, D., Pandini, G., Iuppa, A., Trischitta, V., Vigneri, R. and Frittitta, L. 2000. Insulin/Insulin-Like Growth Factor I Hybrid Receptors Overexpression Is Not an Early Defect in Insulin-Resistant Subjects. *J. Clin. Endocrinol. Metab.* **85**(11), pp.4219–4223.

Sparrow, L.G., McKern, N.M., Gorman, J.J., Strike, P.M., Robinson, C.P., Bentley, J.D. and Ward, C.W. 1997. The disulfide bonds in the C-terminal domains of the human insulin receptor ectodomain. *J. Biol. Chem.* **272**(47), pp.29460-29467.

Sperling, M.A., Tamborlane, W.V., Battelino, T., Weinzimer, S.A. and Phillip, M. 2014. CHAPTER 19 - Diabetes mellitus. In: Sperling, M.A. ed. *Pediatric Endocrinology (Fourth Edition).* W. B. Saunders, pp.846-900.

Sriram, K., Laughlin, J.G., Rangamani, P. and Tartakovsky, D.M. 2016. Shear-Induced Nitric Oxide Production by Endothelial Cells. *Biophys. J.* **111**(1), pp.208-221.

Staiger, K., Hennige, A.M., Staiger, H., Haring, H.-U. and Kellerer, M. 2007. Comparison of the Mitogenic Potency of Regular Human Insulin and its Analogue Glargine in Normal and Transformed Human Breast Epithelial Cells. *Horm. Metab. Res.* **39**(1), pp.65-67.

Steinbrecher, U.P., Parthsarathy, S., Leake, D.S., Witztum, J.L. and Steinberg, D. 1984. Modification of low density lipoprotein by endothelial cells involves lipid peroxidation and degradation of low density lipoprotein phospholipids. *PNAS.* **81**, pp.3883-3887.

Steiner, D.F., Chan, S.J., Welsh, J.M. and Kwok, S.C.M. 1985. STRUCTURE AND EVOLUTION OF THE INSULIN GENE. *Ann. Rev. Genet.* **19**, pp.463-484.

Steiner, D.F., Cunningham, D., Spigelman, L. and Aten, B. 1967. Insulin Biosynthesis: Evidence for a Precursor. *Science.* **157**(3789), pp.697-700.

Steiner, D.F. and Oyer, P.E. 1967. THE BIOSYNTHESIS OF INSULIN AND A PROBABLE PRECURSOR OF INSULIN BY A HUMAN ISLET CELL ADENOMA. *PNAS.* **57**(2), pp.473-480.

Steward, R., Jr., Tambe, D., Hardin, C.C., Krishnan, R. and Fredberg, J.J. 2015. Fluid shear, intercellular stress, and endothelial cell alignment. *Am. J. Physiol. Cell Physiol.* **308**(8), pp.C657-664.

Stroes, E., Kastelein, J., Cosentino, F., Erkelens, W., Wever, R., Koomans, H., Luscher, T. and Rabelink, T. 1996. Tetrahydrobiopterin Restores Endothelial Function in Hypercholesterolemia. *J. Clin. Invest.* **99**, pp.41-46.

Stuehr, D., Pou, S. and Rosen, G.M. 2001. Oxygen reduction by nitric-oxide synthases. *J. Biol. Chem.* **276**(18), pp.14533-14536.

Tabas, I. 2017. 2016 Russell Ross Memorial Lecture in Vascular Biology: Arteriosclerosis, Thrombosis, and Vascular Biology. *Arterioscler. Thromb. Vasc. Biol.* **37**(2), pp.183-189.

Tai, L.K., Okuda, M., Abe, J., Yan, C. and Berk, B.C. 2002. Fluid shear stress activates proline-rich tyrosine kinase via reactive oxygen species-dependent pathway. *Arterioscler. Thromb. Vasc. Biol.* **22**(11), pp.1790-1796.

Tang, H., Hao, Q., Fitzgerald, T., Sasaki, T., Landon, E.J. and Inagami, T. 2002. Pyk2/CAKbeta tyrosine kinase activity-mediated angiogenesis of pulmonary vascular endothelial cells. *J. Biol. Chem.* **277**(7), pp.5441-5447.

Tavafi, M. 2013. Complexity of diabetic nephropathy pathogenesis and design of investigations. *J. Renal. Inj. Prev.* **2**(2), pp.59-62.

Tavian, M., Coulombel, L., Luton, D., Clemente, H.S., Dieterlen-Lievre, F. and Peault, B. 1996. Aorta-associated CD34+ hematopoietic cells in the early human embryo. *Blood.* **87**(1), pp.67-72.

ter Braak, B., Siezen, C.L., Kannegieter, N., Koedoot, E., van de Water, B. and van der Laan, J.W. 2014. Classifying the adverse mitogenic mode of action of insulin analogues using a novel mechanism-based genetically engineered human breast cancer cell panel. *Arch. Toxicol.* **88**(4), pp.953-966.

ter Braak, B., Wink, S., Koedoot, E., Pont, C., Siezen, C., van der Laan, J.W. and van de Water, B. 2015. Alternative signaling network activation through different insulin receptor family members caused by pro-mitogenic antidiabetic insulin analogues in human mammary epithelial cells. *Breast Cancer Res.* **17**, p97.

Thayse, K., Kindt, N., Laurent, S. and Carlier, S. 2020. VCAM-1 Target in Non-Invasive Imaging for the Detection of Atherosclerotic Plaques. *Biology.* **9**(11), p368.

Thirumalai, D., Reddy, G. and Straub, J.E. 2012. Role of Water in Protein Aggregation and Amyloid Polymorphism. *Acc. Chem. Res.* **45**(1), pp.83–92.

Thomas, G.D. and Victor, R.G. 1997. Nitric oxide mediates contraction-induced attenuation of sympathetic vasoconstriction in rat skeletal muscle. *J. Physiol.* **506.3**, p817—826.

Tiwari, S., Halagappa, V.K., Riazi, S., Hu, X. and Ecelbarger, C.A. 2007. Reduced expression of insulin receptors in the kidneys of insulin-resistant rats. *J. Am. Soc. Nephrol.* **18**(10), pp.2661-2671.

Tollefsen, S.E. and Thompson, K. 1988. The Structural Basis for Insulin-like Growth Factor I Receptor High Affinity Binding. *J. Biol. Chem.* **263**(31), pp.16267-16273.

Tollefsen, S.E., Thompson, K. and Petersen, D.J. 1987. Separation of the High Affinity Insulin-like Growth Factor I Receptor from Low Affinity Binding Sites by Affinity Chromatography. *J. Biol. Chem.* **262**(34), pp.16461-16469.

Toshner, M., Dunmore, B.J., McKinney, E.F., Southwood, M., Caruso, P., Upton, P.D., Waters, J.P., Ormiston, M.L., Skepper, J.N., Nash, G., Rana, A.A. and Morrell, N.W. 2014. Transcript analysis reveals a specific HOX signature associated with positional identity of human endothelial cells. *PLoS One.* **9**(3), pe91334.

Tousoulis, D., A-M., K., Tentolouris, C., Papageorgiou , N. and Stefanadis, C. 2012. The Role of Nitric Oxide on Endothelial Function. *Curr. Vasc. Pharmacol.* **10**, pp.4-18.

Truong, K. and Ikura, M. 2001. The use of FRET imaging microscopy to detect protein–protein interactions and protein conformational changes in vivo. *Curr. Opin. Struct. Biol.* **11**, pp.573–578.

Tseng, L.Y.-H., Schwartz, G.P., Sheikh, M., Chen, Z.Z., Joshi, S., Wang, J.-F., Nissley, S.P., Burke, G.T., Katsoyannis, P.G. and Rechler, M.M. 1987. Hybrid molecules containing the A-domain of insulin-like growth factor-I and the B-chain of insulin have increased mitogenic activity relative to insulin. *Biochem. Biophys. Res. Commun.* **149**(2), pp.672-679.

Tsihlis, N.D., Oustwani, C.S., Vavra, A.K., Jiang, Q., Keefer, L.K. and Kibbe, M.R. 2011. Nitric oxide inhibits vascular smooth muscle cell proliferation and neointimal hyperplasia by increasing the ubiquitination and degradation of UbcH10. *Cell Biochem. Biophys.* **60**(1-2), pp.89-97.

Tulloch, P.A., Lawrence, M.C., McKern, N.M., Robinson, C.P., Bentley, J.D., Cosgrove, L.J., Ivancic, N., Lovrecz, G.O., Siddle, K. and Ward, C.W. 1999. Single-Molecule Imaging of Human Insulin Receptor Ectodomain and Its Fab Complexes. *J. Struct. Biol.* **125**, pp.11–18.

Uchikawa, E., Choi, E., Shang, G., Yu, H. and Bai, X.C. 2019. Activation mechanism of the insulin receptor revealed by cryo-EM structure of the fully liganded receptor-ligand complex. *Elife.* **8**.

UK, D. 2020. *Diabetes Prevalence 2019.* [Online]. Available from: https://www.diabetes.org.uk/professionals/position-statements-reports/statistics/diabetes-prevalence-2019

UK, D. 2021. *Diabetes Statistics.* [Online]. Available from: https://www.diabetes.org.uk/professionals/position-statements-reports/statistics

Ullrich, A., Bell, J.R., Chen, E.Y., Herrera, R., Petruzzelli, L.M., Dull, T.J., Gray, A., Coussens, L., Liao, Y.-C., Tsubokawa, M., Mason, A., Seeburg, P.H., Grunfeld, C., Rosen, O.M. and Ramachandran, J. 1985. Human insulin receptor and its relationship to the tyrosine kinase family of oncogenes. *Nature.* **313**, pp.756-761.

Vajo, Z., Fawcett, J. and Duckworth, W.C. 2001. Recombinant DNA Technology in the Treatment of Diabetes: Insulin Analogs. *Endocr. Rev.* **22**, pp.706–717.

van Beem, R.T., Verloop, R.E., Kleijer, M., Noort, W.A., Loof, N., Koolwijk, P., van der Schoot, C.E., van Hinsbergh, V.W. and Zwaginga, J.J. 2009. Blood outgrowth endothelial cells from cord blood and peripheral blood: angiogenesis-related characteristics in vitro. *J. Thromb. Haemost.* **7**(1), pp.217-226.

van der Spoel, D., Lindahl, E., Hess, B., Groenhof, G., Mark, A.E. and Berendsen, H.J.C. 2005. GROMACS: Fast, flexible and free. *J. Comp. Chem.* **26**(16), pp.1701-1718.

van Horn, H., Ekström, C., Ellis, E., Olivecrona, H., Einarsson, C., Tally, M. and Ekstrom, T.J. 2002. GH is a regulator of IGF2 promoter-specific transcription in human liver. *J. Endocrinol.* **172**, pp.457–465.

Vanarotti, M.S., Finkelstein, D.B., Guibao, C.D., Nourse, A., Miller, D.J. and Zheng, J.J. 2016. Structural Basis for the Interaction between Pyk2-FAT Domain and Leupaxin LD Repeats. *Biochemistry.* **55**(9), pp.1332-1345.

Varadi, M., Anyango, S., Deshpande, M., Nair, S., Natassia, C., Yordanova, G., Yuan, D., Stroe, O., Wood, G., Laydon, A., Zidek, A., Green, T., Tunyasuvunakool, K., Petersen, S., Jumper, J., Clancy, E., Green, R., Vora, A., Lutfi, M., Figurnov, M., Cowie, A., Hobbs, N., Kohli, P., Kleywegt, G., Birney, E., Hassabis, D. and Velankar, S. 2022. AlphaFold Protein Structure Database: massively expanding the structural coverage of protein-sequence space with high-accuracy models. *Nucleic Acids Res.* **50**(D1), pp.D439-D444.

Versteyhe, S., Klaproth, B., Borup, R., Palsgaard, J., Jensen, M., Gray, S.G. and De Meyts, P. 2013. IGF-I, IGF-II, and Insulin Stimulate Different Gene Expression Responses through Binding to the IGF-I Receptor. *Front. Endocrinol.* **4**, p98.

Villanueva, C. and Giulivi, C. 2010. Subcellular and cellular locations of nitric oxide synthase isoforms as determinants of health and disease. *Free Radic. Biol. Med.* **49**(3), pp.307-316.

Vincent, A.M. and Feldman, E.L. 2002. Control of cell survival by IGF signaling pathways. *Growth Horm. IGF Res.* **12**(4), pp.193-197.

Viswambharan, H., Yuldasheva, N.Y., Sengupta, A., Imrie, H., Gage, M.C., Haywood, N., Walker, A.M., Skromna, A., Makova, N., Galloway, S., Shah, P., Sukumar, P., Porter, K.E., Grant, P.J., Shah, A.M., Santos, C.X., Li, J., Beech, D.J., Wheatcroft, S.B., Cubbon, R.M. and Kearney, M.T. 2017. Selective Enhancement of Insulin Sensitivity in the Endothelium In Vivo Reveals a Novel Proatherosclerotic Signaling Loop. *Circ. Res.* **120**(5), pp.784-798.

Vivanco, I. and Sawyers, C.L. 2002. The phosphatidylinositol 3-Kinase AKT pathway in human cancer. *Nat. Rev. Cancer.* **2**(7), pp.489-501.

Vogt, B., Carrascosa, J.M., Ermel, B., Ullrich, A. and Haring, H.-U. 1991. The two isotopes of the human insulin receptor (HIR-A and HIR-B) follow different internalisation kinetics. *Biochem. Biophys. Res. Commun.* **177**(3), pp.1013-1018.

Volkmann, N., Martasek, P., Roman, L.J., Xu, X.P., Page, C., Swift, M., Hanein, D. and Masters, B.S. 2014. Holoenzyme structures of endothelial nitric oxide synthase - an allosteric role for calmodulin in pivoting the FMN domain for electron transfer. *J. Struct. Biol.* **188**(1), pp.46-54.

Waller, D.G. and Sampson, A.P. 2018. Diabetes mellitus. *Med. Pharmacol. Therap.*, pp.459-473.

Walter, F., O'Brien, A., Concannon, C.G., Dussmann, H. and Prehn, J.H.M. 2018. ER stress signaling has an activating transcription factor 6alpha (ATF6)-dependent "off-switch". *J Biol Chem.* **293**(47), pp.18270-18284.

Wang, C.-C., Goldfine, I.D., Fujita-Yamaguchi, Y., Gattner, H.G., Brandenburg, D. and De Meyts, P. 1988. Negative and positive site-site interactions, and their modulation by pH, insulin analogs, and monoclonal antibodies, are preserved in the purified insulin receptor. *PNAS.* **85**, pp.8400-8404.

Wang, G.-R., Zhu, Y., Halushka, P.V., Licoln, T.M. and Mendelsohn, M.E. 1998. Mechanism of platelet inhibition by nitric oxide: In vivo phosphorylation of thromboxane receptor by cyclic GMP-dependent protein kinase. *Biochemistry.* **95**, pp.4888-4893.

Wang, H., Wang, A.X., Liu, Z., Chai, W. and Barrett, E.J. 2009. The trafficking/interaction of eNOS and caveolin-1 induced by insulin modulates endothelial nitric oxide production. *Mol. Endocrinol.* **23**(10), pp.1613-1623.

Wang, W., Hein, T.W., Zhang, C., Zawieja, D.C., Liao, J.C. and Kuo, L. 2011. Oxidized low-density lipoprotein inhibits nitric oxide-mediated coronary arteriolar dilation by up-regulating endothelial arginase I. *Microcirculation.* **18**(1), pp.36-45.

Ward, C.W., Menting, J.G. and Lawrence, M.C. 2013. The insulin receptor changes conformation in unforeseen ways on ligand binding: sharpening the picture of insulin receptor activation. *Bioessays.* **35**(11), pp.945-954, doi/910 1002/bies 201370111.

Wassenaar, T.A., Pluhackova, K., Bockmann, R.A., Marrink, S.J. and Tieleman, D.P. 2014. Going Backward: A Flexible Geometric Approach to Reverse Transformation from Coarse Grained to Atomistic Models. *J. Chem. Theory Comput.* **10**(2), pp.676-690.

Webb, B. and Sali, A. 2016. Comparative Protein Structure Modeling Using MODELLER. *Curr. Protoc. Bioinformatics.* **54**, pp.5 6 1-5 6 37.

Weinstein, D., Simon, M., Yehezkel, E., Laron, Z. and Werner, H. 2009. Insulin analogues display IGF-I-like mitogenic and anti-apoptotic activities in cultured cancer cells. *Diabetes Metab. Res. Rev.* **25**(1), pp.41-49.

Weis, F., Menting, J.G., Margetts, M.B., Chan, S.J., Xu, Y., Tennagels, N., Wohlfart, P., Langer, T., Muller, C.W., Dreyer, M.K. and Lawrence, M.C. 2018. The signalling conformation of the insulin receptor ectodomain. *Nat. Commun.* **9**(1), p4420.

Weis, S.M., Lim, S.T., Lutu-Fuga, K.M., Barnes, L.A., Chen, X.L., Gothert, J.R., Shen, T.L., Guan, J.L., Schlaepfer, D.D. and Cheresh, D.A. 2008. Compensatory role for Pyk2 during angiogenesis in adult mice lacking endothelial cell FAK. *J. Cell Biol.* **181**(1), pp.43-50.

Whittaker, J., Groth, A.V., Mynarcik, D.C., Pluzek, L., Gadsboll, V.L. and Whittaker, L.J. 2001. Alanine scanning mutagenesis of a type 1 insulin-like growth factor receptor ligand binding site. *J. Biol. Chem.* **276**(47), pp.43980-43986.

Whittaker, L., Hao, C., Fu, W. and Whittaker, J. 2008. High-affinity insulin binding: insulin interacts with two receptor ligand binding sites. *Biochemistry.* **47**(48), pp.12900-12909.

Whitten, A.E., Smith, B.J., Menting, J.G., Margetts, M.B., McKern, N.M., Lovrecz, G.O., Adams, T.E., Richards, K., Bentley, J.D., Trewhella, J., Ward, C.W. and Lawrence, M.C. 2009. Solution structure of ectodomains of the insulin receptor family: the ectodomain of the type 1 insulin-like growth factor receptor displays asymmetry of ligand binding accompanied by limited conformational change. *J. Mol. Biol.* **394**(5), pp.878-892.

Williams, P.F., Mynarcik, D.C., Yu, G.Q. and Whittaker, J. 1995. Mapping of an NH2-terminal ligand binding site of the insulin receptor by alanine scanning mutagenesis. *J. Biol. Chem.* **270**(7), pp.3012-3016.

Wofsy, C., Goldstein, B., Lund, K. and Wiley, H.S. 1992. Implications of epidermal growth factor (EGF) induced egf receptor aggregation. *Biophys. J.* **63**, pp.98-110.

Wolff, D.J., Datto, G.A., Samatovicz, R.A. and Tempsick, R.A. 1993. Calmodulin-dependent nitric-oxide synthase. Mechanism of inhibition by imidazole and phenylimidazoles. *J. Biol. Chem.* **268**(13), pp.9425-9429.

Wong, A.W., Urisman, A., Burlingame, A.L. and Shokat, K.M. 2019. Chemically reprogramming the phospho-transfer reaction to crosslink protein kinases to their substrates. *Protein Sci.* **28**(3), pp.654-662.

Writing Team for the Diabetes, C., Complications Trial/Epidemiology of Diabetes, I. and Complications Research, G. 2003. Sustained effect of intensive treatment of type 1 diabetes mellitus on development and progression of diabetic nephropathy: the Epidemiology of Diabetes Interventions and Complications (EDIC) study. *JAMA.* **290**(16), pp.2159-2167.

Wu, G., Berka, V. and Tsai, A.L. 2011. Binding kinetics of calmodulin with target peptides of three nitric oxide synthase isozymes. *J. Inorg. Biochem.* **105**(9), pp.1226-1237.

Wu, J.W., Filion, K.B., Azoulay, L., Doll, M.K. and Suissa, S. 2016. Effect of Long-Acting Insulin Analogs on the Risk of Cancer: A Systematic Review of Observational Studies. *Diabetes Care.* **39**(3), pp.486-494.

Xia, C., Misra, I., Iyanagi, T. and Kim, J.J. 2009. Regulation of interdomain interactions by calmodulin in inducible nitric-oxide synthase. *J. Biol. Chem.* **284**(44), pp.30708-30717.

Xu, Y., Kong, G.K., Menting, J.G., Margetts, M.B., Delaine, C.A., Jenkin, L.M., Kiselyov, V.V., De Meyts, P., Forbes, B.E. and Lawrence, M.C. 2018. How ligand binds to the type 1 insulin-like growth factor receptor. *Nat. Commun.* **9**(1), p821.

Yamaguchi, Y., Flier, J.S., Benecke, H., Ransil, B.J. and Moller, D.E. 1993. Ligand-binding properties of the two isoforms of the human insulin receptor. *Endocrinology.* **132**(3), pp.1132-1138.

Yamaguchi, Y., Flier, J.S., Yokota, A., Benecke, H., Backer, J.M. and Moller, D.E. 1991. Functional Properties of Two Naturally Occurring Isoforms of the Human Insulin Receptor in Chinese Hamster Ovary Cells*. *Endocrinology.* **129**(4), pp.2058-2066.

Yang, J., Yan, R., Roy, A., Xu, D., Poisson, J. and Zhang, Y. 2015. The I-TASSER Suite: protein structure and function prediction. *Nat. Methods.* **12**(1), pp.7-8.

Yang, Y.M., Huang, A., Kaley, G. and Sun, D. 2009. eNOS uncoupling and endothelial dysfunction in aged vessels. *Am. J. Physiol. Heart Circ. Physiol.* **297**(5), pp.H1829-1836.

Ye, L., Maji, S., Sanghera, N., Gopalasingam, P., Gorbunov, E., Tarasov, S., Epstein, O. and Klein-Seetharaman, J. 2017. Structure and dynamics of the insulin receptor: implications for receptor activation and drug discovery. *Drug Discov. Today.* **22**(7), pp.1092-1102.

Yu, C. and Huang, L. 2018. Cross-Linking Mass Spectrometry: An Emerging Technology for Interactomics and Structural Biology. *Anal. Chem.* **90**(1), pp.144-165.

Zhang, B. and Roth, R.A. 1991. A region of the insulin receptor important for ligand binding (residues 450-601) is recognized by patients' autoimmune antibodies and inhibitory monoclonal antibodies. *PNAS.* **88**, pp.9858-9862.

Zhang, B. and Roth, R.A. 1992. The insulin receptor-related receptor. Tissue expression, ligand binding specificity, and signaling capabilities. *J. Biol. Chem.* **267**(26), pp.18320-18328.

Zhang, H., Pelzer, A.M., Kiang, D.T. and Yee, D. 2007. Down-regulation of type I insulin-like growth factor receptor increases sensitivity of breast cancer cells to insulin. *Cancer Res.* **67**(1), pp.391-397.

Zhang, W., Gustafson, T.A., Rutter, W.J. and Johnson, J.D. 1994. Positively charged side chains in the insulin-like growth factor-1 C- and D-regions determine receptor binding specificity. *J. Biol. Chem.* **269**(14), pp.10609-10613.

Zhang, Y. 2008. I-TASSER server for protein 3D structure prediction. *BMC Bioinformatics.* **9**, p40.

Zhang, Y., Lee, T.S., Kolb, E.M., Sun, K., Lu, X., Sladek, F.M., Kassab, G.S., Garland, T., Jr. and Shyy, J.Y. 2006. AMP-activated protein kinase is involved in endothelial NO synthase activation in response to shear stress. *Arterioscler. Thromb. Vasc. Biol.* **26**(6), pp.1281-1287.

Zhu, X., Bao, Y., Guo, Y. and Yang, W. 2018. Proline-Rich Protein Tyrosine Kinase 2 in Inflammation and Cancer. *Cancers.* **10**(5).

Ziche, M., Morbidelli, L., Masini, E., Amerini, S., Granger, H.J., Maggi, C.A., Geppetti, P. and Ledda, F. 1994. Nitric Oxide Mediates Angiogenesis In Vivo and Endothelial Cell Growth and Migration In Vitro Promoted by Substance P. *J. Clin. Invest.* **94**, pp.2036-2044.

Ziegler, A.N., Chidambaram, S., Forbes, B.E., Wood, T.L. and Levison, S.W. 2014. Insulin-like growth factor-II (IGF-II) and IGF-II analogs with enhanced insulin receptor-a binding affinity promote neural stem cell expansion. *J. Biol. Chem.* **289**(8), pp.4626-4633.

Zoche, M., Bienert, M., Beyermann, M. and Koch, K.-W. 1996. Distinct Molecular Recognition of Calmodulin-Binding Sites in the Neuronal and

Macrophage Nitric Oxide Synthases: A Surface Plasmon Resonance Study. *Biochemistry.* **35**, pp.8742-8747.

Zoete, V., Meuwly, M. and Karplus, M. 2005. Study of the insulin dimerization: binding free energy calculations and per-residue free energy decomposition. *Proteins.* **61**(1), pp.79-93.

20. Appendices

20.1. Binding Affinities of Insulin and IGF-1 to Insulin Receptor Isoforms, IGF1R and IR/IGF1R Hybrid Receptors

	IR-A	IR-B	IGF1R	References
Insulin	0.91 ± 0.3	1.0 ± 0.4	nd	(Frasca et al., 1999)
	nd	nd	>30	(Pandini et al., 2002)
	0.40 ± 0.10	0.49 ± 0.05	>1000	(Sciacca et al., 2010)
	nd	nd	383 ± 27	(Versteyhe et al., 2013)
	1.57 ± 0.33	nd	nd	(Rajapaksha and Forbes, 2015)
	2.7 ± 0.6	2.6 ± 0.7	nd	(Pierre-Eugene et al., 2012)
IGF-1	>30	>30	0.2 ± 0.3	(Pandini et al., 2002)
	nd	nd	1.49 ± 0.14	(Versteyhe et al., 2013)
	34 ± 13	50 ± 13	nd	(Pierre-Eugene et al., 2012)
IGF-2	3.3 ± 0.4	36.0 ± 3.8	nd	(Frasca et al., 1999)
	nd	nd	0.6	(Pandini et al., 2002)
	nd	nd	13.1 ± 0.7	(Versteyhe et al., 2013)
	15.2 ± 0.2	nd	nd	(Rajapaksha and Forbes, 2015)
	4 ± 0.4	nd	3.4 ± 0.2	(Ziegler et al., 2014)

Table 20-1: EC_{50} Values of Insulin, IGF-1 and IGF-2 for IR-A, IR-B and IGF1R

Cognate ligand concentration required to achieve 50% of maximal receptor activation (EC_{50}, nM) of IR-A, IR-B and IGF1R homodimer species. Table from (Belfiore et al., 2017).

IR-A/IGF1R (HR-A)			IR-B/IGF1R (HR-B)			Method	References
Insulin	*IGF-1*	*IGF-2*	*Insulin*	*IGF-1*	*IGF-2*		
3.7 ± 0.9	0.3 ± 0.2	0.6 ± 0.1	>100	2.5 ± 0.5	15 ± 0.9	PACA	(Pandini et al., 2002)
2.6 ± 1.3	0.01 ± 0.01	nd	2.8 ± 1.4	0.01 ± 0.01	nd	PACA	(Slaaby et al., 2006)
1.1 ± 0.2	0.02 ± 0.006	0.18 ± 0.04	1.1 ± 0.3	0.02 ± 0.07	0.19 ± 0.04	SPA	
4.6 ± 1.9	0.01 ± 0.001	nd	5.1 ± 2.3	0.01 ± 0.01	nd	PEG	
70 ± 12	0.5 ± 0.2	0.7 ± 0.1	76 ± 12	0.3 ± 0.1	0.3 ± 0.1	PACA	(Benyoucef et al., 2007)
60 ± 10	4.0 ± 0.5	nd	40 ± 5	4.0 ± 1.0	nd	BRET	
130 ± 41	3.0 ± 0.66	nd	70 ± 35	2.8 ± 0.66	nd	BRET	(Pierre-Eugene et al., 2012)
342 ± 121	6 ± 3	nd	325 ± 88	12 ± 2	nd	ELISA	(Slaaby, 2015)

Table 20-2: EC_{50} Values of Insulin, IGF-1 and IGF-2 for IR-A/IGF1R and IR-B/IGF1R Hybrids

Cognate ligand concentration required to achieve 50% of maximal receptor activation (EC_{50}, nM) of IR-A/IGF1R and IR-B/IGF1R heterodimer species. Table from (Belfiore et al., 2017).

20.2. Western blotting primary and secondary antibodies

Antibody Name	Antibody ID	Manufacturer	Source	Concentration
Insulin Receptor β (4B8)	#3025	CST	Rabbit	1:1,000
IGF1R β (D23H3) XP®	#9750	CST	Rabbit	1:1,000
β-actin (C4)	Sc-47778	SCBT	Mouse	1:5,000
PYK2	#3292	CST	Rabbit	1:1,000
Phospho-PYK2 (Tyr402)	#3291	CST	Rabbit	1:1,000
eNOS/NOS Type III	AB_397691	BD BS	Mouse	1:1,000
P-eNOS (Tyr-657)/nNOS (Tyr-895)	NP4031	ECM BS	Rabbit	1:1,000
Phospho-eNOS (Ser1177)	#9571	CST	Rabbit	1:1,000
Akt pan (11E7)	#4685	CST	Rabbit	1:1,000
Phospho-Akt (Ser473) (D9E) XP®	#4060	CST	Rabbit	1:1,000
Phospho-Akt (Thr308) (244F9)	#4056	CST	Rabbit	1:1,000
PI3 Kinase p85 (19H8)	#4257	CST	Rabbit	1:1,000
Phospho-PI3 Kinase p85 (Tyr458)/p55 (Tyr199)	#4228	CST	Rabbit	1:1,000
PI3 Kinase p110α (C73F8)	#4249	CST	Rabbit	1:1,000
PI3 Kinase p110β (C33D4)	#3011	CST	Rabbit	1:1,000
P44/42 MAPK (Erk1/2) (137F5)	#4695	CST	Rabbit	1:1,000
Phospho-p44/42 MAPK (Erk1/2) (Thr202/Ty204)	#9101	CST	Rabbit	1:1,000
Anti-Rabbit HRP	NA9341ML	SLS	Rabbit HRP	1:10,000
Anti-Mouse HRP	A27025	Thermo	Mouse HRP	1:10,000

20.3. ESMIRO/Y656F Genotype

Mouse ID	Genotype	
	ESMIRO	*Y656F*
1	TG	Het
2	TG	Het
3	TG	Het
4	WT	Het